

University of Louisville

ThinkIR: The University of Louisville's Institutional Repository

Electronic Theses and Dissertations

12-2020

The utilization of metal-ligand cooperativity for electrocatalytic reduction and catalytic hydration.

Steven Cronin
University of Louisville

Follow this and additional works at: <https://ir.library.louisville.edu/etd>

 Part of the [Inorganic Chemistry Commons](#)

Recommended Citation

Cronin, Steven, "The utilization of metal-ligand cooperativity for electrocatalytic reduction and catalytic hydration." (2020). *Electronic Theses and Dissertations*. Paper 4040.
<https://doi.org/10.18297/etd/4040>

This Doctoral Dissertation is brought to you for free and open access by ThinkIR: The University of Louisville's Institutional Repository. It has been accepted for inclusion in Electronic Theses and Dissertations by an authorized administrator of ThinkIR: The University of Louisville's Institutional Repository. This title appears here courtesy of the author, who has retained all other copyrights. For more information, please contact thinkir@louisville.edu.

THE UTILIZATION OF METAL-LIGAND COOPERATIVITY
FOR ELECTROCATALYTIC REDUCTION AND CATALYTIC
HYDRATION

By

Steven P Cronin

B.A. Northern Kentucky University 2012

M.S. University of Louisville 2018

A Dissertation Submitted to the
Faculty of the College of Arts and Sciences

of the University of Louisville in Fulfillment
of the Requirements for the Degree of

Doctor of Philosophy in Chemistry

Department of Chemistry
University of Louisville, KY

December 2020

© 2020 by Steven Patrick Cronin

All Rights Reserved

THE UTILIZATION OF METAL-LIGAND COOPERATIVITY
FOR ELECTROCATALYTIC REDUCTION AND CATALYTIC
HYDRATION

By

Steven P Cronin

B.A. Northern Kentucky University 2012

M.S. University of Louisville 2018

A Dissertation Approved on

10/21/2020

By the following Dissertation Committee

Advisor: Dr. Craig A. Grapperhaus

Dr. Robert M. Buchanan

Dr. Pawel Kozlowski

Dr. Gatum Gupta

For Mom, Dad, Alicia, Loki, and Leelo

ACKNOWLEDGEMENTS

I would first like to thank Professor Craig Grapperhaus for accepting me into his group as well as providing me guidance over the last five and a half years. Professor Grapperhaus has managed to mold me into the scientist I am today. I know to be skeptical of data, and the most important person to prove something to, is myself. He has taught me to not hold tightly onto theories and only follow the ones you have proof for. He additionally has provided me with many opportunities to grow outside of the lab with the talks and conferences he has sent me too. These conferences also allowed me to gain exposure to the broader chemistry community and the intricacies of working in academia. He has been a fantastic mentor for me, and I am forever indebted to him. I am very grateful to have learned so much from not only a fantastic mentor, but human being.

Next I would like to thank Professor Robert Buchanan for his support, mentorship, and advice over the last five and a half years. While Craig was my “mentor” on paper, Dr. Buchanan was just as much as one. I have learned so much from you and our talks. Our talks were always about what can you do to help give support for a mechanism, how to make a catalyst better, and how to really mentor undergraduates. I appreciate all the prompt edits to manuscripts and guidance in helping me develop my writing ability.

I am grateful for my computational collaborators, Professor Pawel Kozlowski, Brady Garabato, Megan Toda, and Abdullah Al Mamun. These people helped me elevate my computational chemistry from an afterthought, to one where there is comfort in discussion of it. I owe much to Brady, as he did a fantastic job of teaching me the basics of

computational work. Megan and Abdullah did a fantastic job of helping me where I got stuck and brought me all the way to where I am at now.

I am extremely grateful for Dr. Mark Mashuta, who solved many crystal structures for me and showed me how to generate valuable crystals. Mark also has been a fantastic friend throughout my PhD. Whether it was watching football, tailgating, getting lunch, discussing computers, among other things, Mark made getting away from the lab fun and educational.

In that same vein I am extremely grateful for Neal Stolowich, who has helped me tremendously in my understanding of NMR. Without his help, basic NMR problem solving techniques would be beyond me. His friendship is also extremely valuable, and he would often accompany Dr. Mashuta and myself on our adventures.

I would like to thank the lab members who came before me and assisted me through my whole PhD. I would especially like to thank Andrew Haddad for showing me how to be a research scientist, making me feel welcome in the Grapperhaus lab, and pretty much teaching me every technique I know. I also would like to specifically thank Caleb Calvary for teaching me enough organic synthesis to get through my PhD.

I would like to thank Professor Gatum Gupta and Professor Josh Spurgeon. Professor Gupta's group had been a great help for finishing odds and ends for publications, as well as his support while serving on my dissertation committee. Professor Spurgeon and his group did a fantastic job with helping me in my understanding of CO₂ reduction reactions.

Finally, I would like to thank Mike, Bonnie, Alicia, and my brothers Scott, Eric and David. You have all been fantastic influences on my life and have showered me with love and support.

ABSTRACT

THE UTILIZATION OF METAL-LIGAND COOPERATIVITY FOR ELECTROCATALYTIC REDUCTION AND CATALYTIC HYDRATION

Steve P. Cronin

10/21/2020

Small molecules are building blocks for developing larger materials. These small molecules could be extremely small, such as hydrogen, or larger such as a nitrile, but their impact on the global economy is massive. This dissertation describes a catalyst for three reactions involving small molecules; 1) the hydrogen evolution reaction, 2) the carbon dioxide reduction reaction, 3) nitrile hydration. The catalyst Zn(DMTH) (DMTH = diacetyl-2-(4-methyl-3-thiosemicarbazone)-3-(2-pyridinehydrazonato)) use “metal-ligand cooperativity” between the Lewis acid Zn(II) metal ion and an uncoordinated Lewis base nitrogen in the ligand framework to activate substrates. The complex has been analyzed via NMR, UV/Vis, single crystal X-ray crystallography, electrochemical methods, XPS and computationally.

Chapter three discusses the ability of Zn(DMTH) and the methylated form Zn(DMTMH) to utilize solution protons to generate H₂. Zn(DMTH) and Zn(DMTMH) have similar turnover frequencies (TOF) of ~7000 s⁻¹, but their overpotential differs by ~700 mV. The overpotential difference is determined to be from both electronic effects,

and proton rearrangement. These differences are supported by control experiments, computational work (DFT), and isolation of valuable intermediates. Chapter four focuses on the ability of Zn(DMTH) to activate CO₂ for reduction to formate. The catalyst has a TOF of ~70 s⁻¹ albeit at a large overpotential (0.9V). The catalyst is also shown to work at lower operating potentials by using an electrochemical hydride (Pt) and a chemical hydride (NaBH₄). Zn(DMTH) operates in an unprecedented mechanism where it utilizes metal-ligand cooperativity to deprotonate a methanol where CO₂ insertion occurs. This ability allows Zn(DMTH) to bind CO₂ directly from air, making it the first CO₂ reduction catalyst that can do this. Chapter five expands upon this idea of metal-ligand cooperativity to activate methanol, by using the same process to activate water. This activation of water is shown by the generation of amides from nitriles. Zn(DMTH) behaves as a nitrile hydration catalyst with a large quantity of nitriles including difficult to hydrate nitriles. Optimization reactions occurred with acetonitrile with a TOF of almost 50 h⁻¹ at 0°C. Analysis of thermodynamic parameters indicate a mechanism with contributions from multiple steps.

TABLE OF CONTENTS

Acknowledgements.....	iv
Abstract.....	vii
List of Figures.....	xvi
List of Schemes.....	xxi
List of Tables.....	xxii
Chapter I Introduction.....	1
1.1 Lay Summary.....	1
1.2 Scope of Dissertation.....	2
1.3 Small Molecule Activation.....	4
1.3.1 Hydrogen.....	7
1.3.2 Carbon Dioxide.....	9
1.3.3 Nitriles.....	12
1.4 Metal-Ligand Cooperativity.....	13
1.5 Frustrated Lewis Pairs.....	17
1.6 Prior Work on Zn(DMTH).....	18
Chapter II Experimental Methods.....	20
2.1 Materials.....	20
2.2 Physical Methods.....	21

2.3 Precursor Synthesis.....	22
2.3.1 Synthesis of Diacetyl-N-4-methyl thiosemicarbazone	22
2.4 Ligand Synthesis.....	23
2.4.1 Synthesis of Diacetyl-2-(4-methyl-3-thiosemicarbazide)-3-(2-hydrazone-N-methy-pyridine) (H ₂ DMTMH)	23
2.5 Catalysts Syntheses.....	24
2.5.1 Synthesis of ZnDMTH (MeOH).....	24
2.5.2 Synthesis of Zn Diacetyl-2-(4-methyl-3-thiosemicarbazone)-3-(2-hydrazone-N-methy-pyridine) (ZnDMTMH)	25
2.5.3 Synthesis of Zn(HDMTH)(OAc).....	26
2.5.4 Synthesis of Zn(HDMTH)(CO ₃ CH ₃).....	27
2.6 General Electrochemical Techniques	28
2.6.1 Preparation of Electrodes	29
2.6.2 Maintenance of Electrodes.....	30
2.6.3 Purification of Supporting Electrolyte	31
2.6.4 Cyclic Voltammetry Introduction	31
2.6.5 Simple Cyclic Voltammetry for Identification of Potentials.	32
2.6.6 Cyclic Voltammetry for Electrocatalysis.....	33
2.6.7 Reaction Order Experiments.....	33
2.6.8 Controlled Potential Coulometry Experiments	34

2.6.9 Soak Tests	35
2.6.10 Cycle Dip Tests.....	36
2.6.11 CPC Dip Tests.....	36
2.6.12 Square Wave Voltammetry	36
2.6.13 Resistance Measurements	37
2.7 Computational Methods.....	37
2.8 Analysis of Kinetic Data - General.....	38
2.8.1 Calculation of Turnover Frequency (TOF).....	38
2.8.2 Calculation of Faradaic Efficiency	38
2.8.3 Determination of Overpotential for Catalysts.....	39
2.9 Analysis of Kinetic Data – Chapter 3	40
2.9.1 Calculations of pKs and Potentials via Computational Methods.....	40
2.9.2 Determination of Reaction Orders via Electrochemical Methods for HER	41
2.10 Analysis of Kinetic Data – Chapter 4	41
2.10.1 Determination of Reaction Orders via Electrochemical Methods for CO ₂ RR	41
2.10.2 Calculation of Binding Constants	42
Chapter III Utilizing Charge effects and minimizing intramolecular proton rearrangement to improve overpotential of a thiosemicarbazonato Zinc HER catalyst	43
3.1 Background.....	43

3.2 Synthesis and Characterization	48
3.2.1 General Synthesis, NMR, FT-IR, and UV/Vis of Compounds	48
3.2.2 Structural Determination.....	52
3.2.3 Electrochemical Characterization	53
3.3 Homogenous Catalytic Hydrogen Evolution	55
3.3.1 Cyclic Voltammetry.....	55
3.4 Control Experiments	59
3.4.1 Soak Test.....	59
3.4.2 Post CV Dip-test	60
3.4.3 Post Electrolysis Dip-test.....	61
3.4.4 XPS Film Analysis.....	63
3.4.5 Post Electrolysis Rinse Test.....	64
3.5 Density Functional Theory Investigations	64
3.6 Proposed HER Mechanism	69
3.7 Conclusion	70
3.8 Experimental Specific to Chapter 3	72
3.8.1 Crystallographic Studies	72
3.8.2 Electrochemical Methods.....	74
3.8.3 Catalysis Control Experiments	76
3.8.4 XPS Experiments	77

3.8.5 Resistance Measurements	78
3.8.6 Titration Experiments	79
3.8.7 NMR Studies.....	79
3.8.8 Computation Methods.....	79
Chapter IV Exploiting Metal-Ligand Cooperativity to sequester, activate, and Reduce atmospheric carbon dioxide with a neutral zinc complex.....	81
4.1 Background.....	81
4.2 Mechanism.....	84
4.3 CO ₂ Binding	85
4.3.1 UV/Vis Spectroscopy.....	86
4.3.2 Electrochemical Characterization	87
4.3.3 Single Crystal X-Ray Diffraction	88
4.3.4 FT-IR.....	88
4.4 Reactions of Zn(HDMTH)(CO ₃ CH ₃).....	89
4.4.1 Reactions with Chemical Hydride	89
4.4.2 Reactions with Pt Working Electrode.....	90
Run 1 is in black, Run 2 in blue, and the blank in red.	91
4.4.4 Summary of All Reactions.....	96
4.5 Conclusions.....	96
4.6 Experimental Specific to Chapter 4.	97

4.6.1 Materials and Methods.....	97
4.6.2 Physical Methods.....	98
4.6.3 Electrochemical Methods.....	98
4.6.4 Reaction of Zn(DMTH) with CO ₂ and NaBH ₄ in MeOH.....	101
Chapter V Mechanistic Investigations of Nitrile Hydration Catalyzed by Zn(DMTH) under Ambient Conditions.....	102
5.1 Background.....	102
5.2 Preliminary Nitrile Hydration Studies.....	105
5.3 Optimization of Acetonitrile Hydration.....	106
5.4 Temperature Effects.....	111
5.5 Scope of Nitrile Hydration.....	112
5.6 Nitrile Hydration Mechanism.....	116
5.7 Conclusion.....	119
5.8 Experimental Specific to Chapter 5.....	119
5.8.1 UV/Vis Titration.....	119
5.8.2 Calibration Curves.....	120
5.8.3 General Hydration Procedure.....	120
5.8.4 Varying Water Procedure.....	120
5.8.5 Varying Acetonitrile:catalyst Procedure.....	121
5.8.6 Varying %Methanol:Acetonitrile Procedure.....	121

5.8.7 Varying Temperature Procedure.....	121
5.8.8 Varying Substrate (other nitriles) Procedure	122
Chapter VI Conclusions and Future directions.....	123
6.1 Summary	123
6.1 Improving HER Overpotential.....	123
6.2 Metal-Ligand Cooperativity to Sequester, Activate, and Reduce Carbon Dioxide	125
6.3 Metal-Ligand Cooperativity for Nitrile Hydration	127
References.....	129
Appendix A Supplemental Figures.....	136
A.1 Chapter 2 Figures and Tables.....	136
A.2 Chapter 3 Figures and Tables.....	148
A.3 Chapter 4 Figures and Tables.....	179
A.4 Chapter 5 Figures and Tables.....	208
Appendix B Computational Coordinates	219
Curriculum Vita	266

LIST OF FIGURES

Figure I-1. A. Depiction of Zn(DMTH) and the charge locations on the neutral molecule. B. Depiction of the FLP like ability of the zinc and noncoordinating nitrogen.....	3
Figure I-2. Sacconi-type iron complex drawn with B in the linker. ¹⁴	6
Figure I-3. Depiction of the Ishitani Re(bipy)(CO) ₃ (C ₆ H ₁₄ NO ₃) complex.....	7
Figure 1-4. A. CO ₂ emissions over time. ²⁴ B. Global energy usage expectations via EIA. ²⁵	10
Figure I-5. Various oxidation states of Ni bis(stilbenedithiolate). In all cases the nickel center can be assigned as a Ni(II) atom.	14
Figure I-6. A. Mechanism of Cp*Ir(^t BA ^F Ph). B. Mechanism of Cu(II) (2,2'-thiobis(2,4- di-tert-butylphenol)) ₂ , C. Mechanism of ZnATSM (only one depicted although other options exist, see reference) ⁴⁵ D. Mechanism of (P ^h I ₂ P ²⁻)Al(THF)Cl.....	16
Figure I-7. A. Depiction of a Lewis pair. B. Depiction of a frustrated Lewis pair. C. Depiction of the lone pair and acceptors in a frustrated Lewis pair.	17
Figure I-8. Comparison of Zn(DMTH), ATSM and other ATSM derivatives.....	19
Figure II-1. Depiction of crystallographic setup for Zn(HDMTH)(CO ₃ CH ₃).....	27
Figure II-2. Depiction of the polishing pattern for the working electrode.....	30

Figure III-1. A. Metal-centered pathway for HER. B. Ligand-centered pathway for HER.	46
Figure III-2. DuBois catalyst.	46
Figure III-3. CECE mechanism of Zn(ATSM).	48
Scheme III-2. Comparison of BTSC complexes with Zn(DMTH).	48
Figure III-4. UV/visible spectra in acetonitrile of 1 – 3 titrated with acetic acid.	52
Figure III-5. ORTEP ⁹² representations of Zn(HDMTH)(OAc) and Zn(DMTMH)I.	53
Figure III-6. A. CVs of 1.0 mM 1 (black), 2 (blue), and 3 (red) in acetonitrile containing 0.1 M Bu ₄ NPF ₆ as supporting electrolyte.	55
Figure III-7. CVs recorded in acetonitrile at a scan rate of 0.2 V/s in 0.1 M Bu ₄ NPF ₆	57
Figure III-8. Plots of i_c/i_p for ZnDMTH.	58
3.3.2 Controlled Potential Coulometry	58
Figure III-9. Controlled potential coulometry for two hours for 1 at an applied potential of 2.60 V vs. Ag/AgCl (A) and 3 at an applied potential of -1.80 V vs. Ag/AgCl.	59
Figure III-10. Cycle test CVs.	61
Figure III-11. Post CPC CVs.	63
Figure III-12. Lowest energy calculated structures.	67
Protonation sites circled in red for A. 2, B. 2-H ⁺ , C. 2-H, and D. 2-H ₂ ⁺	67
Figure III-13. Three lowest energy calculated structures of 2-H ₂	68

Protonation sites circled in red.....	68
Figure III-14. Relative values of $E_{1/2}$ and $E_{cat/2}$ for 2 and 3'	72
Figure IV-1. A. Half-reactions for the two-electron reduction of CO_2 . B. Generalized pathways for catalytic reduction of CO_2 by two electrons.	83
Figure IV-2. A. Catalytic pathway for the reduction of CO_2 to HCO_2^- by $Zn(DMTH)$. The source of the hydride (H^-) can be chemical or electrochemical. All non-coordinating lone-pair electrons are shown. B. Representation of $Zn(DMTH)$ highlighting the frustrated Lewis pair between the non-coordinating Lewis base (red) and Lewis acid (blue). Formal charges are shown in green. C. Addition of methanol across the frustrated Lewis pair via metal-ligand cooperativity	85
Figure IV-3. A. Photograph of a 3 mM solution of $Zn(DMTH)$ in methanol under ambient conditions. B. Photograph of a 3 mM solution of $Zn(DMTH)$ in methanol, while bubbling with CO_2 . C. UV-visible spectra of a 0.1 mM solution of $Zn(DMTH)$ in methanol under varying concentrations of CO_2 gas. D. UV-visible spectra of a 0.1 mM solution of $Zn(DMTH)$ in methanol before and after bubbling the solution with untreated air from the laboratory using an air pump.	87
Figure IV-4. A. Comparison CV of $Zn(DMTH)$ (black) and $Zn(DMTH)$ under CO_2 atmosphere (blue dashed) in methanol. B. i_{cat} vs [cat] peak at -1.30 V at a scan rate of 200 mV/s. C. i_{cat} vs [cat] peak at -1.75 V at a scan rate of 200 mV/s.	88
Figure IV-5. A. ORTEP ⁹² representation of $[Zn(HDMTH)(CO_3CH_3)]$. B. FT-IR of $[Zn(HDMTH)(CO_3CH_3)]$ from single crystals.	89

Figure IV-6. Controlled potential coulometry of Zn(DMTH) in the presence of CO ₂ and 10 mM acetic acid in methanol with a Pt working electrode.....	91
4.4.3 Reactions with Glassy Carbon Electrode.....	92
Figure IV-7. Cyclic voltammograms of Zn(DMTH) showing reactivity with CO ₂ and acetic acid.....	93
Figure IV-8. Controlled potential coulometry for Zn(DMTH) in the presence of 10 mM acetic acid.....	95
Figure IV-9. Turnovers of formate as a function of [CH ₃ COOH].....	95
Figure IV-10. Depiction of dilution method for obtaining variable concentration of CO ₂	98
Figure V-1. The active site for Fe-NHase.....	103
Figure V-2. The [PtH(PMe ₂ O) ₂ H(PMe ₂ OH)] catalyst and catalytic cycle.....	104
Figure V-3. UV/visible spectra of 0.1 mM Zn(DMTH) in acetonitrile (black) with additions of 0.55 (blue) to 3.3 mM (green) DI H ₂ O.	106
Figure V-4. A. Gas Chromatography for hydration of acetonitrile after 1 h reaction under 12.5% v/v water (black) and 11.0% v/v (blue). B. Corresponding mass-spectrum of the peak at RT 2.4 min.....	107
Figure V-5. Turnover as a function of %V/V water.	108
Figure V-6. Turnover as a function of mmol acetonitrile.....	109
Figure V-7. TOF vs % of solution that is CH ₃ CN.....	110
Figure V-8. TON vs time for acetamide over 30 days of reaction time.	111

Figure V-9. TOF as a function of reaction temperature.....	112
Figure V-10. Proposed catalytic cycle for the hydration of nitriles by Zn(DMTH).....	118
Figure V-11. Depiction of proton shuttling for Zn(DMTH)(H ₂ O) to Zn(HDMTH)(OH)	118

LIST OF SCHEMES

Scheme I-1. The water gas shift reaction.....	8
Scheme I-2. Solar powered hydrogen production from water.....	9
Scheme I-3. Pathway for environmental cleanup of nitriles.....	13
Scheme I-4. The reaction of Pt(IV) (^t BuMe ₂ nacnac)PtMe ₃ reacting with O ₂	17
Scheme II-1. Synthesis of diacetyl-N-4-methyl-thiosemicarbazone.	22
Scheme II-2. Synthesis of diacetyl-2-(4-methyl-3-thiosemicarbazide)-3-(2-hydrazone-N-methyl-pyridine) (H ₂ DMTMH).....	23
Scheme II-3. Synthesis of ZnDMTH (MeOH).	24
Scheme II-4. Synthesis of Zn(HDMTH)I method A.	25
Scheme II-5. Synthesis of Zn(HDMTH)I method B.	26
Scheme III-1 A. Water Gas Shift Reaction. B. Methane Gas Reformation Reaction C. Electrocatalytic Production of Hydrogen.....	44
Scheme III-3. Synthetic routes for compounds 1 – 3.....	49
Scheme III-4. Proposed HER mechanism.	70

LIST OF TABLES

Table I-1. Standard reduction potentials of various CO ₂ reduction processes. ²⁷ Where E° ' is the standard reduction potential at pH 7, and E° is the standard reduction potential under acidic conditions.	11
Table IV-1. Compilation of average faradaic efficiencies for the reduction of carbon dioxide to formate by Zn(DMTH) under various CPC conditions. ^a	96
Table V-1. Compilation of Nitriles and TOF.....	115

CHAPTER I

INTRODUCTION

1.1 Lay Summary

This dissertation describes the activity of a unique zinc catalyst with applications in renewable energy, waste cleanup, and raw material generation. All chemical reactions have an energetic hill that must be overcome for the reaction to occur. A catalyst lowers the hill, which can then allow the reaction to happen under less energetic conditions. The catalyst in this dissertation employs “metal-ligand cooperativity” to activate substrate molecules for conversion to product. The cooperativity results from neighboring Lewis acid “acceptor” and Lewis base “donor” sites. The combination of these two features in close proximity promotes reactivity by either splitting an individual molecule apart or bringing two molecules together to interact. The catalyst in this dissertation has been investigated for three specific reactions: hydrogen evolution, carbon dioxide reduction, nitrile hydration. Hydrogen is an energy carrier and a potential alternative to fossil fuels. Hydrogen is also an important feedstock for industrial processes, such as hydrogenation. Industrially, most hydrogen is produced from fossil fuels, but catalysts like the one in this dissertation can use electricity to produce hydrogen by splitting water. In addition, our catalyst can capture carbon dioxide and help convert it to useful products, like formate. Formate can act as a precursor to making larger carbon containing compounds such as plastics and fuels, or can be a useful fuel source itself as the acid form, formic acid. Traditionally, carbon dioxide capture and reduction required expensive catalysts. Our

catalyst incorporates an earth-abundant metal in an inexpensive ligand framework to capture and reduce carbon dioxide in a single step. Lastly, the catalyst in this dissertation can hydrate nitriles. Nitriles are useful as solvents and are precursor chemicals for various products such as polyacrylamide, which is used as a stabilizer in commercial products like makeup and lotions. While nitriles are useful precursors and solvents, release of them into the environment can be toxic to the wildlife and humans, while also disrupting other vitally important ecosystem components. Additionally, cleanup of these spills can be expensive and cause irreparable damage to the ecosystem. Our catalyst is capable hydrating nitriles at neutral pH and room temperature. This could lead to an inexpensive catalyst that can directly solve some of these issues with waste, waste cleanup, and raw material generation.

1.2 Scope of Dissertation

This dissertation describes catalytic applications of the metal complex (diacetyl-2-(4-methyl-3-thiosemicarbazone)-3-(2-pyridinehydrazonato)zinc(II), Zn(DMTH), Figure 1-1A. The complex employs metal-ligand cooperativity for the activation of small molecules. Specifically, a non-coordinating Lewis base of the ligand framework is positioned near the Lewis acid metal center as shown in Figure 1-1B. The interaction is similar to a frustrated Lewis Pair (FLP). This first chapter provides an overall introduction to the dissertation. It includes a brief history of FLPs and FLP-like systems, their significance in the activation of small molecules, and the relevant history that lead to our study of Zn(DMTH). Some principles of catalyst design are presented to give perspective on why this catalyst was chosen and to show how this one complex is a potential building block for other complexes.

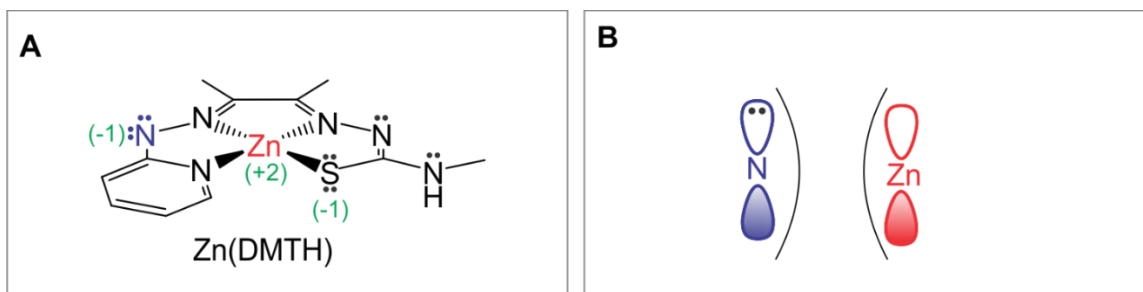


Figure I-1. A. Depiction of Zn(DMTH) and the charge locations on the neutral molecule.

B. Depiction of the FLP like ability of the zinc and noncoordinating nitrogen.

Chapter II includes general experimental details and background on the methodology used in the dissertation. It includes synthetic procedures, details of general characterization techniques, and the methods used for catalyst evaluation. It also describes the electrochemical techniques and computational methodology employed in this work.

Chapters III – V each detail the catalytic activity of Zn(DMTH) for a different reaction. The chapters begin with a specific introduction of the reaction, its importance, and other catalyst for the reaction in the literature. Chapter III focuses on Zn(DMTH) as an electrocatalyst for the hydrogen evolution reaction (HER). It includes electrochemical experiments, isolation of catalytically important intermediates, and computational methods. In addition, it includes the synthesis, characterization, and evaluation of the N-methylated derivative, Zn(DMTMH) which shows a significant drop in overpotential while maintaining HER activity. Chapter IV describes the ability of the Zn(DMTH) complex to capture, activate, and reduce CO₂. Chemical and electrochemical characterization techniques, characterization of catalytically important intermediates, and chemical and electrochemical reduction techniques are included in this chapter. Chapter V reports the catalytic activity of Zn(DMTH) for nitrile hydration, a non-redox process. The chapter

includes important aspects of the catalyst, isolation of intermediates, GC/MS calibration, methods, results kinetic investigations, investigations on the effect of temperature, and substrate scope are also included. The important part of Zn(DMTH) is that the catalyst works at pH neutral conditions.

The dissertation concludes with Chapter VI, which provides a summary and future directions. This chapter begins with a discussion of ligand design, its importance, and possible modifications to the DMTH ligand for the activation of other small molecules or to increase activity. In addition, MLC is discussed in depth, and the need to examine other metals, as they may be active for other reactions. Finally, a brief overview of future directions and the lessons that have been learned from this complex can be found directly in this chapter.

1.3 Small Molecule Activation

Small molecules can be defined as any compound containing five or fewer elements, with a total molecular weight less than 90 g/mol.¹ Examples of small molecules include CO₂, SO₂, N₂, CH₄, and O₂. While some small molecules, such as N₂ and O₂, are beneficial in the quantities that exist in our atmosphere, others have adverse environmental impacts. For example, SO₂ is the primary source of acid rain and concentration of 0.2 ppm in the atmosphere.² The EPA estimated that approximately 0.97 million metric tons of acid rain fell in 2019.³ Another example is CO₂, which has been implicated in global warming and climate change. Although the degree of its impact remains in debate,⁴ the current atmospheric concentration of carbon dioxide (CO₂) is in excess of 415 ppm are more than twice the 1900 level of 200 ppm.⁵⁻⁶

For the activation of small molecules several challenges exist.⁷ For most small molecules, the biggest challenge is that they are either linear or saturated molecules. An example of this is CO₂. The C=O bond is polar in nature which would allow for easy modification by a nucleophilic attack on the C or electrophilic attack on the O. However the overall molecule is linear which makes it difficult to modify either the C or the O in the C=O bond.⁸ An activated form of CO₂, bicarbonate and methylcarbonate, could allow for either nucleophilic attack on the C or electrophilic attack, however these ligands do not often readily bind to metal atoms. Another difficulty in small molecule activation and reduction is lack of polarity, even if the molecule is activated. An example of this is N₂. N₂ is linear molecule, however due to the same electronegativity of each nitrogen atom, there is no dipole, making it more difficult to reduce. Finally, the low solubility of these small molecules in organic solvents or water creates for large challenges. Every gas has its own Henry's constant, and therefore only a fraction of the total gas inlet will be dissolved in solution for activation.

These challenges have been addressed by a large quantity of metal containing and a smaller amount of metal-free catalysts, but more work is still needed for the optimization of these processes. These catalysts can be electrocatalysts or traditional catalysts. For instance, the easiest way to activate CO₂ from being a linear species to an active species is by the use of metal hydroxide species (MOH).⁹ By use of these species, almost all dissolved CO₂ is converted directly to bicarbonate. While bicarbonate is an activated form of CO₂, as it is now trigonal planar, the carbon is not easily reduced at electrode surfaces. There are a small number of non-electrocatalysts that can convert bicarbonate directly to formate, but transitions requiring the transfer of more than two electrons have yet to be shown.¹⁰ Other

catalysts such as the $M(\text{bipy})(\text{CO})_3\text{X}$ ($\text{bipy} = 2,2'$ -bipyridine),¹¹⁻¹² can bind a dissolved CO_2 , and activate it by having it either O-bound or C-bound. This binding as an O-bound or C-bound species can influence product formation. These systems however operate at large overpotentials but are durable and have good selectivity for specific products that are not “dead ends”, bicarbonate and carbonate like species.

One way to deal with the lack of polarity issue is to use metals that are polarizable or ligands that allow the metal center to change from low spin to high spin. The most popular of these is iron, as it is earth abundant and does allow for changes in spin. The Sacconi-type iron complex, $\text{P}_3^{\text{E}}\text{Fe}$ (P_3^{E} is a phosphine donor bonded to a center atom through an ortho-phenylene linker $\text{E} = \text{B}, \text{C}, \text{Si}$) is a prototypical example for nitrogen activation, Figure I-2.¹³ The iron center that is supported by other portions of the ligand, allows for a state in which a hydride is “parked” in the coordination sphere of the iron and a nitrogen of the N_2 , has a change in polarization. This polarization allows for hydride attacks to generate ammonia and hydrazine.

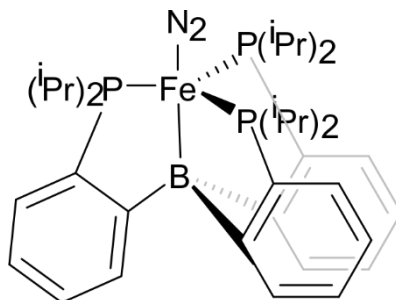


Figure I-2. Sacconi-type iron complex drawn with B in the linker.¹⁴

Due to the majority of redox chemistry occurring in solution or at the solution interface, regardless of the catalyst being heterogenous or homogenous, the catalysts are only able to complete the reactions at the dissolved concentration of small molecules. There

are two direct ways that researchers have circumvented this issue. Ishitani and coworkers developed a $\text{Re}(\text{bipy})(\text{CO})_3(\text{C}_6\text{H}_{14}\text{NO}_3)$ ($\text{C}_6\text{H}_{14}\text{NO}_3 = \text{triethanolamine}$) complex that utilizes the bound triethanolamine, to capture the CO_2 , Figure I-3.¹⁵⁻¹⁶ By capturing of CO_2 for activation, the complex can work at lower pressures of CO_2 , and work around the concentration problem. Another solution for this is to use single pass cells, due to their small volume, and higher surface to volume ratios, the amount dissolved comes into higher contact with the catalysts, generating higher product formations and faradaic yields.¹⁷

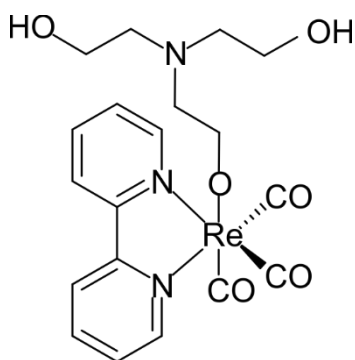


Figure I-3. Depiction of the Ishitani $\text{Re}(\text{bipy})(\text{CO})_3(\text{C}_6\text{H}_{14}\text{NO}_3)$ complex.

This dissertation focuses on the activation of three small molecules; H_2 , CO_2 , and water for the hydration of nitriles. A brief overview of the significance of each molecule is provided below. Detailed introductions, including catalytic activation strategies, for each molecule are provided in the individual chapters.

1.3.1 Hydrogen

Hydrogen has a large number of uses for the developed world. Currently the production of hydrogen to meet these needs largely proceeds via the water-gas shift (WGS) reaction, Scheme I-1.¹⁸ The WGS reaction utilizes carbon monoxide and water to generate carbon dioxide and hydrogen. The WGS reaction is an important reaction as the Haber-

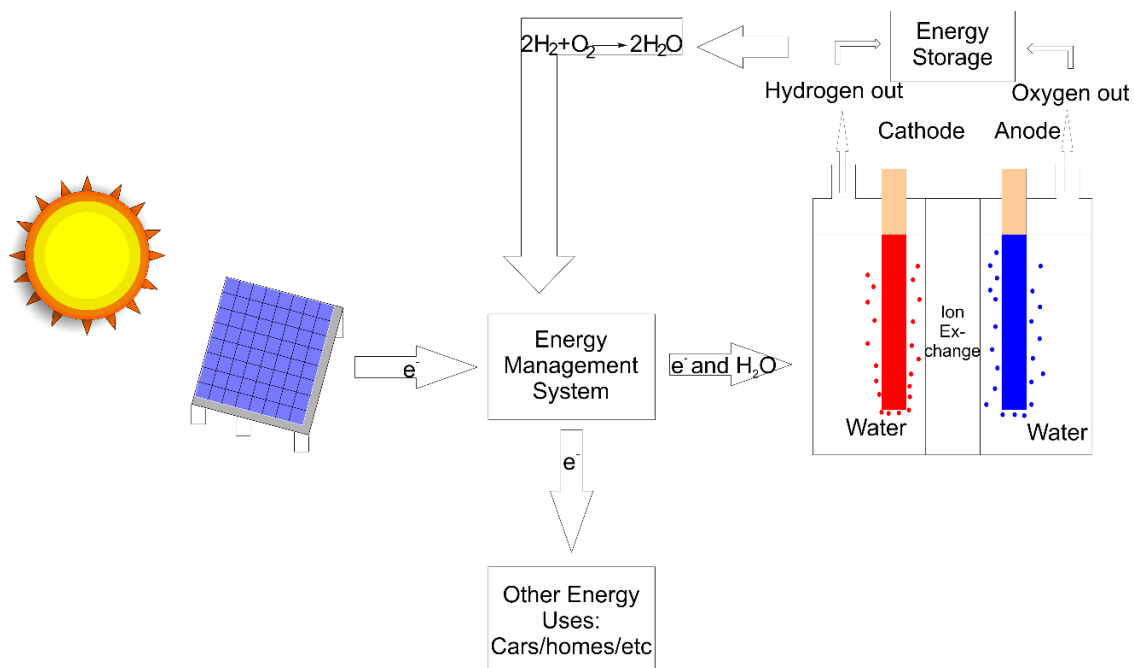
Bosch process utilizes hydrogen and nitrogen for the direct synthesis of ammonia. As a result, the WGS has been combined to the direct gasification of coal, which releases more CO₂ directly into the atmosphere. This process accounts directly for 54% of all hydrogen use.¹⁹ Furthermore 35% of hydrogen use is for hydrogenation and other industrial applications. Reliable and practical renewable sources of hydrogen are far and few between, as nearly all industrial hydrogen is produced directly from fossil fuels.

Scheme I-1. The water gas shift reaction.



Additionally, hydrogen is a promising fuel source. This is because hydrogen can be derived from the electrolysis of water, and the combustion of hydrogen directly would yield water as a product, Scheme I-2. This would be a greener approach as it would allow for a carbon-free fuel source, and it is the simplest product to generate. However, hydrogen does have some challenges when being implemented as a fuel source. Most notably is that hydrogen is a gas, and storage would be one major obstacle.²⁰ Additionally, water is a greenhouse gas as well.²¹ But the use of water as the source of protons, would lead to a “water neutral” cycle.

Scheme I-2. Solar powered hydrogen production from water.



1.3.2 Carbon Dioxide

As mentioned earlier in 1.3, increasing CO_2 concentration in the atmosphere is a major component of climate change and has direct effects on ocean acidification. The change of CO_2 emissions from approximately 799,000 BC to today is shown in Figure I-4A. What is to note is that there is a sharp increase starting at the year 1950. The CO_2 released into the atmosphere comes primarily from two major sources outside of respiration; the burning of fossil fuels and the generation of concrete.²² The first source of CO_2 , burning fossil fuels, is obvious to see where each metric ton of CO_2 is generated. Whether it is directly for use in travel, generation of electricity, or as simple as generation of heat, fossil fuels are a huge component of human life. The second source, concrete, is a large polluter that should be curtailed.²³ Concrete is usually generated from limestone, $CaCO_3$, and is heated until the calcium carbonate is decarbonated to generate calcium

oxide, which later can have water added prior to pouring.. This means at the bare minimum, for one ton of CaO to be produced, approximately half a ton of CO₂ must be released. Additionally, these processes must utilize large quantities of heat, which leads to larger CO₂ emissions.

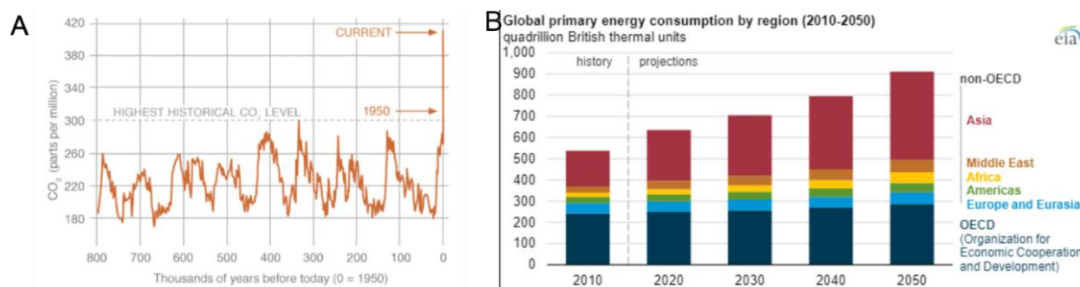


Figure 1-4. A. CO₂ emissions over time.²⁴ **B.** Global energy usage expectations via EIA.²⁵

According to the U.S. Energy Information Administration (EIA), a 50% increase in world energy usage is expected by 2050.²⁶ This large growth is expected to be primarily involve Asia, Figure I-4b. Growing energy usage highlights two major concerns associated with climate change. First, how does the already “developed” world wean its dependence on fossil fuels and begin generating alternative carbon neutral sources of energy that will not require trillions of dollars in infrastructure changes? Second, how does the developing world, Asia in particular, accommodate the massive increase in energy needs without burning fossil fuels.

While CO₂ is associated with a large amount of negative effects, it can be used as a feedstock to generate other large carbon containing compounds, including but not limited to polymers and fuels. These compounds are more attractive immediately than that of hydrogen generated from hydrogen evolution; because existing infrastructure can utilize

the compounds generated from CO₂ as a feedstock. Additionally, CO₂ in theory requires less energy to reduce than that of hydrogen, table I-1. While lower voltages are required to reduce CO₂, as mentioned earlier in section 1.3 the compound is linear. Because the compound is linear, it becomes difficult to add protons to the carbon center or the oxygen terminal atoms. Additionally, and more importantly, it is difficult to have two carbon dioxides bent in such a way that a C-C coupling reaction can occur and the large carbon containing fuels and polymers can be accessed.

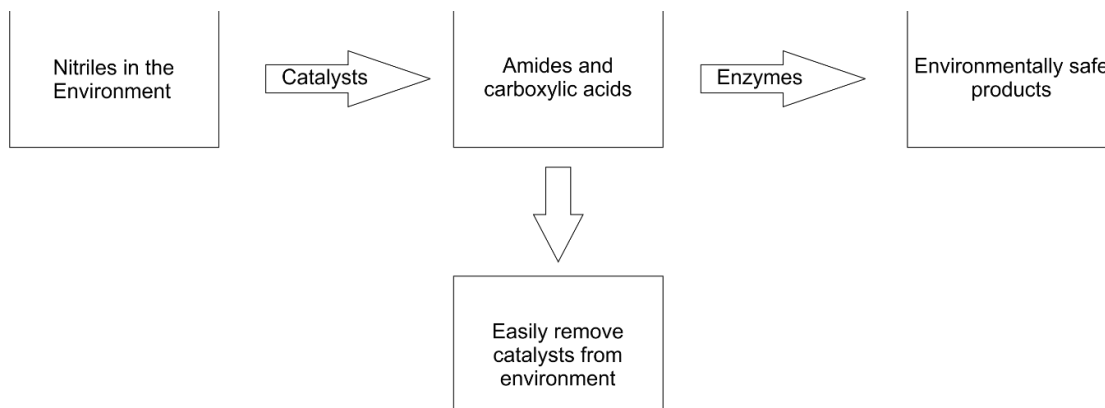
Table I-1. Standard reduction potentials of various CO ₂ reduction processes. ²⁷ Where E°' is the standard reduction potential at pH 7, and E° is the standard reduction potential under acidic conditions.		
Reaction	E°'	E°
$\text{CO}_2(\text{aq}) + \text{e}^- \rightarrow \text{CO}_2^{\cdot-}(\text{aq})$	-1.9 V	-1.9 V
$\text{CO}_2(\text{g}) + 2\text{H}^+ + 2\text{e}^- \rightarrow \text{CO}(\text{g}) + \text{H}_2\text{O}$	-0.52 V	-0.12 V
$\text{CO}_2(\text{g}) + \text{H}^+ + 2\text{e}^- \rightarrow \text{HCO}_2^-(\text{aq})$	-0.43 V	-0.11 V
$\text{CO}_2(\text{g}) + 4\text{H}^+ + 4\text{e}^- \rightarrow \text{HCHO}(\text{aq}) + \text{H}_2\text{O}$	-0.51 V	-0.14 V
$\text{CO}_2(\text{g}) + 6\text{H}^+ + 6\text{e}^- \rightarrow \text{CH}_3\text{OH}(\text{aq}) + \text{H}_2\text{O}$	-0.38 V	-0.01 V
$\text{CO}_2(\text{g}) + 8\text{H}^+ + 8\text{e}^- \rightarrow \text{CH}_4(\text{g}) + 2\text{H}_2\text{O}$	-0.24 V	+0.15 V
$2\text{H}^+ + 2\text{e}^- \rightarrow \text{H}_2$	-0.41 V	0 V

1.3.3 Nitriles

Nitriles (RCNs) are industrially very important as solvents and as precursors. Acrylamide which is produced from acrylonitrile, is produced on a scale of over 200 metric tons.²⁸ These amides have been often used to make things such as polyacrylamide, which has uses such as water treatment, screen printing, papermaking, aid in oil recovery, toys and used in PAGE, a biological technique for the electrophoresis of proteins.²⁹⁻³⁰ Industrially acrylamide is hydrated using Nitrile Hydratase (NHase). The bacteria that contain this enzyme are valued because they operate at pH neutral, 20-40° C, and do not cause further hydrolysis to carboxylic acids.³¹

While nitriles are useful industrial solvents, they can be problematic as industrial waste.³² The cyano-groups can be absorbed easily by the mucous membrane of the respiratory tract, and react with methemoglobin in the bloodstream. Additionally, these compounds can disrupt the process of cellular respiration and can effectively behave as a rapidly acting poison.³³ In 2014, Kang and Shin determined that in the gum river alone there was approximately 1 µg/L of nitrile containing compounds including HCN.³⁴ In 2004 Giurtiati *et al* found Italy contained approximately 5 µg/L and Frizzarian and Rocha found Brazil contained approximately 25-50 µg/L in environmental samples.³⁵⁻³⁶ One remedy is to hydrate the nitriles to an amide or further hydrolyze the amide to a carboxylic acid, which have less environmental impact than that of the nitriles, Scheme I-3. However, this needs to be done at pH neutral and ambient conditions as to not affect the wildlife in the area.

Scheme I-3. Pathway for environmental cleanup of nitriles.



1.4 Metal-Ligand Cooperativity

The concept of metal-ligand-cooperativity (MLC) has its origins in the seminal work of Jørgensen in 1966 that addressed the confusion related to oxidation state assignments for complexes with certain ligands.³⁷ This led to ligands being termed either as “innocent” or “non-innocent” depending on the ability for the oxidation states of their complexes to be defined. An innocent ligand is defined as any ligand that directly allows for the identification of the oxidation state of the central atom. An example is the carbonyl ligand (CO), which always acts as a 2 electron back bonding ligand, in monometallic species. However, the CO ligand does not alter the charge on the metal center, and thus is considered innocent. A non-innocent ligand, on the other hand, results in various oxidation states for the metal center and thus can be considered ambiguous. An example is dithiolenes such as bis(stilbenedithiolate) Ni, which exists with the ligand charge states of 0, -1, and -2, Figure I-5.³⁸ Non-innocent ligands have been exploited in the development of catalysts.³⁹ The benefit of this is the ligand can cooperate with the metal in a synergistic manner that helps to facilitate the chemical processes. This synergy can often be referred to as a subset

of metal-ligand cooperativity. As described by Milstein and coworkers in a 2015 review,⁴⁰ metal-ligand cooperativity includes:

1. Both the metal and ligand participate in the bond cleavage or bond formation steps.
2. Both the metal and the ligand are chemically modified during bond activation.
3. The coordination mode of the cooperative ligand undergoes significant changes in the first coordination sphere as a result of bond activation.
4. Systems with redox non-innocent ligands, where the ligand participates only in transferring electrons to or from the metal but not in the bond cleavage or formation steps.
5. Hemilabile ligands whose main function is to create a coordinative unsaturation at the metal center, while bond activation takes place primarily at the metal surface.
6. Metal and ligand setups that involve only the second coordination sphere.

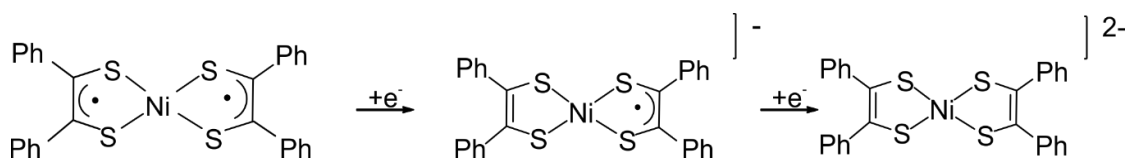


Figure I-5. Various oxidation states of Ni bis(stilbenedithiolate). In all cases the nickel center can be assigned as a Ni(II) atom.

Redox non-innocence can have a variety of effects on catalysis, Figure I-6. First the non-innocent ligands can modify the Lewis acidity of a metal. An example of this was shown by Rauchfuss and coworkers in the $\text{Cp}^*\text{Ir}(\text{}^t\text{BA}^{\text{F}}\text{Ph})$ complex, where $\text{H}_2\text{}^t\text{BA}^{\text{F}}\text{Ph}$ is 2-(2-trifluoromethyl)anilino-4,6-di-tert-butylphenol. This catalyst activates H_2 in a redox-switchable manner, Figure I-6A.⁴¹ Oxidation of the ligand generates a ligand radical, which in turn tunes the acidity of the Ir metal in such a way that it can then bind the H_2 and

generate H^+ as a product using a sacrificial oxidant. A second way redox non-innocent ligands can affect catalysis is through them behaving as electron reservoirs. A common example of this is the 2,6-diiminepyridine ligand, and the iron complex of it, Figure I-6B. This iron(II) complex delocalizes the oxidative processes required to do a [2 + 2] cycloaddition across the 2,6-diiminepyridine ligand.⁴²⁻⁴³ The third way in which redox non-innocent ligands can be used is as a part of the bond-activation process. A common alcohol to aldehyde oxidation catalyst, the dinuclear Cu(II) (2,2'-thiobis(2,4-di-tert-butylphenol))₂, can also form diols from secondary alcohols, Figure I-6C.⁴⁴ In this catalyst, the proximal oxygens deprotonate the alcohols, which allow for the diol formation reaction. Finally, the ligand itself can conduct all the chemistry. In the case of Zn(ATSM)⁴⁵ and (PhI₂P²⁻)Al(THF)Cl⁴⁶ reported by Grapperhaus and coworkers and Berben and coworkers, respectively, all of the hydrogen are produced via the ligand as opposed to via the metal, Figure I-6D.

This concept of cooperation between the ligand and metal is not limited to inorganic catalytic systems. They can also be found directly in active sites of metalloenzymes. Galactose oxidase and hydrogenase are two examples of metalloenzymes that utilize non-innocent ligands as a way to activate small molecules. Galactose oxidase uses a free radical ligand coordinated directly to the copper center which allows the enzyme to activate O₂ to hydrogen peroxide.⁴⁷ Hydrogenase on the other hand uses coordinating sulfurs that can allow for the docking of protons and the metal center(s) themselves as a way to oxidize H₂.⁴⁸ These metalloenzymes have become an additional inspiration for the development of homogeneous electrocatalysts utilizing metal-ligand cooperativity.

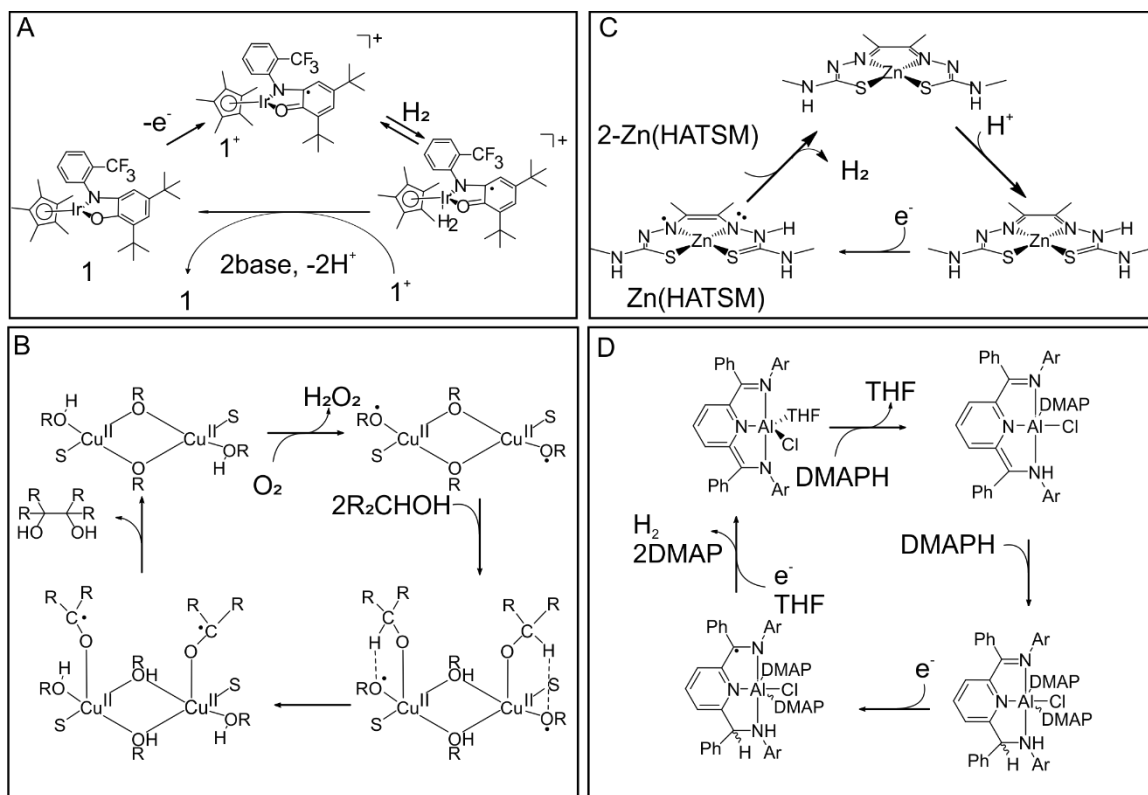
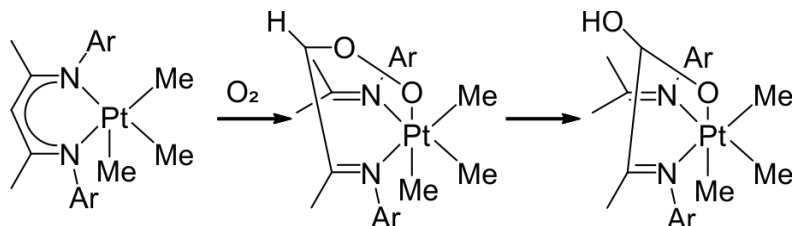


Figure I-6. A. Mechanism of $\text{Cp}^*\text{Ir}(\text{BA}^{\text{F}}\text{Ph})$. B. Mechanism of $\text{Cu}(\text{II})$ $(2,2'$ -thiobis(2,4-di-*tert*-butylphenol)) $_2$, C. Mechanism of ZnATSM (only one depicted although other options exist, see reference)⁴⁵ D. Mechanism of $(\text{PhI}_2\text{P}^2)\text{Al}(\text{THF})\text{Cl}$.

In some of the cases of the non-innocent ligand, both the ligand and metal are directly cooperating to generate a product or activate a species, through metal-ligand cooperativity. One of the first examples of this was by Goldberg *et. al.*,⁴⁹ where they showed the $\text{Pt}(\text{IV})$ complex $(\text{tBuMe}_2\text{nacnac})\text{PtMe}_3$ reacting with O_2 , Scheme I-4. The metal and the redox non-innocent ligand work in tandem to split the O_2 using the *nacnac* ligand into a metal-oxo and carbon-hydroxy species.

Scheme I-4. The reaction of Pt(IV) (^tBuMe₂nacnac)PtMe₃ reacting with O₂.



1.5 Frustrated Lewis Pairs

A typical Lewis pair results from the interaction of a Lewis acid (electron pair acceptor) and a Lewis base (electron-pair donor) forming an adduct, Figure I-7A. However, if the acid and base incorporate bulky substituents, steric interactions may prevent the orbital overlap required for adduct formation, Figure I-7B. In these cases, a frustrated Lewis pair (FLP) exists. The FLP has the advantage of containing both a Lewis base lone pair and a Lewis acid acceptor for the activation of small substrates, Figure I-7C. This activation can allow for protons or electrons to incorporate into the small molecule and allow for reduction of the small molecule into a useful fuel source.

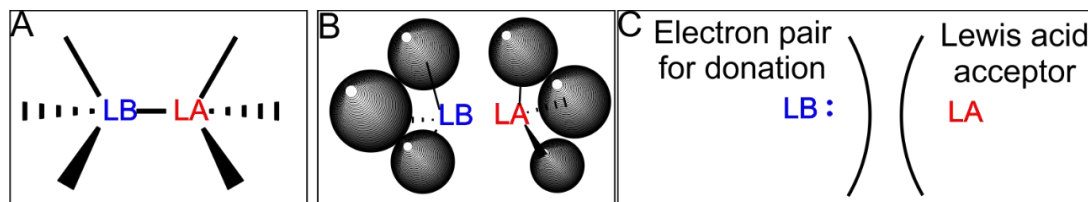


Figure I-7. A. Depiction of a Lewis pair. B. Depiction of a frustrated Lewis pair. C.

Depiction of the lone pair and acceptors in a frustrated Lewis pair.

The term FLPs was coined by Douglas Stephan.⁵⁰ Initial reports of FLPs focused on the heterolytic activation or release of hydrogen across the FLP. For example, (4-(bis(perfluorophenyl)boranyl)-2,3,5,6-tetrafluorophenyl)dimesitylphosphane

[Mes₂PH(C₆F₄)BH(C₆F₅)₂], releases hydrogen gas upon heating above 150°C. Introduction of 1 atm H₂ at 25°C to the resulting solution regenerates the initial [Mes₂PH(C₆F₄)BH(C₆F₅)₂] species, making the FLP competent at hydrogen activation and release.

More recently silylene/borane-based FLPs have been reported by Driess and coworkers that react with O₂, N₂O, and CO₂ to give silnanoes,⁵¹⁻⁵² Additional reactions with S₈ and H₂ generate silathiones and silanes, respectively. Similar work by Rauch and coworkers who used terminal hydrides with Zn and Mg with the tris[1-isopropylbenzimidazol-2-yl]dimethylsilyl]methyl ligand with B(C₆F₅)₃ and R₃SiH to generate methane directly from CO₂.⁵³ All three catalysts directly demonstrate the versatility of FLPs for the activation of small molecules.

1.6 Prior Work on Zn(DMTH)

The use of bis(thiosemicarbazone)s in the field of radiotherapeutics have been widely examined.⁵⁴ The popularity and use of these compounds has led to a similar ligand, one in which one thiosemicarbazone has been replaced by that of a pyridine, Figure I-8. The copper complex of this ligand, DMTH, was first reported by Cowley *et al.*⁵⁵ While the crystal structure of the doubly deprotonated ligand containing copper was not reported, the Zn complex was reported in this publication to show that the ligand can be doubly deprotonated. The synthesis of this complex was then reported with other group 12 metals such as cadmium in 2012.⁵⁶ Prior to this dissertation these complexes and similar bis(thiosemicarbazone) complexes have been examined as molecular imaging agents.⁵⁷ The related bis(thiosemicarbazone) complexes have been reported as electrocatalysts, however prior to this dissertation DMTH has not been examined as a catalyst.^{45, 58-65}

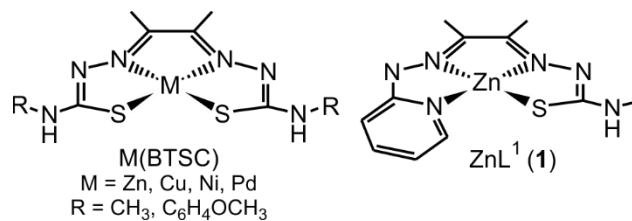


Figure I-8. Comparison of Zn(DMTH), ATSM and other ATSM derivatives.

Redox non-innocent ligands such as DMTH, have been explored for various catalytic activities, however not many have been explored for multiple chemical reactions. The similar ATSM and derivatives have been shown to be catalytic for HER. The Zn(DMTH) is structurally similar, however due to the additional basicity of the hydrazino nitrogen, the Zn(DMTH) complex can behave like a FLP and utilizes MLC to activate small molecules in the HER, CO₂RR, and water in the nitrile hydration reactions. Therefore, this thesis evaluates Zn(DMTH) for the HER, CO₂RR and nitrile hydration reactions. The Zn(DMTH) complex generates a large quantity of avenues to explore and generates a scaffold for other exciting levels of chemistry to examine.

CHAPTER II

EXPERIMENTAL METHODS

2.1 Materials

All chemicals were obtained from commercially available sources and were used as received unless otherwise noted. In the case of 2-chloropyridine, only fresh unopened bottles were used. After opening, the bottle was used in its entirety, as over the course of a month the reagent degraded and gave poor yields or impure products. In cases where dry glassware is noted in the procedure, the glassware was flame-dried under vacuum three times prior to use and refilled with argon. All solvents other than methanol and acetone were purified and dried using a solvent purification systems (SPS) supplied by MBraun. For the drying of methanol and acetone, the glassware was flame dried as described above, and then filled with molecular sieves. The solvent was added while the glassware was still hot, and then sealed with a septum. The solvent was then purged with argon for 30 minutes prior to use.

All gases were supplied directly from Welders Supply, Louisville, KY. In the case of use of “laboratory air” an UL-40 pump was purchased from Amazon. The pump was attached through tigon tubing to generate an inlet. All uses of the air pump were done at the highest speed setting. Diacetyl-2-(4-methyl-3-thiosemicarbazone)-3-(2-pyridinehydrazide) (H_2DMTH) was prepared by the methods of Cowley *et al.*⁵⁵ The synthesis of the precursor compound 2-hydrazinopyridine was synthesized by prior published methods with the modification of running the reaction for 16h.⁶⁶ The precursor compound, 1-methyl-1-(pyridine-2-yl)hydrazine was synthesized by prior published

methods.⁶⁷ One synthesis route for Zn(DMTH) was completed by prior published methods.⁵⁶ Crystallization of Zn(DMTH) also occurred via prior published methods.⁵⁵

2.2 Physical Methods

Elemental analyses were obtained from Midwest Microlab (Indianapolis, IN). Infrared spectra (ATR) were recorded using a Perkins Elmer spectrum 100 with a diamond tip as a powder or crystal. ¹H, ¹³C, and HSQC NMR spectra were obtained using either a Bruker 400-MHz or Bruker 500-MHz NMR. All UV/vis measurements were completed on a Variant Cary 50 Bio with fast scan capabilities. Electrospray Ionization mass spectrometry (+ESI-MS) was performed by the Laboratory for Biological Mass Spectrometry at Texas A&M University. Matrix-assisted laser desorption/ionization (MALDI-TOF) were completed by Caleb Calvary with the help of the Maurer Lab.

Cyclic voltammetry (CV), controlled potential coulometry (CPC), and all other electrochemical tests were carried out using a Gamry Interface potentiostat/galvanostat. A three-electrode setup was employed with a glassy carbon working electrode (3.0 mm diameter surface area = 0.07 cm²) or platinum disk electrode (3.0 mm diameter surface area 0.07 cm²), a platinum counter electrode and a Ag/Ag⁺ or Ag/AgCl reference electrode when applicable. The electrodes were prepared using the methods in section 2.7.1.

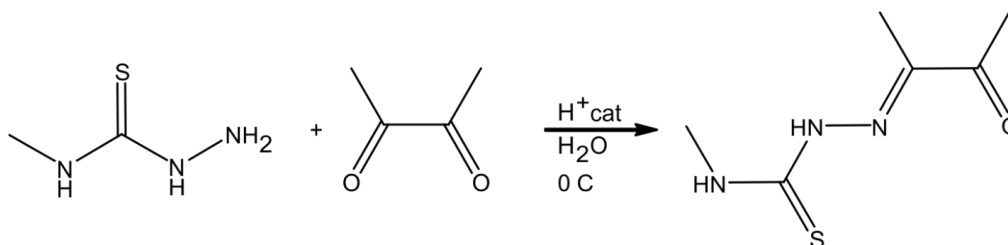
Hydrogen production was determined via the use of gas chromatography. The gas chromatogram was a Gow-MAC series 400 GC-TD fitted with a molecular sieve column. The column was heated to 130 °C under N₂ gas flow with 250 μL injections. Identification of product was conducted using a standard for the product expected and matching retention times. Identification of hydrated amines was conducted by GC/MS. The GC/MS employed was an Agilent 7820A equipped with a 5975 MSD. The column equipped was a carbowax

column, that is 85% nonpolar in nature. There were two methods employed depending on products. The first method used: the oven was set to 60°C and ramped to 140°C and held for 2 min. The ramp was set to 20°C/min at a flow rate of 1 mL/min. Each run lasted 7 min. The other methodology employed was the oven was set to 60°C and ramped to 275°C and held for 2 min. The ramp was set for 20°C/min at a flow rate of 1 mL/min. Each run lasted 13.75 min.

2.3 Precursor Synthesis

2.3.1 Synthesis of Diacetyl-N-4-methyl thiosemicarbazone

Scheme II-1. Synthesis of diacetyl-N-4-methyl-thiosemicarbazone.



Diacetyl-N-4-methyl thiosemicarbazone was prepared according to a modified literature procedure.⁶⁸ To a 250 mL round bottom flask 1.7 mL (0.019 mol) 2,3-butanedione and 5 drops of concentrated H₂SO₄ were added. In a beaker 2.0 g (0.019 mol) of 4-methyl-3-thiosemicarbazide was dissolved in 200.0 mL of DI water. The 4-methyl-3-thiosemicarbazide solution was added dropwise to the 2,3-butanedione solution at 0°C. *Note: When scaling up the reaction any mass addition of >2g of 4-methyl-3-thiosemicarbazide, the solution must be filtered after addition of one half the 4-methyl-3-thiosemicarbazide.* Once the addition is completed, the solution was filtered, and a white solid obtained. The white solid was dissolved in a 9:1 ethanol:water solution and kept in the freezer for at least 24 h before filtering and drying. Yield = 85 % ¹H NMR (Appendix

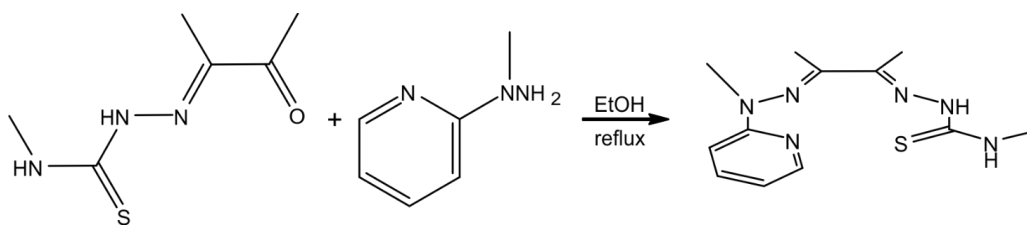
A, Figure A-1) *DMSO-d*₆ δ /ppm: 10.62 (N-NH), 8.62 (CH₃-NH), 3.04 (NH-CH₃), 2.41 (CH₃), 1.95 (CH₃).

If the isolated product contains >3% ATSM (diacetyl-bis(N-4-methyl-3-thiosemicarbazide)), further purification was performed by short path chromatography using a silica plug with ethyl acetate as the mobile phase. In a typical experiment, 0.200 g of crude compound was dissolved in 100 mL of dichloromethane (DCM) and deposited on the column and eluted with ethyl acetate. The combined eluted solutions were evaporated under vacuum producing pure product.

2.4 Ligand Synthesis

2.4.1 Synthesis of Diacetyl-2-(4-methyl-3-thiosemicarbazide)-3-(2-hydrazone-N-methyl-pyridine) (H₂DMTMH)

Scheme II-2. Synthesis of diacetyl-2-(4-methyl-3-thiosemicarbazide)-3-(2-hydrazone-N-methyl-pyridine) (H₂DMTMH).



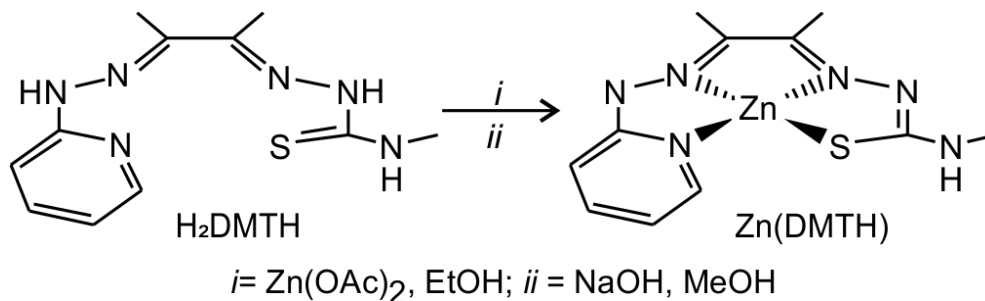
4.24 g of (Z)-N-methyl-2-(3-oxobutan-2-ylidene)hydrazine-1-carbothioamide was placed in a round bottom flask with 3.0g of 1-methyl-1-(pyridine-2-yl)hydrazine and 40 mL ethanol. The solution was refluxed for 16 hours. The solution was then concentrated to approximately 10 mL, and then diethyl ether was added and a grey precipitate formed. The grey precipitate was then filtered and washed with cold diethyl ether. Yield = 40 % ¹H NMR *DMSO-d*₆ δ /ppm: 10.34 (N-NH), 8.36 (CH₃-NH), 8.23 (Ar-H), 7.62 (Ar-H), 6.98 (Ar-

H), 6.85 (Ar-H), 3.35 (N-CH₃, can be obscured by H₂O), 3.06 (NH-CH₃), 2.33 (C-CH₃), 2.23 (C-CH₃). ¹³C NMR DMSO-*d*₆ δ/ppm: 179.02 (C=S), 161.49 (C=N), 160.16 (C=N), 148.69 (N-C-N), 147.32 (Ar C), 137.63 (Ar C), 115.47 (Ar C), 109.78 (Ar C), 38.98 (N-C), 31.37 (N-C), 15.55 (C-CH₃), 11.16 (C-CH₃) HSQC δ/ppm: (2.23, 11.16), (2.33, 15.55), (3.06, 31.37), (3.35, 38.98), (6.85, 115.47), (6.98, 109.78), (7.62, 137.63), (8.23, 147.32).

2.5 Catalysts Syntheses

2.5.1 Synthesis of ZnDMTH (MeOH)

Scheme II-3. Synthesis of ZnDMTH (MeOH).

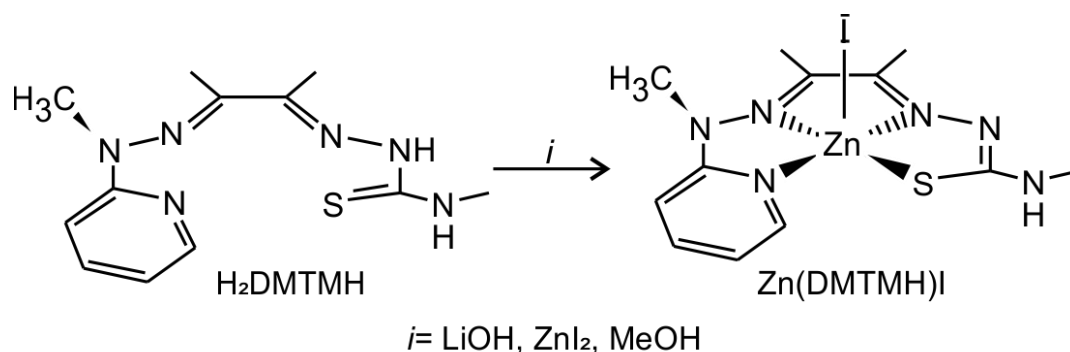


An alternative route to the one published by Cowley and coworkers is shown above.⁵⁶ In a 250 mL round bottom flask, 0.245 g (0.927 mmol) of DMTH and 0.225 g (1.23 mmol) of Zn(OAc)₂·2H₂O was dissolved in 30 mL ethanol. The solution was refluxed for 16 h under N₂ yielding a yellow solid upon cooling. This yellow solid contained the Zn(HDMTH)(OAc) as an impurity and was washed with cold ethanol and diethyl ether. Crude yield = 85 %. To purify the crude compound was dissolved in methanol and a 6 fold excess of NaOH (based on crude mass) was added and stirred for 5 days. The solution was filtered under vacuum and the solid discarded. The filtrate was removed under vacuum and dissolved in minimal amount of methanol (2 mL) and layered with 30 mL of diethyl ether. An orange/red solid was isolated the next day by vacuum filtration and rinsed with diethyl

ether. Isolated yield was 0.182 g (0.556 mmol, 60%). NMR and IR match reported literature except for resonances assigned to methanol adduct.

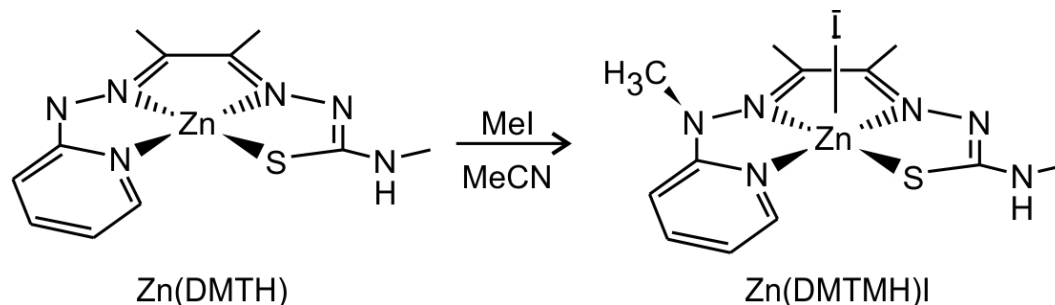
2.5.2 Synthesis of Zn Diacetyl-2-(4-methyl-3-thiosemicarbazone)-3-(2-hydrazone-N-methyl-pyridine) (ZnDMTMH)

Scheme II-4. Synthesis of Zn(HDMTH)I method A.



Method A. The Zn complex can be synthesized by first dissolving 0.200 g of diacetyl-2-(4-methyl-3-thiosemicarbazide)-3-(2-hydrazone-N-methyl-pyridine) (H_2DMTMH) in 50 mL of methanol containing 0.030 g of LiOH and stirring for 15 minutes. After which time 0.249 g of $\text{ZnI}_2 \cdot 2\text{H}_2\text{O}$ was added and stirred for 5 days. The solution was then concentrated under vacuum to approximately 4 mL and filtered. Yield = 65 % ^1H NMR $\text{DMSO-}d_6$) δ/ppm : 8.10 (Ar-H), 8.04 (Ar-H), 7.86(NH- CH_3), 7.38 (Ar-H), 7.16 (Ar-H), 3.62 (N- CH_3), 2.90 (NH- CH_3), 2.33, 2.07(C- CH_3).

Scheme II-5. Synthesis of Zn(HDMTH)I method B.



Method B. Conversely the complex can be generated via methylation of ZnDMTH directly. 0.300 g (0.909 mmol) of ZnDMTH was flame dried and then dissolved in 50 mL of acetonitrile. To this 0.057 mL (0.909 mmol) of iodomethane was added and then the solution was refluxed for 24 h. The solution was then concentrated to approximately 5 mL under vacuum and placed in the freezer for 4 h. The resulting solid was filtered and washed with diethyl ether. Yield = 78% $^1\text{H NMR DMSO-}d_6$) δ /ppm: 8.10 (Ar-H), 8.04 (Ar-H), 7.86(NH-CH₃), 7.38 (Ar-H), 7.16 (Ar-H), 3.62 (N-CH₃), 2.90 (NH-CH₃), 2.33, 2.07(C-CH₃). Synthesis of X-ray quality crystals: 0.042 g of Zn(DMTMH)I was dissolved in 30 mL of a 1:1:1 mixture of acetone:acetonitrile:methanol (3 mM). This was then distributed into a series of test tubes and covered with parafilm with a small quantity of holes poked in it. This yielded X-ray quality single crystals in 3 days.

2.5.3 Synthesis of Zn(HDMTH)(OAc)

ZnDMTH (10 mg, 0.00258 mmol) was dissolved in 10 mL of a 1:1:1 mixture of methanol:acetonitrile:acetone. To this was added 10 drops of glacial acetic acid (17.4 M) resulting in a color change from orange to yellow. Zn(HDMTH)(OAc) was isolated as X-ray quality yellow crystals upon slow evaporation over several days at room

temperature. Yield: 8.4 mg (0.00217 mmol), 83.7%. ^1H NMR (400 MHz, DMSO-d_6) δ/ppm : 9.73 (N-NH), 8.14 (Ar-H), 7.82(NH- CH_3), 7.67(Ar-H), 7.23(Ar-H), 6.80 (Ar-H), 2.82(NH- CH_3), 2.19(C- CH_3), 1.80 ($\text{O}_2\text{C-CH}_3$)

2.5.4 Synthesis of $\text{Zn}(\text{HDMTH})(\text{CO}_3\text{CH}_3)$

An h-tube was flame-dried prior to addition of 0.004 g (0.012 mmol) of $\text{Zn}(\text{DMTH})$, and the tube was sealed with a septum and then wired with copper. Ten milliliters of a 50:50 mixture of dried methanol and acetone was added to the tube to dissolve $\text{Zn}(\text{DMTH})$. Great care was taken to ensure that the solution stayed in the vertical portion of the h-tube, and solvent levels did not go larger than the shoulder of the h. CO_2 was passed through a drying tube prior to bubbling in the $\text{Zn}(\text{DMTH})$ solution for 15 min. Further, the headspace of the tube was filled with pure CO_2 , which was the portion after the shoulder of the h-tube was submerged in an ice bath (Figure II-1). This ice bath was changed every 24 h, and yellow X-ray quality crystals of $\text{Zn}(\text{HDMTH})(\text{CO}_3\text{CH}_3)$ were obtained after 5 days.

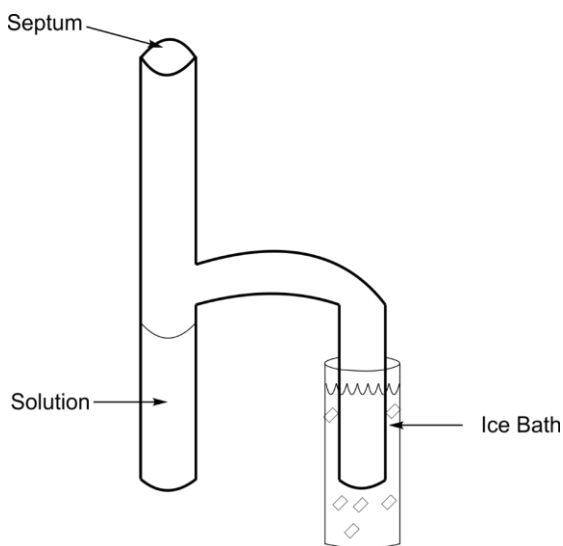


Figure II-1. Depiction of crystallographic setup for $\text{Zn}(\text{HDMTH})(\text{CO}_3\text{CH}_3)$

2.6 General Electrochemical Techniques

For electrocatalysis, mastery of these techniques is paramount. The most commonly used are cyclic voltammetry, square wave, and controlled potential coulometry. The most important things to generating useable electrochemical data are proper cleanliness and maintenance of electrodes, purity of sample, dryness of solvent, purity of supporting electrolyte, and choosing the solvent with the appropriate window. Herein, the cleaning and maintenance of electrodes and purification of supporting electrolyte are described. With the exception of methanol, all solvents are obtained from the solvent purification system with flame dried glassware that is purged under inert gas after collection. Methanol was dried using magnesium and iodine and then stored over molecular sieves. Choosing the proper solvent can be difficult as understanding non-covalent interactions between the complex and solvent is often critical to catalytic activity. Additionally, various solvents will have varying solvent windows. For a list of common solvent windows see Dempsey and coworkers⁶⁹ and Yan and coworkers.⁷⁰

Another common issue when conducting electrochemical measurements is uncompensated resistance associated with iR drop. In the case of electrochemistry, a voltage is passed through the cell generating some current. The solution has an inherent resistance that is often times mitigated by supporting electrolytes. Changes of observed current can be seen even when using the proper supporting electrolyte and is often referred to as “ iR drop”. The most common way to avoid iR drop is proper positioning of electrodes and use of a supporting electrolyte. Typically, a three-electrode setup is employed in electrochemical techniques. In this setup, a working, counter, and reference electrode are employed. The further apart the three electrodes are the larger the iR drop, therefore with

careful positioning iR drops can be mitigated. One way to check if your solution is undergoing iR drop issues, is to run a cyclic voltammetry experiment of a solution containing ferrocene. The peak to peak separation of ferrocene should be 59-60 mV. If the peak to peak separation is larger, that may indicate iR drop issues. This iR drift can be a bigger problem when monitoring catalysis, as the peak potential can shift to more negative or positive potentials vs the true value, thereby raising the overpotential. Most modern machines have iR compensation tools, and for the Gamry instruments the auto iR compensation yields the best results.

2.6.1 Preparation of Electrodes

Prior to the conducting of an experiment, the working and counter electrodes must be polished, cleaned, and sonicated. To polish glassy carbon working electrodes, place approximately 0.3 mL of cleaning slurry on the polishing pad. Then take the electrode and move it in a figure 8 motion in the center of the polishing pad, Figure II-2. When polishing is complete, the electrode should be washed with water, ethanol, and acetone the solvent being used in the electrochemical measurement. For platinum disk electrodes the polishing and cleaning procedure is the same as the glassy carbon working electrode. For platinum wire electrodes, sandpaper is used to generate a mirror finish. After this the rinse procedure is employed as the same as the working electrode. Once the electrodes are cleaned and polished, they are placed in a test tube with the electrochemical solvent and sonicated for at least 15 minutes. For the reference electrode, rinse directly with water and then the electrochemical solvent and place in the electrochemical cell.

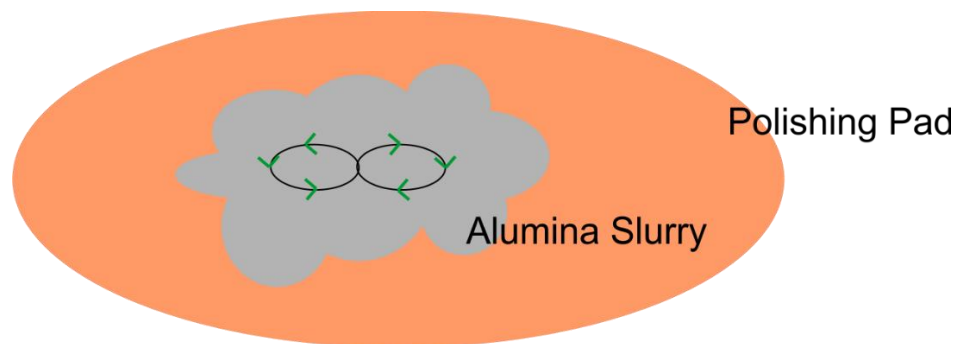


Figure II-2. Depiction of the polishing pattern for the working electrode.

2.6.2 Maintenance of Electrodes

Cleanliness and proper maintenance is essential for proper function of the electrodes. In the case of the glassy carbon electrodes, proper polishing and cleaning prior to and after experiments must be conducted. If the electrodes are not cleaned and polished, cracks can occur in the electrode/casing surrounding the electrode. If this occurs the electrode will stop working or will stop generating the correct current.

In the case of platinum electrodes, they should be cleaned and polished before and after each use. If buildup of substrates occurs on the platinum electrodes, then they should be dipped into acid and rinsed with a large quantity of DI H₂O. If the substrate still exists after a strong acid like HNO₃, then try aqua regia. If that still doesn't work, the last option is sandpaper until the substrate comes off.

The most common reference electrode is the Ag/AgCl electrode. To generate an electrode, first dissolve 3 M KCl in DI H₂O. Typically, this is made in a scintillation vial, which is 20 mL. After generation of this, the capillary tube fitted with a frit, that the electrode is placed in, should be rinsed with acetone, dried, and soaked in the 3 M KCl solution. The silver wire should be polished to a mirror finish, usually with sandpaper, and

then rinsed with acetone and allowed to air dry. Using a syringe, take approximately 0.5 mL of the KCl solution and fill the capillary tube and then plastic cap encapsulating the silver wire top. Then very carefully, twist the capillary tube into the plastic cap, making sure that the frit is not “popped” out of the capillary tube. To add a frit to a capillary tube if one is not there already, take the capillary tube and a small amount of the shrink tubing and a glass frit and fit the shrink tubing around the capillary and the frit. Then using a heat gun, shrink the tubing around the frit and the glass tubing.

2.6.3 Purification of Supporting Electrolyte

All supporting electrolytes can be purchased at the electrochemical grade. However, the most common used, tetrabutylammonium hexafluorophosphate, is often purchased as reagent grade, not electrochemical grade. Purification is done via recrystallization with boiling ethanol. If the recrystallized product does not give full needles, then a second recrystallization must be done prior to use in electrochemical experiments. If this is not done, false peaks will occur in the oxidative region.

2.6.4 Cyclic Voltammetry Introduction

The most common electrochemical technique employed in the Grapperhaus laboratory is cyclic voltammetry (CV). A CV is recorded by in scanning the potential in one direction to a switching point, and then scanning back in the opposite direction to a desired potential. The current is measured as a function of the applied potential. In a reversible process, the peak current for both the reductive and oxidative directions should be the same value from the baseline. An example would be scanning from 0.0 V to -2.50 V to 0.5 V to 0.0 V. CVs can be conducted at any potential and cycled for any number of times.

2.6.5 Simple Cyclic Voltammetry for Identification of Potentials.

In the electrochemical cell, 0.1 M supporting electrolyte, the three electrodes, a septum, and the gas circulator were placed in the 5 compartments. The solvent was filled to 25 mL, and then purged with inert gas for at least 15 minutes. Then a “blank” potential scan is completed. In this scan, the limits of the solvent window are scanned to identify the full solvent window and solvent oxidation or reduction. Once this is completed, the substrate, in this case the catalyst, was added to the solution and the solvent was purged with inert gas. From here the full solvent window should be scanned with the catalyst. If the catalyst has multiple oxidation or reduction events, the potential should be varied as to “capture” those events for their reversibility and coupling. For example, if the catalyst has two reduction events at -1.5 and -2.0 V and one oxidation at -1.4 V. A simple experiment would be to scan to -1.6 V from any potential prior to -1.6 V and look for if the -1.4 V oxidation appears when scanning to a potential more positive than -1.4 V. This will tell the “coupling” of events. A final scan is completed of all the events that can be seen. Once this is completed the scan rate should be varied from 100 mV/s to 1,000 mV/s. The current should be plotted vs the inverse square root of the scan rate in V/s, to generate the square root of the D_0 of the complex. This is called a Cottrell plot and generated from the Cottrell equation, as equation 1. For the Cottrell equation, the variables can be defined as n = number of electrons, F = Faraday’s constant, A = area of the electrodes active surface, C = bulk concentration, t = *time*, D = diffusion coefficient. In the varying scans, the $nFAC$ and $\sqrt{\pi}$ are constant, therefore plotting I vs $1/\sqrt{t}$ generates \sqrt{D} as the slope of the line.

$$i = \frac{nFAC\sqrt{D}}{\sqrt{\pi t}} \quad (1)$$

2.6.6 Cyclic Voltammetry for Electrocatalysis

In electrocatalytic experiments the catalytic substrates are added to the solution. For instance, in HER conditions, the chosen acid was added to the solution and allowed to equilibrate ~5 min, and a CV was performed. If the current generated is greater than that of the original current, then catalysis is being observed. It should be noted that knowledge of at what potential and where the substrate added appears is paramount to identifying if the new peaks are catalytic. The substrate was added until a “saturated” current is observed. Saturated current implies that as you add more substrate, the current does not increase. After this is obtained, a scan rate independence should be completed. In this experiment, the scan rate should be stepped up by 500 mV/s until a consistent current is obtained. It also should be noted that the larger the current generated, along with features of the catalyst, the observed catalytic potential may shift. In the case of HER, the catalytic wave may be at -1.5 V initially, but at saturation it may be at -1.8 V. Another case could be that the faster the scan rate the same catalytic wave changes could be observed. When the experiment is finished, less than 5 mg of ferrocene should be added to the solution, and a CV completed in the oxidative direction. This allows for direct referencing to the internal standard. NOTE: Ferrocene current should not exceed 20 μA . If a large quantity of Ferrocene is added, iR changes can occur, and result in faulty referencing to the internal standard.

2.6.7 Reaction Order Experiments

If the reaction is catalytic, it is important to understand how many components are involved in a catalytic step. There are two separate cases that should be examined: varying the substrate and varying the catalyst. In the case of varying substrate, the same catalytic

solution from 2.7.3.2 should be enough. When that experiment is completed, care should be taken to get multiple data points from start of catalysis to saturation. If the catalysis is “overshot” i.e. there are only 4-5 data points from the experiment, the experiment should then be recompleted, to generate a minimum of 10 data points prior to saturation, and an additional 3-4 data points after saturation.

In the case of catalyst variance there are two separate types of experiments that can be done. In one case, the solution can be made from a stock concentration of catalyst and saturation concentration of substrate. The catalyst can then be added to this solution to vary the concentration, with scans of each addition, such that 4-6 data points are obtained. An example of this is the solution starts at 0.5 mM, and each time the mass that corresponds to 0.5 mM catalyst is added to the solution. There also can exist separate mechanisms depending on concentration, or the catalyst may only be soluble up to 1.0 mM, which would make the addition of catalyst to generate smaller concentrations. For example, 0.5 mM starting solution and addition of the mass to generate a 0.1 mM increase in concentration. It should be noted that after each addition, the solution should be purged with inert gas.

The second case is if side reactions or inconsistent data is observed from the first set of experiments, “fresh” solutions should be generated. In these experiments catalysis is completed at one concentration, and then the solution is removed from the cell, and the cell cleaned and dried. Then a new concentration was added, and that catalytic experiment was completed. This was completed to generate 4-6 data points.

2.6.8 Controlled Potential Coulometry Experiments

Controlled potential coulometry (CPC) experiments are completed to analyze products of reactions. These are necessary, as in CV experiments only the portions that

appear in the diffusion layer catalytically turnover. Because of this it is difficult to analyze the products via that methodology as the concentration of products is minor in comparison to the bulk. In a CPC experiment, two compartment cells are employed separated by fritted glassware. In one compartment the “working” portion contains 0.1 M supporting electrolyte, the catalyst, a stir bar, solvent, and substrate. In this portion of the cell the working electrode and the reference electrode are employed. The counter cell contains the 0.1 M supporting electrolyte, solvent, and the counter electrode. One way to lower the resistance of the cell, is to put the counter electrode as close as possible to the frit of the working cell. The CPC should be conducted by first conducting a CV. From there, there are two ways to complete the catalytic experiment. The potential can be held at the potential of $\frac{1}{2}$ the catalytic potential. This can help increase the Faradaic Efficiency of the system. The potential can also be held at just past the catalytic peak. The reason for picking just past the catalytic peak, are two-fold. First, if background production is higher at that potential, it would be hard to differentiate background production from catalytic production. Second, if at the better Faradaic efficiency, an undetectable amount of product is generated. Once the catalytic runs are completed, blank runs, or runs in the absence of catalyst, at the same potentials, to generate a faradaic efficiency.

2.6.9 Soak Tests

One concern of homogenous catalysis is the catalyst adheres the electrode surface throughout catalysis, making the catalyst heterogeneous in nature. One way to determine if the catalyst adheres chemically to the surface of the electrode is the soak test. In this experiment, all of the components of the catalytic cycle, the supporting electrolyte, the catalyst, the solvent, the substrate are placed in a beaker or scintillation vial. After this, the

working electrode after being polished and cleaned, is placed in the solution for at least 16 h. After the soaking the outside of the electrode is rinsed with DI H₂O, and then the electrode is placed in a fresh solution with supporting electrolyte and solvent, and a CV is completed. Additionally, substrate can be added at this point, to determine if the catalytic current is observed.

2.6.10 Cycle Dip Tests

This is a variation of the “Rinse Test” often employed by catalytic groups. In a rinse test the electrode is removed from a post catalytic experiment, and washed with DI H₂O, then placed in a fresh solution with electrolyte and solvent. However, the number of scans is variable, and the reproducibility requires the completion of the same experiment presented by the author of their catalytic experiment. In a cycle dip test, the catalytic solution is produced at substrate saturating conditions. Then at one scan rate, the solution is cycled for a predetermined number of cycles. Once the cycling is complete the electrode is removed, washed with DI H₂O and placed into a fresh solution with electrolyte. Substrate can be added post the first cycle after washing to determine catalytic viability of the film.

2.6.11 CPC Dip Tests

A CPC dip test, is completed by completing a CPC at a given potential, then removing the electrode from the solution. After removal from the solution, the electrode is washed with DI H₂O, and then placed into a fresh solution with supporting electrolyte. After the CV, the substrate can be added to the solution, and a second CV completed.

2.6.12 Square Wave Voltammetry

Square wave voltammetry is a form of linear sweep voltammetry that combines square wave and staircase potential. Due to the current being sampled at two times,

resolution of peaks that do not separate in CV can be observed. Completion of a square wave voltammetry, is similar to that of a CV, as all the setup is the same, however the scan is from one potential, to another, i.e. 0.0 V to -1.0 V. The scan pulse can help with the resolution of peaks. To help with resolution, smaller pulses can be used.

2.6.13 Resistance Measurements

Resistance measurements are a way to determine the inherent resistance of the solution with whatever components are dissolved. This is done by determining the open circuit potential, and then measuring the impedance of electron flow. The more ionic the solution, the lower the resistance of the solution. Resistance measurements were conducted using a Metroham Autolab potentiostat. 0.5 mM solutions of catalyst, tetrabutylammonium hexafluorophosphate, and para-nitroaniline were prepared. A 5 mL aliquot of each solution was placed in separate beakers between two graphite rods that were 2.5 cm apart. This was then subjected to resistance measurement experiment provided by the Nova software made by Metroham Autolab.

2.7 Computational Methods

Density Functional Theory (DFT) is often successfully employed to calculate and validate the experimental observables. DFT is less expensive than other computational methods and can predict the energetics and the geometrical structures of a model system with a considerable accuracy. The accuracy of the DFT is largely depend on the choice of a proper functional. Based on our previous studies of related complexes it was shown that the B3LYP hybrid functional can produce better agreement with experimental parameters such as bond lengths, bond angles and torsional angles.⁵⁵ In this regard we have applied B3LYP functional to optimize the structures with 6-311g (d,p) basis set.⁷¹⁻⁷² This level of

theory was also applied in our previous studies and found to be quite accurate. The calculations were conducted in a polarizable continuum model (PCM).⁷³ The appropriate solvent was used as a solvent in PCM. The optimized structures were confirmed by frequency calculations. No imaginary frequencies were found for the optimized geometries which confirms the optimized structure were true stationary points. All corresponding cartesian coordinates were added in Appendix B. Gaussian 09 was used to conduct the calculations.⁷⁴ Chemcraft and gaussview were used to visualize the structures.⁷⁵

2.8 Analysis of Kinetic Data - General

2.8.1 Calculation of Turnover Frequency (TOF)

In terms of direct chemical reactions, a turnover frequency can be defined as the number of turnovers in a given period of time. This means that direct TOF can be determined from bulk solutions in direct chemical reactions. Due to the fact that turnovers only occur in the diffusion layer, the TOF can be calculated in a different manner electrochemically. The derivation of this can be found by Haddad et al, and as equation 2.⁵⁸

$$TOF = 1.94 \nu \left(\frac{I_c}{I_p} \right)^2 \quad (2)$$

2.8.2 Calculation of Faradaic Efficiency

In a general CPC experiment a value of charge is passed over the length of the experiment. To determine the quantity of charge generated via catalysis, the charge passed through the catalytic run must be subtracted from the blank run, equation 3. In terms this can then be defined as:

$$Q_{cat} = Q_{total} - Q_{blank} \quad (3)$$

After this the quantity of product is determined, via NMR, gas chromatography, etc. This is commonly referred to as the turnover number (TON) or the number of turnovers. This can then be compared to the amount of product determined via the blank run, as shown in equation 4. In terms this can then be defined as:

$$n_{\text{cat}} = n_{\text{total}} - n_{\text{blank}} \quad (4)$$

The quantity of moles that should be generated by the total charge generated from the CPC experiment can be defined as equation 5.

$$n_{\text{calc}} = Q_{\text{cat}} \times \frac{1 \text{ mol } e^-}{96485 \text{ C}} \times \frac{1 \text{ mole product}}{x \text{ mol } e^-} \quad (5)$$

In this general equation the moles of electrons passed are a function of the total number of electrons required to generate the product. Finally, with these two numbers in hand the faradaic efficiency can be calculated as equation 6.

$$\text{Faradaic efficiency} = \frac{n_{\text{cat}}}{n_{\text{calc}}} \times 100\% \quad (6)$$

2.8.3 Determination of Overpotential for Catalysts

Overpotential is the difference between the thermodynamic potential and the operating potential of the electrochemical cell. The overpotential is then defined by equation 7.

$$\eta = |E_{1/2}^T - E_{\text{cat}/2}| \quad (7)$$

Where η is the overpotential, $E_{\text{cat}/2}$ is the potential at which the current is one half the maximum catalytic current, and $E_{1/2}^T$ is the thermodynamic potential. The thermodynamic potential can be defined by equation 8 described by Formound et al.⁷⁶

$$E_{1/2}^T = E_{H^+/H_2}^0 - \frac{2.303RT}{F} pK_a + \epsilon_D + \frac{RT}{2F} \ln(2K_c^2 C_0 C_{H_2}^0) \quad (8)$$

Where E_{H^+/H_2}^0 is the standard reduction potential for hydrogen in the solvent, R is the ideal gas constant, T is the temperature, F is faraday's constant, pK_a is the $-\log K_a$ for the acid, ϵ_D is the a measure of how fast the diffusion of the products are with respect to the reactants, C_0 is the concentration of the acid used and $C_{H_2}^0$ is the concentration of dissolved hydrogen in the solvent used.

2.9 Analysis of Kinetic Data – Chapter 3

2.9.1 Calculations of pKs and Potentials via Computational Methods

The overall governance of pK and reduction potential starts with one of the following two reactions:



In the case for calculation of pK, the optimized geometries of substrate, catalyst, and product are generated. In the case where the product has a non-coordinating anion, the anion is calculated separately. These calculations are done in a PCM model to simulate additional solvent interactions. Once the calculations have been completed, the products are subtracted from the reactants, to generate a value for the K overall for the reaction. The $-\log$ of this value generates the pK of the reaction. In the case for reduction potentials, the calculation uses ferrocene and ferrocenium as the way to balance the charge, and the reduced and nonreduced calculations are completed. A difference from the reduced and ferrocenium and ferrocene and nonreduced are completed. This allows for direct mechanistic comparison of the reduction potential and the chemical feasibility of a step.

2.9.2 Determination of Reaction Orders via Electrochemical Methods for HER

The equation that governs the catalytic current can be derived from the Randles-Sevcik, equation 11. Where n = number of electrons, F = faraday's constant, A = area of the electrode, D = diffusion coefficient and n' = number of electrons effectively used by the catalyst during reduction.⁷⁷

$$i_{\text{cat}} = nFA C_p^0 \sqrt{Dn'k_{\text{obs}}}. \quad (11)$$

However under more practical conditions it can be rewritten as: $i_{\text{cat}} = nFA[\text{cat}] \sqrt{Dn'k_{\text{obs}}}$, as C_p^0 is the concentration of the bulk catalyst. In the case of HER $n'K_{\text{obs}}$ can be rewritten as $k[\text{H}^+]$ generating equation 12. In this case k = catalytic rate constant, $[\text{H}^+]$ = concentration of protons.

$$i_{\text{cat}} = nFA[\text{cat}] \sqrt{kD[\text{H}^+]}. \quad (12)$$

2.10 Analysis of Kinetic Data – Chapter 4

2.10.1 Determination of Reaction Orders via Electrochemical Methods for CO₂RR

The derivation to this point is the exact same as for the HER presented in 2.7.1.2. When CO₂ is varied in a system that is using the solvent as the acid concentration the equation can be rewritten as equation 13.⁷⁸⁻⁷⁹

$$i_{\text{cat}} = nFA[\text{cat}] \sqrt{kD[\text{CO}_2]}. \quad (13)$$

However, the case protons are added to the solution and must be accounted for in as they are accounted for in HER by equation 5.

Combination of equations 5 and 13 yields equation 14:

$$i_{\text{cat}} = nFA[\text{cat}] \sqrt{kD[\text{CO}_2][\text{H}^+]}. \quad (14)$$

All subsequent catalytic orders were determined by analysis of i_{cat} vs $[\text{cat}]^n$ or i_{cat} vs $[\text{H}^+]^{n/2}$, where n is the reaction order.

2.10.2 Calculation of Binding Constants

The binding constants followed the reaction shown in equation 15. The equilibrium constants can then be calculated as the result of equation 16. Due to the calculations being from UV/Vis spectroscopy, the concentration of a substrate at equilibrium can be defined as $[\text{Substrate}] = A/\epsilon$.



$$K = \frac{[\text{Cat-Substrate}]}{[\text{Cat}][\text{Substrate}]} \quad (16)$$

CHAPTER III
UTILIZING CHARGE EFFECTS AND MINIMIZING INTRAMOLECULAR
PROTON REARRANGEMENT TO IMPROVE OVERPOTENTIAL OF A
THIOSEMICARBAZONATO ZINC HER CATALYST

3.1 Background

Work in this chapter has been previously published in *Inorganic Chemistry*.⁸⁰ Hydrogen has several major uses in the developed world. It is a primary component in the Haber-Bosch process, a reagent in hydrogenation reactions, and a potential carbon-free fuel source. However almost the entirety of the hydrogen produced industrially is through the water-gas shift (WGS) reaction, Scheme III-1a.⁸¹ In the WGS reaction, for every 1 mol of H₂ produced, 1 mol of CO₂ minimum is released. Considering that last year 70 million tons of H₂ were produced, and that 95% of all hydrogen produced is through non-renewable energy sources, a minimum of 1.45 billion tons of CO₂ were produced through the production of hydrogen for industrial processes.⁸² Currently there are two promising ways to produce hydrogen while reducing CO₂ emissions; methane gas reformation and electrocatalysts, Scheme III-1b,c. In the case of methane gas reformation, carbon monoxide (CO) is a byproduct that must be either separated from the stream to give pure H₂. Alternately, the H₂/CO gas mixture can be then used in the Fischer-Tropsch process to generate liquid hydrocarbons.⁸³ In the case of electrocatalysis, the product H₂ would be the only gaseous product, and thus separation would not be necessary. Additionally, electrocatalysts can operate using water as a proton source and use the electricity generated

from renewable sources such as wind and solar. This chapter will focus on the use of electrocatalysts to drive hydrogen production.

Scheme III-1 A. Water Gas Shift Reaction. B. Methane Gas Reformation Reaction C. Electrocatalytic Production of Hydrogen



Hydrogen production from electrocatalysts can occur using heterogeneous or homogeneous catalysts. In the case of heterogeneous electrocatalysts, the standard is platinum. Platinum, while expensive, generates hydrogen at zero overpotential and has high turnover frequencies (TOFs). Overpotential is the difference between the potential at which the redox event is experimentally observed and the thermodynamically determined reduction potential. In other words, it is how much additional energy must be put into the system for the system to catalytically turnover. The major drawbacks to platinum are that it is expensive and a scarce metal. For these reasons, other heterogeneous catalysts such as MoS_x and homogeneous electrocatalysts deposited on electrode surfaces have been evaluated.^{63, 84} Due to its low overpotential with high activity, MoS_x is an attractive electrode material. This electrode is proposed to react through an edge site S mechanism.⁸⁵ Mimics of this edge site selectivity have been extensively explored in the homogeneous phase.⁸⁶ Another promising heterogeneous electrode is that of homogeneous electrocatalysts either being chemically tethered, electrodeposited, or physically deposited on the electrodes surface.⁸⁷ In general, these have resulted in maintaining the homogeneous activity, however they typically result in lowering the overpotentials of the deposited catalysts.⁶³

While homogenous electrocatalysts may be a largely academic processes at this point, understanding the mechanisms for these catalysts and their reactivity can help for screening of the most promising candidates for deposition on an electrode surface. In the case of homogenous electrocatalysts, there are two distinct pathways that can exist: a metal-centered pathway and a ligand centered pathway, Figure III-1. A. In the case of a metal-centered pathway, the complex must be reduced to activate the complex. Then upon the protonation and reduction, generation of a metal hydride occurs and that hydride is free to attack a solution proton or the proton on the ligand framework. An example of this is the DuBois catalyst which boasts a TOF of over $100,000 \text{ s}^{-1}$ and at a very low overpotential, Figure III-2.⁸⁸ In fact due to the effectiveness of DuBois' initial catalyst, a large quantity of derivatives with modification of the ligands have been developed.⁸⁹ Furthermore, this has now become a candidate for the production of fuel cells, where hydrogen is needed to be produced. The $\text{Ni}(\text{P}^{\text{Ph}}_2\text{N}^{\text{Ph}})_2$ catalyst undergoes a reduction which allows the complex to be protonated on the ligand framework at the pendant amine which brings the proton in proximity to the nickel center. Then upon further reduction, migration to the nickel center of the H atom generates a Ni(II)-hydride. The Ni(II)-hydride then attacks a proton that is “shuttled” in by the pendant amine and H_2 is released.

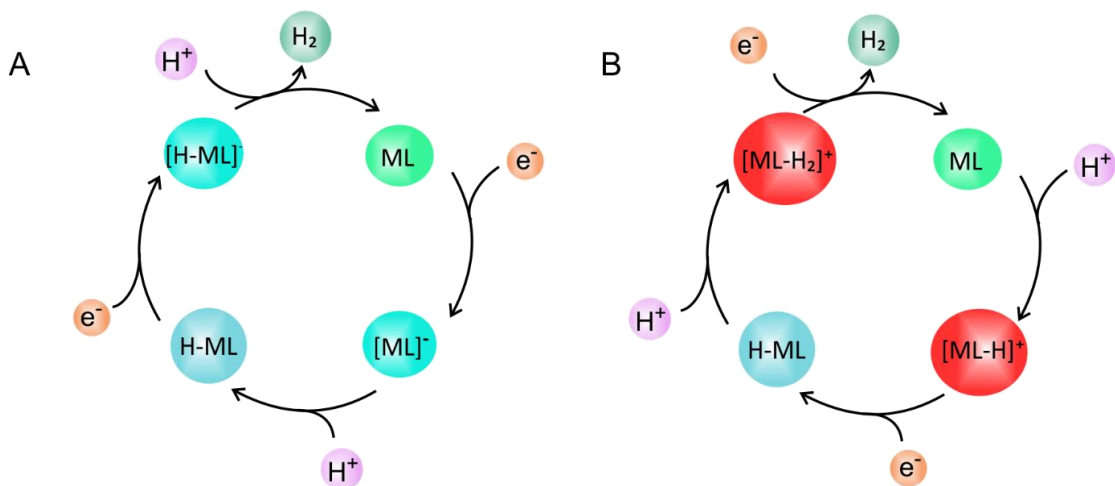


Figure III-1. A. Metal-centered pathway for HER. B. Ligand-centered pathway for HER.

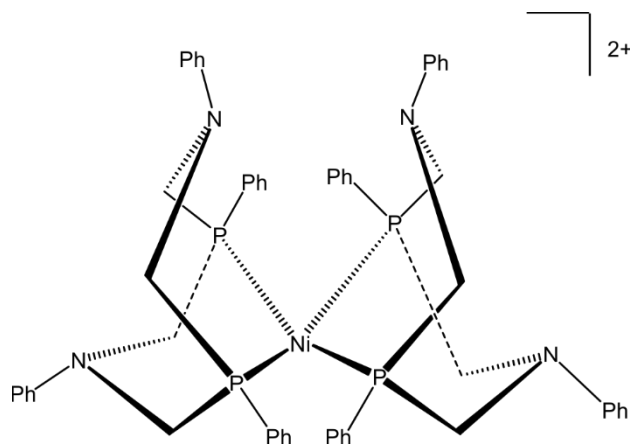


Figure III-2. DuBois catalyst.

While the metal-hydride centered pathway has been shown to be operable at lower overpotentials, the ligand centered pathway can also generate similar TOFs using less expensive materials and potentially metal-free. In the ligand centered route, a protonation event is typically seen well before reduction, Fig III-1.B. Upon protonation and reduction, a second protonation is usually added with hydrogen released in a following reduction step. There have been a few examples of this in the literature first with the $Re(PS)_3$ system

developed by Grapperhaus and coworkers.⁹⁰ This coordinatively saturated molecule had a ligand centered “route” that was available to it, but the researchers could not rule out the possibility of the generation of a rhenium hydride.⁹¹ Another ligand centered route was exploited by Berben and coworkers with their $(^{\text{Ph}}\text{I}_2\text{P}^2)\text{Al}(\text{THF})^+$ species.⁴⁶ While the reported TOF was low at 3.3 h^{-1} , they were the first to show that a ligand centered route was unambiguously possible.

The direct inspiration for the choice of DMTH as a ligand for the work described in this chapter is $\text{Zn}(\text{ATSM})$, which generates hydrogen from the Zn catalyst with large TOFs.⁴⁵ Additionally, the ligand H_2ATSM , also generated H_2 at similar overpotentials. In the case of $\text{Zn}(\text{ATSM})$ the mechanism was more complicated than just a CECE mechanism, as the catalyst was second order, Figure III-3. Due to the reaction order of $\text{Zn}(\text{ATSM})$ a molecule could be protonated and reduced and combined with a second protonated and reduced species to generate H_2 . Additionally, it could also undergo a second protonation step prior to dimerization to generate H_2 . Due to the dimerization, proton rearrangement was not seen. The related complexes, $\text{Cu}(\text{ATSM})$ and $\text{Ni}(\text{ATSM})$ as well as their derivatives, saw proton rearrangement prior to the release of H_2 .⁵⁸⁻⁵⁹ This proton rearrangement in all cases saw the complexes achieve HER, albeit at larger overpotentials. In the current study, we show that the HER activity previously reported for the related BTSC complex $\text{Zn}(\text{ATSM})$ is retained upon substitution of one thiosemicarbazone with a pyridyl functional group, Scheme III-2.

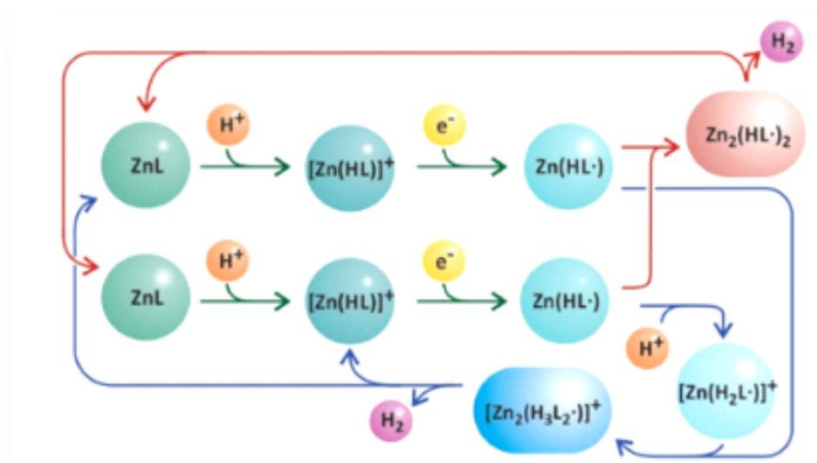
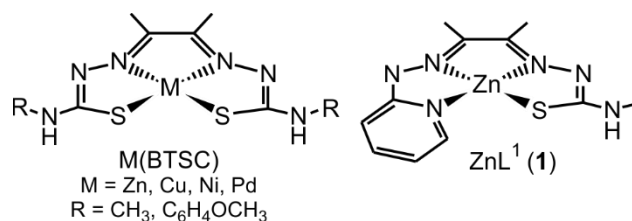


Figure III-3. CECE mechanism of Zn(ATSM). *Reproduced from Beyond Metal Hydrides: Non-Transition-Metal and Metal-Free Ligand-Centered Electrocatalytic Hydrogen Evolution and Hydrogen Oxidation.*⁴⁵

Scheme III-2. Comparison of BTSC complexes with Zn(DMTH).



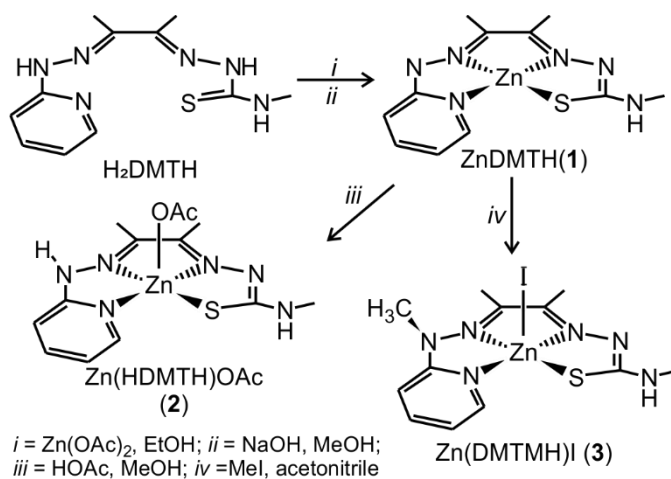
3.2 Synthesis and Characterization

3.2.1 General Synthesis, NMR, FT-IR, and UV/Vis of Compounds

The compounds $\text{Zn}(\text{DMTH})(\text{CH}_3\text{OH})$ (**1**), $\text{Zn}(\text{HDMTH})\text{OAc}$ (**2**), and $\text{Zn}(\text{DMTMH})\text{I}$ (**3**) were prepared as shown in Scheme III-3. The ligand H_2DMTH was synthesized as previously reported by Cowley.⁵⁵ The single crystal X-ray structure of **1**· CH_3OH was published previously by Dilworth and coworkers, however no synthetic procedure for **1** was reported.⁵⁶ The synthesis of the related aqua complex $[\text{Zn}(\text{DMTH})\text{H}_2\text{O}] \cdot 2\text{H}_2\text{O}$ is known.⁵⁶ We prepared **1** by addition of zinc acetate to an

ethanol solution of the H₂DMTH yielding a yellow precipitate following reflux. Addition of excess sodium hydroxide to the crude product in methanol allowed isolation of pure **1** as a dark orange solid upon workup. The ¹H and ¹³C NMR of **1** is consistent with those reported for [Zn(DMTH)H₂O]·2H₂O, including resonances for the coordinated methanol, Appendix A Figure A-5. The FT-IR of **1** is consistent with that of [Zn(DMTH)H₂O]·2H₂O, with the exception that **1** shows a broad absorption peak at 3300 cm⁻¹ characteristic of the methanol O-H stretch, while [Zn(DMTH)H₂O]·2H₂O shows a broad water absorption peak near 3200 cm⁻¹, Appendix A Figure A-6. For **1**, a band at 1388 cm⁻¹ assigned to the C-O-H stretch of methanol is also observed.

Scheme III-3. Synthetic routes for compounds 1 – 3.



Protonation of **1** with acetic acid in methanol or acetonitrile resulted in a color change from orange to yellow associated with formation of **2**. The electronic spectrum of **1** in MeCN has a broad feature near 500 nm and sharp peaks at 324 and 274 nm, Figure III-4A. Upon addition of acetic acid, the solution changes color from red-orange to yellow due to loss of intensity of the 500 nm band. The new features of **2** grow in at 329 and 420

nm with isosbestic points at 295 and 360 nm consistent with protonation of the hydrazino-nitrogen.

The ^1H NMR for **2** in DMSO-d_6 displays a peak at 9.73 ppm that indicates protonation of the hydrazino pyridine moiety, Appendix A Figure A-11. Furthermore, a peak at 1.80 indicates a coordinated acetate. Analysis of the region from 6.8-8.2 ppm shows five prominent signals: 6.80, 7.21, 7.23, 7.82, and 8.14 corresponding to the protons on the pyridine moiety and the amine on the TSC. The FT-IR reveals an N-H stretch at 3360 cm^{-1} and three bands at 3241, 2935, and 1640 cm^{-1} assigned to the coordinated acetate, Appendix A Figure A-12. Resistance measurements, Appendix A Table A-4, show that the $\text{Zn}(\text{HDMTH})(\text{OAc})$ complex is mostly covalent in nature, indicating the acetate anion stays bound to the axial position.

The UV-visible spectrum of **2** in acetonitrile shows two bands at 329 nm and 420 nm, Figure III-4B. Upon addition of acid the peak at 420 nm decreases in intensity and the band at 329 nm increases with an isosbestic point at 360 nm. To confirm the identity of new species as $\mathbf{2-H}^+$, crystals of **2** were dissolved in DMSO-d_6 and HPF_6 was added, Appendix A Figure A-14. Analysis via ^1H NMR showed two new peaks at 11.54 and 10.30 ppm, each integrating to 0.37 H with respect to the hydrazino nitrogen, attributed to two forms of $\mathbf{2-H}^+$ in equilibrium. One protonation site is assigned as the neighboring imido on the pyridine side and the other to the opposite hydrazino nitrogen on the thiosemicarbazone side.

Compound **3** was prepared as an air stable, brown/yellow solid by methylation of **1** in MeCN upon reflux. The ^1H NMR in DMSO shows a resonance at 3.62 ppm assigned

to the N-CH₃ protons in addition to the backbone methyl resonances at 2.07 and 2.33 ppm and the peak at 2.90 is the TSC methyl resonance, Appendix A Figure A-7. The region from 7.2 – 8.1 ppm contains a single set of peaks at 7.16, 7.38, 8.04, and 8.10 ppm assigned to the pyridine moiety and a broad singlet at 7.86 ppm for the NH of the pendant amine of the TSC. The FT-IR of **3** reveals a broad peak at 1080 cm⁻¹, and a shift in a peak at 1219 cm⁻¹ from 1214 cm⁻¹. These are indicative of changes in the C=N in the imines of the backbone, Appendix A Figure A-8. Resistance measurements, Appendix A, Table A-4, show that the complex is more ionic in nature, indicating an on/off coordination environment for the iodide anion.

The UV/vis spectrum of **3** in MeCN includes two bands at 304 nm and 420 nm, Figure III-4C. Upon addition of acid the band at 304 nm increases along with a decrease in intensity of the band at 420 nm. This results in an isosbestic point at 380 nm. To further probe the identity of **3-H**⁺, complex **3** was dissolved in DMSO-d₆ and an excess of HPF₆ was added, Appendix A Figure A-15. The ¹H NMR clearly demonstrates new features at 11.54, 10.53, and 10.24 ppm consistent with protonation at the coordinated amido nitrogens and the hydrazino nitrogen. The integration of all three new peaks is approximately 1/3 of a proton each with respect to the backbone methyl integration indicating tautomerization over the three sites.

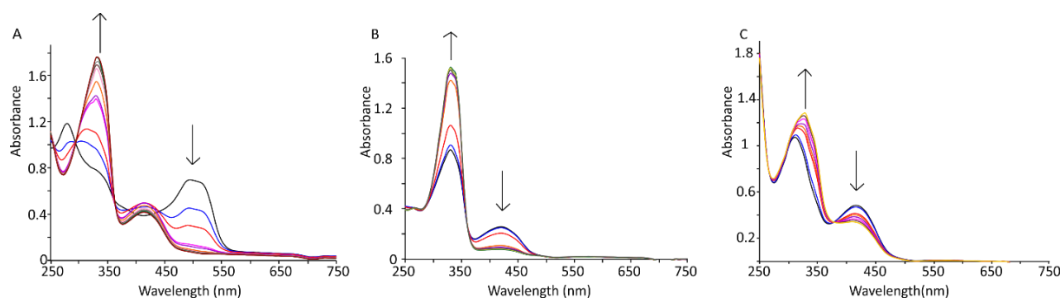


Figure III-4. UV/visible spectra in acetonitrile of **1** – **3** titrated with acetic acid.

(pathlength = 1 cm) of: A. 0.1 mM of **1** titrated with 0.01 M acetic acid from 0.1 equivalent to **1** equivalent. B. 0.1 mM **2** titrated with 0.1 M acetic acid from 2 to 16 equivalents. C. 0.1 mM of **3** titrated with 0.1 M acetic acid from 2 to 16 equivalents.

3.2.2 Structural Determination

Slow evaporation of a methanol solution of **1** yielded triclinic crystals with unit cell parameters consistent with those of the previously reported **1** structure. Single crystals of **2** and **3** were obtained upon slow evaporation of an acetonitrile:methanol:acetone mixture (1:1:1). Crystal data and structure refinement details for **2** and **3** are listed in Appendix A, Table A-1. A comparison of selected metric parameters for **1** – **3** and the related complex $[\text{Zn}(\text{HDMTH})\text{H}_2\text{O}]\text{NO}_3$ (**2'**)⁵⁶ is provided in Appendix A, Table A-3.

ORTEP representations⁹² of **2** and **3** are provided in Figure III-5. Each complex contains Zn in a square pyramidal environment with the metal sitting slightly above the basal plane defined by the N₃S donor atoms of the L¹ chelate. The axial position is occupied by acetate in **2** and iodide in **3**. The protonated hydrazino N in **2** is best described as trigonal planar with a C-N_{ImPyr}-N_{HyPyr}-H torsion angle of 14°, which is similar to that in **2'**, 6.7°. In contrast, the methylated hydrazino N in **3** is distorted towards pyramidal as evidenced by

the C-N_{ImPyr}-N_{HyPyr}-CH₃ torsion angle of 43°. This is attributed to steric interactions between the hydrazino-N and backbone methyl groups. The metal-ligand bond distances in **2** and **3** are similar to those in **1** and **2'**, Appendix A, Table A-3. Differences in the Zn-N_{Pyr} and Zn-N_{ImPyr} bond distances between the complexes are attributed to electronic effects associated with modification of the nearby hydrazino N environments and coordination of anions in the axial position.

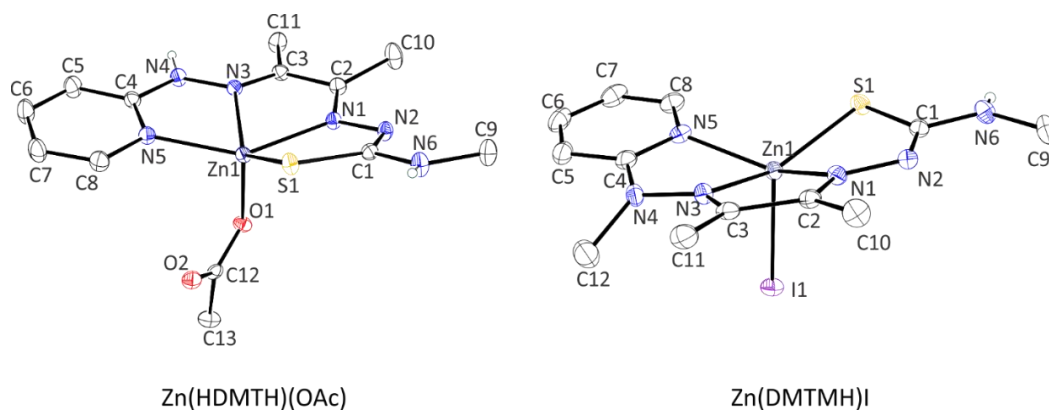


Figure III-5. ORTEP⁹² representations of Zn(HDMTH)(OAc) and Zn(DMTMH)I.

3.2.3 Electrochemical Characterization

The cyclic voltammogram (CV) of **1** in acetonitrile, Figure III-6A black, displays an irreversible one electron reduction at -2.47 V and an irreversible one electron oxidation at -0.36 V. Scans of only the anodic region confirm the one electron oxidation is not coupled to the one electron reduction, Figure III-6B black. All reported potentials listed are referenced to the Fc⁺/Fc couple ($E_{1/2} = 0.48$ V vs Ag/Ag⁺). The reduction of -2.47 V is slightly more cathodic than that of ZnATSM, which is -2.15 V in acetonitrile.⁴⁵ The CV of **2** in acetonitrile shows three one-electron reduction events at -2.23 V, -2.46 V, and -2.87 V and a one electron oxidation event at -0.17 V, Figure III-6A blue. The reduction event at -2.23 V is assigned to the **2/2**⁻ redox couple, which is shifted by +0.23 V with respect to

1/1⁻. Reduction of **2** to **2**⁻ increases the basicity of the ligand resulting in proton transfer near the electrode to generate a mixture of **1**, **2**, and **2-H**. This process facilitates the peak at -2.46 V, which is at the same potential of that of **1/1**⁻. The final reduction event at -2.87 V is attributed to generation of a small amount of H₂. Furthermore, the oxidation peak is likely associated with the **2/2**⁻ couple as no peak exists if an anodic scan is completed, Figure III-6B blue. The CV of **3** in acetonitrile shows two irreversible reduction events at -1.79 V and -2.02 V and three irreversible oxidation events at -0.19 V, 0.06 V, and 0.38 V, Figure III-6A red. The more cathodic reduction is assigned to **3/3**⁻ couple, for which the iodide remains coordinated to the metal center. The event at -1.79 V is attributed to reduction of **3'**, which results from dissociation of iodide from Zn in solution. The oxidation event at 0.38 V is attributed the oxidation I⁻ to I₂.⁹³ All oxidations are observed when only the anodic region is scanned, Figure III-6B red. A compilation of diffusion coefficients can be found in Appendix A, Table A-5.

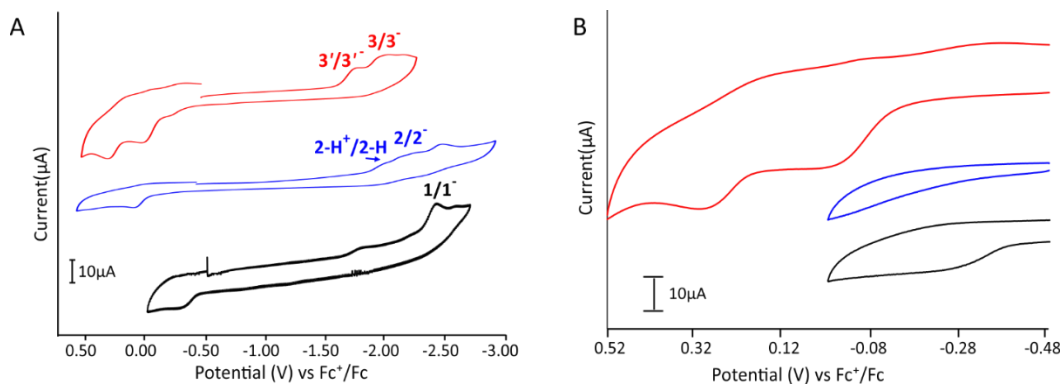


Figure III-6. A. CVs of 1.0 mM **1** (black), **2** (blue), and **3** (red) in acetonitrile containing 0.1 M Bu₄NPF₆ as supporting electrolyte. Data were recorded at a scan rate of 0.2 V/s. B. Vs of 1.0 mM **1** (black), **2** (blue), and **3** (red) in acetonitrile containing 0.1 M Bu₄NPF₆ as supporting electrolyte when scanned anodically.

3.3 Homogenous Catalytic Hydrogen Evolution

The catalysts Zn(DMTH) and Zn(DMTMH) were both examined for the hydrogen evolution reaction (HER). They were first examined through cyclic voltammetry experiments and then through controlled potential coulometry for faradaic yields and proof of catalysis.

3.3.1 Cyclic Voltammetry

Addition of acetic acid to a 1 mM solution of **1** in acetonitrile exhibits a catalytic wave at -3.29 V, Figure III-7A. The current is significantly higher than the background reduction of acetic acid at the glassy carbon electrode. At lower acid concentrations, a pre-peak attributed to **2-H**⁺ is observed at -1.81 V that shifts to -1.74 V under successively more acidic conditions. Under saturating acid conditions this peak is hidden by the catalytic wave. Based on the background corrected current under saturating conditions, the estimated TOF is calculated as 7700 s⁻¹. The overpotential was calculated as 1.27 V from

the $E_{\text{cat}/2}$ value of -2.67 V using the method of Artero and coworkers.⁷⁶ However, due to homoconjugation, the real overpotential is 1.45 V. The reaction is first-order in **1** and second order in acid, Figure III-8A-C. Under large acid concentrations it is clear that some side phenomena could be observed as the CV appears not under diffusion control, Appendix A Figure A-17. The most common side phenomena are “consumption of the substrate, deactivation of the catalyst, and inhibition by products.”⁹⁴ The most likely of this is consumption of the substrate at the electrode as this process is undergoing catalysis, however it is also possible that this is evidence for a buildup of an electroactive film. Since acetic acid in acetonitrile can sometimes give “false” second order plots,⁹⁵ catalytic experiments were repeated with phenol, Appendix A Figure A-19. These experiments confirmed the reaction is second order with respect to acid, Figure III-8D,E. Kinetic isotope studies done using *d*₁-acetic acid (CH₃OOD) yielded a KIE of $1.66 \pm .15$, Appendix A Figure A-20,A-21. The KIE is similar to that reported for Zn-ATSM, which is proposed to proceed via a ligand hydride mechanism with attack by the hydride on a proton in solution or bound to ligand/metal framework.⁴⁵ Further studies using the exceedingly weak acid methanol show no catalysis, indicating that methanol is not strong enough to doubly protonate the complex **1**, Appendix A Figure A-22.

Addition of acetic acid to a 1 mM acetonitrile solution of **3** yielded a catalytic wave with peak current at -2.15 V and an onset potential of -1.49 V. A pre-peak is observed at -1.81 V under low acid concentrations (< 0.030 M). The pre-peak is indicative of protonation of **3** to generate **3-H**⁺. At acid concentrations > 0.030 M, the pre-peak is obscured by the catalytic wave. Notably, at acid concentrations > 0.072 M the catalyst becomes inactivated. Based on the current under scan-rate independent conditions in 0.072

M acetic acid solution, the TOF is calculated as 6700 s^{-1} at an overpotential of 0.56 V with $E_{\text{cat}/2} = -1.95 \text{ V}$, Figure III-7B. However, when recalculated due to homoconjugation the overpotential is 0.72 V. The catalytic current shows a second-order dependence with respect to acid and first-order dependence with respect to catalyst, Figure III-8F,G. Kinetic isotope studies with deuterated acetic acid resulted in a KIE of 1.30 ± 0.23 similar to **1**, Appendix A Figure A-27,A-28.

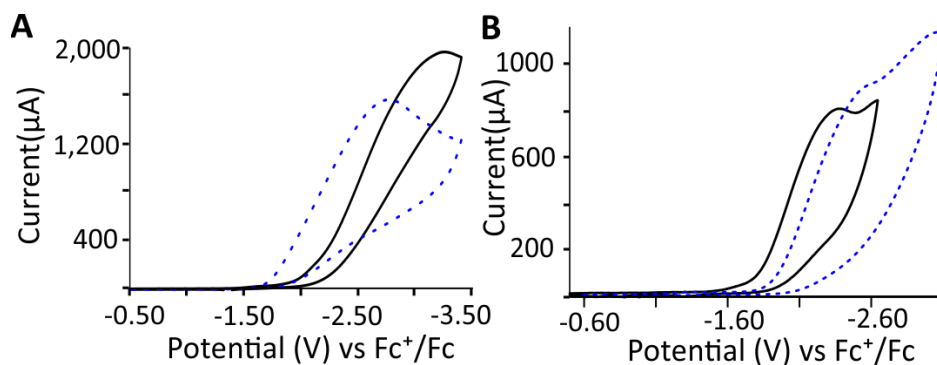


Figure III-7. CVs recorded in acetonitrile at a scan rate of 0.2 V/s in 0.1 M Bu₄NPF₆. A) The blue dashed line is the background scan of 0.240 M acetic acid with no catalyst. The solid black line is the scan of **1** in the presence of 0.240 M acetic acid with the background scan of 0.240 M acetic acid subtracted. B) The blue dashed line is the background scan of 0.072 M acetic acid with no catalyst. The solid black line is the scan of **3** in the presence of 0.072 M acetic acid with the background scan of 0.072 M acetic acid subtracted.

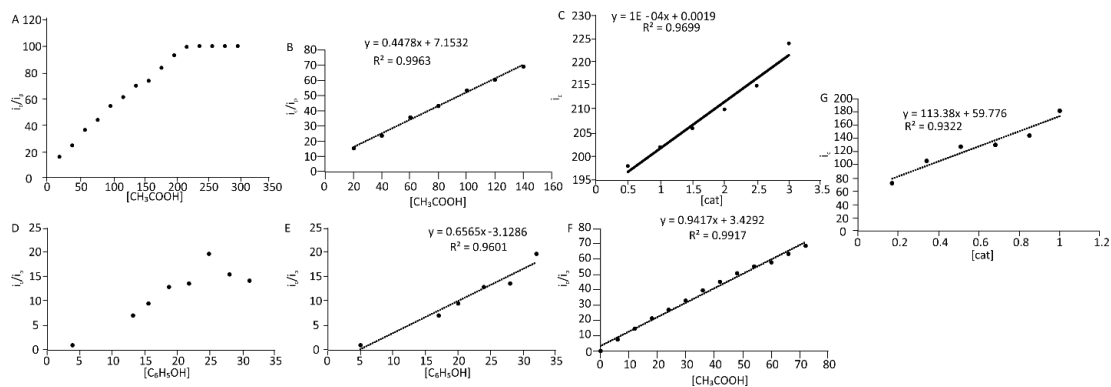


Figure III-8. Plots of i_c/i_p for ZnDMTH. A. i_c/i_p as a function of acid concentration for ZnDMTH B. The linear region of i_c as a function of acetic acid showing second order dependence. C. i_c/i_p as a function of catalyst concentration. D. i_c/i_p as a function of acid concentration for ZnDMTH utilizing phenol as a proton source. E. The linear region of i_c/i_p as a function of phenol for ZnDMTH showing second order dependence. F. The linear region of i_c/i_p as a function of acetic acid for Zn(DMTMH)I. G. i_c as a function of catalyst concentration for Zn(DMTMH)I.

3.3.2 Controlled Potential Coulometry

To quantify gas production and determine faradic efficiency, controlled potential coulometry was conducted in acetonitrile at an applied potential of -2.60 V for **1** and -1.80 V for **3** vs Ag/AgCl, Figure III-9. Analysis of a sample of the headspace gas by gas chromatography confirmed the product as hydrogen. Compound **1** generated 6.89 mL of gas over a two hour period. Control experiments in the absence of **1** at this potential yielded 2.26 mL over the same time period. Based on a total volume of hydrogen generated by the catalyst of 4.63 mL, this corresponds to a TON of 189 in 2 hours and a faradaic efficiency of 71%. For **3**, the total volume of gas produced, after correcting background reactivity of 0.20 mL associated with a TON of 8.4 and a faradaic efficiency of 89%. Data for these

experiments is tabulated in the supporting information, Appendix A, Table A-9. The relatively low TONs as compared to the TOFs results from the fact that only catalyst at the electrode surface actively generates hydrogen, but the bulk concentration of the catalyst is used to calculate the TON values.

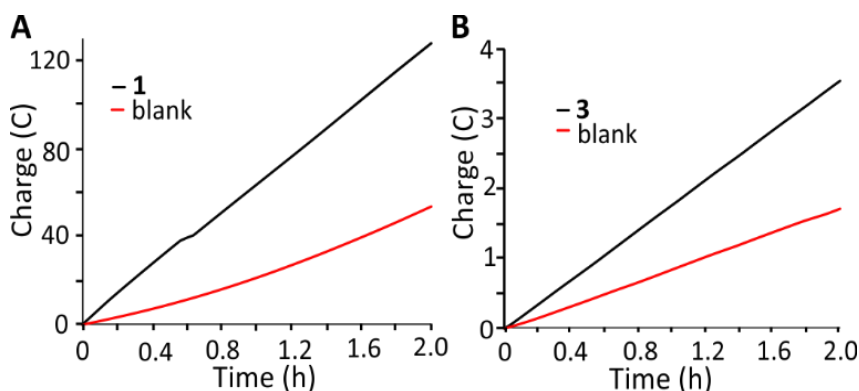


Figure III-9. Controlled potential coulometry for two hours for **1** at an applied potential of -2.60 V vs. Ag/AgCl (A) and **3** at an applied potential of -1.80 V vs. Ag/AgCl.

3.4 Control Experiments

Due to the adhesion of CuATSM to the electrodes surface after large periods of electrocatalysis, control experiments were conducted in the same manner.⁶³ The findings were that under prolonged electrochemical experiments Zn(DMTH) and Zn(DMTMH) bound to the electrodes surfaces after prolonged electrochemical experimentation, however did not bind under short term or fresh scans.

3.4.1 Soak Test

To determine if complexes chemically adsorb to the glassy carbon electrode, a soak test was performed for both **1** and **3**. The electrode was placed in a solution containing catalyst, substrate, solvent, and supporting electrolyte overnight. The electrode was removed from the solution, rinsed, and placed into a fresh solution of electrolyte. For both

1 and **3**, no peaks were observed, even upon addition of substrate, indicating that no significant quantities of catalyst chemically adsorbed on to the electrode under these conditions, Appendix A Figures A-31,A-32.

3.4.2 Post CV Dip-test

To determine if catalysts adsorb to the electrode under electrocatalytic conditions, a post CV dip test was performed for both **1** and **3**. CV data were collected under acid saturating electrocatalytic conditions. The glassy carbon electrode was removed, rinsed, and placed into a fresh solution of electrolyte and the CV recorded. For **1**, after 10 cycles the electrode showed no significant peaks when placed in a fresh solution, even upon addition of 0.240 M acetic acid, Figure III-10A and Appendix A Figure A-33. However, when the test was repeated using 30 cycles a peak at -2.65 V was observed upon placing the electrode in fresh electrolyte suggesting that some of **1** had adsorbed on the electrode, Figure III-10B and Appendix A Figure A-34. Addition of acid confirmed that the adsorbed species was catalytically active for HER, Figure III-10C. For **3**, after 10 cycles under acid saturated conditions, the electrode showed small peaks at -1.72 V and -2.04 V when placed in a fresh solution of electrolyte consistent with adsorption of **3**, Figure III-10D, and Appendix A Figure A-35. Upon addition of acid, electrocatalytic HER is observed, Figure III-10E. These results indicated that upon prolonged cycling, a significant amount of HER activity is likely due to adsorbed catalyst. However, since initial cycles show catalytic activity that cannot be attributed to adsorbed complex, both **1** and **3** are competent homogeneous HER catalysts.

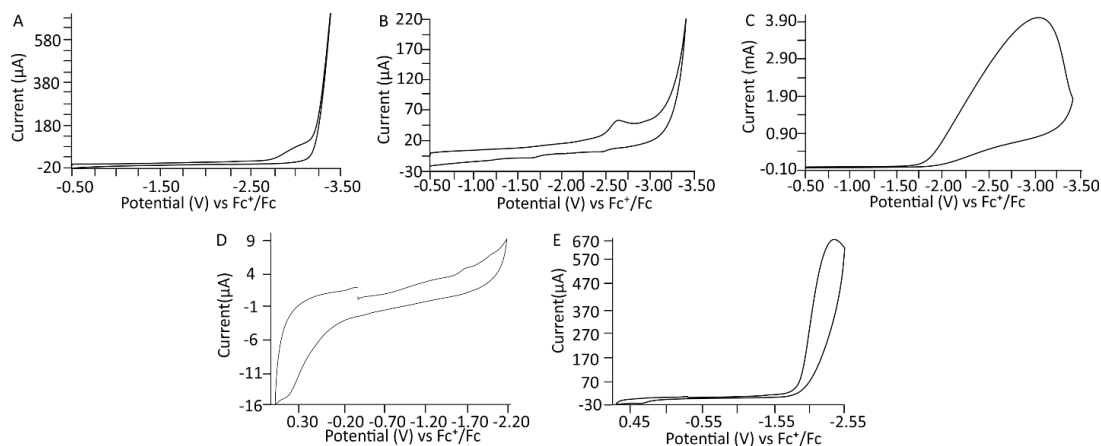


Figure III-10. Cycle test CVs. A. Cyclic voltammetry of post 10-cycle test of Zn(DMTH). B. Cyclic voltammetry of post 30-cycle test of Zn(DMTH). C. Cyclic voltammetry of post 30-cycle test of Zn(DMTH) with 0.240 M acetic acid. D. Cyclic voltammetry of post 10-cycle test of Zn(DMTMH)I. E. Cyclic voltammetry of post 10-cycle test of Zn(DMTMH)I with 0.072 M acetic acid.

3.4.3 Post Electrolysis Dip-test

To further investigate the adsorption of catalyst on the electrode during prolonged electrocatalytic activity, bulk electrolysis was performed in acetonitrile with 0.240 M or 0.072 M acetic acid for **1** and **3** at applied potentials of -3.10 V and -2.30 V, respectively. 0.240 M and 0.072 M acetic acid were chosen due to those being the concentrations used in the CPC experiments. As in the other control experiments, the electrode was then rinsed and placed in a fresh solution of electrolyte and CV data was collected. As described below, the results confirm the adsorption of both **1** and **3** as catalytically active films on glassy carbon.

For **1**, the CV of the glassy carbon electrode post-electrolysis showed reduction events at -0.60 V and -2.10 V in the absence of acid, Figure III-11A. Additionally, an

oxidation occurs at -0.10 V that is substantially larger in current in comparison to the reduction events attributed to desorption of complex from the electrode's surface. When 0.240 M acetic acid is added to this solution a pre-peak is observed at -1.10 V along with a catalytic peak at -2.10 V, Figure III-11B. Notably, the catalytic peak for HER is shifted by 1.2 V relative to the homogeneous solution value of -3.29 V. A similar shift of ~1.2 V was observed for the HER activity of Cu(ATSM) upon adsorption on glassy carbon.⁵⁸ Recently, we also reported significant anodic shifts in HER overpotential for planar Ni(ATSM) derivatives adsorbed on glassy carbon upon conditioning of the electrode through repeated cycling.⁶³ To confirm the identity of the adsorbed species deposited during bulk electrolysis of **1**, the film was removed from the electrode surface and analyzed by XPS.

For **3**, the catalyst was subjected to a bulk electrolysis over 24 hours at an applied potential of -2.30 V. After CPE, the electrode was rinsed with DI H₂O and placed into a fresh electrolyte solution and the CV was scanned between -2.40 and 0.60 V. Two reductions events were observed at -1.30 V and -1.90 V along with two oxidation events at -0.30 V and 0.10 V, implying an electroactive compound is deposited on the electrode surface during electrolysis, Figure III-11C. The film is catalytically active for HER with a peak current of 690 μ A at -2.05 V under acid saturating conditions, Figure III-11D. This is similar to the catalytic activity observed for the film of **3** deposited during the post-CV dip test.

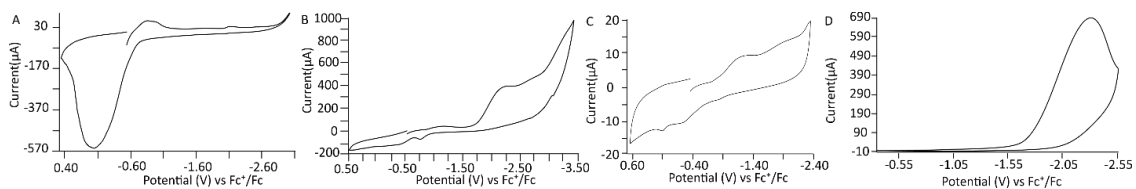


Figure III-11. Post CPC CVs. A. CV of the electrode post 24 hour CPC of Zn(DMTH) and 0.240 M acetic acid. B. CV of the electrode with 0.240 M acetic acid added post 24 hour CPC of Zn(DMTH) and 0.240 M acetic acid. C. CV of the electrode post 24 hour CPC of Zn(DMTMH)I and 0.072 M acetic acid. D. CV of the electrode with 0.072 M acetic acid added post 24 hour CPC of Zn(DMTMH)I and 0.072 M acetic acid.

3.4.4 XPS Film Analysis

To identify the composition of the catalytically active films deposited during the control experiments, the electrolysis conditions for the post-electrolysis dip-test were repeated and the coating on the electrode surface was analyzed by XPS Appendix A Figures A-38-A-42 and Tables A-10-A-12. For **1**, the coating showed atomic percentages for N:Zn:S in an approximately 6:1:1 ratio consistent with the parent compound. Further, the XPS showed two peaks for nitrogen consistent with the intact complex having a sp^2 and a sp^3 hybridized nitrogen. The carbon percentage in the coating could not be determined due to the large signal from the glassy carbon electrode and/or adventitious carbon. Films of **3** showed a N:Zn ratio of 6:1 with a variable amount of S (0.3 – 0.5 equivalents) and less than 0.1 equivalent of iodide. Since XPS is extremely surface sensitive, the variability and low quantity of the S could indicate that not all of the sulfurs are on the surface of the adsorbed species. However, we cannot exclude the possibility that some ligand degradation of **3** occurs. The marginal amount of iodide indicates the film contains the cation **3'** (iodide dissociated) that is charge balanced by PF_6^- . Further XPS

elemental mapping shows that the N1s and Zn2p elemental maps overlap, indicating that the complex is likely still intact despite the low sulfur concentrations.

3.4.5 Post Electrolysis Rinse Test

Since the post-electrolysis dip-test produced an electrocatalytically active film over a prolonged timeframe (24 hours), a post-electrolysis rinse test was conducted over a shorter timeframe (2 hours) for comparison with the CPC experiments. In a typical experiment, an acetonitrile solution of **1** containing 0.1 M NBu₄PF₆ and 0.240 M acetic acid was subjected to CPC for 2 hours. The electrodes were then removed and rinsed with DI H₂O. The electrodes were then placed into a clean cell containing 0.1 M NBu₄PF₆ and 0.240 M acetic acid, but no catalyst. A second 2 hour CPC was then completed. Similar experiments were conducted for **3**. For both complexes **1** and **3**, appreciable charge was produced in the initial CPC but after rinsing the electrode no significant charge above the acid-blank experiment was observed, Appendix A Figure A-42,A-43. This indicates that an electrocatalytically active film is not generated over the timeframe of the 2 hour CPC experiments. All catalysis under these conditions is attributed to homogeneous catalysis and not heterogenous catalysis.

3.5 Density Functional Theory Investigations

To explore the mechanism of the H₂ evolution a series of density functional theory (DFT) calculations were performed on **1** (S = 0, q = 0) and its protonated and reduced derivatives **2** (S = 0, q = 0), **2-H⁺** (S = 0, q = +1), **2-H** (S = ½, q = 0), **2-H₂⁺** (S = ½, q = +1), and **2-H₂** (S = 0, q = 0). The initial structure for the calculations were taken from crystal structure data. The model structures were then optimized with DFT using the B3LYP functional and 6-311g (d,p) basis set.⁷¹⁻⁷² This level of theory has been shown to be reliable

for similar complexes.⁵⁹ The calculations were carried out in solvent employing polarizable continuum model (PCM) using acetonitrile as a solvent.⁷³ Verification of the computational methods were done by comparing the optimized bond distances to that of the crystallographic parameters, Appendix A, Table A-13. The thermodynamic feasibility of the interconversion of complexes through protonation or reduction steps was evaluated by the calculation of equilibrium constant (K) for chemical steps or reduction potential ($E_{1/2}$) for reduction steps. The thermodynamic parameter K was calculated by optimizing products and reactants and utilizing both acetic acid and acetate ions as independent calculations. The thermodynamic parameter $E_{1/2}$ was calculated by using both a direct reference to ferrocene and a Born-Haber cycle.⁹⁶ A summary of the calculations and a comparison of calculated vs experimental reduction potentials can be found Appendix A Table A-4 Figure A-46-A-54. It should be noted that the calculated K values are lower estimates as outer sphere interactions between the metal-containing cation and acetate counterion, which could stabilize the products, were not included.

The initial optimized structural model of the **1** was in good agreement with the crystal structure. The optimized structure is square planar with Zn-S and Zn-N bond distances within 0.1 Å of the experimentally determined values. To verify the location of the additional proton in **2**, the optimized structure of **1** was modified by addition of an acetate at the Zn center and addition of a hydrogen at all possible protonation sites of the ligand. Geometry optimizations were conducted for all the possible structures. Frequency calculations were also conducted after geometry optimizations to confirm that the optimized structure corresponds to a true minimum. Protonation at the hydrazino nitrogen N₄ was found to be energetically most stable, Figure III-12A. The next lowest energy

structure, with protonation at the opposite hydrazino nitrogen N2, was 7.6 kcal/mol higher. The calculated K for the protonation of **1** to **2** is 214 indicating the step is thermodynamically favorable.

Next, the protonation of **2** to **2-H⁺** was evaluated by addition of a proton to the lowest energy structures of **2**. Structures were then optimized and the stationary points were confirmed by frequency calculations. Protonation at the opposite hydrazino nitrogen N2 was energetically most stable, Figure III-12B, whereas protonation on sulfur was 8.0 kcal/mol energetically less favorable. Protonation at other nitrogen sites are 10.6 kcal/mol or higher in energy. The calculated K for the protonation of **2** to **2-H⁺** is 9.2×10^{-3} . While this step is not as favorable as **1** to **2**, under acid saturating conditions (0.240 M) **2-H⁺** should be the only component in solution.

To evaluate the initial reduction event, the possible structures of **2-H⁺** were re-evaluated as neutral, spin doublets and optimized with the same level of theory. The structure with protons at both N2 and N4 remains the lowest energy structure for **2-H**, Figure III-12C. However, a tautomer with protons at the adjacent imido and hydrazino nitrogens N1 and N2 is only 1.6 kcal/mol higher in energy. The spin density distribution of the lowest energy structure shows delocalization over the ligand backbone. The calculated reduction potential for **2-H⁺** to **2-H** of -1.82 V is in good agreement with the experimental reduction potential of -1.97 V.

Based on the experimental observation that HER with **2** is second-order in acid, we next evaluated the addition of another proton to the lowest energy structures of **2-H** to yield the cationic, spin doublet **2-H₂⁺**, Figure III-12D. The possible protonation combinations

were then optimized with frequency calculations. The most favorable of all the optimized structures has protons at N1, N2, and N4, Figure III-12D. The next lowest energy structure is 5.3 kcal/mol higher in energy with protons on N2, N4, and N5. The calculated K for the protonation of **2-H** to **2-H₂⁺** was found to be 56 indicating that this is a thermodynamically competent route under acid saturating conditions.

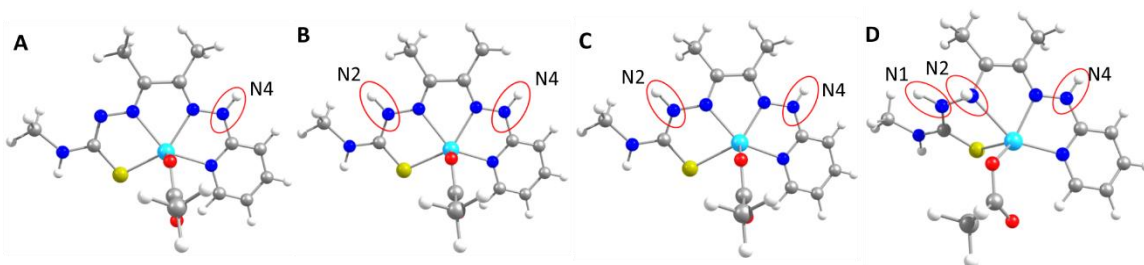


Figure III-12. Lowest energy calculated structures. Protonation sites circled in red for A. **2**, B. **2-H⁺**, C. **2-H**, and D. **2-H₂⁺**.

Since the protonation of **2-H** to **2-H₂⁺** is thermodynamically favorable, we further evaluated its potential role in HER. Addition of an electron to **2-H₂⁺** yields the proposed hydrogen evolving complex **2-H₂**. Three viable structures are located within 4.6 kcal/mol of each other, Figure III-13. Interestingly, the lowest energy structure is distorted towards trigonal bipyramidal of the central zinc atom with protons at N1, N3, and N4. The H-N3-N4-H torsion angle is 48.2°. The next lowest energy structure (+1.4 kcal/mol) is tetrahedral with protons at N2, N3, and N4 with a H-N3-N4-H torsion angle of 96.6°. The final optimized structure is a distorted square pyramid with protons at N1, N2, and N4 is 4.6 kcal/mol above the minimum. The H-N1-N2-H torsion angle is 54.7° respectively. The calculated reduction potential was found to be between -1.1 and -1.3 V indicating that reduction of **2-H₂⁺** is much easier than reduction of **2-H**. This event is observed

experimentally in the CV under acid saturating conditions in which case the prepeak associated with reduction of **2-H** is obscured by the catalytic current. Based on these calculations it cannot be determined which of these species, or combination of species, contributes to H₂ evolution.

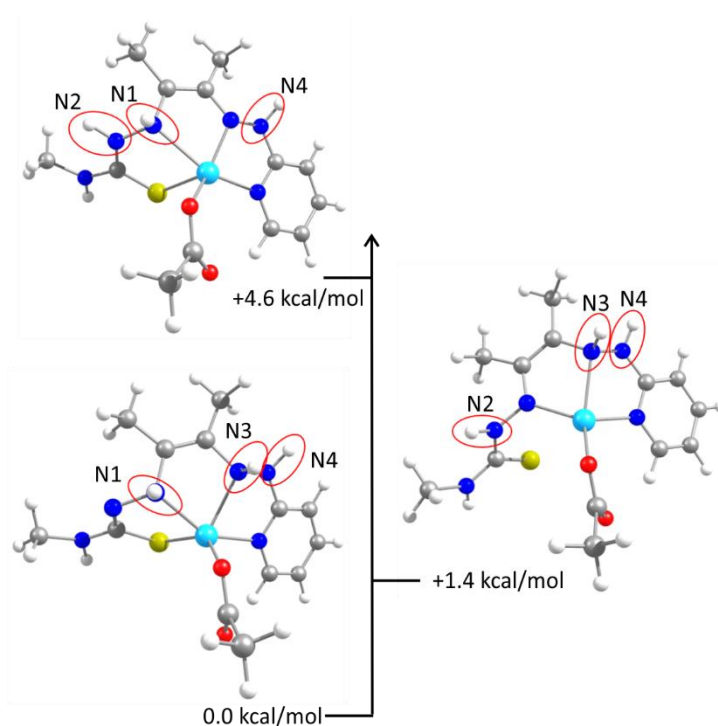


Figure III-13. Three lowest energy calculated structures of **2-H₂**. Protonation sites circled in red.

The analogous methylated species was calculated as the monocation **3-H₂⁺** with no coordinated acetate. In the absence of coordinated acetate, the complex adopts a tetrahedral-like environment for the central zinc atom. The likely hydrogen evolving N1, N2 protonated species was lowest in energy. However, other tautomers are within 3.3 kcal/mol. The coordination of acetate is proposed to occur under high concentrations of acid corresponding with the loss of HER activity.

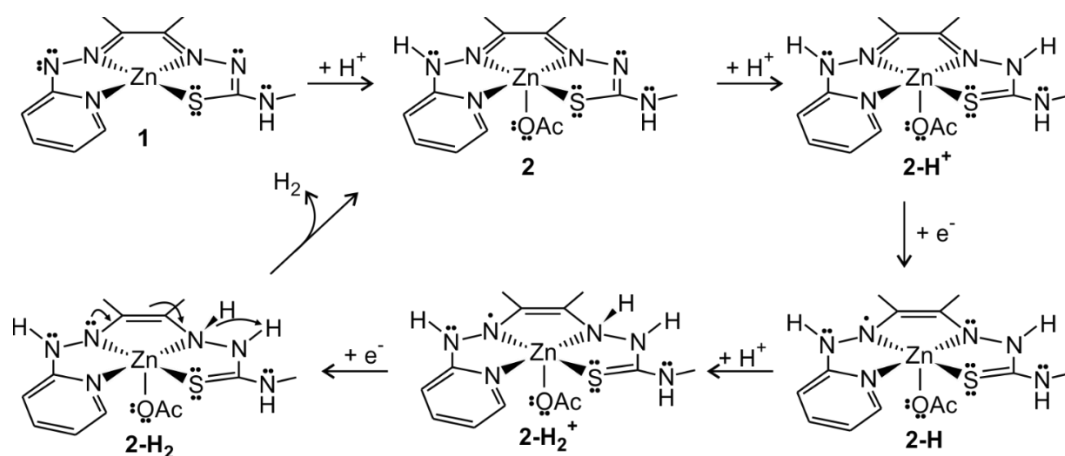
An alternate HER pathway for **2**, which does not require protonation to **2-H₂⁺** was also considered. This route presumes H₂ release upon direct reduction of the low lying HN1-N2H tautomer of **2-H**. The calculated reduction potential for **2-H**, -2.47 V, is accessible at E_{cat/2} value of -2.67 V and this route cannot be excluded. This route is not available for **3** due to the methylation of the hydrazino nitrogen N2.

3.6 Proposed HER Mechanism

A proposed HER mechanism based on experimental and computational results is shown in Scheme III-4. Compound **1** serves as a precatalyst that is protonated to yield the active catalyst **2**. Complex **2** evolves hydrogen via a CECE mechanism in which C represents a chemical step (protonation) and E is an electrochemical step (reduction). Ligand-centered protonation of **2** to **2-H⁺** is followed by ligand-centered reduction to yield **2-H**. The second protonation step of the cycle yields **2-H₂⁺**. The final reduction yields the hydrogen evolving complex **2-H₂** for which three energetically plausible structures were identified computationally. Our proposed mechanism prefers the distorted square pyramidal structure as it yields the lowest energy structure of **2** upon H₂ evolution, Scheme III-4. The proposed mechanism for **3** is an analogous CECE pathway in which the proton on N4 in **2** is substituted with a methyl group, and no coordination of the acetate ligand. The mechanism for Zn(DMTH) is clearly wildly different from that of Zn(ATSM) and much closer to that of Cu(ATSM). In the case of Zn(ATSM), Cu(ATSM), Zn(DMTH), and Zn(DMTMH), protonation occurs on the hydrazino nitrogen in the first step. From there the mechanism varies. In the case of Zn(ATSM) and Cu(ATSM), both undergo a reduction event post protonation. For Cu(ATSM), this results in a protonation event on the opposing hydrazino nitrogen. For Zn(ATSM), complication occurs at this point as it can either

undergo a protonation like that of Cu(ATSM), or it can combine with another protonated reduced species to release H₂. It can also after undergoing the second protonation combine with a neutral protonated reduced species to release H₂. These complications are not seen with Cu(ATSM) as after it is protonated, reduced, and protonated, it can be reduced again and from there proton tautomerization is seen to generate H₂.

Scheme III-4. Proposed HER mechanism.



3.7 Conclusion

In the current study, we show that the HER activity previously reported for the related BTSC complex Zn(ATSM) is retained upon substitution of one thiosemicarbazone with a pyridyl functional group in **2** and **3** allowing for further expansion and refinement of this class of non-innocent ligands for HER. Re-evaluation of the TOF for Zn(ATSM) using the equation $\text{TOF} = 1.94v(i_c/i_p)^2$ gives a value of 4000 s^{-1} for Zn(ATSM) at an overpotential of 1.04 V. Catalysts **2** and **3** yield a TOF of $\sim 7000 \text{ s}^{-1}$ at scan rate independent conditions. This indicates a higher TOF was achieved, albeit at a higher overpotential.

The protonated complex **2** requires a significantly larger overpotential, 1.45 V, than the methylated complex **3**, 0.72 V, to achieve similar TOFs. The 730 mV shift in overpotential is attributed to a combination of two factors, see Figure III-14. The first is a charge effect (a) accounting for a 440 mV shift in overpotential. Whereas **2** is neutral in solution with a coordinated acetate, the weakly coordinating iodide of **3** dissociates in solution to generate the monocationic species **3'**. As a result, $E_{1/2}$ for the cationic **3'** is 440 mV more accessible than the $E_{1/2}$ for **2**. This accounts for the majority of the 730 mV difference in overpotential for the two catalysts. A similar shift was seen by Rochford and coworkers where a protonation first pathway reduced the reduction potential by 450 mV.⁹⁷

The remaining difference in overpotential of ~290 mV is attributed to differences in the rate of intramolecular proton transfer. As noted by Nocera and co-workers, catalysts operating via intermolecular proton transfer typically show $E_{cat/2}$ values near the thermodynamic $E_{1/2}$ value of the catalyst, while intramolecular proton transfer shifts $E_{cat/2}$ to more negative reduction potentials dependent on the scan rate.⁹⁸ As shown in Figure III-14, the difference between $E_{cat/2}$ and $E_{1/2}$ is larger for **2** (440 mV) than for **3'** (160 mV) indicating a larger kinetic barrier to intramolecular proton transfer in the former. Whereas the hydrogen evolving complex **2-H₂** has three energetically accessible tautomers, Figure 7, only one tautomer is possible in the **3'** derivative due to methylation at the N4 site. The 280 mV difference in these kinetic values accounts for the remaining ~290 mV difference in overpotential.

Overall, the ~730 mV difference in overpotential for **2** and **3'** results from a combination of charge effects, ~440 mV, and kinetic effects, ~290 mV. The results demonstrate the utility of ligand design to combine factors to substantially lower

overpotential. Further, the HER activity of **2** and **3'** demonstrates the flexibility of the thiosemicarbazone framework as a platform for non-innocent ligand derived electrocatalysts.

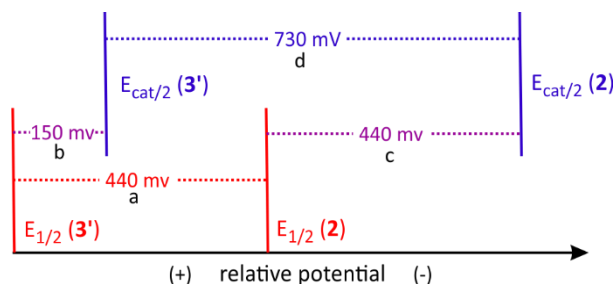


Figure III-14. Relative values of $E_{1/2}$ and $E_{cat/2}$ for **2** and **3'**. The difference in $E_{1/2}$ values (a) reflects the difference in charge of the two catalysts. The difference between $E_{cat/2}$ and $E_{1/2}$ for each catalyst (b and c) represents the kinetic barrier due to intramolecular proton rearrangement in that catalyst. The difference in overpotential is determined by the difference in $E_{cat/2}$ (d), which equals $a + c - b$.

3.8 Experimental Specific to Chapter 3

Synthesis for all compounds in Chapter 3 can be found in Chapter 2.

3.8.1 Crystallographic Studies

A thin yellow prism $0.27 \times 0.08 \times 0.06 \text{ mm}^3$ crystal of **2** grown from a solution of acetonitrile/methanol/acetone was mounted on a CryoLoop for collection of X-ray data on an Agilent Technologies/Oxford Diffraction Gemini CCD diffractometer. The CrysAlisPro⁹⁹ CCD software package (v 1.171.36.32) was used to acquire a total of 727 thirty second frame ω -scan exposures of data at 100 K to a $2\theta_{\text{max}} = 54.12^\circ$ using monochromated $\text{MoK}\alpha$ radiation (0.71073 \AA) from a sealed tube. Frame data were processed using CrysAlisPro⁹⁹ RED to determine final unit cell parameters: $a = 7.2770(3) \text{ \AA}$, $b = 7.6340(3) \text{ \AA}$, $c =$

17.8924(7) Å, $\alpha=91.102(3)$, $\beta=92.654(3)^\circ$, $\gamma=115.763(4)^\circ$, $V=893.35(6)$ Å³, $D_{\text{calc}}=1.442$ Mg/m³, $Z=2$ to produce raw hkl data that were then corrected for absorption (transmission min./max. = 0.907 /1.000; $\mu=1.508$ mm⁻¹) using SCALE3 ABSPACK.¹⁰⁰ The structure was solved by Direct methods in the space group P-1 using SHELXS¹⁰¹ and refined by least squares methods on F^2 using SHELXL¹⁰¹. Non-hydrogen atoms were refined with anisotropic atomic displacement parameters. Imine H's were located by difference maps and refined isotropically. Methyl hydrogen atoms were placed in their geometrically generated positions and refined as a riding model and these atoms were assigned $U(\text{H})=1.5 \times U_{\text{eq}}$. For all 3915 unique reflections ($R(\text{int}) 0.037$) the final anisotropic full matrix least-squares refinement on F^2 for 236 variables converged at $R1=0.033$ and $wR2=0.075$ with a GOF of 1.08.

A yellow prism 0.20 x 0.20 x 0.03 mm³ crystal of **3** grown from a solution of acetonitrile/methanol/acetone was mounted on a glass fiber for collection of X-ray data on an Agilent Technologies/Oxford Diffraction Gemini CCD diffractometer. The CrysAlisPro⁹⁹ CCD software package (v 1.171.36.32) was used to acquire a total of 857 forty second frame ω -scan exposures of data at 100K to a $2\theta_{\text{max}}=60.20^\circ$ using monochromated MoK α radiation (0.71073 Å) from a sealed tube. Frame data were processed using CrysAlisPro⁹⁹ RED to determine final unit cell parameters: $a=7.2994(3)$ Å, $b=12.8478(5)$ Å, $c=17.248(2)$ Å, $\alpha=90.0^\circ$, $\beta=90.0^\circ$, $\gamma=90.0^\circ$, $V=1617.5(2)$ Å³, $D_{\text{calc}}=1.929$ Mg/m³, $Z=4$ to produce raw hkl data that were then corrected for absorption (transmission min./max. = 0.663/1.00; $\mu=3.558$ mm⁻¹) using SCALE3 ABSPACK¹⁰⁰. The structure was solved by Direct methods in the orthorhombic space group P 2₁ 2₁ 2₁ using SHELXS¹⁰¹ and refined by least squares methods on F^2 using SHELXL¹⁰¹. Non-hydrogen

atoms were refined with anisotropic atomic displacement parameters. Imine H's and pyridyl H's were located by difference maps and refined isotropically. Methyl hydrogen atoms were placed in their geometrically generated positions and refined as a riding model and these atoms were assigned $U(H) = 1.5 \times U_{eq}$. For all 4750 unique reflections ($R(int) = 0.041$) the final anisotropic full matrix least-squares refinement on F^2 for 236 variables converged at $R^1 = 0.029$ and $wR^2 = 0.056$ with a GOF of 1.08.

3.8.2 Electrochemical Methods

General methods for cyclic voltammetry and CPC measurements can be found in Chapter 2. All cyclic voltammetry (CV) and controlled potential coulometry (CPC) measurements were recorded using a Gamry Interface potentiostat/galvanostat connected to a glassy carbon working electrode (3.0 mm diameter surface area = 0.07 cm²), a platinum counter electrode and Ag/Ag⁺ reference electrode. Before use, the working electrode was polished using an aqueous alumina slurry. The working and counter electrode were rinsed with ethanol, acetone, DI water and finally acetonitrile, and then sonication for 15 min in acetonitrile. CV experiments were conducted in a five-neck electrochemical cell. Three necks were used for each electrode. The other necks were used to maintain a constant Ar atmosphere during data acquisition and to introduce solids, acids, and solvent levels. Overpotential and turnover frequency calculations were performed as previously reported.^{58, 76}

CPC measurements were conducted to determine Faradaic efficiencies were performed using an H-tube fitted with a frit. The working compartment contained a glassy carbon and a Ag/Ag⁺ reference electrode. The counter electrode compartment was fitted with a platinum wire. All CV and CPC measurements were performed using solutions

containing 0.1 M Bu_4NPF_6 in acetonitrile and 1 mM **1** or **3**. In CPC studies, the H-tube was charged with 44 mL of 1 mM **1** or **3** in acetonitrile and 0.240 M acetic acid and purged with Ar for 15 minutes. The H-tube was then inverted, and CPC was conducted at -2.60 V vs Ag/AgCl for 2h. In the case of the control experiment for **2**, the concentration was 0.5 mM and 0.286 mM respectively. Ferrocene was used as an internal standard, except during the concentration dependence studies and control experiments. Evolved gas from the cathode compartment displaced solvent in a cylinder with diameter 1.12 cm. Each volume of gas were then calculated via the volume of a cylinder and then using the ideal gas law a value for number of moles of hydrogen was determined. The amount of gas produced was subtracted from the gas produced via experiments sans catalyst, or the “blank” experiment. The total charge passed was also subtracted from the “blank” experiment and from there the theoretical moles of gas was determined (see SI). From there the faradaic efficiency equation was utilized to determine the faradaic efficiencies of each catalyst in each solvent.

To identify the gaseous product of electrocatalysis, CPC measurements were completed in a two-compartment electrolysis cell, that was fitted with a frit to separate the two compartments. The working compartment was charged with 1 mM **1** or **3**, 0.1 M NBu_4PF_6 , and acid saturating glacial acetic acid and filled with acetonitrile, with both the working electrode and reference electrode. The other compartment was charged with 0.1 M NBu_4PF_6 and acetonitrile with a platinum counter electrode. The CPC was done for 24 hours and the evolved gas was subjected to gas chromatography (GC-TCD) analysis at the end of electrolysis using a Gow-MAC series 400 GC-TCD equipped with a molecular sieve column for product detection. The column was heated to 130 °C under N_2 gas flow with

250 μ L injection samples. Control studies of the CV and CPC experiments were done under the exact same conditions with the absence of 1 mM **1**, **2**, or **3**.

3.8.3 Catalysis Control Experiments

Soak Test. For a general explanation of the Soak Test see Chapter 2. The glassy carbon electrode was immersed in a scintillation vial containing an acetonitrile solution of 1 mM of **1**, 0.1 M Bu₄NPF₆ and 0.240 M acetic acid for 24 hours. The same conditions were applied to **3**, with the exception that 0.072 M acetic acid was used. The electrode was removed from the vial and the outside edge rinsed carefully with DI H₂O, taking care not to touch the working portion of the electrode. The rinsed electrode was immersed in a fresh solution of 0.1 M Bu₄NPF₆ in acetonitrile and CVs were recorded at scan rates of 0.2, 0.5, 1.0 V/s.

Cycle Test. For a general explanation of the Cycle Test see Chapter 2. A polished glassy carbon electrode was immersed in an acetonitrile solution containing 1 mM **1** or **3**, 0.1 M Bu₄NPF₆ and enough acetic acid to reach acid saturation conditions. The electrode was repeatedly cycled between -0.5 V and the ending catalysis potential (-3.4 V for **1** and -2.2 V for **3**) vs Fc⁺/Fc for 10 to 30 cycles at a scan rate of 0.2 V/s. The electrodes were then removed from solution rinsed carefully with DI H₂O. The rinsed electrode was immersed in a fresh solution of 0.1 M Bu₄NPF₆ in acetonitrile and CVs were recorded at scan rates of 0.2, 0.5, 1.0 V/s. Acetic acid was then added to obtain acid saturating conditions and the CVs recollected.

Controlled Potential Coulometry Test. For a general explanation of a Controlled Potential Coulometry Test see Chapter 2. The CPC for stability and electrode deposition were done

in a two-compartment cell separated via a frit. One compartment housed a stir bar, 1 mM **1** or **3**, 0.1 M Bu₄NPF₆ and enough acetic acid to reach acid saturation conditions in acetonitrile and the working and reference electrode. The other compartment held the Pt counter and 0.1 M Bu₄NPF₆ in acetonitrile. The working compartment was purged with Ar for 15 min. The potential was then held at -2.60 V for **1** or -2.20 V for **3** for 24 h. The electrodes were then removed from solution rinsed carefully with DI H₂O, and placed in a fresh solution of 0.1M Bu₄NPF₆ in acetonitrile. CVs were recorded (see Supplemental Information). Acid at saturating conditions was then added to these solutions and CVs were also recorded. Samples for XPS analysis were collected by scraping material from the dried electrode surface.

Post-electrolysis rinse test. A CPC was done in the H-Cell as described above in the CPC test. After that CPC the electrode was removed, rinsed with DI H₂O, and placed into a fresh solution with 0.240 M or 0.072 M acetic acid, 0.1 M NBu₄PF₆ in acetonitrile. A second CPC was conducted over 2 hours.

3.8.4 XPS Experiments

The XPS experiments were carried out using PHI VersaProbe II instrument equipped with a focused monochromatic Al K(alpha) source. The instrument base pressure was ca. 8×10^{-10} Torr. For all experiments, X-ray power of 25 W at 15 kV was used with a 100 micron beam size at the X-ray incidence and take off angles of 45°. Additional mapping experiments were completed using a 20 micron beam size. The instrument work function was calibrated to give a binding energy (BE) of 84.0 eV for Au 4f 7/2 line for metallic gold and the spectrometer dispersion was adjusted to give a BE's of 284.8 eV, 932.7 eV and of 368.3 eV for the C 1s line of adventitious (aliphatic) carbon presented on the non-sputtered

samples, Cu 2p_{3/2} and Ag 3d_{5/2} photoemission lines, respectively. For all samples the patented PHI dual charge neutralization system was used. High resolution I 3d, Zn2p and N1s spectra were taken with a minimum of 10 - 60 s scans using 0.1 eV steps and 93.9 eV, and 23.15 eV pass energy for C1s, respectively. Signal above background measurement and Shirley background subtraction was made using MultiPak v9.0 PHI software. At the ultimate PHI Versa Probe II instrumental resolution the temperature spread (at 14/86%) of the metallic silver Fermi edge was less than 120 meV. All XPS spectra were recorded using PHI software SmartSoft –XPS v2.0 and processed using PHI MultiPack v9.0 and/or CasaXPS v.2.3.14. The relative sensitivity factors from MultiPack library were used to determine atomic percentages. Peaks were fitted using GL line shapes utilizing a combination of Gaussians and Lorentzians. Wherever possible, conclusions were drawn from the number of resolved signals for a given element, so as to minimize reliance on absolute binding energies for the nonconductive molecular materials. A given sample was examined at 5-6 different spots on the mounted specimen to assure that consistent, reproducible results were obtained. The high resolution I 3d_{5/2} XPS spectra have been deconvoluted into two components I₁ and I₂ which generates reasonably good fits.

3.8.5 Resistance Measurements

For a general explanation of Resistance Measurements see Chapter 2. Resistance measurements were conducted using a Metroham Autolab potentiostat. 0.5 mM solutions of **2**, **3**, tetrabutylammonium hexafluorophosphate, and para-nitroaniline were prepared. A 5 mL aliquot of each solution was placed in separate beakers between two graphite rods that were 2.5 cm apart. This was then subjected to resistance measurement experiment provided by the Nova software made by Metroham Autolab.

3.8.6 Titration Experiments

A series of 1 mM solutions (10 mL) of **1**, **2**, and **3** were prepared in acetonitrile. The solutions were then diluted to a 0.1 mM and titrated with a 0.1 M solution of acetic acid in acetonitrile. Titrations were monitored by UV-Vis spectroscopy. After each addition, solutions were allowed to equilibrate for three minutes.

3.8.7 NMR Studies

In an NMR tube 5 mg of **2** was dissolved in DMSO- d_6 . To this solution 25 μ L of HPF_6 (45% wt) in water was added. The solution turned from red to yellow and displayed peaks at δ/ppm 11.58 (imido (N-H)), 10.30 (hydrazino N-H), 10.16 (hydrazino N-H), 8.45 (Ar-H), 8.33 (Ar-H), 8.08 (Ar-H), 7.45 (NH- CH_3), 7.13 (Ar-H), 3.15 (N- CH_3), 2.16 (C- CH_3) (6), 1.88 (O-C(O)- CH_3).

In an NMR tube 5 mg of **3** was dissolved in DMSO- d_6 . To this solution 25 μ L of HPF_6 (45% wt) in water was added. The solution turned from red to yellow and displayed peaks at δ/ppm 11.54 (imido (N-H)), 10.53 (hydrazino N-H), 10.24 (imido N-H), 8.45 (Ar-H), 8.08 (Ar-H), 7.97 (Ar-H), 7.42(NH- CH_3), 7.33 (Ar-H), 3.12 (N- CH_3) (1proton), 3.00 (NH- CH_3), 2.76 (N- CH_3) (1proton), 2.66 (N- CH_3) (1proton), 2.26 (C- CH_3), 2.20 (C- CH_3).

3.8.8 Computation Methods

For a general explanation of Computational Methods see Chapter 2. Density Functional Theory (DFT) has been successfully employed to calculate and validate the experimental observables. DFT is less expensive than other computational methods and can predict the energetics and the geometrical structures of a model system with a considerable accuracy. The accuracy of the DFT is largely depend on the choice of a proper functional. Based on

our previous studies of related complexes it was shown that the B3LYP hybrid functional can produce better agreement with experimental parameters such as bond lengths, bond angles and torsional angles.⁵⁹ In this regard we have applied B3LYP functional to optimize the structures with 6-311g (d,p) basis set.⁷¹⁻⁷² This level of theory was also applied in our previous studies and found to be quite accurate. The calculations were conducted in a polarizable continuum model (PCM).⁷³ Acetonitrile was used as a solvent in PCM as this has been used in our experiment. The optimized structures were confirmed by frequency calculations. No imaginary frequencies were found for the optimized geometries which confirms the optimized structure were true stationery points. All corresponding cartesian coordinates were added in Appendix B. Gaussian 09 was used to conduct the calculations.⁷⁴ Chemcraft and Gaussview were used to visualize the structures.⁷⁵

CHAPTER IV
EXPLOITING METAL-LIGAND COOPERATIVITY TO SEQUESTER, ACTIVATE,
AND REDUCE ATMOSPHERIC CARBON DIOXIDE WITH A NEUTRAL ZINC
COMPLEX

4.1 Background

The work in this chapter was previously reported in *Inorganic Chemistry*.¹⁰² Although the degree of its effects remains in debate,⁴ the current atmospheric concentration of carbon dioxide (CO₂) is in excess of 415 ppm creating substantial impacts on climate, global temperatures, and ocean acidification. Goal 13 of The 2030 Agenda for Sustainable Development by the United Nations identifies the need to “take urgent action to combat climate change and its impacts.”¹⁰³ The 2018 U. N. report calls for “urgent and accelerated action” as the five-year global temperature from 2013 – 2017 is the highest on record.¹⁰⁴

As mentioned in Chapter I, there is a direct question of how does the “developed” world develop carbon neutral sources of energy that does not require trillions of dollars in infrastructure changes. One way to combat this is to directly bring balance to the carbon cycle, through the reduction of CO₂, through renewable resources, to energy dense fuels. These energy dense fuels would be prized for a number of reasons. First, they have a significantly higher energy density than that of hydrogen. Second, most of the developed world runs on these fuels. Additionally, reduction of CO₂ to carbon containing compounds could have other uses such as solvents or precursors to generate larger molecular weight products. These energy dense fuels could then in theory be recaptured after burning and put back into the cycle. Currently, the initial steps of this process requires one direct method

to capture low concentrations of CO₂ from the atmosphere or flue gas¹⁰⁵⁻¹⁰⁸ and a second system to reduce CO₂^{8, 17, 27, 109-112} to value added products such as energy dense fuels. In this chapter, we report the combination of these two steps for the reduction of CO₂ to formate (HCO₂⁻) from (1) pure CO₂ and (2) from air using an inexpensive catalyst containing zinc.

Just like HER the CO₂RR catalysts can fall into the heterogeneous or homogenous pathways. There are advantages and disadvantages to both pathways. In the case of heterogeneous catalysis the biggest advantage is products that require more than 2 electrons are available. There is a large quantity of electrodes that have been studied for heterogeneous CO₂RR, with a focus on both single metal and mixed/modified systems.¹⁷ In the case of almost all single metal systems, one product, typically carbon monoxide (CO) or HCO₂⁻, is observed, at a high selectivity for that product.^{8, 112} The exception is that copper electrodes have been able to access C₂⁺ products, however they have had poor selectivity for specific carbon containing compounds.¹¹³ While these are products are attractive and processes are on the cutting edge, none of these catalysts are practical solutions due to the fact that none work at low concentrations of CO₂. This implies that one catalyst is necessary to capture the CO₂ prior to reduction and as a result larger energy expenditures would be seen.

In the case of homogenous electrocatalysis, only the two-electron reduction pathway is known. The two-electron reduction of CO₂ in the presence of a proton donor typically yields HCO₂⁻ or carbon monoxide (CO), Figure IV-1 A, through common pathways that dictate the product distribution, Figure IV-1 B.⁸ A significant limitation of these pathways is the requirement for reduction prior to CO₂ binding, which limits the

catalysts ability to fix CO₂ at low pressure. To date, no catalyst following these pathways can utilize CO₂ from air or 3 – 13% streams commonly found in power plant exhaust.^{8, 27,}

112

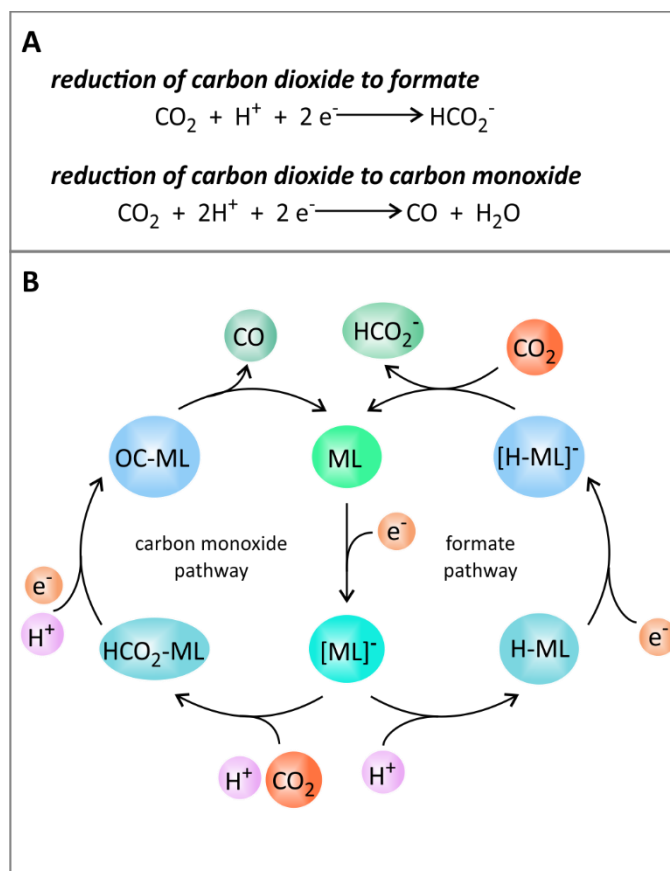


Figure IV-1. A. Half-reactions for the two-electron reduction of CO₂. B. Generalized pathways for catalytic reduction of CO₂ by two electrons.

Recently, two catalysts that bind substrate prior to reduction have been reported demonstrating the potential of alternate mechanistic approaches to improve catalytic activity. Protonation of fac-Mn([(MeO)₂Ph]₂bpy)(CO)₃(CH₃CN))(OTf) ([(MeO)₂Ph]₂bpy) = 6,6'-bis(2,6-dimethoxyphenyl)-2,2'-bipyridine, OTf = triflate) prior to reduction lowers the overpotential for CO₂ reduction to CO by 450 mV⁹⁷ relative to Re(bpy)(CO)₃(X) (bpy = 2,2'-bipyridine, X = halide). The Re(bpy)(CO)₃(X) derivative developed by Ishitani and

coworkers, where X is a deprotonated triethanolamine, facilitates CO₂ binding from air without prior reduction.¹⁵⁻¹⁶ Similar complexes with Ru¹¹⁴ and Mn¹¹⁵ also sequester low levels of CO₂, but only the Re derivative has been reported to catalytically reduce low pressure CO₂.¹⁶ The Ishitani catalyst underscores the necessity to bind CO₂ first in order to reduce CO₂ at low concentrations. Previously, Ito reported CO₂ fixation yielding zinc-alkylcarbonate complexes (Zn-CO₃R) from air with alcohol solutions of N₄ macrocycles, such as Me₄[14]aneN₄, containing Zn(II) and base.¹¹⁶ Building upon these ideas, we developed Zn(DMTH) (DMTH = diacetyl-2-(4-methyl-3-thiosemicarbazone)-3-(2-pyridinehydrazonato)) as a sustainable catalyst for the reduction of CO₂ to formate from air.

4.2 Mechanism

The reduction of CO₂ to HCO₂⁻ by Zn(DMTH) follows an unprecedented mechanism employing metal-ligand cooperativity, Figure IV-2A.⁴⁰ The catalyst contains a frustrated Lewis pair (FLP)¹¹⁷ between the Zn(II) ion (Lewis acid) and the non-coordinating nitrogen of the 2-pyridinehydrazonato group (Lewis base), Figure IV-2B. The FLP facilitates deprotonation of methanol (CH₃OH) to generate the active catalyst Zn(HDMTH)(OCH₃) in equilibrium with Zn(DMTH)(HOCH₃), Figure IV-2C. As previously reported for other metal-alkoxides,^{114-115, 118} insertion of CO₂ into the Zn-OCH₃ bond yields a stable methylcarbonate intermediate Zn(HDMTH)(CO₃CH₃). The methylcarbonate provides an activated form of CO₂ that is susceptible to reduction by a hydride source generating HCO₂⁻ and CH₃OH. The hydride source can be chemically (NaBH₄) or electrochemically generated from Pt or Zn(DMTH). The electrochemical hydride is generated in a similar method presented for the HER of Zn(DMTH).⁸⁰ Ligand

substitution of CH_3OH for HCO_2^- regenerates $\text{Zn}(\text{DMTH})(\text{HOCH}_3)$ to complete the cycle. It should be noted an alternate route via C-O isomerization cannot be completely ruled out.¹¹⁹

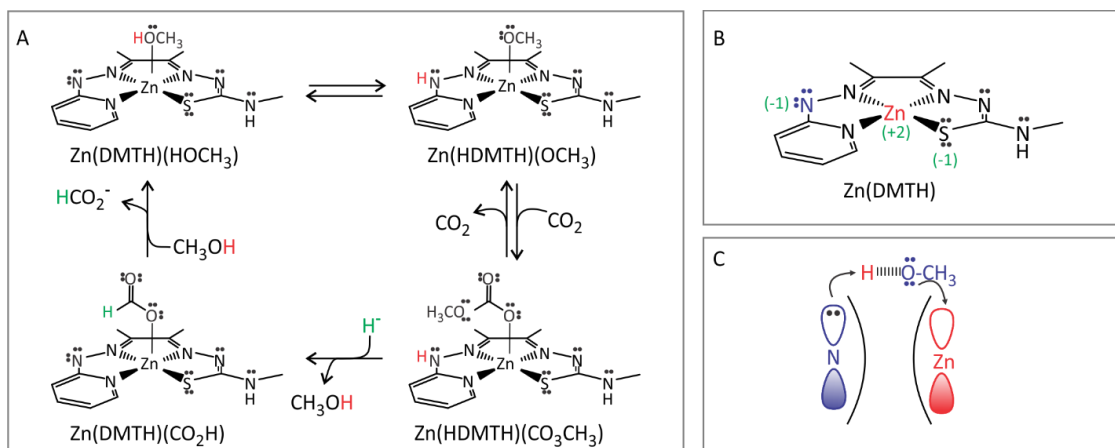


Figure IV-2. A. Catalytic pathway for the reduction of CO_2 to HCO_2^- by $\text{Zn}(\text{DMTH})$.

The source of the hydride (H^-) can be chemical or electrochemical. All non-coordinating lone-pair electrons are shown. B. Representation of $\text{Zn}(\text{DMTH})$ highlighting the Frustrated Lewis pair between the non-coordinating Lewis base (red) and Lewis acid (blue). Formal charges are shown in green. C. Addition of methanol across the frustrated Lewis pair via metal-ligand cooperativity

4.3 CO_2 Binding

A critical feature of our system is the ability of $\text{Zn}(\text{DMTH})$ to bind CO_2 prior to reduction. In methanol, $\text{Zn}(\text{DMTH})(\text{CH}_3\text{OH})$ yields a bright orange solution, Figure IV-3 A, that changes to bright yellow upon bubbling with CO_2 , Figure IV-3 B. The solution returns to the original orange color when sparged with an inert gas (N_2 or Ar).

4.3.1 UV/Vis Spectroscopy

To quantify the CO₂ binding affinity, UV-visible spectra were recorded using different concentrations of CO₂, Figure IV-3 C. In the absence of CO₂, the UV-visible spectrum of Zn(DMTH)(CH₃OH) shows a peak at 424 nm and a peak at 309 nm with a shoulder at 500 nm. Bubbling with 100% CO₂ results in a shift of the lower energy peak to 420 nm and loss of the shoulder at 500 nm. At lower CO₂ concentrations (400 – 1000 ppm), the intensity of the shoulder at 500 nm varies as a function of CO₂ concentration. Analysis of the data (see sample calculations and Appendix A Table A-14) to determine a CO₂ binding constant (K) of $(6.9 \pm 1.8) \times 10^3$, which is similar to the value of 1.7×10^3 reported for the Ishitani catalyst.¹⁵ Based on our measured value of K, Zn(DMTH) should be able to bind CO₂ from air (~415 ppm) in methanol. To confirm this, an air pump was used to introduce non-purified air from the surroundings into solutions of the complex, Figure IV-3 D. The results clearly demonstrate the ability of Zn(DMTH) to sequester CO₂ from the atmosphere without first reducing the catalysts or pre-treating the air sample. The square wave voltammetry was inconclusive as it appeared that an alternate EC mechanism also exists, Figure A-56.

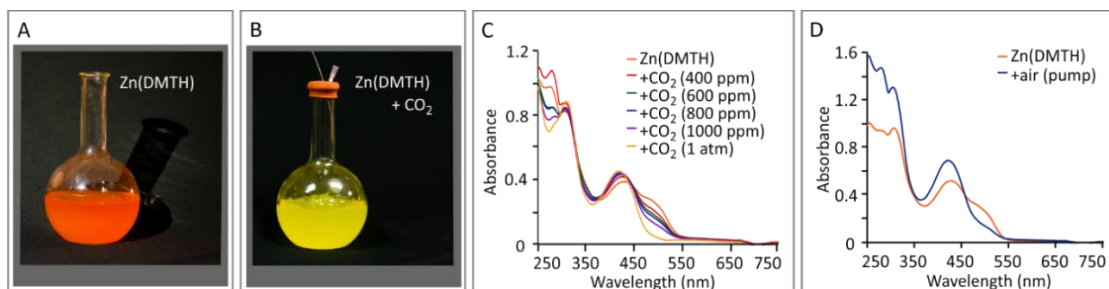


Figure IV-3. A. Photograph of a 3 mM solution of Zn(DMTH) in methanol under ambient conditions. B. Photograph of a 3 mM solution of Zn(DMTH) in methanol, while bubbling with CO₂. C. UV-visible spectra of a 0.1 mM solution of Zn(DMTH) in methanol under varying concentrations of CO₂ gas. D. UV-visible spectra of a 0.1 mM solution of Zn(DMTH) in methanol before and after bubbling the solution with untreated air from the laboratory using an air pump.

4.3.2 Electrochemical Characterization

The reversible CO₂ binding to Zn(DMTH)(CH₃OH) can also be observed by changes in cyclic voltammetry (CV). In methanol, the CV of Zn(DMTH)(CH₃OH) displays an irreversible reduction event with peak cathodic current (E_{pc}) at -1.77 V and an irreversible oxidation with peak anodic current (E_{pa}) at -0.06 V, vs. Fc⁺/Fc, at a scan rate of 200 mV/s. Introduction of CO₂ shifts the reduction peak anodically to -1.66 V and a pre-peak develops at -1.23 V, Figure IV-4 A. Analysis of the peak currents at -1.23 V and -1.66 V as a function of catalyst concentration show that both are first order with respect to catalyst, Figure IV-4 B,C and Appendix A Figure A-55 indicating that Zn(HDMTH)(CO₃CH₃) formation occurs via CO₂ insertion into Zn(DMTH)(CH₃OH) through internal proton rearrangement. Sparging with an inert gas restores the initial CV confirming that CO₂ fixation is reversible.

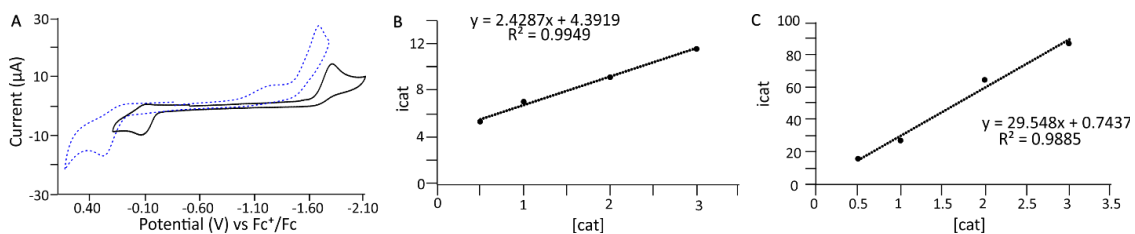


Figure IV-4. A. Comparison CV of Zn(DMTH) (black) and Zn(DMTH) under CO₂ atmosphere (blue dashed) in methanol. B. i_{cat} vs [cat] peak at -1.30 V at a scan rate of 200 mV/s. C. i_{cat} vs [cat] peak at -1.75 V at a scan rate of 200 mV/s.

4.3.3 Single Crystal X-Ray Diffraction

The CO₂ bound complex was identified as the methylcarbonate intermediate, Zn(HDMTH)(CO₃CH₃), by single crystal X-ray diffraction, Figure IV-5A. The Zn(II) ion sits in a distorted square pyramidal arrangement with the N₃S donors of (HDMTH)-chelate in the equatorial plane and a methylcarbonate in the apical position. The hydrogen atom H₄N on the 2-pyridinehydrazonato nitrogen N₄ was located in the electron difference map. The metric parameters are similar to previously reported structures of [Zn(HDMTH)(OH₂)]NO₃, [Zn(HDMTH)(OAc)] (OAc = acetate), and Zn(DMTH)(HOCH₃),^{55-56, 80} Appendix A, Table A-3. The methylcarbonate is coordinated to Zn through the formally anionic O1 with a Zn-O1 distance of 1.991(3) Å, which is similar to the distance of 1.965(3) Å in [Zn(Me₄[14]aneN₄)(CO₃CH₃)] (ClO₄).¹¹⁸ The planarity of the carbonate carbon, C12, is consistent with a change in hybridization to sp² from sp in CO₂.

4.3.4 FT-IR

The infrared spectrum of Zn(HDMTH)(CO₃CH₃) crystals further confirms the fixation of CO₂ as a methylcarbonate with concomitant protonation of the 2-pyridinehydrazonato nitrogen Figure IV-5B. The infrared spectra of monoalkylcarbonato zinc(II) complexes display characteristic ν_1 and ν_2 stretching vibrations near 1650 and 1300 cm⁻¹, respectively, and an out-of-plane bending mode (π) at ~810 cm⁻¹.¹¹⁶ These bands are present in the spectrum of Zn(HDMTH)(CO₃CH₃) as an intense band at 1681

cm^{-1} , a shoulder at 1298 cm^{-1} , and a peak at 814 cm^{-1} . The protonation of the 2-pyridinehydrazone nitrogen is confirmed by the appearance of a broad N-H stretch at 2889 cm^{-1} , which is similar to the acetate bound species, 2937 cm^{-1}

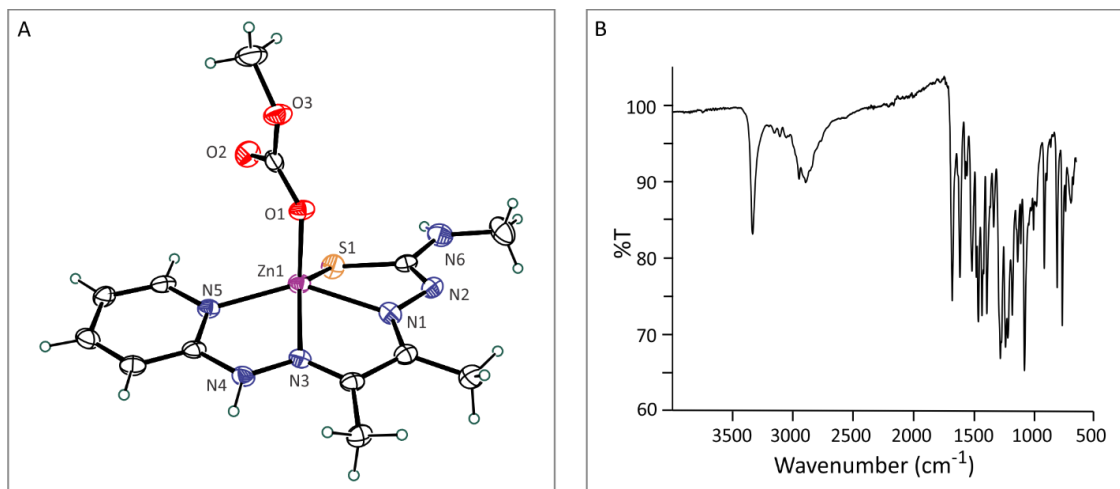


Figure IV-5. A. ORTEP⁹² representation of [Zn(HDMTH)(CO₃CH₃)]. B. FT-IR of [Zn(HDMTH)(CO₃CH₃)] from single crystals.

4.4 Reactions of Zn(HDMTH)(CO₃CH₃)

Next, we evaluated the reactivity of Zn(HDMTH)(CO₃CH₃) with hydride sources to complete the reduction of CO₂ to HCO₂⁻. Previously, Ito established the nucleophilic character of zinc-methylcarbonate complexes in reactions with alkylsulfonates (FSO₃R),¹¹⁶ which has been further exploited for epoxide copolymerization.¹²⁰⁻¹²¹ However, to our knowledge the reactivity of zinc-methylcarbonate complexes with nucleophiles has not been previously evaluated.

4.4.1 Reactions with Chemical Hydride

First, the reaction of a chemical source of hydride, NaBH₄, with Zn(HDMTH)(CO₃CH₃) was examined. In a typical experiment, the Zn(HDMTH)(CO₃CH₃) complex was generated from the parent complex in methanol

under constant bubbling of CO₂. An excess of NaBH₄ was added and the reaction stirred for 30 minutes. Analysis of the reaction mixture by ¹H NMR confirmed the formation of HCO₂⁻ with 170 turnovers, Appendix A Figure A-60. Since NaBH₄ is known to produce formate under CO₂ in ethanol,¹²² control experiments in the absence of Zn(DMTH)(CO₃CH₃) were conducted yielding 62 turnovers for the uncatalyzed reaction, Appendix A Figure A-61. The results confirm Zn(DMTH)(CH₃OH) is able to fix CO₂ from a gaseous stream and catalyze its reduction to HCO₂⁻ with a hydride source.

4.4.2 Reactions with Pt Working Electrode

To test if the reduction of CO₂ to HCO₂⁻ can be achieved electrocatalytically, controlled potential coulometry (CPC) was conducted using a platinum (Pt) working electrode, Figure IV-6. Pt electrodes are known to catalyze the hydrogen evolution reaction (HER) via a Pt-hydride intermediate with no observed CO₂ reduction in the absence of a co-catalyst.¹²³⁻¹²⁴ A solution of Zn(HDMTH)(CO₃CH₃) was prepared in methanol under constant bubbling of CO₂. A potential of -2.00 V vs. ferrocenium/ferrocene (Fc⁺/Fc) was applied for 24 hours during which 55.8 C of charge was consumed. Analysis of the reaction mixture by ¹H NMR confirmed the presence of HCO₂⁻ with a total of 8.70 turnovers, Appendix A, Figure A-62-A-64. The relatively low number of turnovers as compared the NaBH₄ study results from the fact that catalytic turnover in electrochemical reaction only occurs in the diffusion layer, whereas the chemical reaction occurs throughout the bulk. The faradaic efficiency for CO₂ reduction based on the total charge is 30.1%, Appendix A, Table A-16. A substantial portion of the charge is associated with hydrogen evolution at Pt, which was found to account for 38.6 C in control experiments in the absence of our co-catalyst. Of the additional 17.2 C consumed upon addition Zn(DMTH)(CH₃OH), 97.8% is

associated with HCO_2^- production. Spectroelectrochemical FT-IR experiments done using a Pt working electrode in acetonitrile saw a few major points, Appendix A, Figure A-65-A-67. First, the complex utilized residual water and water within the acetic acid solution to hydrate the acetonitrile, as acetamide was detected as a product. Second the complex utilized the residual water as a way to capture the CO_2 as a carbonate species, and the complex showed it was an efficient carbonate production catalyst.¹²⁵

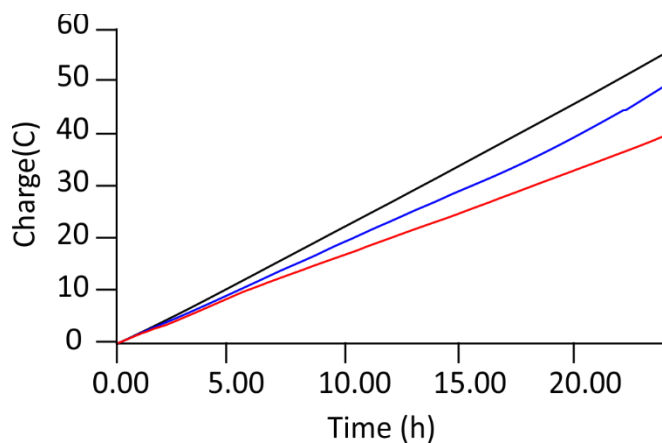


Figure IV-6. Controlled potential coulometry of $\text{Zn}(\text{DMTH})$ in the presence of CO_2 and 10 mM acetic acid in methanol with a Pt working electrode. Run 1 is in black, Run 2 in blue, and the blank in red.

4.4.3 Reactions with Glassy Carbon Electrode

To determine if Zn(DMTH)(CH₃OH) is able to catalyze CO₂ reduction in the absence of external hydride sources, CV experiments using a glassy carbon working electrode were performed. Recently, we reported Zn(DMTH) as an electrocatalyst for ligand-centered HER in acetonitrile upon addition of acetic acid.⁸⁰ The CV of Zn(DMTH) in acetonitrile:methanol (9:1) at a scan rate of 200 mV/s shows an irreversible reduction ($E_{pc} = -2.12$ V vs. Fc⁺/Fc) and two irreversible oxidations ($E_{pa1} = -0.27$ and $E_{pa2} = -0.13$ V), Figure IV-7 black. Upon addition of CO₂, a new peak attributed to the reduction of Zn(HDMTH)(CO₃CH₃) is observed at -1.87 V with a small catalytic peak at -2.37 V, Figure IV-7 red. Addition of acetic acid results in a substantial increase in the current of the catalytic peak at -2.37 V and an additional reduction event at -1.40 V, Figure IV-7 blue. The peak at -1.40 V is attributed to the [Zn(H₂DMTH)(CO₃CH₃)]⁺⁰ couple resulting from the protonation of the hydrazonato nitrogen of the thiosemicarbazone group. This event is shifted by +470 mV relative to the [Zn(HDMTH)(CO₃CH₃)]^{0/-} couple at -1.87 V. It should be noted the presence of both peaks indicates an equilibrium between [Zn(HDMTH)(CO₃CH₃)] and [Zn(H₂DMTH)(CO₃CH₃)]. The catalytic peak at -2.39 V is associated with the further reduction of Zn(H₂DMTH)(CO₃CH₃), which is the proposed hydride source based on prior HER studies.⁸⁰ Analysis of the catalytic peak under scan rate independent conditions with 10 mM acetic acid yield a turnover frequency (TOF) of 73.4 s⁻¹ with an overpotential of 0.86 V.⁷⁶ Recalculation due to homoconjugation yields an overpotential of 0.96 V. Since Zn(DMTH) is known to adhere to glassy carbon under extended catalytic conditions, data were analyzed from CV traces on fresh electrode surfaces.⁸⁰ Notably, if acetic acid is added to Zn(DMTH) prior to CO₂ fixation, only

catalytic HER is observed. This is attributed to protonation of the 2-pyridylhydrazone N, which is the internal base required for CO₂ fixation. Under turnover conditions, the insertion of CO₂ into Zn(DMTH)(CH₃OH) is kinetically preferred to protonation at acetic acid concentrations of 10 mM or less. At acetic acid concentrations above 10 mM in 9:1 acetonitrile:methanol only catalytic HER is observed at -3.29 V vs. Fc⁺/Fc.⁸⁰ Attempts using phenol (96.8 mM) as a weaker acid showed no catalytic wave above background catalyst and CO₂, Appendix A, Figure A-74.

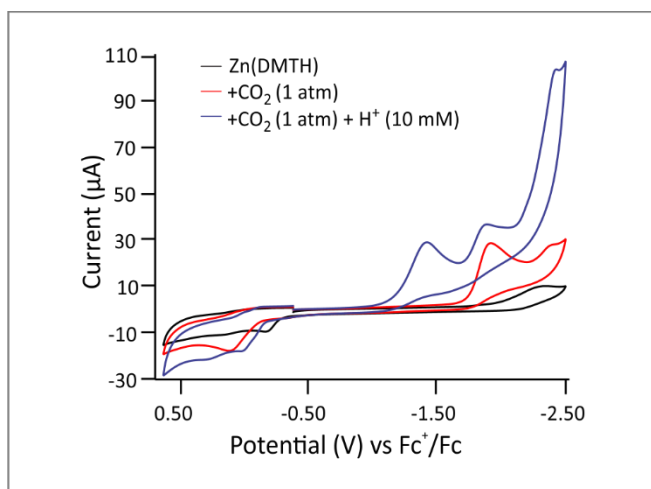


Figure IV-7. Cyclic voltammograms of Zn(DMTH) showing reactivity with CO₂ and acetic acid. Data recorded at a scan rate of 200 mV/s in 9:1 acetonitrile:methanol solution containing 0.1 M tetrabutylammonium hexafluorophosphate as supporting electrolyte with a glassy carbon working electrode, platinum counter electrode, and a Ag/AgCl reference electrode. Potentials are scaled to an internal Fc⁺/Fc standard. Traces shown are Zn(DMTH) (black), Zn(DMTH) + 1 atm CO₂ (red), and Zn(DMTH) + 1 atm CO₂ then + 10 mM acetic acid (blue). All scans are from -0.48V to -2.5 V to 0.60 V to -0.48V and background corrected.

To quantify the product of CO₂ reduction with Zn(DMTH) at a glassy carbon electrode, a series of CPC experiments were performed in the presence of acetic acid and slow bubbling of CO₂ for 24 hours (Table IV-1) at a potential of -2.30 V vs Fc⁺/Fc. The current remained constant over the course of the experiment with no sign of catalyst degradation. In all cases, including control experiments, H₂ was observed as a product in the headspace via gas chromatography. Analysis of the reaction solution via ¹H NMR revealed the production of formate or formic acid, depending on the reaction solvent, when Zn(DMTH) was present as a catalyst. No formate or formic acid was detected in control experiments in the absence of Zn(DMTH). The highest average charge and best average faradaic efficiencies were observed with Zn(DMTH) in 9:1 acetonitrile:methanol solution saturated with a stream of CO₂ at a glassy carbon electrode, Figure IV-8A. Based on total charge consumed, these solutions yielded a faradaic efficiency of 29.2% for formic acid with a total of 16 turnovers. Notably, formic acid production accounts for 95.5% of the charge in excess of the background.

The subtraction of the background activity allows evaluation of the faradaic efficiency for the homogeneous catalyst.^{78, 126-127} In methanol solution, Zn(DMTH) at a glassy carbon electrode provided a total of 12 turnovers with a faradaic efficiency of 24.1% based on total charge under a stream of CO₂, Figure IV-8B. Variation of the acid concentration shows optimal HCO₂⁻ production between 8.3 and 10 mM acetic acid, Figure IV-9. At lower acid concentrations, significantly less HCO₂⁻ is detected, while higher concentrations favor HER. To confirm that HCO₂⁻ is derived from CO₂, isotopic labeling studies with ¹³CO₂ were conducted. The resulting experiment showed a doublet centered at 8.44 ppm (J = 139 Hz) for H¹³CO₂⁻ and a singlet at 8.44 ppm for H¹²CO₂⁻, Appendix A,

Figure A-84.¹²⁸⁻¹²⁹ The singlet intensity for $\text{H}^{12}\text{CO}_2^-$ is attributed to CO_2 generated by oxidation of solvent at the anode. Remarkably, when the reaction was repeated using air pumped into solution from the surroundings in place of a CO_2 stream, reduction to HCO_2^- was observed with a total of 4 turnovers. The optimal faradaic efficiency is 15.8% based on total charge consumed and 47.6 % for background corrected charge, Figure IV-8C. To our knowledge, this is the first reported electrocatalytic reduction of CO_2 to HCO_2^- from air.

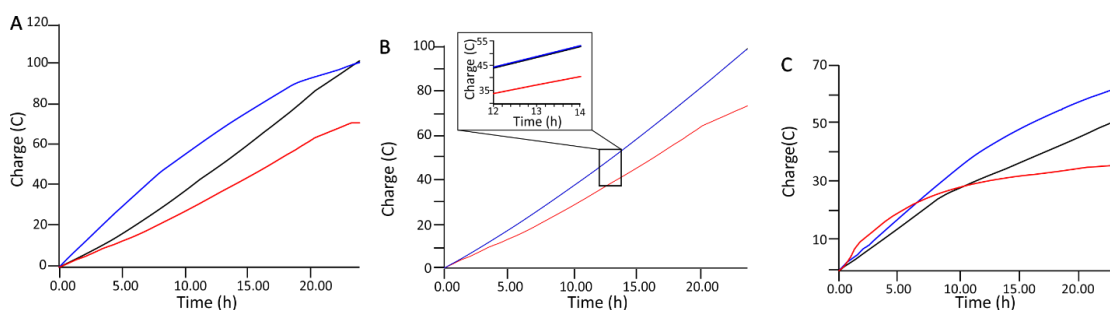


Figure IV-8. Controlled potential coulometry for Zn(DMTH) in the presence of 10 mM acetic acid. A. 9:1 Acetonitrile:methanol and pure CO_2 . B. Methanol and pure CO_2 . C. Methanol and air from an air pump. For all traces run 1 is black, run 2 blue, blank red.

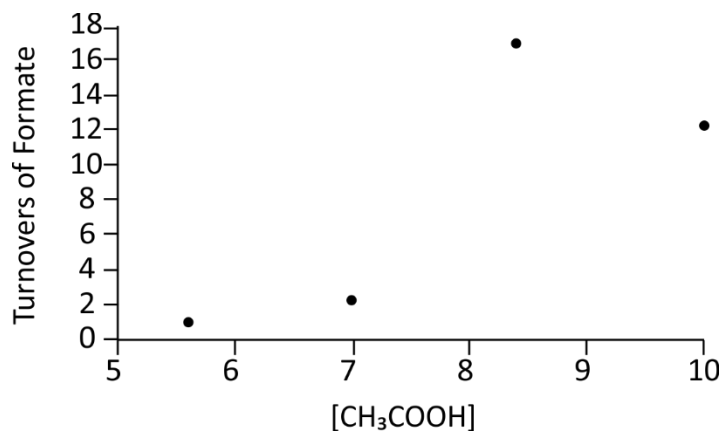


Figure IV-9. Turnovers of formate as a function of $[\text{CH}_3\text{COOH}]$

4.4.4 Summary of All Reactions

Table IV-1. Compilation of average faradaic efficiencies for the reduction of carbon dioxide to formate by Zn(DMTH) under various CPC conditions.^a

Working Electrode	Solvent	CO ₂ Source ^b	Charge Consumed (C)		Faradaic Efficiency (%)	
			Total	Corrected ^c	Overall	Corrected ^d
Pt	MeOH	1 atm	49.7-55.8	11.1-17.2	15.6-30.1	70.3-97.8
GC	MeCN:MeOH	1 atm	102.7-101.1	29.4-31.4	27.7-29.2	93.9-95.6
GC	MeOH	1 atm	98.0-98.3	24.6-24.9	18.7-24.1	75.0-95.0
GC	MeOH	Air	51.9-63.3	15.7-27.1	14.3-15.8	36.9-47.6

a) All experiments conducted for 24 hours; CPC = controlled potential coulometry, Pt = platinum electrode, GC = glassy carbon electrode, MeOH = methanol, MeCN = acetonitrile (MeCN). b) 1 atm CO₂ was obtained from a CO₂ cylinder (99.9%), gas was passed through a drying tube prior to introduction to the cell; CO₂ from air was obtained by using an air pump to introduce laboratory air into the solution with no pre-purification. c) The corrected charge is the total charge obtained in the presence of substrate and Zn(DMTH) minus the charge obtained under identical substrate conditions without Zn(DMTH). d) The overall faradaic efficiency is calculated based the quantity of formate produced relative to the total charge consumed; the corrected faradaic efficiency is calculated using the corrected charge.

4.5 Conclusions

In conclusion, Zn(DMTH) catalyzes the sequestration, activation, and reduction of CO₂ to HCO₂⁻ on its own or in tandem with a hydride source. Modification of this hydride source from the catalyst to a supporting co-catalyst (Pt) lowers the overpotential of the reaction. Notably, Zn(DMTH) maintains its activity at low pressure in the presence of oxygen and water allowing for direct capture and reduction of CO₂ from air. The unprecedented activity of Zn(DMTH) results from the inclusion of a FLP for CO₂ fixation in a redox-active ligand framework that facilitates CO₂ reduction at a non-redox active Zn(II). Further, Zn(DMTH) is a stable catalyst that incorporates a sustainable earth abundant metal in an oxygen and water tolerant complex that can be synthesized from inexpensive chemical reagents. Our ligand-centric approach combining features to fix and reduce CO₂ at a single redox non-active metal site is different from all other CO₂ reduction catalysts and provides a new strategy to mitigate global CO₂ levels. While our work focuses

on reactivity at the cathode, a significant remaining challenge is the coupling of the reduction with a sustainable oxidation at the anode.^{9, 130} As noted by a reviewer, in the current system the methanol solvent is most likely being oxidized, probably all of the way to CO₂. Careful consideration of the overall stoichiometry and enhancing the rate of CO₂ reduction are required to further develop this approach.

4.6 Experimental Specific to Chapter 4.

4.6.1 Materials and Methods.

All reagents were obtained from commercially available sources and used as received unless otherwise noted. Solvents were dried and purified using an MBraun solvent purification system, except methanol which was dried using magnesium and iodide and then stored over molecular sieves. The complexes in this study are air and water stable as solids and were handled on the benchtop with no required protection from the atmosphere unless noted. Zn(DMTH) was synthesized and characterized by previous reported methods,⁵⁶ with slight modifications. The solid was collected as the dihydrate and placed under vacuum to dry. The container of Zn(DMTH) was subjected to flame drying prior to storage and use. It is important to note the solid is red in color after flame drying, while its initial color is orange.

All experiments with pure CO₂ were conducted by passing CO₂ through a drying column filled with CaSO₄. For experiments using air as the CO₂ source, an Uniclife air pump UL40 purchased from Amazon was used. The pump has two ports, one of which was sealed with parafilm. The other port was connected to a piece of tygon tubing first sealed with parafilm and then fitted with a nozzle containing a needle that was inserted into the

septum on the reaction vessel. The pump was operated at its highest setting for all experiments.

4.6.2 Physical Methods.

All ^1H NMRs were done using DMSO-d_6 as a solvent on a 500 MHz Bruker NMR spectrometer. Infrared spectra were recorded on freshly prepared crystalline sample using a Nicolet 360 FT-IR with a smart iTR attachment. UV-vis spectra were obtained on 0.1 mM solutions of Zn(DMTH) in dry methanol using a Variant Cary 50 Bio with fast scan capabilities. To determine the equilibrium binding constant, various concentrations of CO_2 were bubbled through the solutions for 30 min prior to recording the spectra. Concentrations were obtained via the scheme depicted in Figure IV-10. Acid titration studies were conducted using 0.1 M acetic acid in methanol.

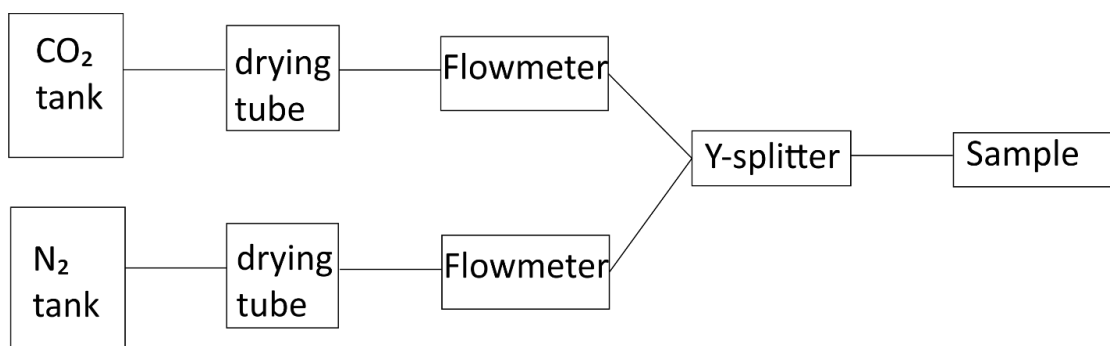


Figure IV-10. Depiction of dilution method for obtaining variable concentration of CO_2 .

4.6.3 Electrochemical Methods.

All cyclic voltammetry (CV) and controlled potential coulometry (CPC) measurements were recorded using a Gamry Interface potentiostat/galvanostat connected to a glassy carbon working electrode (3.0 mm diameter, surface area = 0.071 cm^2), a platinum auxiliary electrode and Ag/Ag^+ reference electrode. Before use, the working

electrode was polished using an aqueous alumina slurry. The working and counter electrodes were rinsed with ethanol, acetone, DI water and finally methanol or methanol/acetonitrile, followed by sonication for 15 min in methanol or methanol/acetonitrile. CV experiments were conducted using a five-neck electrochemical cell. Separate necks were used for the three electrodes. The remaining necks were used to maintain a constant Ar or CO₂ atmosphere during data acquisition and to introduce solids, acids, and adjust solvent levels. Solutions were purged with Ar gas to remove oxygen and prior recording initial voltammograms of the complex. CO₂ was then bubbled through the solutions for 15 min prior to recording voltammograms for each experiment. All data presented are background subtracted. CPC measurements were conducted to determine faradaic efficiencies and were performed using a U-shaped tube containing a frit to separate the two compartments. The working compartment contained a glassy carbon (3.0 mm diameter, surface area=0.071 cm²) or platinum disk (3.0 mm diameter, surface area = 0.071 cm²) electrode and an Ag/Ag⁺ reference electrode. The counter electrode compartment was fitted with a platinum wire. All CV and CPC measurements were performed using solutions containing 0.1 M Bu₄NPF₆ in methanol or 9:1 acetonitrile:methanol and 1 mM Zn(DMTH). Ferrocene was used as an internal standard and added at the end of each experiment. For concentration dependent studies, a fresh solution for each concentration of complex was used. Prior to each CPC study a cyclic voltammogram of the complex was recorded. Potentials were then chosen from the potential of the catalytic peak. Following CPC studies, 100 μL of the reaction solution was transferred to an NMR tube containing 10 μL of DMF (standard solution which is calibrated to 30 mM) as an internal standard and 600 μL of DMSO-d₆. NMR spectra were recorded at a minimum of 128 scans with a

2 second relaxation delay. It should be explicitly noted that CO₂ or air is always added prior to the addition of acid in catalytic studies.

All calculations of overpotential and turnover frequency were done in the manner described by Haddad et. al.⁵⁸ and Fourmond et. al.⁷⁶ The faradaic efficiency for formation of formate was confirmed by ¹H NMR and mmol quantity generated was determined based on integration against a 30 mM DMF standard. The total number of coulombs passed during CPE was corrected by subtracting the coulombs associated with a blank solution and used to determine the theoretical amount of formate that should be produced in mM. The following formula was used to determine the faradaic efficiency.

Faradaic efficiency = $\frac{\text{Actual moles of HCO}_2^-}{\text{Theoretical moles of HCO}_2^-}$ x 100%, which would then determine the faradaic efficiency.

For isotopic labeling studies, a 5 L tank of ¹³CO₂ was purchased from Cambridge Isotopes. This tank was connected through swagelocks and a regulator to the airtight electrochemical cell containing 0.1 M NBu₄PF₆ and 1.0 mM Zn(DMTH) in methanol. This cell contained a working glassy carbon and a Ag/AgCl reference. The flow rate adjusted to 10.0 cc/min. and the cell was purged with the ¹³CO₂ for 15 minutes. Then, 8.3 mM acetic acid was added to the solution and it was stirred. The counter compartment containing 0.1 M NBu₄PF₆ in methanol and a platinum mesh electrode was placed as close to the working cell as possible. The solution was held at -2.30 V vs Fc/Fc⁺ for 2 hours using a Biologic SP200. A 500 μL aliquot of this solution was removed and added to 100 μL of DMSO-d₆ and a ¹H NMR spectrum was recorded.

4.6.4 Reaction of Zn(DMTH) with CO₂ and NaBH₄ in MeOH

Zn(DMTH) (0.0066g, 2.0mM) was added to a 50 mL round bottom flask. This flask was then flame dried and filled with 10 mL of dry methanol. The methanol solution was stirred for 5 min to make sure all of the Zn complex had dissolved. Then the solution was bubbled with dry CO₂ for 15 min to ensure saturation. In a second flame dried flask, 0.3783g (10.00 mmol) of NaBH₄ was dissolved in 2 mL of MeOH. The solution was transferred to the flask containing the Zn complex using a syringe and the mixture was stirred for 30 minutes under a stream of CO₂. A control was conducted in the absence of Zn(DMTH).

CHAPTER V
MECHANISTIC INVESTIGATIONS OF NITRILE HYDRATION CATALYZED BY
ZN(DMTH) UNDER AMBIENT CONDITIONS

5.1 Background

The production of polymers, lubricants, drug stabilizers, detergents, dyes, and herbicides by the hydration of nitriles to amides is of large importance industrially.^{28, 131} Furthermore, hydrolysis of the amide to generate carboxylic acids has even more widespread uses.¹³² Traditionally, hydration reactions are accomplished under some combination of the following conditions: (1) use of very low or high pH,¹³³⁻¹³⁷ (2) use of temperatures significantly higher than room temperature,¹³⁸⁻¹³⁹ (3) use of expensive catalysts that contain expensive metals such as platinum,¹⁴⁰⁻¹⁴² (4) molybdenum,¹⁴³ or ruthenium.¹³⁸ Recently less expensive metals such as nickel,¹⁴⁴ copper,¹⁴⁵ and zinc¹⁴⁶⁻¹⁴⁸ have been examined, however none of these operate at both neutral pH and room temperature.

Industrially the enzyme, Nitrile Hydratase (NHase),¹⁴⁹⁻¹⁵⁰ is used as it has a significantly lower operating temperature and has high selectivity for nitrile hydration with hydrolysis to carboxylic acids essentially nonexistent. NHase was first identified in 1980.¹⁵¹ Yamada and Kobayashi were the first to carry out the industrial-scale production of acrylamide using NHase in 1996.³¹ NHase-mediated hydration of acrylonitrile to acrylamide was the first industrial-scale organic biotransformation.¹⁵² This also marks the first application of biotechnology in the petroleum industry.¹⁵² Further biotransformations of nitrile to valuable amides with NHase has been further examined.¹⁵³

NHase applications beyond synthesis of important amides are numerous. NHase has been explored for the bioremediation of toxic nitriles with emphasis on toxic waste water,¹⁵⁴ shale oil,¹⁵⁵ and herbicide¹⁵⁶ and other contaminated soils.¹⁵⁶⁻¹⁵⁷ The active site of NHase contains either a mononuclear low-spin non-heme iron (III) or non-corrinoid cobalt (III).¹⁴⁹ The Fe-NHase preferentially hydrates aliphatic nitriles, as Co-NHase hydrates aromatic nitriles. Both NHase active sites contains a highly conserved C-S-L-C-S-C motif that serves as the metal-binding domain, Figure V-1. Cys-109 is in the oxidation state of -2, while Cys-114 has been oxidized to a sulfenate (RSO-) with an oxidation state of 0. Cys-112 is also present as a sulfinate with an oxidation state of +2. The posttranslational sulfur-oxygenation has been determined to be critical for hydratase activity.

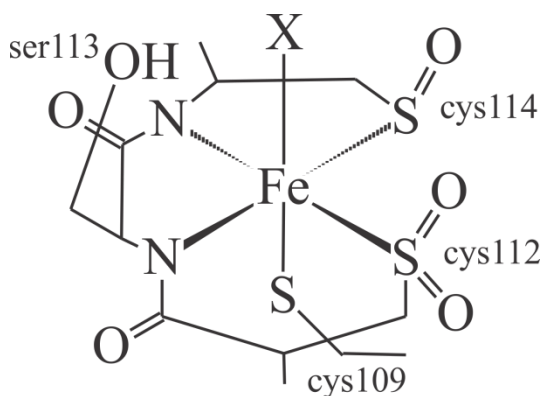


Figure V-1. The active site for Fe-NHase. X represents the nitrile binding site.

The only small molecule catalyst that has been able to both use neutral pH and room temperature is the $[\text{PtH}(\text{PMe}_2\text{O})_2\text{H}(\text{PMe}_2\text{OH})]$ catalyst developed by Parkins and coworkers, Figure V-2.^{141, 158} A key mechanistic feature of this catalyst is the release of H_2 to create an open site at the Pt metal. This open site is then capable of binding the desired nitrile, which can create a metalacyclic intermediate from attack by the neighboring hydroxyl group. This can then be hydrated to give the amide product. Parkins catalyst is

also effective in natural product synthesis, biologically active molecules and pharmaceuticals, and other catalytic reactions like amidation.¹⁴² However, the Parkins catalyst is not without limitations. Most importantly that it uses an expensive and rare metal, platinum, as its active site.

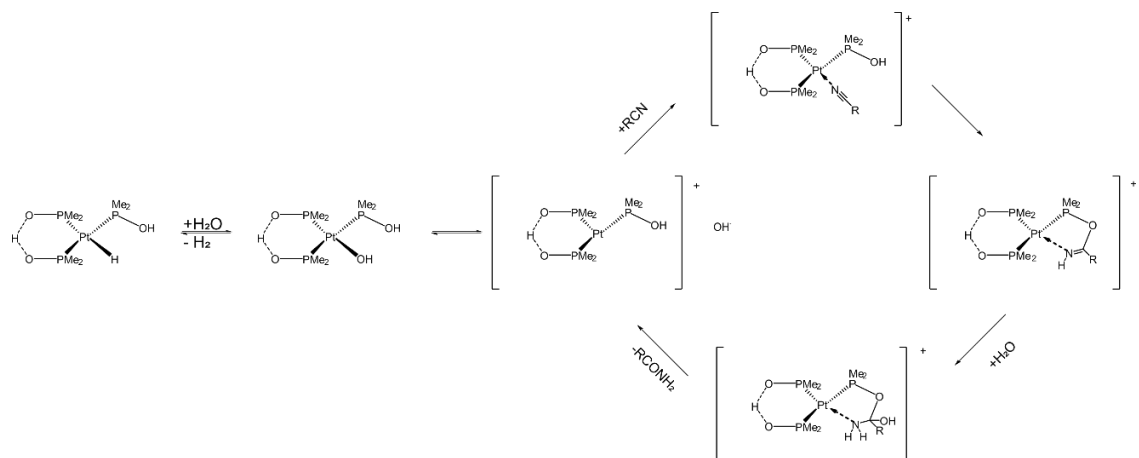


Figure V-2. The $[PtH(PMe_2O)_2H(PMe_2OH)]$ catalyst and catalytic cycle.

Nitriles and cyano- compounds also have significant environmental impacts.³² Companies routinely release these compounds into water supplies as is seen in Brazil and Italy where $25\text{-}50\ \mu\text{g/L}$ ³⁶ and $5.11\ \mu\text{g/L}$ ³⁵ of cyano- containing compounds are detectable in surface water. Furthermore soil samples in Japan have been reported as high as $0.060\ \text{mg/L}$.¹⁵⁹ Environmental cleanup of these compounds is not only difficult, but expensive. The only room temperature catalyst for nitrile hydration is platinum based, and adding a new bacterium containing an enzyme such as Nitrile Hydratase into an ecosystem can have further problematic effects on the environment. Therefore, there is a need for a molecular catalyst that can operate at ambient temperatures, including lower temperatures, that is inexpensive to produce.

A growing amount of interest is shown in Frustrated Lewis Pairs (FLPs).¹¹⁷ have been employed in a variety of reactions such as the CO₂ reduction, the hydrogen evolution reaction, and the nitrogen reduction reaction.¹⁶⁰ As described in Chapters 4, Zn(DMTH) behaves as a FLP like system in its ability to capture, activate, and then reduce CO₂ to formate from pure streams or air.¹⁰² Of note the catalyst is able to deprotonate a methanol to generate a methoxide, which is then capable of CO₂ insertion. In a similar vein, Zn(DMTH) should be able to split water into a proton, docked on the ligand framework, and a subsequent hydroxide bound to the metal center. In doing so this can result in a hydration of the nitrile by the hydroxide at a neutral pH in a very similar manner to which base assisted hydration of nitriles occurs. In this chapter, the catalytic activity of Zn(DMTH) to hydrate nitriles at room temperature and pH neutral conditions is described.

5.2 Preliminary Nitrile Hydration Studies

While performing the electrocatalytic studies described in chapters 3 and 4, it was observed that when Zn(DMTH) was allowed to stand in acetonitrile solution for several days, a white precipitate was observed. The solid was identified as acetamide by ¹H NMR. To confirm this activity, the following experiment was performed under controlled conditions. Zn(DMTH) was dissolved in acetonitrile to give an orange solution, Figure V-3, with peaks at in the UV/visible spectrum at 336 nm and 494 nm, Figure V-3. Upon addition of 5.5 to 33 molar equivalents of water, the intensity at 494 nm decreases with a concomitant increase at 336 nm and an isosbestic point at 363 nm. Additions of water beyond 33 molar equivalents resulted in a secondary reaction (not shown). After the solution was allowed to stand for several days, colorless crystals of acetamide were collected and characterized by ¹H NMR.

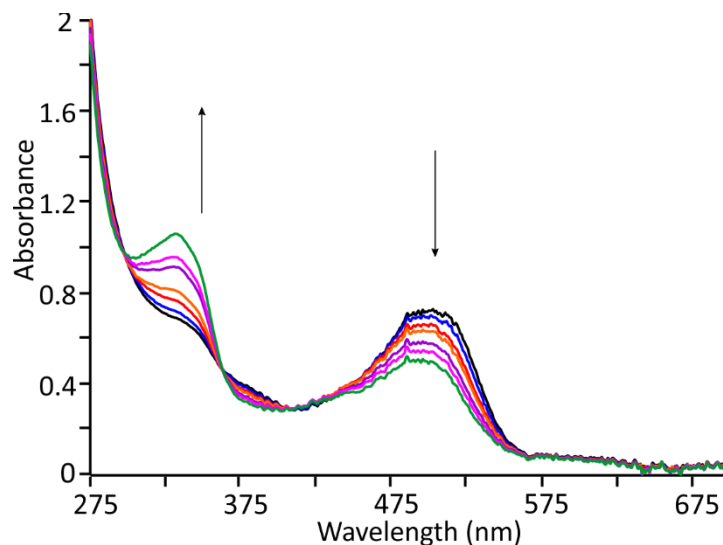


Figure V-3. UV/visible spectra of 0.1 mM Zn(DMTH) in acetonitrile (black) with additions of 0.55 (blue) to 3.3 mM (green) DI H₂O.

5.3 Optimization of Acetonitrile Hydration

Optimizations of the nitrile hydration were conducted using acetonitrile as the substrate with product quantification by gas chromatography affixed with mass spectrometry (GC/MS). For the GC, an Agilent 1909S-433 carbowax column was used with an injection temperature of 60°C and ramped to 140°C and held for 2 minutes with a ramp rate at 20°C/min. Under these conditions, the desired hydration acetamide product is observed at 2.4 minutes and the hydrolysis product, acetic acid, is observed at 2.75 minutes, Figure V-4.

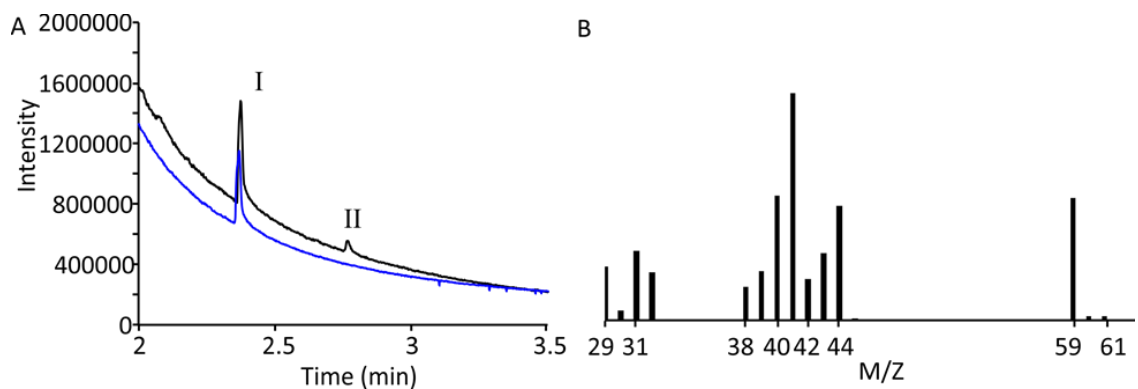


Figure V-4. A. Gas Chromatography for hydration of acetonitrile after 1 h reaction under 12.5% v/v water (black) and 11.0% v/v (blue). B. Corresponding mass-spectrum of the peak at RT 2.4 min. Tailing is from background acetonitrile. Peak (I) is acetamide production. Peak (II) is acetic acid production. First, the volume percentage (%v/v) of water was optimized by adding variable quantities of water to a mixture composed of 10 mL of a 1 mM (0.01 mmol) methanol solution of Zn(DMTH) and 2.61 mL (100 mmol, 17.5%-19.6% of the total volume) of acetonitrile. Under these conditions, the catalyst loading is 0.02 mol%. The volume of water was varied from 0.70 mL (5.3% v/v, 0.039 mmol) to 2.3 mL (15.4% v/v, 0.13 mmol). The amount of acetamide produced after one hour was quantified and calculated as a turnover frequency (TOF). Each reaction was run in duplicate. As shown in Figure V-5, the optimal water amount was 12.5 % v/v. Under these conditions the hydration of acetonitrile is maximized with minimal hydrolysis of the C-NH₂ bond of acetamide to acetic acid (<5%) was observed. A TOF of $0.83 \pm 0.02 \text{ h}^{-1}$ was calculated. At volumes of water >12.5% the selectivity of the amide dramatically decreases and the hydrolysis product, acetic acid, is observed.

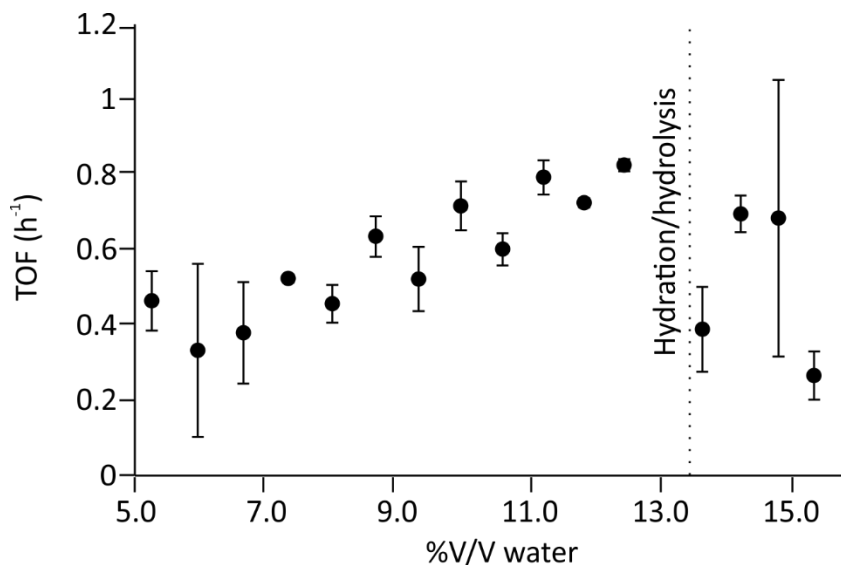


Figure V-5. Turnover as a function of % V/V water. Dashed line indicates where selectivity for hydrolysis product is favored.

The nitrile hydration reaction was further optimized for catalyst loading, which was quantified as the ratio of catalyst to acetonitrile. In these reactions, 10 mL methanol of a 1 mM (0.01 mmol) methanol solution of Zn(DMTH) was mixed with a variable volume of acetonitrile from 58 mL (1.1 mol) to 139 mL (2.7 mol) to vary the catalyst:nitrile ratio from 3.76 to 9.00 ppm, Figure V-6. Water was added to maintain a constant 12% v/v concentration based on the total volume. Reactions were run for one hour in duplicate. The TOF was calculated based on the observed quantity of acetamide. In general, the TOF increased as when the quantity of nitrile was increased with a maximum TOF of 24 ± 4 h⁻¹ at catalyst:nitrile ratio 4.14 ppm (0.01mmol ZnDMTH:2.4 mol acetonitrile). It should be noted that at catalyst:nitrile ratios below 4 ppm the TOF decreases substantially with a value of 1.06 h⁻¹ observed at 3.76 ppm. This observation is consistent with substrate inhibition.¹⁶¹ The inhibition of hydration activity with excess nitrile is consistent with a water/hydroxide bound species (Zn(DMTH)(H₂O) or Zn(HDMTH)OH) as the active form

of the catalyst. In solution, the catalyst exists as a mixture of this active form with inactive nitrile-, $\text{Zn}(\text{DMTH})(\text{CH}_3\text{CN})$, and solvent-bound, $\text{Zn}(\text{DMTH})(\text{CH}_3\text{OH})$, species. Ligand exchange to the aquo bound species must occur prior to hydration.

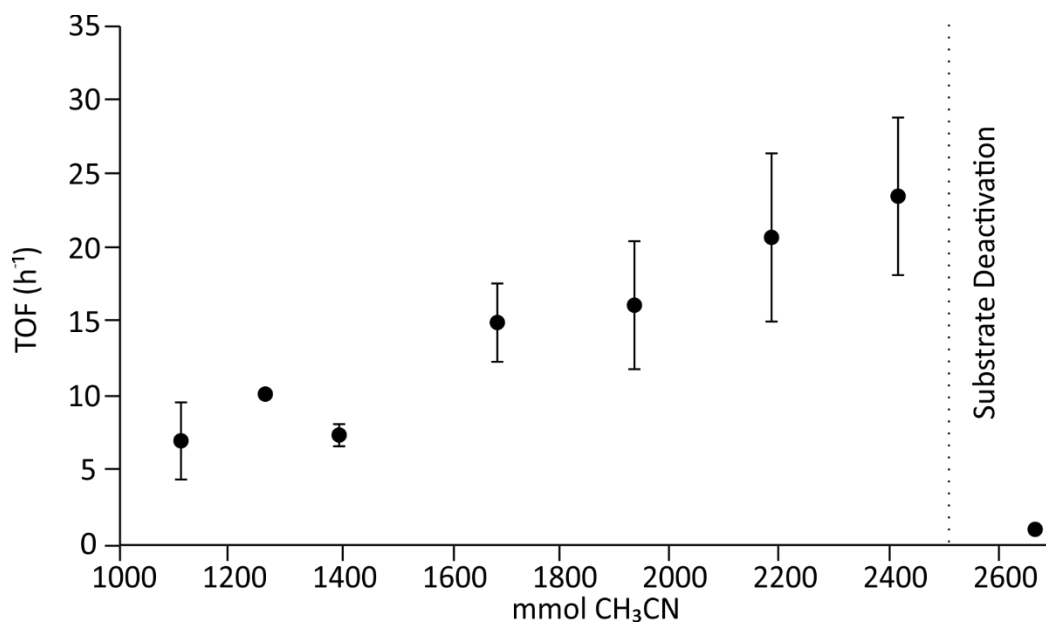


Figure V-6. Turnover as a function of mmol acetonitrile. Dashed line indicates substrate deactivation as a function of nitrile inhibition.

Finally, the % of nitrile relative to catalyst solution was examined. In these experiments, 10 mL of a 0.5 to 2.0 mM (0.005 mmol to 0.02 mmol) methanol solution of $\text{Zn}(\text{DMTH})$ was mixed with variable quantities of acetonitrile to maintain a constant catalyst:nitrile ratio of 4.1 ppm. The volume of water was varied to keep a constant % H_2O (v/v) of 12.5%. Reactions were run in triplicate and the TOF calculated based on the observed quantity of acetamide after one hour. As shown in Figure V-7, % nitrile solutions of 80% or higher results in similar TOFs, while % nitrile solutions less than 80% significantly lower TOFs are observed. This indicates that when the methanol % is $> 7.5\%$

of the total solution, ligand exchange favors $\text{Zn}(\text{DMTH})(\text{CH}_3\text{OH})$ over $\text{Zn}(\text{DMTH})(\text{H}_2\text{O})$ and there is insufficient active catalyst for optimal activity.

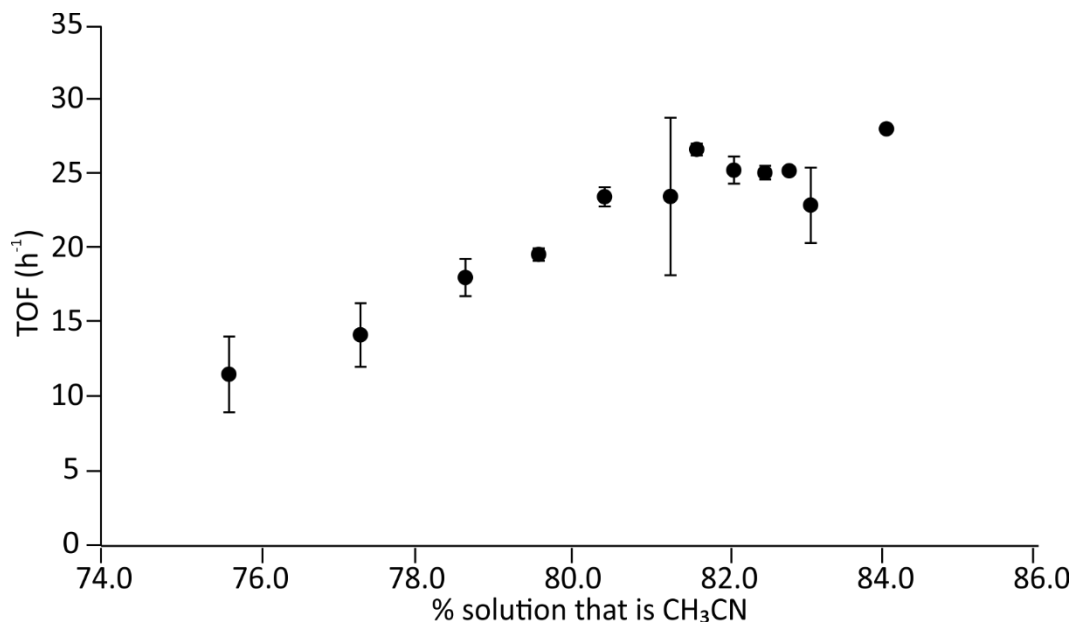


Figure V-7. TOF vs Percent of solution that is CH_3CN .

The optimization studies underscore several facts with this system. First, the methanol solvent used to dissolve $\text{Zn}(\text{DMTH})$ plays a specific role in inhibition of the catalyst. This inhibition of the catalyst indicates that the first step of the mechanism must be a ligand exchange of $\text{Zn}(\text{DMTH})(\text{CH}_3\text{OH})$ to $\text{Zn}(\text{DMTH})(\text{H}_2\text{O})$ or $\text{Zn}(\text{DMTH})(\text{CH}_3\text{CN})$. Second, due to substrate inhibition exhibited in Figure V-6, the first step of the mechanism must be $\text{Zn}(\text{DMTH})(\text{CH}_3\text{OH})$ to $\text{Zn}(\text{DMTH})(\text{H}_2\text{O})$. Third, water at volume percentages $>12.5\%$ yields hydrolysis products instead of hydration products. Fourth, completion studies in which all of the nitrile substrate is converted to product under optimized conditions are not possible as the molar quantity of nitrile far exceeds the amount of water. Finally, catalyst concentration studies are not possible as changing the

catalyst loading also changes the catalyst:nitrile ratio and/or the v/v % methanol in the solution.

To evaluate the durability of the catalyst, a long-term study was performed over 1 month. A solution containing 0.01 mmol Zn(DMTH), 126 mL of acetonitrile, 10 mL of methanol, and 12.5 % (1.03 mol) V/V water was stirred constantly for 30 days. A maximum concentration of acetamide of 205 mM achieved after 21 days, Figure V-8, Appendix A-86. Based on the catalyst concentration of 0.064 mM, the quantity of product represents 3200 turnovers. No further activity was observed after 21 days. By this point, 0.205 mol of water is consumed and the solution became colorless indicating the catalyst was inactive at this point.

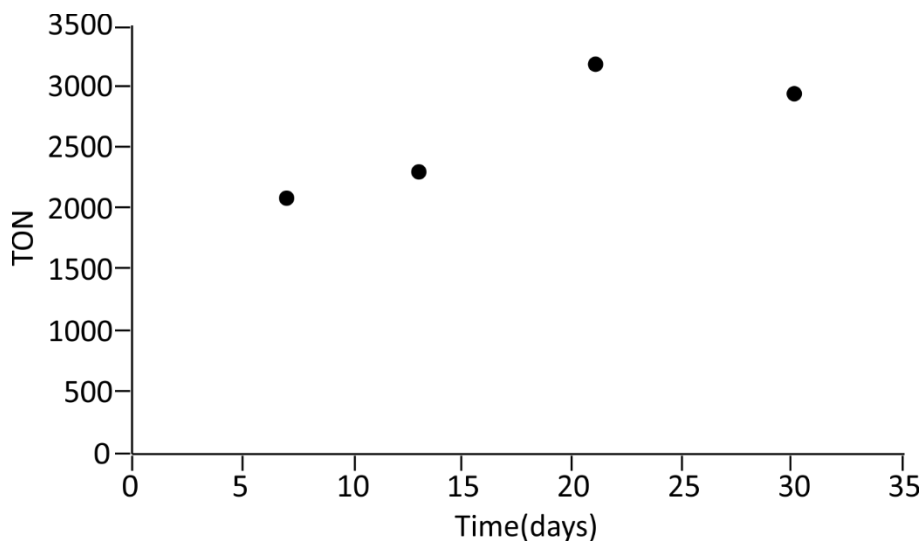


Figure V-8. TON vs time for acetamide over 30 days of reaction time.

5.4 Temperature Effects

To further understand the reactivity of Zn(DMTH) for the hydration of nitriles, variable temperature studies were completed. Data was collected using a reaction solution consisting of a 10 mL methanol solution of 1.0 mM Zn(DMTH), 126 mL acetonitrile, and

18.6 mL (12.5 % v/v) water. Hydration reactions were evaluated at six different temperatures from 273 to 323 K for one hour with TOF calculated based on the quantity of amide determined by GC at the end of the reaction. Reactions were run in duplicate or triplicate and the average TOFs were plotted versus temperature, Figure V-9. Notably, the highest TOF of $48 \pm 7.4 \text{ h}^{-1}$ is observed at the lowest temperature of 273 K. Increasing the temperature results in a steady decrease in TOF to a minimum of 23 h^{-1} at 298 K. As the temperature was increased above room temperature, the TOF increased to 26 h^{-1} at 308 K and 40 h^{-1} at 323 K. The V-shaped plot of TOF versus temperature indicates the hydration mechanism is complex with an activation parameter that is best described as a collective parameter that includes contributions of terms from multiple steps.¹⁶²

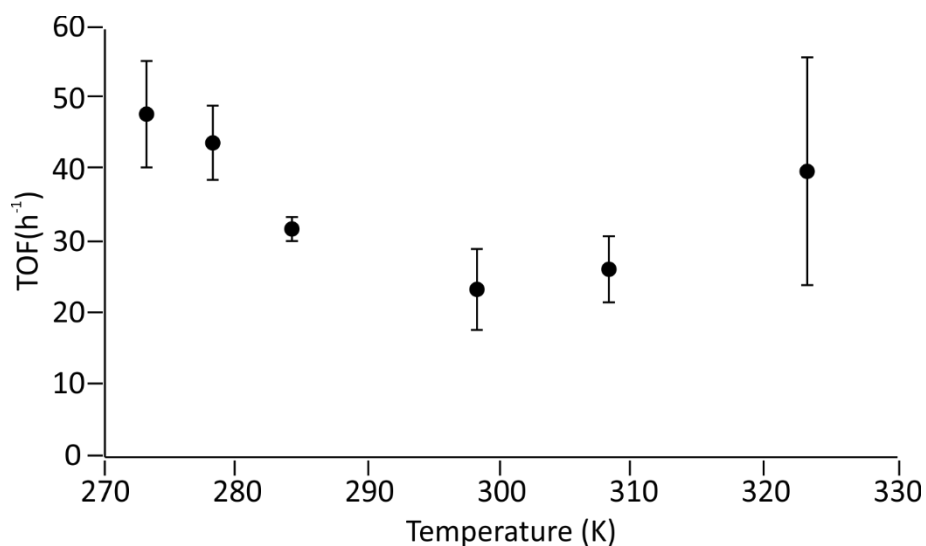


Figure V-9. TOF as a function of reaction temperature.

5.5 Scope of Nitrile Hydration

To evaluate the scope of nitrile hydration using Zn(DMTH) as a catalyst, its hydration activity with a variety of nitriles were explored, Table V-1. The nitriles evaluated include a series of aromatic nitriles and linear aliphatic nitriles. In a typical reaction, a 10

mL methanol solution of 1.0 mM Zn(DMTH) was mixed with 1.0 mL of water (10% v/v) and 40 equivalents of nitrile. The reaction was allowed to run for one hour after which the quantity of amide product was quantified by GC/MS.

A series of aromatic nitriles (entries 1-9) were examined to evaluate the effect of substituent groups relative to benzonitrile. A TOF of 0.80 h^{-1} was observed for the hydration of benzonitrile. Generally, nitrile hydration is favored for electron withdrawing groups and disfavored for electron donating groups.¹⁶³ A comparison of the para substituted methoxy, methyl, and chloro derivatives (entries 2 – 4) do not follow this trend. The hydration rate constants for the methyl and chloro derivatives of 0.19 and 0.086 h^{-1} , respectively, were significantly lower than the value for benzonitrile. The para-methoxy derivative had the highest TOF with a value of 5.8 h^{-1} . A relatively high TOF of 2.3 h^{-1} was retained when the methoxy substituent was moved to the meta position (entry 5). These results deviate from the general trend seen by other nitrile hydration catalysts. The significantly higher TOF results for the methoxy derivatives suggest electronic effects are not the controlling factor. The O-Me group may be behaving as a water shuttle and/or facilitating substrate release. Direct activation of the nitrile by a neighboring oxygen in the phenoxyacetonitrile (entry 6) increases reactivity, as expected, resulting in a large TOF increase to 24 h^{-1} .

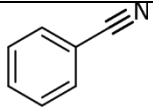
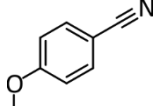
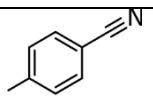
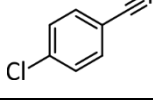
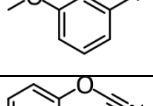
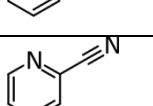
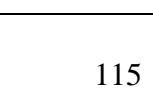
The pyridyl nitrile derivatives (entries 7 – 9) are consistent with the hypothesis that functional groups on the substrate facilitate reactivity. The substrates with the pyridine nitrogen in the ortho and para positions have enhanced TOFs of 9.1 and 7.4 h^{-1} , respectively. Moving the nitrogen to the meta position results in a TOF of 0.89 h^{-1} , which

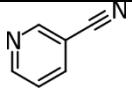
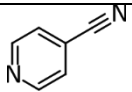
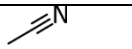
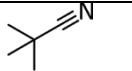
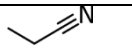
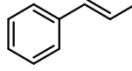
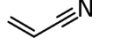
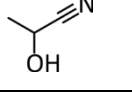
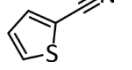
is similar to benzonitrile. The high TOF of the ortho is attributed to the close proximity of the nitrogen lone pair to the activated nitrile, which could serve as a base for amide release.

Next, saturated aliphatic nitriles were examined (entries 10-13). Under the reaction descriptions of this study, the TOF for acetonitrile was 0.21 h^{-1} . The bulkier trimethylacetone nitrile, saw a 3-fold rate increase to 0.60 h^{-1} . This result indicates that sterics do not hinder the hydration of nitriles. The long chain propionitrile had a slower TOF of 0.011 h^{-1} . This nitrile has been shown in enzymatic systems to occur at slower rates relative to acetonitrile.¹⁶⁴ Additionally, the long chain propionitrile saw large quantities of carboxylic acid in the resulting chromatogram. The large quantity of hydrolysis products suggests amide dissociation to be slow for this long chain nitrile, and that amide dissociation might be the rate determining step. Finally, attempts to hydrate malonitrile resulted in product peaks in the GC/MS with masses of larger than 180. This likely is the result of polymerization of the product. This lack of selectivity makes malonitrile an unlikely candidate for Zn(DMTH).

After saturated aliphatic nitriles were examined, unsaturated aliphatic nitriles were tested (entries 14-15). The TOF for hydration of cinnamonitrile, 0.39 h^{-1} , is nearly twice that of acetonitrile. However, the unsaturation of the long chain did result in a decrease in reaction rate in comparison to the activated benzonitrile. For further examination of the effect of unsaturated nitriles, acrylamide was tested. Hydration experiments under the general conditions employed for other nitriles resulted in products in the GC/MS consistent with a reaction between methoxide and acrylonitrile. Runs in “neat” acrylonitrile resulted nitrile hydration, but with a TOF of just 0.064 h^{-1} .

Overall, the results show that Zn(DMTH) is able to hydrate a number of aromatic and aliphatic nitriles. As noted above, malonitrile and acrylonitrile substrates were incompatible with the catalyst. Some additional nitriles also had issues with hydration (entries 16-17), as the target product was either not obtained or obtained with very low selectivity. Nitriles containing OH functional groups tended to polymerize, as a result of the activation of the alcohol functionality which resulted in no conversion to the amide species. The solvent, methanol, played a major issue in getting quantifiable product from 2-thiophenecarbonitrile as the methoxide form instead of the amide was detected. Neat runs resulted in a large amount of non-quantifiable hydration products.

Table V-1. Compilation of Nitriles and TOF				
Entry	Nitrile	Structure	TOF (h ⁻¹)	% of products containing amides
1	Benzonitrile		0.80 ± 0.16	> 99% ^a
2	4-methoxybenzonitrile		5.8 ± 1.2	87% ^b
3	p-tolunitrile		0.086 ± 0.020	>99% ^a
4	4-chlorobenzonitrile		0.19 ± 0.023	> 99% ^a
5	3-methoxybenzonitrile		2.3 ± 0.18	88% ^b
6	Phenoxyacetonitrile		24 ± 2.1	85% ^b
7	2-pyridinecarbonitrile		9.1 ± 3.1	> 99% ^a

8	3-pyridinecarbonitrile		0.89 ± 0.014	$> 99\%^a$
9	4-pyridinecarbonitrile		7.4 ± 1.3	$> 99\%^a$
10	Acetonitrile		0.21 ± 0.034	$> 99\%^a$
11	Trimethylacetoneitrile		0.60 ± 0.25	$72\%^b$
12	Propionitrile		0.011 ± 0.0015	$5\%^c$
13	Malonitrile		0.040 ± 0.0013	$< 1\%^d$
14	Cinnamonitrile		0.39 ± 0.097	$> 99\%^a$
15	Acrylonitrile		0.064 ± 0.041	$> 99\%^{a,e}$
16	Lactonitrile		0.0096 ± 0.0039	$< 1\%^f$
17	2-thiophenecarbonitrile		No quantifiable product	$0\%^g$

All nitrile hydrations occurred with 1 mM (0.01 mmol) Zn(DMTH) in 10 mL methanol (unless otherwise specified) 10% V/v water and 40 mmol of nitrile. a. Only product observed was the corresponding amide. b. direct comparison of amide to carboxylic acid products. c. conversion to carboxylic acid and M/Z > 180 observed in large quantities in comparison to amide. d. Large quantity of oligomers with M/Z > 180 observed as primary product e. Ran neat as methoxy derived products were the only products observed when methanol was the solvent. f. Hydration products from the hydroxyl group were observed along with polymers (>2 lactamides combined). g. methoxide attack on the nitrile was observed and no amide product generated. Additionally opening of the thiophene ring was observed.

5.6 Nitrile Hydration Mechanism

A proposed catalytic cycle for Zn(DMTH) is shown in Figure V-10. The cycle is consistent with results from section 5.3 that show decreased activity with increasing methanol percentage and inhibition at high nitrile:catalyst ratios. Dissolution of Zn(DMTH) in methanol yields the pre-catalyst Zn(DMTH)(CH₃OH) (A). In the reaction

mixture, complex **A** is in equilibrium with the active catalyst $\text{Zn}(\text{DMTH})(\text{OH}_2)$ (**B**) and the nitrile inhibition complex $\text{Zn}(\text{DMTH})(\text{RCN})$ (**E**). At high nitrile:catalyst ratios complex **E** is the dominant species and hydration activity does not occur. Likewise, when the reaction solution contains a large percentage of methanol the amount of active complex **B** is small. The aqua complex **B** is in equilibrium with the hydroxide derivative $\text{Zn}(\text{HBMTH})\text{OH}$ (**C**), in which the deprotonated nitrogen in **B** serves as an internal base. This likely requires a second equivalent of water or the methanol solvent to act as a proton bridge, Figure V-11. The hydroxy group of **C** then attacks a nitrile in solution, as proposed in other nitrile hydration pathways, generating the amidate bound species $\text{Zn}(\text{HDMTH})(\text{RCONH})$ (**D**).^{136-137, 139, 165} Release of the amide upon addition of water regenerates **B** completing the catalytic cycle. Alternately, methanol or nitrile could displace the amide to generate **A** or **E**, respectively. Hydrolysis of **D** occurs if the product release rate is slow and/or if the volume percentage of water in the mixture is high.

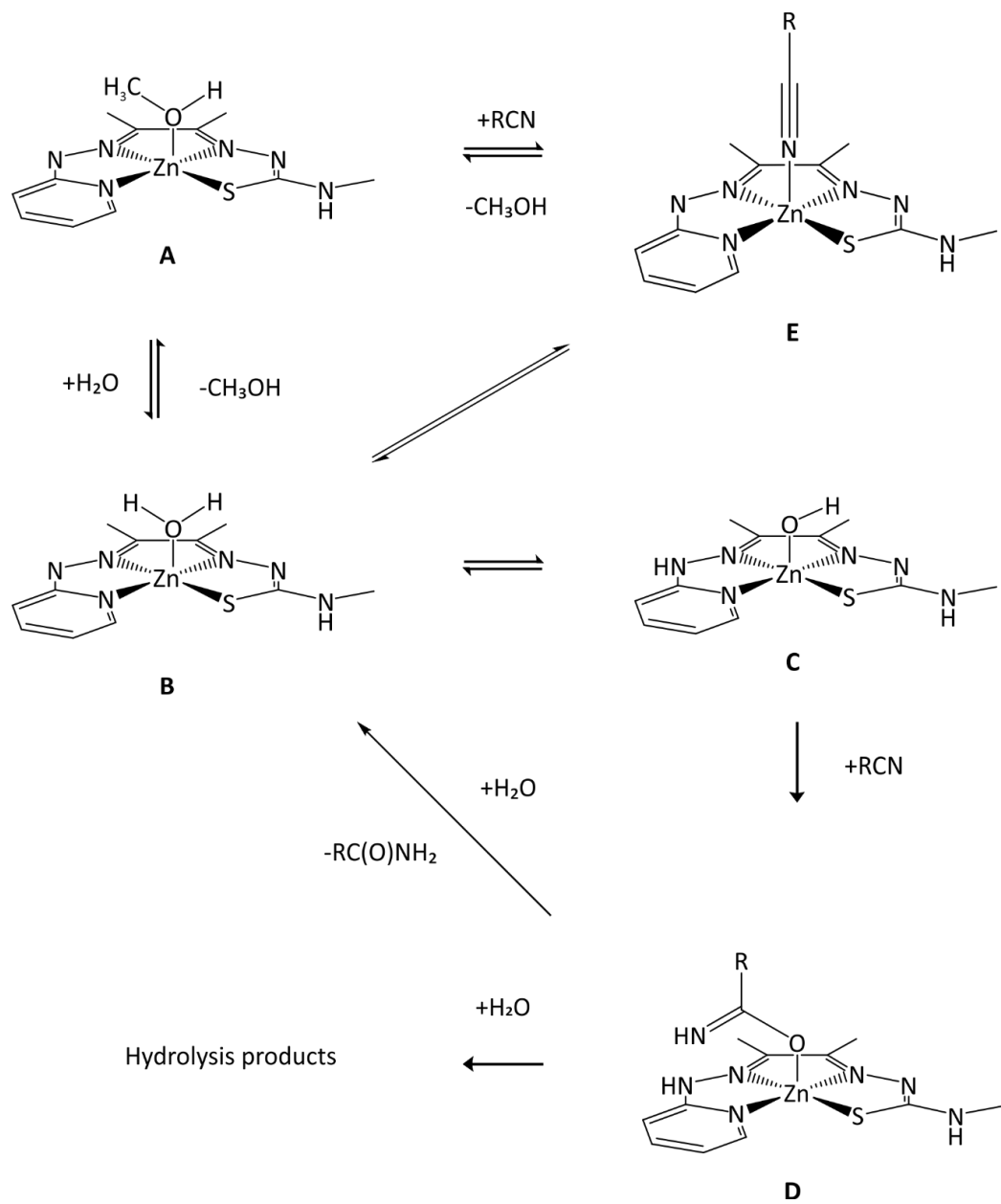


Figure V-10. Proposed catalytic cycle for the hydration of nitriles by Zn(DMTH).

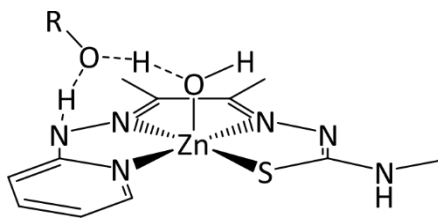


Figure V-11. Depiction of proton shuttling for Zn(DMTH)(H₂O) to Zn(HDMTH)(OH)

5.7 Conclusion

As shown throughout the chapter, Zn(DMTH) utilizes metal-ligand cooperativity, to deprotonate a water to “capture” a nitrile in a similar manner as it does CO₂. This nitrile “capture” results in formation of a proposed amidate intermediate, that can then be released as an amide. These methods are similar to that of NHase, which uses a proximal base to deprotonate water. The Hammett parameters, show that sterics and water shuttling could inhibit or enhance hydration of nitriles. Further hydration of the amidate intermediate results in formation of the carboxylic acid, which deactivates the catalyst. The benefits of the Zn(DMTH) catalyst are numerous, as it is inexpensive, works at room temperature, is pH neutral, and is capable of hydrating of challenging nitriles. While the catalyst has major benefits it also has major drawbacks such as catalyst runs going to completion are difficult, the catalyst cannot distinguish the -OH functional group from that of water, and the reaction rate increases at low T. Optimization of rate, solvent combination, and heterogenization of the catalyst system remain as major frontiers to solve.

5.8 Experimental Specific to Chapter 5

5.8.1 UV/Vis Titration

A 0.1 mM solution of Zn(DMTH) was prepared by dissolving 0.0033g (0.01 mmol) of Zn(DMTH) in 100 mL of dry acetonitrile using a volumetric flask. After collection of the first scan of the complex, 10.0 μL (5.5 molar equivalents) of DI H₂O was added to the cuvette and let stand for 5 minutes. Each subsequent addition followed this same protocol until 60.0 μL (33 molar equivalents) of water was added.

5.8.2 Calibration Curves

A 10 mM stock solution of the amide was prepared in 100 mL of methanol using a volumetric flask. Serial dilution was then performed to generate the solutions for the remaining five data points. All six solutions were sampled by GC/MS to determine the retention time and quantify the peak intensity. From each abundance and concentration, a curve was created in Excel, and ensured that the curve went through the origin with a high R^2 value.

5.8.3 General Hydration Procedure

The corresponding catalysts amount was massed to be 1.0 mM (0.0098 g) in a round bottom Schlenk-flask, with the exception of varying catalyst concentrations experiments. This Schlenk-flask was then affixed with a septum and copper wired shut. Using Schlenk techniques the flask was flame dried and the color of the solid went from orange to dark red. The flask was then charged with 30 mL of dry methanol, to generate a 1.0 mM solution. A second Schlenk-flask was fitted with a stir bar, and then sealed with a septum and copper wired shut. This was then also flame dried using Schlenk techniques. The second flask was then charged with 10.0 mL of the catalyst solution prepared earlier and then a corresponding amount of dried nitrile. The solution was then charged with the corresponding amount of DI H₂O, and then stirred for one hour. The Schlenk-flask was then opened to the atmosphere and an aliquot of reaction mixture removed to then be placed in a GC/MS vial for analysis.

5.8.4 Varying Water Procedure

Varying water experiments were carried out in the methodology for the general hydration experiments. However, the acetonitrile was held constant at 2.61 mL. Then 0.8

mL to 2.3 mL of water was added to the solution and stirred for one hour. Each experiment was done in triplicate and then the quantity of amide and carboxylic acid was analyzed via GC/MS. From this data optimal water concentration was used for all other optimizations.

5.8.5 Varying Acetonitrile:catalyst Procedure

Varying acetonitrile experiments were carried out in the same methodology for the general hydration experiments, except the acetonitrile concentration was varied from 115,000 equivalents to 275,000 equivalents. After the volume of acetonitrile was calculated the %v/v of 10% was held for water and added to the solution. Each reaction ran for one hour before sampling. Each experiment was repeated in triplicate.

5.8.6 Varying %Methanol:Acetonitrile Procedure

Varying catalyst experiments were carried out in the methodology for the general hydration experiments. However, the massed quantity of catalysts was varied from 0.5 mM to 2.0 mM. The amount of acetonitrile used was held constant at 250,000 equivalents of acetonitrile, and 10 % v/v water. Each experiment was repeated in triplicate.

5.8.7 Varying Temperature Procedure

A 1.0 mM solution of Zn(DMTH) was prepared as consistent with the general hydration experiment methodology. The second Schlenk-flask would then be charged with 10 mL of catalyst solution, then 250,000 equivalents of acetonitrile and 10 % v/v water added. For $T < 25^{\circ} \text{C}$ an icebath was employed and held constant at the desired temperature. For $T > 25^{\circ} \text{C}$ an oil bath was used to hold the temperature at the desired temperature. Each reaction was run in triplicate for one hour and then analyzed by GC/MS.

5.8.8 Varying Substrate (other nitriles) Procedure

A 1.0 mM solution was prepared as consistent with the general hydration experiment methodology. In a second Schlenk-flask 10 mL of the catalysts solution was added and then 40 molar equivalents of nitrile was added. To this 10 % v/v water was added and the solution stirred at RT for 1 hour. The Schlenk-flask was then opened to the atmosphere and a GC/MS vial filled with the reaction mixture, and subjected to GC/MS. Each experiment was run in triplicate. In the case of reactions run “neat” as a result of methoxide products, only one Schlenk-flask was used and charged with the solid catalyst. The flask was then “flame-dried” and then charged with 40 molar equivalents of nitrile and 10 % v/v water added. These were also stirred for 1 hour and ran in triplicate.

CHAPTER VI

CONCLUSIONS AND FUTURE DIRECTIONS

6.1 Summary

The results described in Chapters 3 – 5 demonstrate the effectiveness of Zn(DMTH) as a catalyst for a variety of reactions from hydrogen evolution to CO₂ reduction to nitrile hydration. As noted in Chapter 1, this activity is attributed to metal-ligand cooperativity associated with the positioning a non-coordinating Lewis base within close proximity of the Lewis acid metal center. In the following sections, the key points from the dissertation are summarized and future directions are discussed.

6.1 Improving HER Overpotential

As summarized in Chapter III, Zn(DMTH) and Zn(DMTMH)I catalyze the HER with TOFs of $\sim 7000 \text{ s}^{-1}$ at overpotentials of 1.45 V and 0.72 V, respectively. The significant differences in overpotential for the two catalysts result from a combination of effects as mapped out in Figure III-14. For this study, $\sim 450 \text{ mV}$ of overpotential change was directly related to a change in the charge of the catalyst, whereas an additional $\sim 290 \text{ mV}$ of overpotential change was attributed to the removal of one “option” for proton rearrangement. The change in HER overpotential demonstrates the flexibility of the thiosemicarbazone framework for the HER reaction and leaves the door open for future study. A key takeaway from this study is the understanding of the differences in the ligand framework of the catalysts and their effect on catalysis. Upon coordination to Zn²⁺ the DMTH ligand is a dianion whereas the methylated DMTMH ligand is a monoanion. Coordination of DMTMH to other metals, such as Ni(II), could take advantage of the

charge effects to lower HER overpotential. Since the Ni(II) complex of DMTMH, would likely be $[\text{Ni}(\text{DMTMH})]^+$ with the corresponding coordinating anion free in solution, the charge effect would likely already be present. It has been shown with ATSM frameworks that the Ni(II) complex operates at roughly 200-250 mV of lower overpotential than the Cu or Zn counterparts.^{45, 58} If this holds true for the DMTMH counterparts, then an overpotential of 0.31-0.36 V could be observed when utilizing acids that do not have homoconjugation. This is the “sweet spot” for most homogenous HER catalysts as most homogenous HER catalysts average an overpotential of approximately 0.40 V.¹⁶⁶

The second key direction that can be taken from this work is that of the fact that upon prolonged electrolysis the Zn(DMTH) adheres to the electrode and remains intact per XPS data. This adhesion is seen with an onset potential (all potentials are reported vs the Fc^+/Fc couple) of ~ -1.60 V with a peak potential of ~ -1.70 V as opposed to an onset potential of ~ -2.00 V with a peak potential of ~ -3.30 V. This potential of -1.70 V is roughly 200-300 mV from the operating potential of platinum disk electrodes, electrodes that operate at 0 overpotential. Therefore, the bound Zn(DMTH) catalyst could be a useful catalyst for exploration for heterogenous HER catalysis.

Finally, the Zn(DMTH) and Zn(DMTMH)I complexes demonstrate the necessity to limit “options” in catalytic design. The DMTH framework has four potential protonation sites when undergoing HER reactions, the two hydrazino nitrogens and the two imido nitrogens. By removing one of these protonation sites in DMTMH, the over potential is lowered by approximately 270 mV. Smart catalyst design would limit the number of basic sites, to a point. The work done on the DuBois catalyst shows that some basicity is needed for reactivity, but too much basicity requires significant overpotentials.¹⁶⁷ In terms of the

HER ability of the bis(thiosemicarbazones) and asymmetric thiosemicarbazones for the HER reaction, limiting the basicity should result in less proton rearrangement, thus lower overpotentials.

6.2 Metal-Ligand Cooperativity to Sequester, Activate, and Reduce Carbon Dioxide

In Chapter IV, it is shown that Zn(DMTH) is a capable CO₂ reduction catalyst for formate production. It is also shown that Zn(DMTH) is capable of binding CO₂ from air. This catalyst is the first homogeneous catalyst shown to reduce CO₂ directly with unfiltered air. This catalyst operates in the same regard as many other CO₂ capture catalysts by splitting a bound methanol to generate an alkoxide that is bound directly to the zinc metal. From this CO₂ insertion occurs to generate a methylcarbonate bound species. This methylcarbonate is then susceptible to hydride attack, either electrochemical or chemical in nature. The way that Zn(DMTH) likely generates a hydride is similar to that of the way it generates a hydride for HER reactivity.

The Zn(DMTH) complex has plenty of future directions that the catalyst could go in, for the CO₂RR reaction. First, recent published work from Vishnosky *et al.*¹⁶⁸ suggest modification of the “backbone” can result in changes for the overall reduction potential of the complex. In the case of H₂DMTH, there are two potential results of modification of the backbone. First and foremost, the reduction potential could be modified as seen in similar bis(thiosemicarbazone) complexes. Second the basicity of the N₄ nitrogen can be modified depending on the position and the electronics of the backbone group added. Changes in the reduction potential to make the overpotential more accessible would allow for potentially higher reactivity, as well as more commercial applications. Changing the basicity of the N₄ nitrogen could result in higher CO₂ uptake from air, lending to higher faradaic yields

of formate relative to hydrogen. Another potential change to the ligand framework that could see similar results to changing the backbone is changing the substituents on the pyridine ring para to the N4 nitrogen. Changing these substituents could have the same effects as changing the backbone substituents.

Another future direction that can be employed with the DMTH framework is that of changing the metal center from Zn to something that is more electrochemically active like Cu or Ni. Changing the metal center would most certainly directly affect the overall mechanism for CO₂RR as was seen by the Zn, Cu, and Ni complexes of ATSM. Changing the overall mechanism for the CO₂RR could result in different product formation such as CO or products that are generated with more than 2 electrons. Carbon monoxide would be a more desirable product as that could be used directly in Fisher-Tropsch processes.

Another direction that this work can be taken in is the modification of the working electrode. It was shown that by changing the electrode from glassy carbon to platinum, formate production occurred at a lower applied potential. This lower applied potential could have varying effects. First and foremost, Pt electrodes are notoriously good at producing H₂, so choosing an electrode that is a good hydride donor, but not as good as Pt, such as palladium, could result in less hydrogen production. Another alternative is changing the electrode to one in which CO₂RR is known, such as gold or copper, and see if product formation changes as a result of changing the electrode. This could result in a tandem process that could conceivably open the door to doing CO₂RR directly from air on an industrial scale.

Zn methylcarbonate species are well known to undergo epoxide copolymerization. Since Zn(DMTH) is known to generate a methylcarbonate species, this species could likely

undergo epoxide copolymerization using minimal methanol to generate the methylcarbonate species. This could lead to potentially generating polymers directly from low pressures of CO₂ or air.

6.3 Metal-Ligand Cooperativity for Nitrile Hydration

In Chapter V, it was shown that Zn(DMTH) is capable of hydrating various nitriles at room temperature. This hydration shows the versatility of the Zn(DMTH) as a catalyst. The benefits of Zn(DMTH) as a hydration catalyst include: 1) it generates a hydroxide *in-situ* allowing for the hydration of nitriles at “pH neutral” conditions; 2) it generates the hydroxide at room temperature; 3) Zn(DMTH) is inexpensive; and 4) it works at a wide variety of other temperatures. There are drawbacks though to the Zn(DMTH) catalyst for nitrile hydration. First, the catalyst cannot operate in “neat” environments, as too much nitrile leads to a non-reactive nitrile bound species. Second, the catalyst is prone to deactivation if too much water is added to the solution, as hydrolysis products are observed. Third, optimal catalytic conditions would result in a “completed” reaction in over a year.

While there are many things left to be desired with the Zn(DMTH) complex for nitrile hydration, there are specific routes that can be done to improve the complex. Both routes which were mentioned in 6.2 about changing the basicity of the N4 nitrogen could be of use. As creating a more basic N4 group could aid with the splitting of water, allowing for larger or smaller water concentrations, as well as potentially running in neat environments. Lowering the basicity for the N4 group could result in faster substrate release, which might allow the complex to operate at faster TOFs as the rate determining step, water splitting, or substrate release is not known. Additionally, the complex could be adhered to a silicone bead, which would allow it to operate in “neat” conditions. The

advantage would be that the catalyst works at room temperature, and operation in “neat” conditions would allow multiple pass throughs onto a packed column, to generate large quantities of nitriles. While there is more work to be done on the specifics of this catalyst for these reactions listed in this dissertation, it has been made obvious the need to explore this by the versatility of the Zn(DMTH) complex.

REFERENCES

1. Milani, B.; Licini, G.; Clot, E.; Albrecht, M., Dalton Trans. **2016**, *45*, 14419-14420.
2. Lewis, P. R.; Gagg, C., 1 - Introduction. In *Forensic Polymer Engineering*, Lewis, P. R.; Gagg, C., Eds. Woodhead Publishing: 2010; pp 1-41.
3. EPA Power Plant Emission Trends. (accessed 04/03).
4. Voosen, P., Science **2019**, *364*, 222.
5. Lüthi, D.; Le Floch, M.; Bereiter, B.; Blunier, T.; Barnola, J.-M.; Siegenthaler, U.; Raynaud, D.; Jouzel, J.; Fischer, H.; Kawamura, K.; Stocker, T. F., PANGAEA: CO₂ record from the EPICA Dome C 1999 (EDC99) ice core (Antarctica) covering 650 to 800 kyr BP measured at the University of Bern, Switzerland 2008.
6. R. F. Keeling, S. C. P., A. F. Bollenbacher, and S. J. Walker, Scripps CO₂ Program, S. I. o. O., Ed. Modern Records of Atmospheric Carbon Dioxide (CO₂) and a 2000-year Ice-core Record from Law Dome, Antarctica University of California, La Jolla, California USA 92094-0244, 2010.
7. Zhang, W.; Lai, W.; Cao, R., Chem. Rev. **2017**, *117*, 3717-3797.
8. Francke, R.; Schille, B.; Roemelt, M., Chem. Rev. **2018**, *118*, 4631-4701.
9. Xia, C.; Zhu, P.; Jiang, Q.; Pan, Y.; Liang, W.; Stavitski, E.; Alshareef, H. N.; Wang, H., Nat. Energy **2019**, *4*, 776-785.
10. Bulushev, D. A.; Ross, J. R. H., Catal. rev. **2018**, *60*, 566-593.
11. Smieja, J. M.; Kubiak, C. P., Inorg. Chem. **2010**, *49*, 9283-9289.
12. Machan, C. W.; Stanton, C. J.; Vandezande, J. E.; Majetich, G. F.; Schaefer, H. F.; Kubiak, C. P.; Agarwal, J., Inorg. Chem. **2015**, *54*, 8849-8856.
13. Liu, H.; Wei, L.; Liu, F.; Pei, Z.; Shi, J.; Wang, Z.-j.; He, D.; Chen, Y., ACS Catal. **2019**, *9*, 5245-5267.
14. Del Castillo, T. J.; Thompson, N. B.; Peters, J. C., J. Am. Chem. Soc. **2016**, *138*, 5341-5350.
15. Morimoto, T.; Nakajima, T.; Sawa, S.; Nakanishi, R.; Imori, D.; Ishitani, O., J. Am. Chem. Soc. **2013**, *135*, 16825-16828.
16. Kumagai, H.; Nishikawa, T.; Koizumi, H.; Yatsu, T.; Sahara, G.; Yamazaki, Y.; Tamaki, Y.; Ishitani, O., Chem. Sci. **2019**, *10*, 1597-1606.
17. Zhao, G.; Huang, X.; Wang, X.; Wang, X., J. Mater. Chem. A **2017**, *5*, 21625-21649.
18. Pal, D. B.; Chand, R.; Upadhyay, S. N.; Mishra, P. K., Renew. Sust. Energ. Rev. **2018**, *93*, 549-565.
19. Chaubey, R.; Sahu, S.; James, O. O.; Maity, S., Renew. Sust. Energ. Rev. **2013**, *23*, 443-462.
20. Crabtree, G. W.; Dresselhaus, M. S.; Buchanan, M. V., Phys. Today **2004**, *57*, 39-44.
21. Society, A. C. It's Water Vapor, Not the CO₂. (accessed 04/08/2020).

22. Koytsoumpa, E. I.; Bergins, C.; Kakaras, E., J. Supercrit. Fluids **2018**, *132*, 3-16.
23. Lim, T.; Ellis, B. R.; Skerlos, S. J., Environ. Res. Lett. **2019**, *14*, 114014.
24. NASA Graphic: The relentless rise of carbon dioxide. https://climate.nasa.gov/climate_resources/24/graphic-the-relentless-rise-of-carbon-dioxide/ (accessed 4/27/2020).
25. Kahan, A. EIA projects nearly 50% increase in world energy usage by 2050, led by growth in Asia. <https://www.eia.gov/todayinenergy/detail.php?id=41433>.
26. EIA *Annual Energy Outlook 2020*; U.S. Energy Information Administration: eia.gov/aeo, January 2020, 2020; p 81.
27. Appel, A. M.; Bercaw, J. E.; Bocarsly, A. B.; Dobbek, H.; DuBois, D. L.; Dupuis, M.; Ferry, J. G.; Fujita, E.; Hille, R.; Kenis, P. J. A.; Kerfeld, C. A.; Morris, R. H.; Peden, C. H. F.; Portis, A. R.; Ragsdale, S. W.; Rauchfuss, T. B.; Reek, J. N. H.; Seefeldt, L. C.; Thauer, R. K.; Waldrop, G. L., Chem. Rev. **2013**, *113*, 6621-6658.
28. Ahmed, T. J.; Knapp, S. M. M.; Tyler, D. R., Coord. Chem. Rev. **2011**, *255*, 949-974.
29. Bai, B.; Zhou, J.; Yin, M., Pet. Explor. Dev. **2015**, *42*, 525-532.
30. Maizel, Jr, J. V., Trends Biochem. Sci **2000**, *25*, 590-592.
31. Yamada, H.; Kobayashi, M., Biosci. Biotechnol. Biochem. **1996**, *60*, 1391-1400.
32. Jaszczak, E.; Polkowska, Z.; Narkowicz, S.; Namieśnik, J., Environ Sci Pollut Res Int **2017**, *24*, 15929-15948.
33. Zanchett, G.; Oliveira-Filho, E. C., Toxins (Basel) **2013**, *5*, 1896-1917.
34. Kang, H.-I.; Shin, H.-S., Anal. Chim. Acta **2014**, *852*, 168-173.
35. Giuriati, C.; Cavalli, S.; Gorni, A.; Badocco, D.; Pastore, P., J. Chromatogr. A **2004**, *1023*, 105-112.
36. Frizzarin, R. M.; Rocha, F. R. P., Anal. Chim. Acta **2013**, *758*, 108-113.
37. Jørgensen, C. K., Coord. Chem. Rev. **1966**, *1*, 164-178.
38. Obanda, A.; Martinez, K.; Schmehl, R. H.; Mague, J. T.; Rubtsov, I. V.; MacMillan, S. N.; Lancaster, K. M.; Sproules, S.; Donahue, J. P., Inorg. Chem. **2017**, *56*, 10257-10267.
39. Lyaskovskyy, V.; de Bruin, B., ACS Catal. **2012**, *2*, 270-279.
40. Khusnutdinova Julia, R.; Milstein, D., Angew. Chem. Int. Ed. **2015**, *54*, 12236-12273.
41. Ringenberg, M. R.; Kokatam, S. L.; Heiden, Z. M.; Rauchfuss, T. B., J. Am. Chem. Soc. **2008**, *130*, 788-789.
42. Chirik, P. J.; Wieghardt, K., Science **2010**, *327*, 794.
43. Bart, S. C.; Lobkovsky, E.; Bill, E.; Chirik, P. J., J. Am. Chem. Soc. **2006**, *128*, 5302-5303.
44. Chaudhuri, P.; Hess, M.; Flörke, U.; Wieghardt, K., Angew. Chem. Int. Ed. **1998**, *37*, 2217-2220.
45. Haddad, A. Z.; Garabato, B. D.; Kozlowski, P. M.; Buchanan, R. M.; Grapperhaus, C. A., J. Am. Chem. Soc. **2016**, *138*, 7844-7847.
46. Thompson, E. J.; Berben, L. A., Angew. Chem. Int. Ed. **2015**, *54*, 11642-11646.
47. Whittaker, J. W., Chem. Rev. **2003**, *103*, 2347-2364.
48. Lubitz, W.; Ogata, H.; Rüdiger, O.; Reiherse, E., Chem. Rev. **2014**, *114*, 4081-4148.
49. Scheuermann, M. L.; Fekl, U.; Kaminsky, W.; Goldberg, K. I., Organometallics **2010**, *29*, 4749-4751.

50. Welch, G. C.; Juan, R. R. S.; Masuda, J. D.; Stephan, D. W., *Science* **2006**, *314*, 1124.
51. Luecke, M.-P.; Pens, E.; Yao, S.; Driess, M., *Chem. Eur. J.* **2020**, *26*, 4500-4504.
52. Mo, Z.; Szilvási, T.; Zhou, Y.-P.; Yao, S.; Driess, M., *Angew. Chem. Int. Ed.* **2017**, *56*, 3699-3702.
53. Rauch, M.; Parkin, G., *J. Am. Chem. Soc.* **2017**, *139*, 18162-18165.
54. Mckenzie-Nickson, S.; Bush, A. I.; Barnham, K. J., *Curr. Top. Med. Chem.* **2016**, *16*, 3058-3068.
55. Cowley, A. R.; Dilworth, J. R.; Donnelly, P. S.; White, J. M., *Inorg. Chem.* **2006**, *45*, 496-498.
56. Calatayud, D. G.; López-Torres, E.; Dilworth, J. R.; Antonia Mendiola, M., *Inorg. Chim. Acta* **2012**, *381*, 150-161.
57. Christlieb, M.; Dilworth, J. R., *Chem. Eur. J.* **2006**, *12*, 6194-6206.
58. Haddad, A. Z.; Cronin, S. P.; Mashuta, M. S.; Buchanan, R. M.; Grapperhaus, C. A., *Inorg. Chem.* **2017**, *56*, 11254-11265.
59. Jain, R.; Mamun, A. A.; Buchanan, R. M.; Kozlowski, P. M.; Grapperhaus, C. A., *Inorg. Chem.* **2018**, *57*, 13486-13493.
60. Calvary, C. A.; Hietsoi, O.; Strain, J. M.; Mashuta, M. S.; Spurgeon, J. M.; Buchanan, R. M.; Grapperhaus, C. A., *Eur. J. Inorg. Chem.* **2019**, *2019*, 3782-3790.
61. Straistari, T.; Fize, J.; Shova, S.; Réglie, M.; Artero, V.; Orio, M., *ChemCatChem* **2016**, *9*, 2262-2268.
62. Straistari, T.; Hardré, R.; Massin, J.; Attolini, M.; Faure, B.; Giorgi, M.; Réglie, M.; Orio, M., *Eur. J. Inorg. Chem.* **2018**, *2018*, 2259-2266.
63. Gupta, A. J.; Vishnosky, N. S.; Hietsoi, O.; Losovyj, Y.; Strain, J.; Spurgeon, J.; Mashuta, M. S.; Jain, R.; Buchanan, R. M.; Gupta, G.; Grapperhaus, C. A., *Inorg. Chem.* **2019**, *58*, 12025-12039.
64. Jiang, W.-X.; Liu, W.-X.; Wang, C.-L.; Zhan, S.-Z.; Wu, S.-P., *New J. Chem.* **2020**, *44*, 2721-2726.
65. Gulati, S.; Hietsoi, O.; Calvary, C. A.; Strain, J. M.; Pishgar, S.; Brun, H. C.; Grapperhaus, C. A.; Buchanan, R. M.; Spurgeon, J. M., *Chem. Commun.* **2019**, *55*, 9440-9443.
66. Padalkar, V. S.; Patil, V. S.; Phatangare, K. R.; Umape, P. G.; Sekar, N., *Synth. Commun.* **2011**, *41*, 925-938.
67. Li, J.-M.; Yu, Y.; Weng, J.; Lu, G., *Org. Biomol. Chem.* **2018**, *16*, 6047-6056.
68. Xie, D.; King, T. L.; Banerjee, A.; Kohli, V.; Que, E. L., *J. Am. Chem. Soc.* **2016**, *138*, 2937-2940.
69. Elgrishi, N.; Rountree, K. J.; McCarthy, B. D.; Rountree, E. S.; Eisenhart, T. T.; Dempsey, J. L., *J. Chem. Educ.* **2018**, *95*, 197-206.
70. Gong, K.; Fang, Q.; Gu, S.; Li, S. F. Y.; Yan, Y., *Energy Environ. Sci.* **2015**, *8*, 3515-3530.
71. Lee, C.; Yang, W.; Parr, R. G., *Phys. Rev. B. Condens. Matter* **1988**, *37*, 785-789.
72. Wah Wong, M.; Gill, P.; H. Nobes, R.; Radom, L., 1988; Vol. 92.
73. Scalmani, G.; Frisch, M. J., *J. Chem. Phys.* **2010**, *132*, 114110.
74. Frisch, M. J.; Trucks, G. W.; Schlegel, H. B.; Scuseria, G. E.; Robb, M. A.; Cheeseman, J. R.; Scalmani, G.; Barone, V.; Petersson, G. A.; Nakatsuji, H.; Li, X.; Caricato, M.; Marenich, A. V.; Bloino, J.; Janesko, B. G.; Gomperts, R.; Mennucci, B.;

- Hratchian, H. P.; Ortiz, J. V.; Izmaylov, A. F.; Sonnenberg, J. L.; Williams; Ding, F.; Lipparini, F.; Egidi, F.; Goings, J.; Peng, B.; Petrone, A.; Henderson, T.; Ranasinghe, D.; Zakrzewski, V. G.; Gao, J.; Rega, N.; Zheng, G.; Liang, W.; Hada, M.; Ehara, M.; Toyota, K.; Fukuda, R.; Hasegawa, J.; Ishida, M.; Nakajima, T.; Honda, Y.; Kitao, O.; Nakai, H.; Vreven, T.; Throssell, K.; Montgomery Jr., J. A.; Peralta, J. E.; Ogliaro, F.; Bearpark, M. J.; Heyd, J. J.; Brothers, E. N.; Kudin, K. N.; Staroverov, V. N.; Keith, T. A.; Kobayashi, R.; Normand, J.; Raghavachari, K.; Rendell, A. P.; Burant, J. C.; Iyengar, S. S.; Tomasi, J.; Cossi, M.; Millam, J. M.; Klene, M.; Adamo, C.; Cammi, R.; Ochterski, J. W.; Martin, R. L.; Morokuma, K.; Farkas, O.; Foresman, J. B.; Fox, D. J. *Gaussian 16 Rev. B.01*, Wallingford, CT, 2016.
75. Chemcraft.
76. Fourmond, V.; Jacques, P.-A.; Fontecave, M.; Artero, V., *Inorg. Chem.* **2010**, *49*, 10338-10347.
77. Rountree, E. S.; McCarthy, B. D.; Eisenhart, T. T.; Dempsey, J. L., *Inorg. Chem.* **2014**, *53*, 9983-10002.
78. Roy, S.; Sharma, B.; Pécaut, J.; Simon, P.; Fontecave, M.; Tran, P. D.; Derat, E.; Artero, V., *J. Am. Chem. Soc.* **2017**, *139*, 3685-3696.
79. Grills, D. C.; Matsubara, Y.; Kuwahara, Y.; Golisz, S. R.; Kurtz, D. A.; Mello, B. A., *J. Phys. Chem. Lett.* **2014**, *5*, 2033-2038.
80. Cronin, S. P.; Mamun, A. A.; Toda, M. J.; Mashuta, M. S.; Losovyj, Y.; Kozłowski, P. M.; Buchanan, R. M.; Grapperhaus, C. A., *Inorg. Chem.* **2019**, *58*, 12986-12997.
81. Chen, W.-H.; Chen, C.-Y., *Appl. Energy* **2020**, *258*, 114078.
82. Song, C., *Introduction to Hydrogen and Syngas Production and Purification Technologies*. In *Hydrogen and Syngas Production and Purification Technologies*, 2009; pp 1-13.
83. Jahangiri, H.; Bennett, J.; Mahjoubi, P.; Wilson, K.; Gu, S., *Catal. Sci. Technol.* **2014**, *4*, 2210-2229.
84. Grutza, M.-L.; Rajagopal, A.; Streb, C.; Kurz, P., *Sustain. Energ. Fuels.* **2018**, *2*, 1893-1904.
85. Garrett, B. R.; Polen, S. M.; Pimplikar, M.; Hadad, C. M.; Wu, Y., *J. Am. Chem. Soc.* **2017**, *139*, 4342-4345.
86. Karunadasa, H. I.; Montalvo, E.; Sun, Y.; Majda, M.; Long, J. R.; Chang, C. J., *Science* **2012**, *335*, 698.
87. Zeng, M.; Li, Y., *J. Mater. Chem. A* **2015**, *3*, 14942-14962.
88. Helm, M. L.; Stewart, M. P.; Bullock, R. M.; DuBois, M. R.; DuBois, D. L., *Science* **2011**, *333*, 863.
89. Shaw, W. J.; Helm, M. L.; DuBois, D. L., *Biochem. Biophys. Acta* **2013**, *1827*, 1123-1139.
90. Haddad, A. Z.; Kumar, D.; Ouch Sampson, K.; Matzner, A. M.; Mashuta, M. S.; Grapperhaus, C. A., *J. Am. Chem. Soc.* **2015**, *137*, 9238-9241.
91. Tang, H.; Brothers, E. N.; Grapperhaus, C. A.; Hall, M. B., *ACS Catal.* **2020**, *10*, 3778-3789.
92. Farrugia, L. J., *J. Appl. Crystallogr.* **1997**, *565*, 565.
93. Bentley, C. L.; Bond, A. M.; Hollenkamp, A. F.; Mahon, P. J.; Zhang, J., *J. Phys. Chem. C* **2015**, *119*, 22392-22403.

94. Costentin, C.; Drouet, S.; Robert, M.; Savéant, J.-M., *J. Am. Chem. Soc.* **2012**, *134*, 11235-11242.
95. McCarthy, B. D.; Martin, D. J.; Rountree, E. S.; Ullman, A. C.; Dempsey, J. L., *Inorg. Chem.* **2014**, *53*, 8350-8361.
96. Ding, S.; Ghosh, P.; Darensbourg, M. Y.; Hall, M. B., *Proc. Natl. Acad. Sci. U.S.A.* **2017**, *114*, E9775.
97. Ngo, K. T.; McKinnon, M.; Mahanti, B.; Narayanan, R.; Grills, D. C.; Ertem, M. Z.; Rochford, J., *J. Am. Chem. Soc.* **2017**, *139*, 2604-2618.
98. Roubelakis, M. M.; Bediako, D. K.; Dogutan, D. K.; Nocera, D. G., *Energy Environ. Sci.* **2012**, *5*, 7737-7740.
99. Technologies, A. *CrysAlis Pro (CCD and RED)*, 2013.
100. *SCALE3 ABSPACK included in CrysAlis PRO RED*, 1.171.36.32.
101. Sheldrick, G. M., *Acta Crystallogr* **2008**, *A64*, 112-122.
102. Cronin, S. P.; Strain, J. M.; Mashuta, M. S.; Spurgeon, J. M.; Buchanan, R. M.; Grapperhaus, C. A., *Inorg. Chem.* **2020**.
103. Assembly, U. G. *Transforming our world: the 2030 Agenda for Sustainable Development*; A/RES/70/1, available at: <https://www.refworld.org/docid/57b6e3e44.html>, 2015.
104. Guterres, A. *The Sustainable Development Goals Report*; New York, New York, 2018.
105. Leung, D. Y. C.; Caramanna, G.; Maroto-Valer, M. M., *Renew. Sust. Energ. Rev.* **2014**, *39*, 426-443.
106. Aghaie, M.; Rezaei, N.; Zendejboudi, S., *Renew. Sust. Energ. Rev.* **2018**, *96*, 502-525.
107. Trickett, C. A.; Helal, A.; Al-Maythalony, B. A.; Yamani, Z. H.; Cordova, K. E.; Yaghi, O. M., *Nature Reviews Materials* **2017**, *2*, 17045.
108. Banerjee, R.; Phan, A.; Wang, B.; Knobler, C.; Furukawa, H.; Koeffe, M.; Yaghi, O. M., *Science* **2008**, *319*, 939.
109. Qiao, J.; Liu, Y.; Hong, F.; Zhang, J., *Chem. Soc. Rev.* **2014**, *43*, 631-675.
110. Lu, Y.; Han, B.; Tian, C.; Wu, J.; Geng, D.; Wang, D., *Electrochem. Commun.* **2018**, *97*, 87-90.
111. Kornienko, N.; Zhao, Y.; Kley, C. S.; Zhu, C.; Kim, D.; Lin, S.; Chang, C. J.; Yaghi, O. M.; Yang, P., *J. Am. Chem. Soc.* **2015**, *137*, 14129-14135.
112. Jiang, C.; Nichols, A. W.; Machan, C. W., *Dalton Trans.* **2019**, *48*, 9454-9468.
113. Zhao, J.; Xue, S.; Barber, J.; Zhou, Y.; Meng, J.; Ke, X., *J. Mater. Chem. A* **2020**, *8*, 4700-4734.
114. Arikawa, Y.; Nakamura, T.; Ogushi, S.; Eguchi, K.; Umakoshi, K., *Dalton Trans.* **2015**, *44*, 5303-5305.
115. Mandal, S. K.; Ho, D. M.; Orchin, M., *Organometallics* **1993**, *12*, 1714-1719.
116. Kato, M.; Ito, T., *Inorg. Chem.* **1985**, *24*, 504-508.
117. Stephan, D. W., *Science* **2016**, *354*.
118. Kato, M.; Ito, T., *Inorg. Chem.* **1985**, *24*, 509-514.
119. Nichols, A. W.; Chatterjee, S.; Sabat, M.; Machan, C. W., *Inorg. Chem.* **2018**, *57*, 2111-2121.
120. Cheng, M.; Moore, D. R.; Reczek, J. J.; Chamberlain, B. M.; Lobkovsky, E. B.; Coates, G. W., *J. Am. Chem. Soc.* **2001**, *123*, 8738-8749.

121. Trott, G.; Saini, P. K.; Williams, C. K., *Philos. Trans. Royal Soc. A* **2016**, *374*.
122. Zhao, Y.; Zhang, Z.; Qian, X.; Han, Y., *Fuel* **2015**, *142*, 1-8.
123. Costentin, C.; Canales, J. C.; Haddou, B.; Savéant, J.-M., *J. Am. Chem. Soc.* **2013**, *135*, 17671-17674.
124. Barton Cole, E.; Lakkaraju, P. S.; Rampulla, D. M.; Morris, A. J.; Abelev, E.; Bocarsly, A. B., *J. Am. Chem. Soc.* **2010**, *132*, 11539-11551.
125. Figueiredo, M. C.; Ledezma-Yanez, I.; Koper, M. T. M., *ACS Catal.* **2016**, *6*, 2382-2392.
126. Taheri, A.; Thompson, E. J.; Fettingner, J. C.; Berben, L. A., *ACS Catal.* **2015**, *5*, 7140-7151.
127. Sampson, M. D.; Nguyen, A. D.; Grice, K. A.; Moore, C. E.; Rheingold, A. L.; Kubiak, C. P., *J. Am. Chem. Soc.* **2014**, *136*, 5460-5471.
128. Paris, A. R.; Bocarsly, A. B., *ACS Catal.* **2019**, *9*, 2324-2333.
129. Franco, F.; Cometto, C.; Nencini, L.; Barolo, C.; Sordello, F.; Minero, C.; Fiedler, J.; Robert, M.; Gobetto, R.; Nervi, C., *Chem. Eur. J.* **2017**, *23*, 4782-4793.
130. Yang, H.; Kaczur, J. J.; Sajjad, S. D.; Masel, R. I., *ECS trans.* **2017**, *77*, 1425-1431.
131. Kukushkin, V. Y.; Pombeiro, A. J. L., *Inorg. Chim. Acta* **2005**, *358*, 1-21.
132. Yang, S.-T.; Huang, H.; Tay, A.; Qin, W.; De Guzman, L.; Nicolas, E. C. S., Chapter 16 - Extractive Fermentation for the Production of Carboxylic Acids. In *Bioprocessing for Value-Added Products from Renewable Resources*, Yang, S.-T., Ed. Elsevier: Amsterdam, 2007; pp 421-446.
133. Snyder, H. R.; Elston, C. T., *J. Am. Chem. Soc.* **1954**, *76*, 3039-3040.
134. Eby, C. J.; Hauser, C. R., *J. Am. Chem. Soc.* **1957**, *79*, 723-725.
135. Vorozhtov, N. I.; Golubeva, G. A., *Chem. Heterocycl. Compd.* **2005**, *41*, 1307-1313.
136. Tu, T.; Wang, Z.; Liu, Z.; Feng, X.; Wang, Q., *Green Chem.* **2012**, *14*, 921-924.
137. Schmid, T. E.; Gómez-Herrera, A.; Songis, O.; Sneddon, D.; Révolte, A.; Nahra, F.; Cazin, C. S. J., *Catal. Sci. Technol.* **2015**, *5*, 2865-2868.
138. Kumar, D.; Nguyen, T. N.; Grapperhaus, C. A., *Inorg. Chem.* **2014**, *53*, 12372-12377.
139. Bala, M.; Verma, P. K.; Sharma, U.; Kumar, N.; Singh, B., *Green Chem.* **2013**, *15*, 1687-1693.
140. Jiang, X.-b.; Minnaard, A. J.; Feringa, B. L.; de Vries, J. G., *J. Org. Chem.* **2004**, *69*, 2327-2331.
141. Parkins, A. W., *Platinum Met. Rev.* **1996**, *40*, 169.
142. Cadierno, V., *Appl. Sci.* **2015**, *5*.
143. Chakraborty, S.; Berke, H., *ACS Catal.* **2014**, *4*, 2191-2194.
144. Rode, C. V.; Arai, M.; Shirai, M.; Nishiyama, Y., *Appl. Catal., A* **1997**, *148*, 405-413.
145. Marcé, P.; Lynch, J.; Blacker, A. J.; Williams, J. M. J., *Chem. Commun.* **2016**, *52*, 1436-1438.
146. Kopylovich, M. N.; Kukushkin, V. Y.; Haukka, M.; Fraústo da Silva, J. J. R.; Pombeiro, A. J. L., *Inorg. Chem.* **2002**, *41*, 4798-4804.
147. Barbosa, L. A. M. M.; van Santen, R. A., *J. Mol. Catal. A: Chem.* **2001**, *166*, 101-121.
148. Barbosa, L. A. M. M.; van Santen, R. A., *J. Catal.* **2000**, *191*, 200-217.

149. Prasad, S.; Bhalla, T. C., *Biotechnol. Adv.* **2010**, *28*, 725-741.
150. Cheng, Z.; Xia, Y.; Zhou, Z., *Front. bioeng. biotech.* **2020**, *8*.
151. Asano, Y.; Tani, Y.; Yamada, H., *Agr. Biol. Chem.* **1980**, *44*, 2251-2252.
152. Kobayashi, M.; Shimizu, S., *Nat. Biotechnol.* **1998**, *16*, 733-736.
153. Chen, J.; Zheng, R. C.; Zheng, Y. G.; Shen, Y. C., *Adv. Biochem. Eng. Biotechnol.* **2009**, *113*, 33-77.
154. Li, T.; Liu, J.; Bai, R.; Ohandja, D. G.; Wong, F. S., *Water Res.* **2007**, *41*, 3465-73.
155. Aislabie, J.; Atlas, R. M., *Appl. Biochem. Biotechnol.* **1989**, *20*, 799-807.
156. Holtze, M. S.; Sørensen, S. R.; Sørensen, J.; Aamand, J., *Environ. Pollut.* **2008**, *154*, 155-168.
157. Baxter, J.; Garton, N. J.; Cummings, S. P., *Folia Microbiologica* **2006**, *51*, 591-597.
158. Ghaffar, T.; Parkins, A. W., *Tetrahedron Lett.* **1995**, *36*, 8657-8660.
159. Matsumura, M.; Kojima, T., *J. Hazard. Mater.* **2003**, *97*, 99-110.
160. Jupp, A. R.; Stephan, D. W., *Trends Chem.* **2019**, *1*, 35-48.
161. Kaplan, N. O.; Everse, J.; Admiraal, J., *Ann. N.Y. Acad. Sci.* **1968**, *151*, 400-412.
162. Vyazovkin, S., *PCCP* **2016**, *18*, 18643-18656.
163. Zhang, S.; Xu, H.; Lou, C.; Senan, A. M.; Chen, Z.; Yin, G., *Eur. J. Org. Chem.* **2017**, *2017*, 1870-1875.
164. DiGeronimo, M. J.; Antoine, A. D., *Appl. Environ. Microbiol.* **1976**, *31*, 900-906.
165. Wang, N.; Ma, P.; Xie, J.; Zhang, J., *Mol. Divers.* **2020**.
166. Bullock, R. M.; Das, A. K.; Appel, A. M., *Chem. Eur. J.* **2017**, *23*, 7626-7641.
167. Klug, C. M.; Cardenas, A. J. P.; Bullock, R. M.; O'Hagan, M.; Wiedner, E. S., *ACS Catal.* **2018**, *8*, 3286-3296.
168. Vishnosky, N. S.; Mashuta, M. S.; Buchanan, R. M.; Grapperhaus, C. A., *Inorg. Chim. Acta* **2017**, *461*, 45-51.
169. Binder, H. Z., *Naturforsch B* **1973**, *28*.
170. Turner, N. H.; Murday, J. S.; Ramaker, D. E., *Anal. Chem.* **1980**, *52*, 84-92.
171. Fogg, P. G. T.; Clever, L. H.; Cramer, A. L.; Derrick, E. M.; Gjaldbaek, J. C.; Hayduk, W.; Johnson, S. A.; Kittredge, T. D.; Long, P. L.; Young, C. L. *Carbon Dioxide in Non-aqueous Solvents at Pressures Less Than 200 KPa*; Oxford; New York, 1992.

APPENDIX A
SUPPLEMENTAL FIGURES

A.1 Chapter 2 Figures and Tables

Note: Some figures will have overlap with later chapters

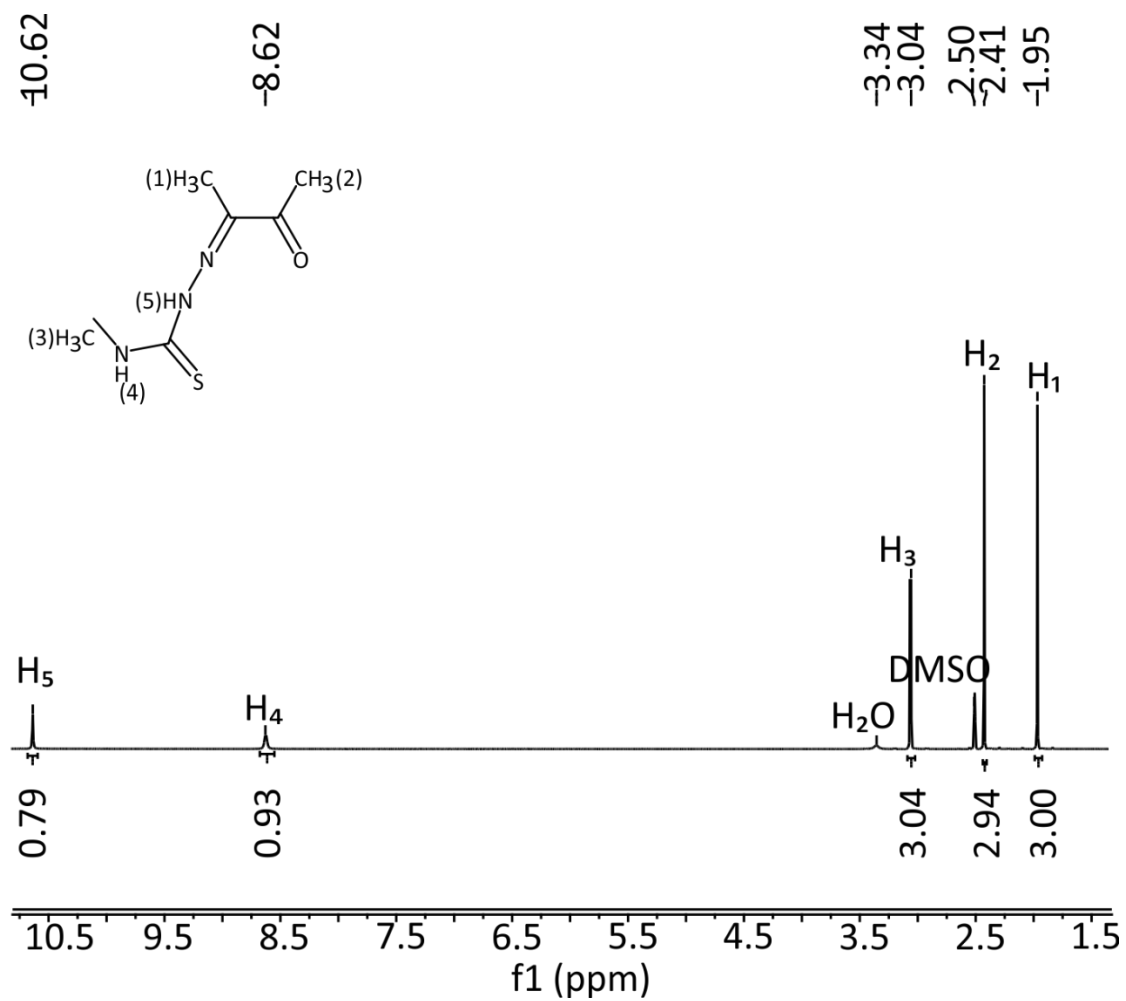


Figure A-1. ¹H NMR of Diacetyl-N-4-methyl thiosemicarbazone.

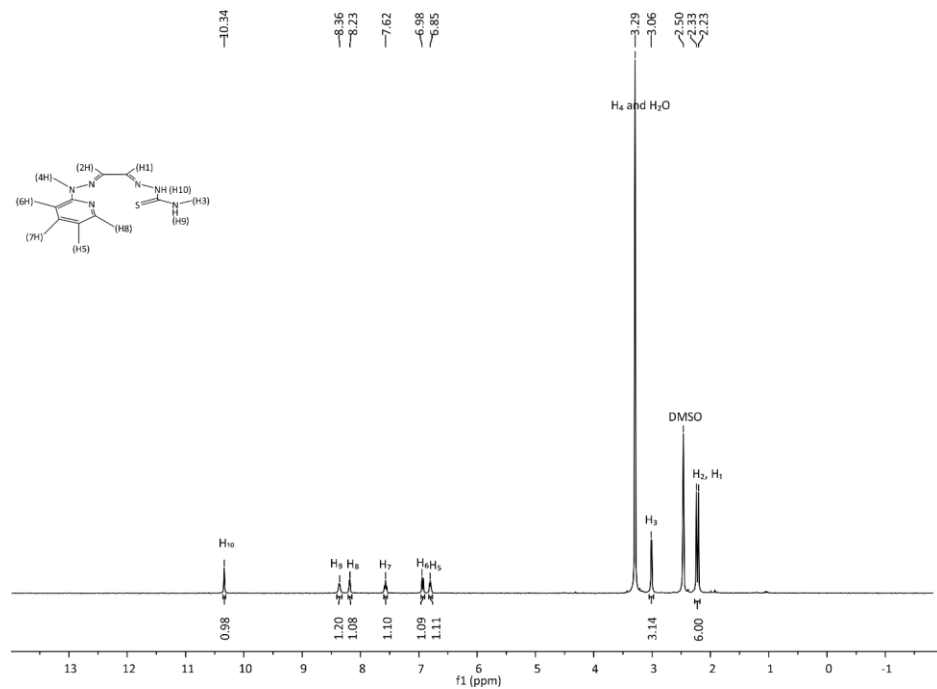


Figure A-2. ¹H NMR of diacetyl-2-(4-methyl-3-thiosemicarbazide)-3-(2-hydrazone-N-methyl-pyridine) (H₂DMTMH).

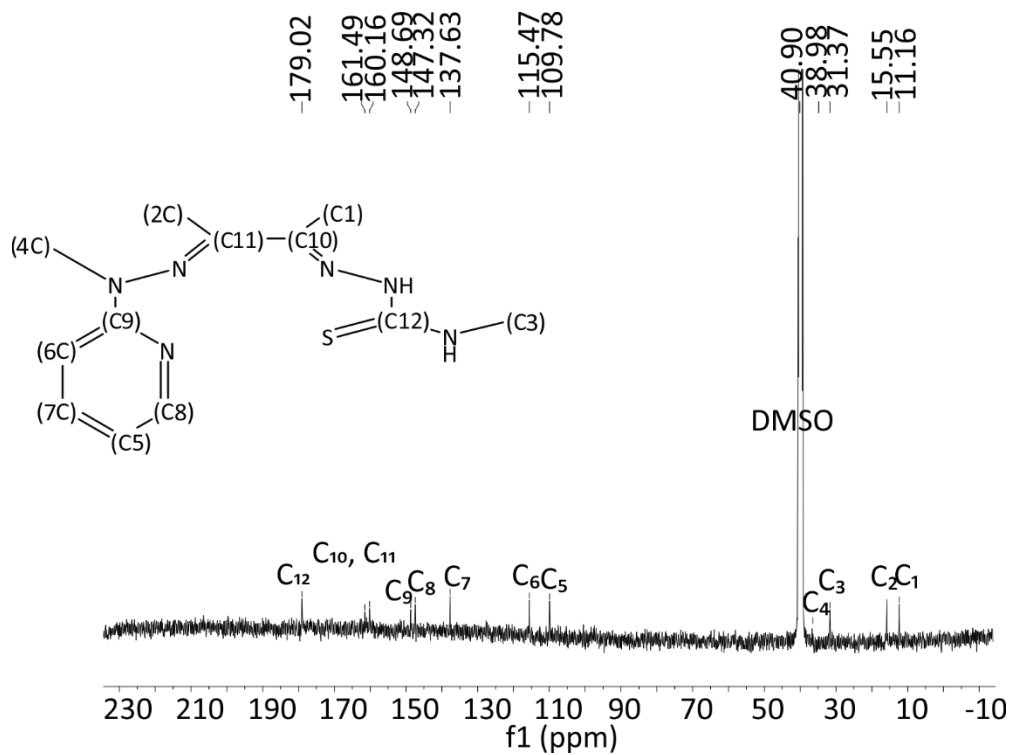


Figure A-3. ¹³C NMR of diacetyl-2-(4-methyl-3-thiosemicarbazide)-3-(2-hydrazone-N-methyl-pyridine) (H₂DMTMH).

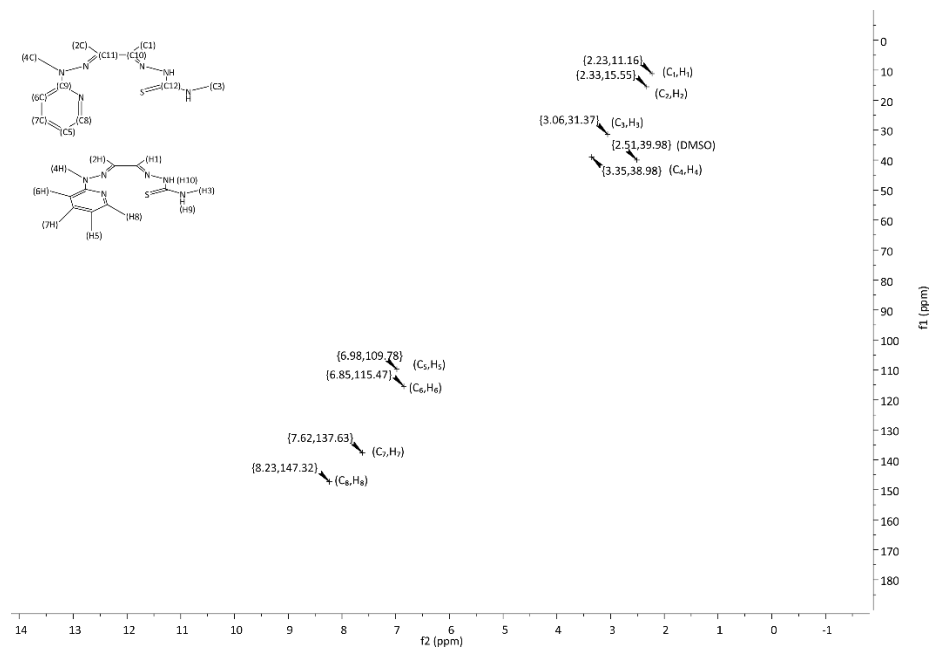


Figure A-4. HSQC NMR of diacetyl-2-(4-methyl-3-thiosemicarbazide)-3-(2-hydrazone-N-methyl-pyridine) (H₂DMTMH).

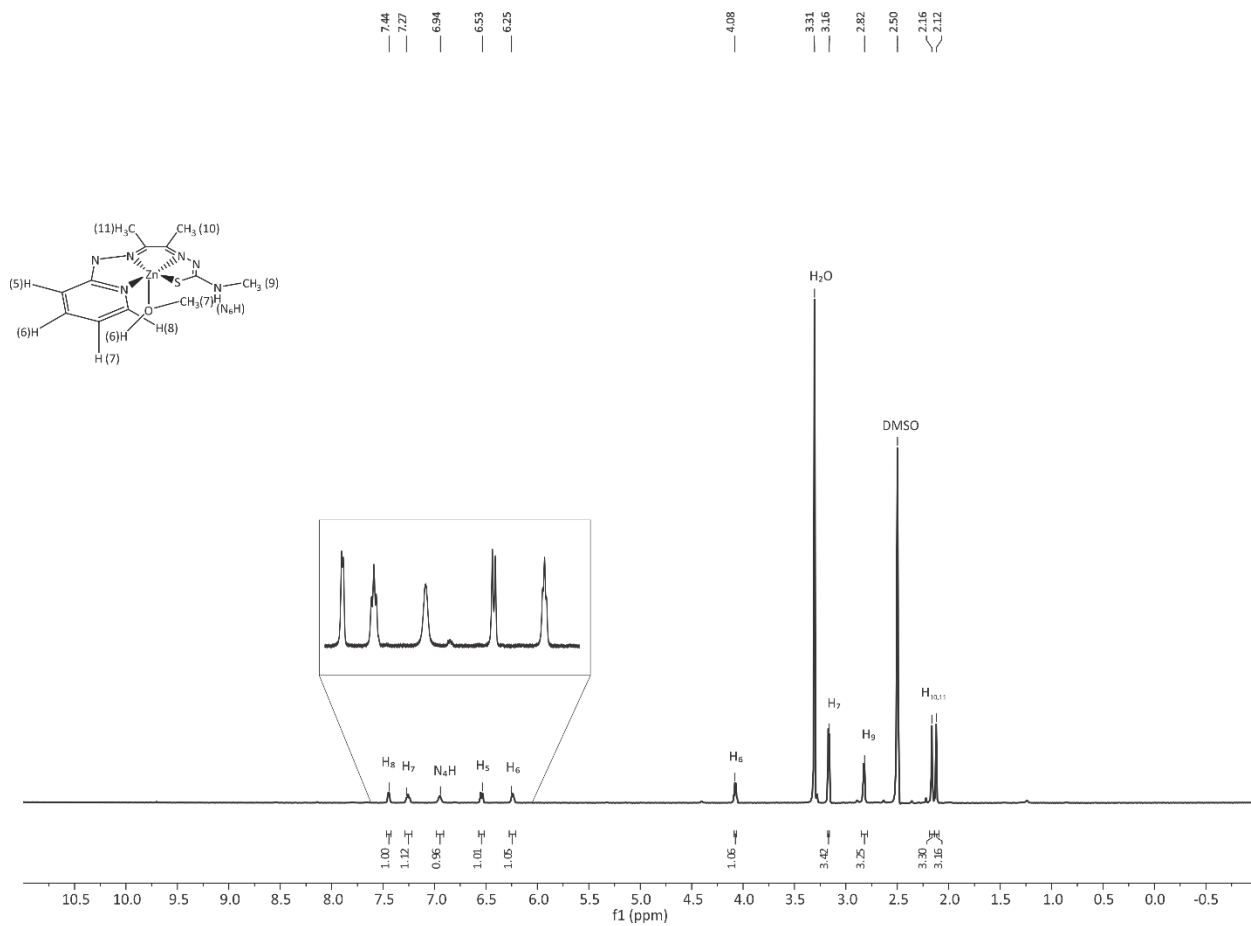


Figure A-5. ¹H NMR of ZnDMTH(MeOH).

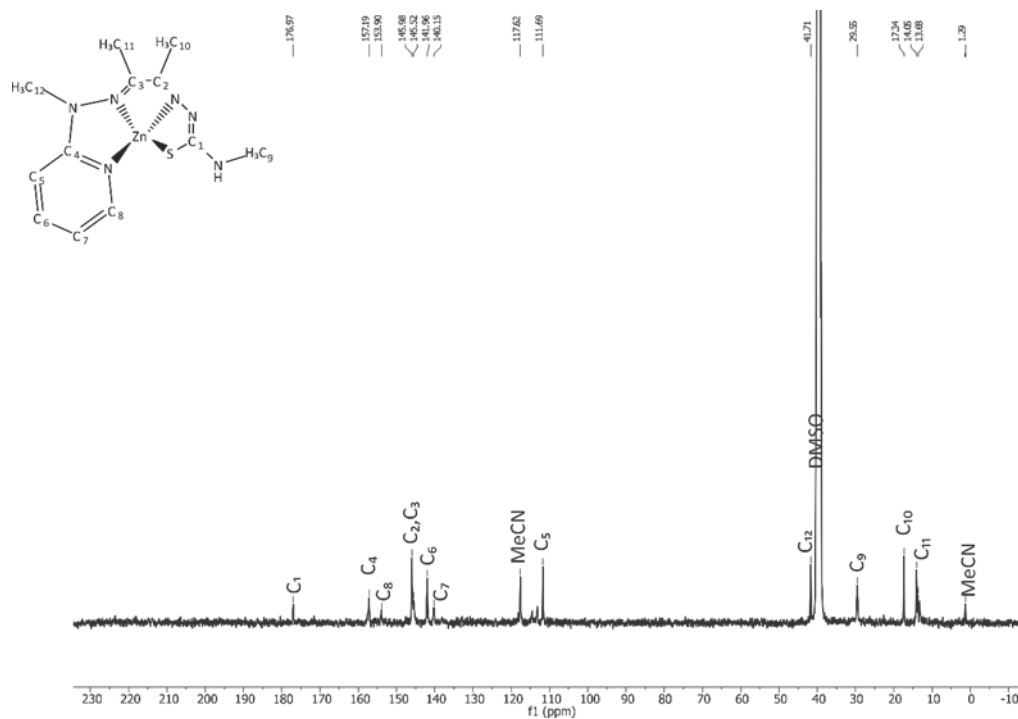


Figure A-8. ^{13}C NMR of Zn(DMTMH)I.

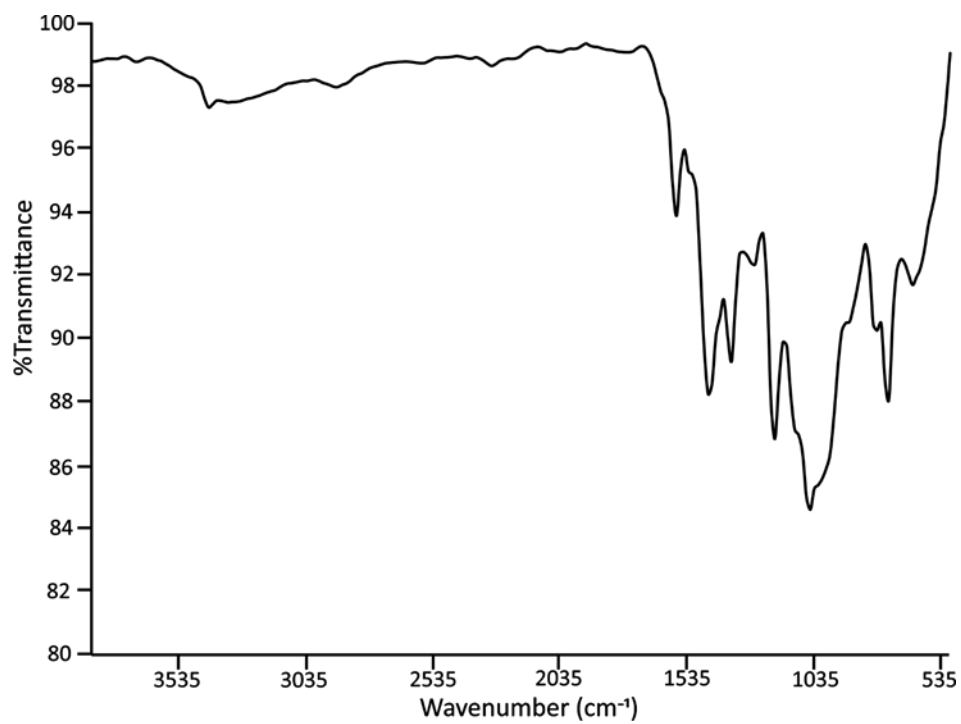


Figure A-9. FT-IR of Zn(DMTMH)I.

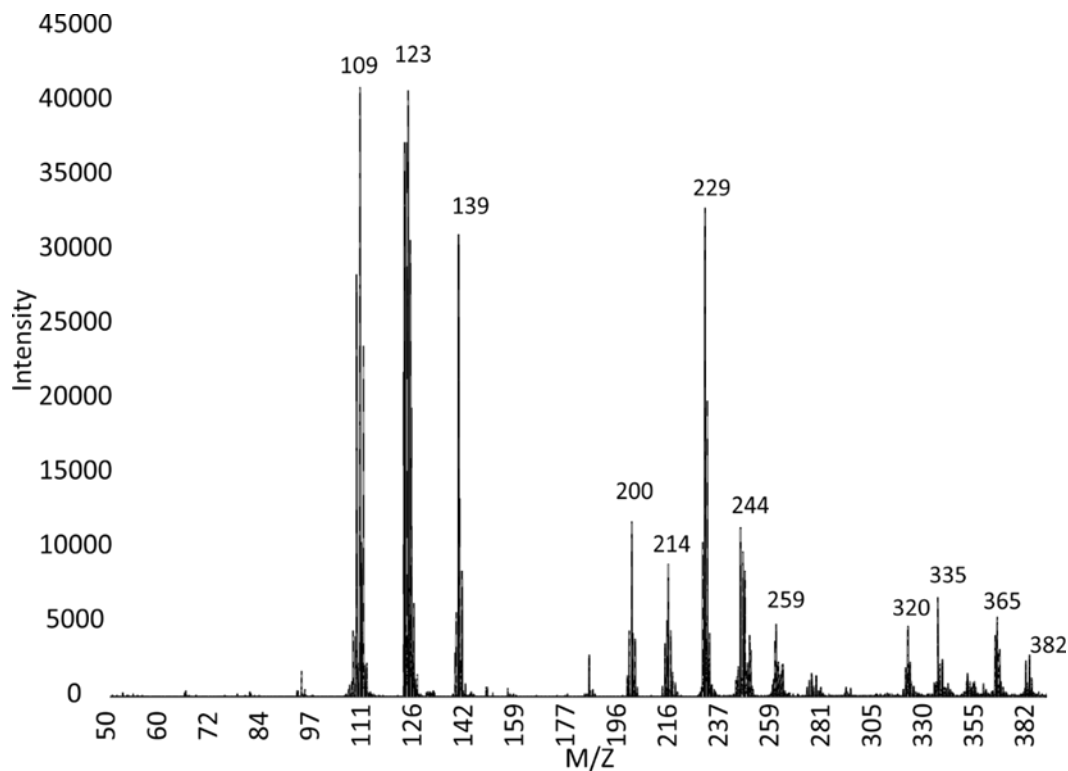


Figure A-10. Mass Spectrum of Zn(DMTMH)I.

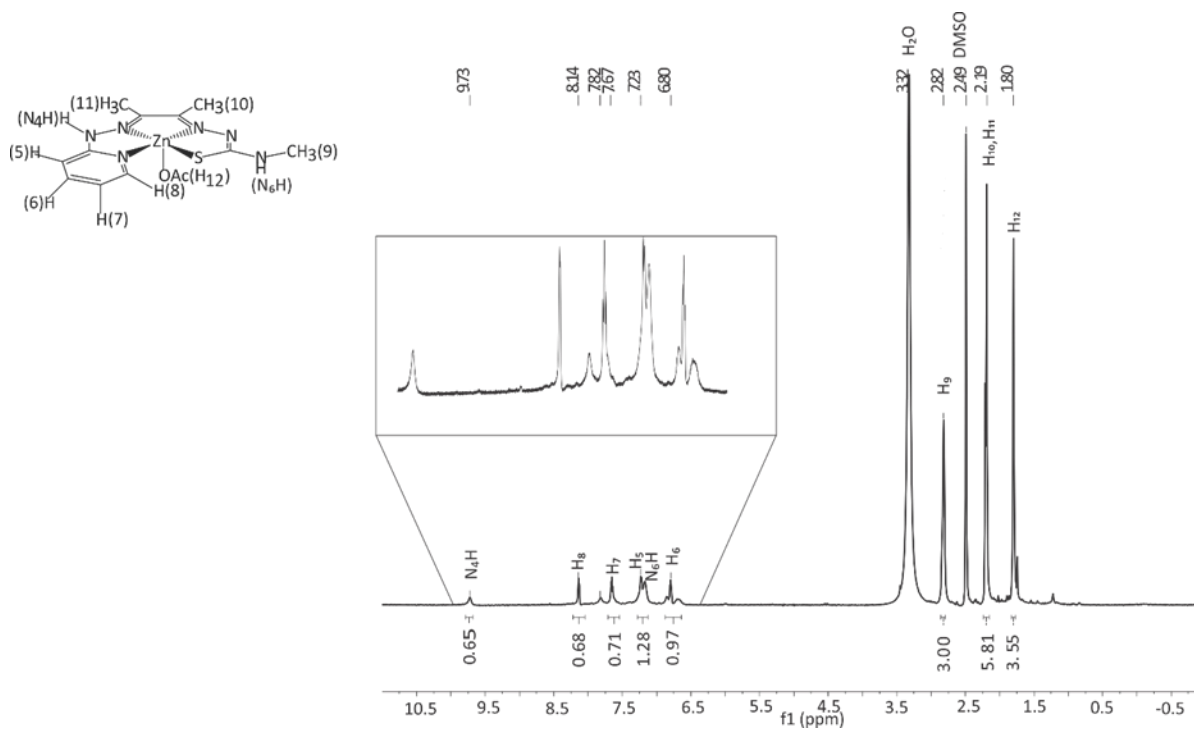


Figure A-11. ¹H NMR of Zn(HDMTH)(OAc).

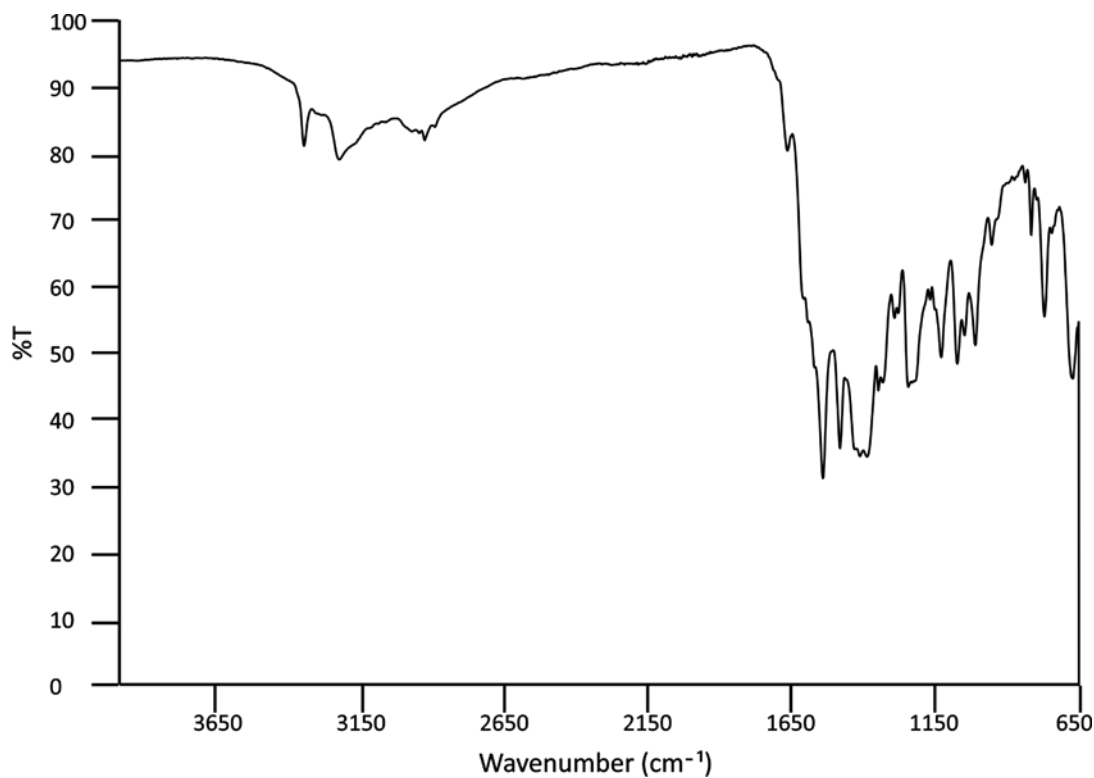


Figure A-12. FT-IR of Zn(HDMTH)(OAc).

043018-1h #122-203 RT: 0.54-0.90 AV: 81 NL: 1.62E6
 T: FTMS + p ESI Full ms [66.7000-1000.0000]

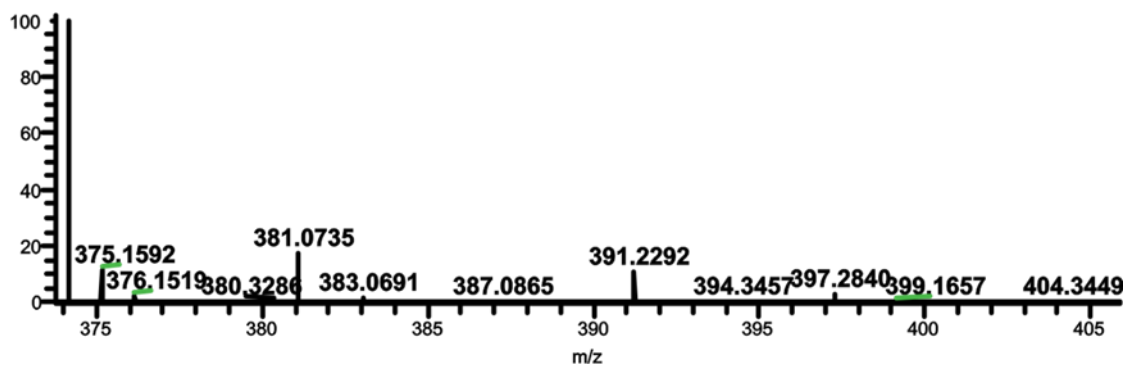


Figure A-13. Mass Spectrum of Zn(HDMTH)(OAc).

Table A-1. Crystal Data and Structural Refinement for Zn(HDMTH)(OAc) and Zn(DMTMH)I.

Empirical formula	ZnSN ₆ C ₁₃ O ₂ H ₁₈	ZnSIN ₆ C ₁₂ H ₁₇
Formula Weight	387.76	469.65
Temperature(K)	100.3(3)	100.8(2)
Wavelength(Å)	0.71073	0.71073
Crystal System	Triclinic	Orthorhombic
Space Group	P-1	P 21 21 21
Unit Cell Dimensions	a = 7.2770(3) Å	a = 7.2994(3) Å
	b = 7.6340(3) Å	b = 12.8478(5) Å
	c = 17.8924(7) Å	c = 17.248(2) Å
	α = 91.102(3)°	α = 90°
	β = 92.654(3)°	β = 90°
	γ = 115.763(4)°	γ = 90°
Volume (Å ³)	893.35(6)	1617.5(2)
Z	2	4
ρ _{calcd} (Mg m ⁻³)	1.442	1.929
Abs. coeff. (mm ⁻¹)	1.508	3.558
F(000)	400	920
Crystal color, habit	Yellow prism	Yellow prism with red tint
Crystal size (mm ³)	0.27 x 0.08 x 0.06	0.20 x 0.20 x 0.03
θ range data collection (°)	3.38 to 27.06	3.21 to 30.10
Index ranges	-9 ≤ h ≤ 9	-10 ≤ h ≤ 10
	-9 ≤ k ≤ 9	-17 ≤ k ≤ 18
	-22 ≤ l ≤ 22	-24 ≤ l ≤ 24
Reflections collected	20923	41111
Independent reflections	3915	4750
	[R(int) = 0.0369]	[R(int) = 0.0413]
Completeness to θ _{max}	99.8%	99.8%
Absorption correction	Semi-empirical from equivalents	Semi-empirical from equivalents
Max. and min. trans.	1.000 and 0.907	1.000 and 0.663
Refinement method	Full-matrix least-squares of F ²	Full-matrix least-squares on F ²
Data/restraints/parameters	3915/0/236	4750/0/236
Goodness-of-fit on F ²	1.076	1.075
Final R indices [I > 2σ(I)] ^a , b	R1 = 0.0304	R1 = 0.0251
	wR2 = 0.0738	wR2 = 0.0541

R indices (all data) ^{a, b}	R1 = 0.0330	R1 = 0.0297
	wR2 = 0.0750	wR2 = 0.0557
Largest difference peak and hole (e·Å ³)	0.700 and -0.338	0.009(13)

Table A-2. Crystal Data and Structural Refinement for Zn(HDMTH)(CO₃CH₃).

Empirical formula	C ₁₃ H ₁₈ N ₆ O ₃ S Zn
Formula Weight	403.76
Temperature	101.4 (3) K
Wavelength	0.71073 Å
Crystal system	Monoclinic
Space group	P21/c
Unit cell dimensions	a = 9.4736 (14) Å
	b = 20.760 (2) Å
	c = 9.3671 (13) Å
	α = 90°
	β = 112.821(16)°
	γ = 90°
Volume	1698.1(4) Å ³
Z	4
Density (calculated)	1.579 Mg/m ³
Absorption coefficient	1.594 mm ⁻¹
F(000)	832
Crystal color, habit	Yellow prism
Crystal size	0.23 x 0.04 x 0.02 mm ³
Theta range for data	3.76 to 25.67°
Index ranges	-11 ≤ h ≤ 11, -25 ≤ k ≤ 24, -
Reflections collected	17621
Independent reflection	3211 [R(int) = 0.1119]
Completeness to theta =	99.6%
Absorption correction	Multi-scan
Max. and min. transmission	1.000 and 0.919
Refinement method	Full-matrix least-squares on F ²
Data/restraints/parameters	3211/0/237
Goodness-of-fit on F ²	1.014
Final R indices [I > 2σ(I)]	R ₁ = 0.0578 wR ₂ = 0.0791
R indices (all data)	R ₁ = 0.1053 wR ₂ = 0.0923
Largest diff peak and hole	0.562 and -0.588 e·Å ⁻³

Table A-3. Comparison of known crystals of Zn(DMTH) and derivatives

All distances in Å all angles in °.

Complex	Zn(HDMTH) (CO ₃ CH ₃)	Zn(DMTH) (HOCH ₃)	ZnHDMT H(CO ₂ CH ₃)	ZnHDMTH(H ₂ O)NO ₃
Zn-N _{ImTSC}	2.125(4)	2.106(2)	2.1511(18)	2.0985(19)
Zn-N _{Pyr}	2.091(4)	2.057(2)	2.1245(18)	2.082(2)
Zn-N _{ImPyr}	2.139(3)	2.098(2)	2.138(17)	2.109(2)
Zn-S1	2.3245(14)	2.3279(7)	2.3113(6)	2.324(7)
C-N _{HyPyr}	1.389(6)	1.376(3)	1.382(3)	1.385(3)
N _{ImPyr} -N _{HyPyr}	1.344(5)	1.361(3)	1.355(2)	1.345(3)
Zn-O	1.991(3)	2.0443(19)	1.9868(15)	1.9974(18)
N _{Pyr} -Zn-S	117.33(11)	118.99(1)	117.82(5)	118.93(1)
N _{ImPyr} -Zn-O	101.87(13)	97.55(1)	95.11(6)	98.76(1)
N _{ImPyr} -Zn-S	137.29(11)	150.27(1)	137.61(5)	150.65(1)
N _{Pyr} -Zn-N _{ImTSC}	144.72(14)	147.19(1)	144.68(1)	145.49(1)
C-N _{ImPyr} - N _{HyPyr} -H	15.50	-	14	7

A.2 Chapter 3 Figures and Tables

Table A-4. Resistance measurements of Zn(HDMTH)(OAc), Zn(DMTMH)I, (NBu₄PF₆), and 4-nitroaniline.

Compound	Resistance (Ω)
Zn(HL ¹)Ac	24,126
ZnL ² I	9,586
NBu ₄ PF ₆	1,882
4-Nitroaniline	59,660

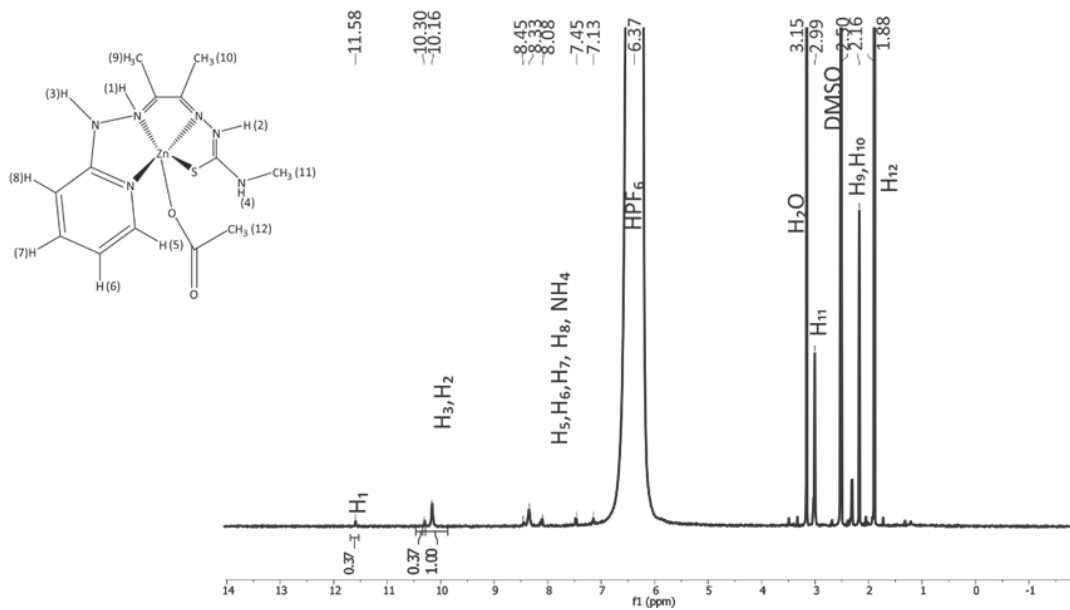


Figure A-14. ¹H NMR of Zn(HDMTH)(OAc) with HPF₆.

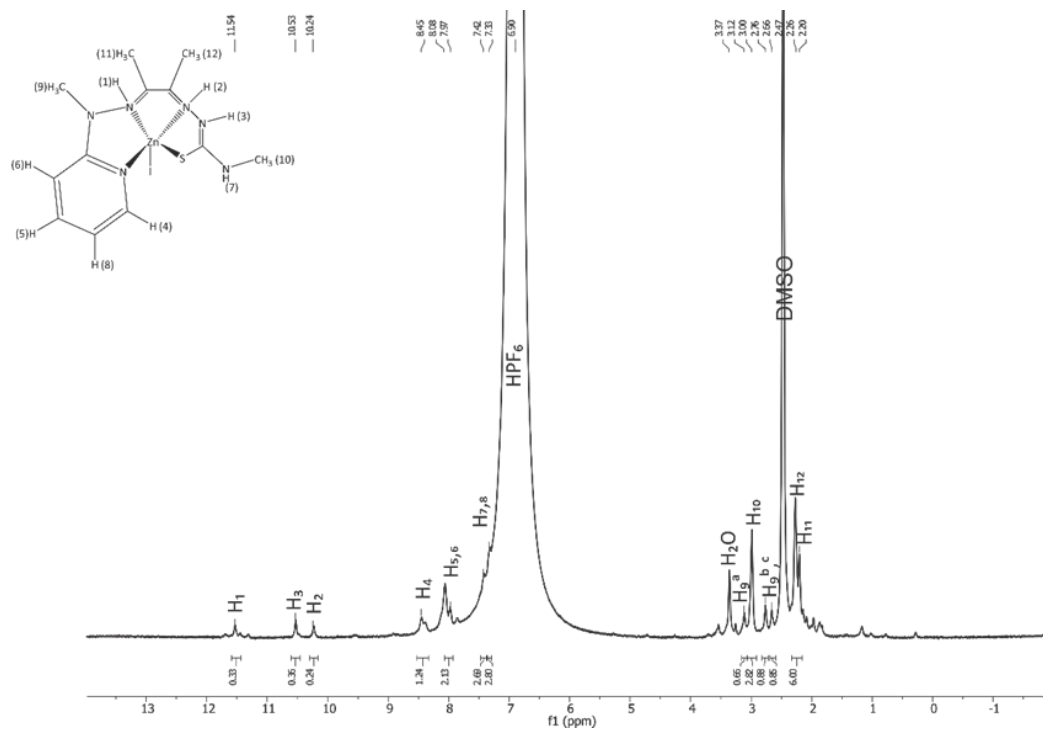


Figure A-15. ¹H NMR of Zn(DMTMH)I with HPF₆.

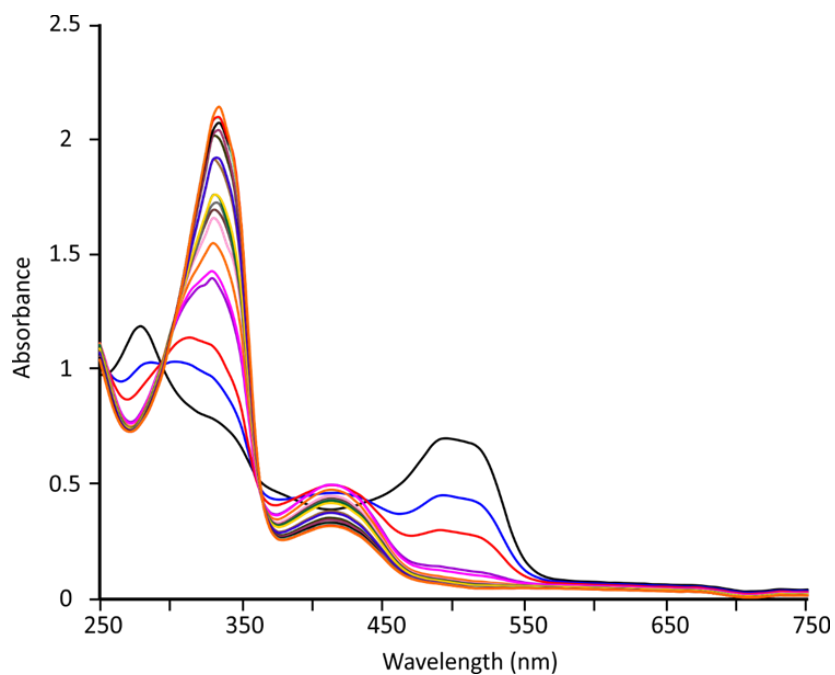


Figure A-16. UV/Vis of Zn(DMTH) with acetic acid beyond 1 equivalent

No acid in black. Traces are .01mM to .1mM, then .1mM to 1.9 mM

Table A-5. Compilation of diffusion coefficients.

Catalyst	Solvent	Slope	[cat]	D ₀
ZnL ¹	Acetonitrile	5.0 x 10 ⁻⁵	1 mM	6.87 x 10 ⁻⁶ cm ² /s
Zn(HL ¹)Ac	Acetonitrile	3.0 x 10 ⁻⁵	0.58 mM	7.35 x 10 ⁻⁶ cm ² /s
ZnL ²	Acetonitrile	5.0 x 10 ⁻⁵	1 mM	6.87 x 10 ⁻⁶ cm ² /s

Table A-6. TOF_{max} for all catalysts and conditions

Catalyst	Solvent	Acid source	ν	I _{cat} (μA)	ip(μA)	I _{cat} /ip	TOF _{max} s ⁻¹
ZnL ¹	Acetonitrile	Acetic Acid	1.1 V/s	3200	53.4	59.93	7700
ZnL ²	Acetonitrile	Acetic Acid	2.0 V/s	1628	39.08	41.66	6700

Table A-7. Data for the calculation of E^T_{1/2}

Catalyst	Solvent	pKa	C ⁰ _{H₂} (mM)	C ⁰ _{AA} (mM)	E ^T _{1/2} (V)
ZnL ¹	Acetonitrile	22.3	3.30	240	-1.40
ZnL ²	Acetonitrile	22.3	3.30	72	-1.39

Table A-8. Overpotential values for each catalyst and solvent.

Catalyst	Solvent	E ^T _{1/2} (V)	E _{cat/2} (V)	η vs Fc/Fc ⁺ (V)
ZnL ¹	Acetonitrile	-1.22	-2.67	1.45
ZnL ²	Acetonitrile	-1.23	-1.95	0.72

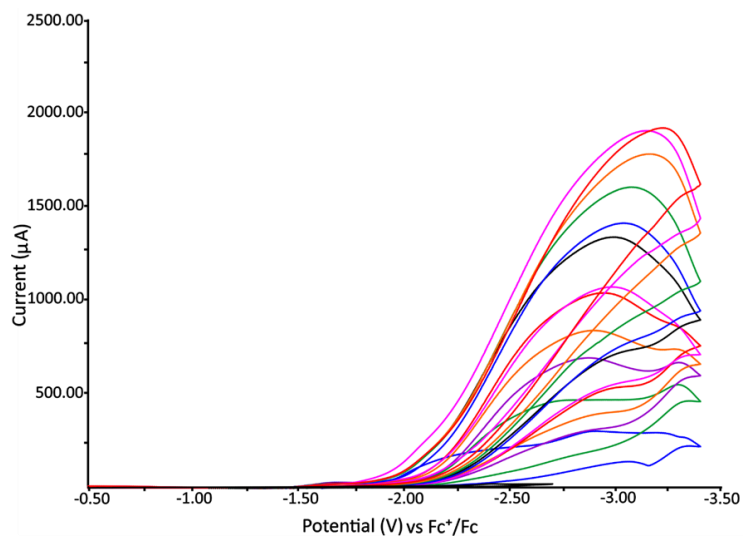


Figure A-17. Cyclic voltammetry of Zn(DMTH) in acetonitrile with acetic acid, full data, scan rate (0.2 V/s).

Each scan is with 30 mM acetic acid addition with background subtraction of the corresponding concentration of acid.

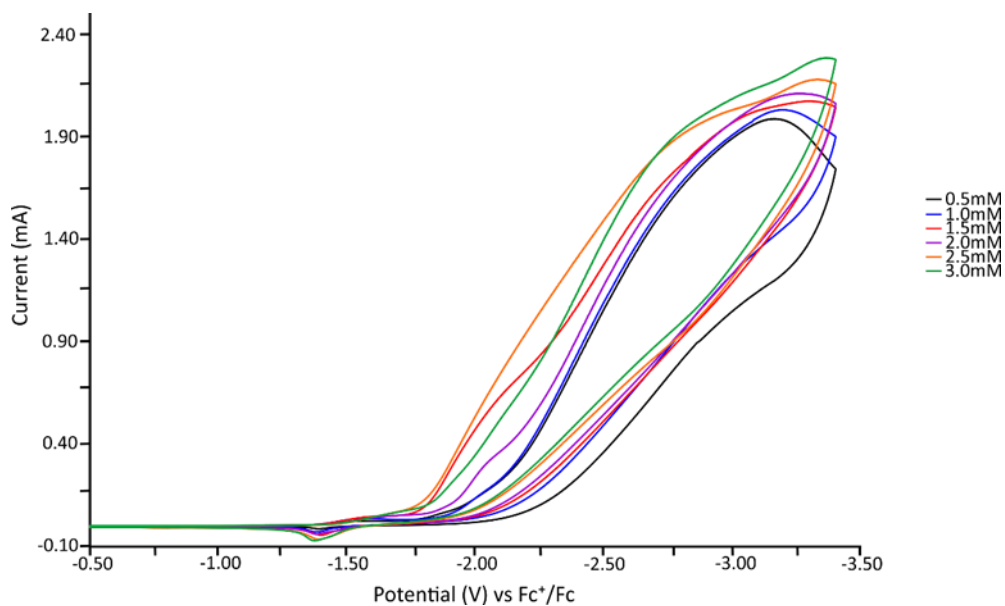


Figure A-18. Catalyst Dependence study for Zn(DMTH) in acetonitrile, scan rate (0.2 V/s).

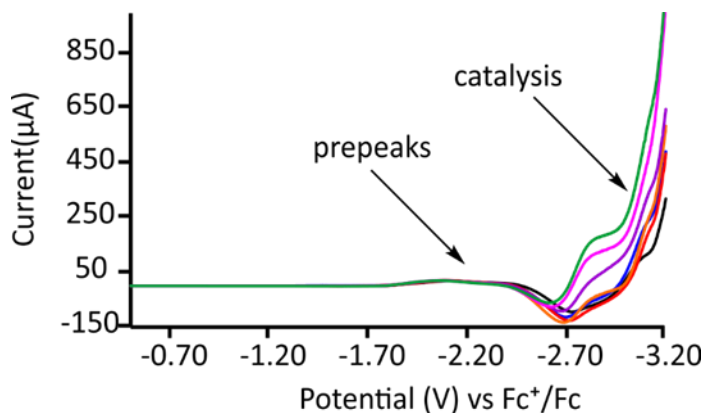


Figure A-19. Cyclic voltammetry of Zn(DMTH) in acetonitrile with phenol, full data, scan rate (0.2 V/s).

After subtraction of the corresponding concentration of phenol 17mM, 20mM, 24mM, 28mM, 32 mM, 36 mM, 40mM shown

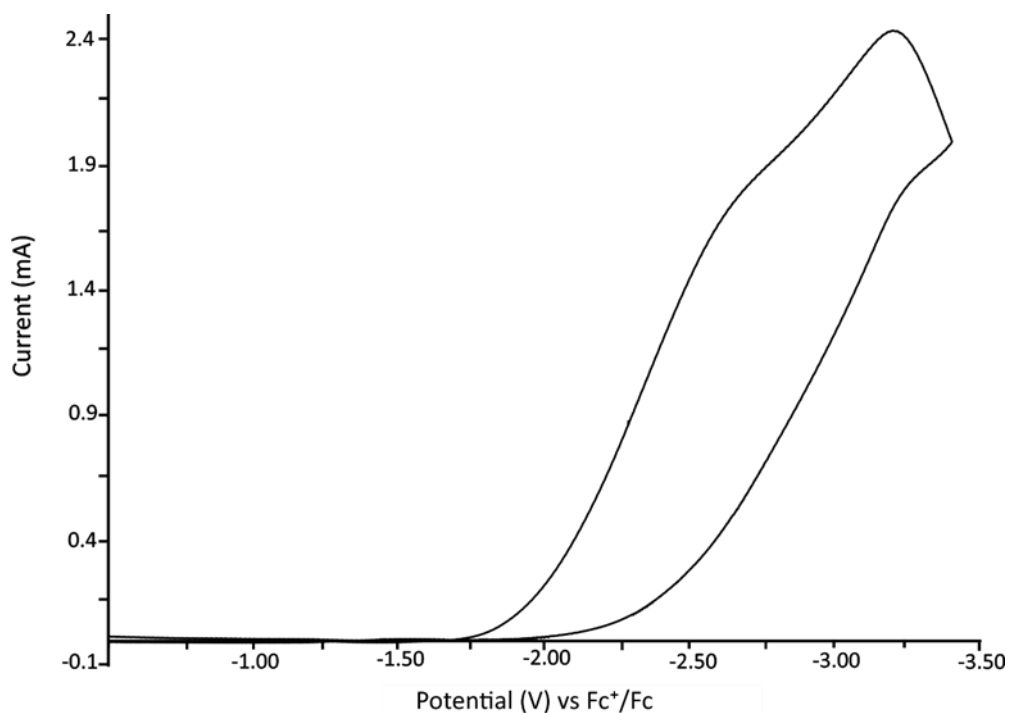


Figure A-20. Cyclic voltammetry of Zn(DMTH) in acetonitrile with acetic acid (D₄), (scan 1) scan rate (1.0 V/s).

With background subtraction of the corresponding concentration of acid.

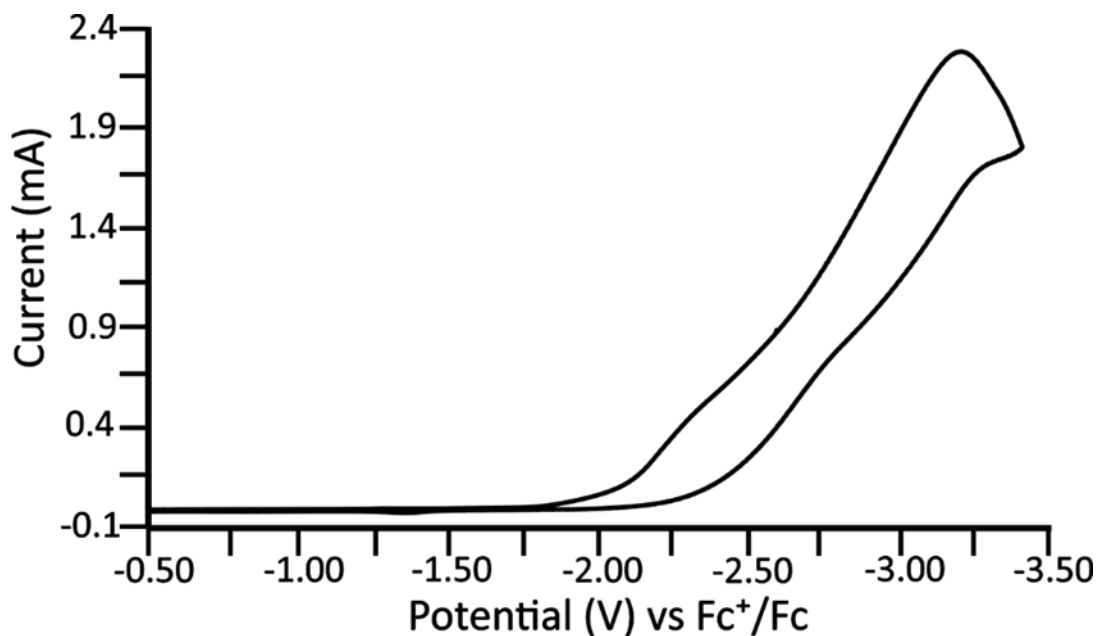


Figure A-21. Cyclic voltammetry of Zn(DMTH) in acetonitrile with acetic acid (D₄), (scan 2) scan rate (1.0 V/s).

With background subtraction of the corresponding concentration of acid.

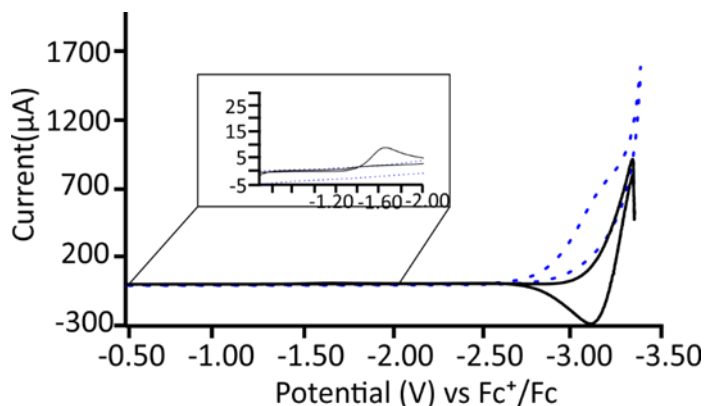


Figure A-22. Cyclic voltammetry of Zn(DMTH) in acetonitrile with 2.74 M methanol, full data, scan rate (0.2 V/s).

Blue Dashed 2.74 M methanol in acetonitrile. Black **1** in 2.74M methanol and acetonitrile with blue dashed subtracted. Inset, Reduction of **1** in 2.74M methanol and acetonitrile.

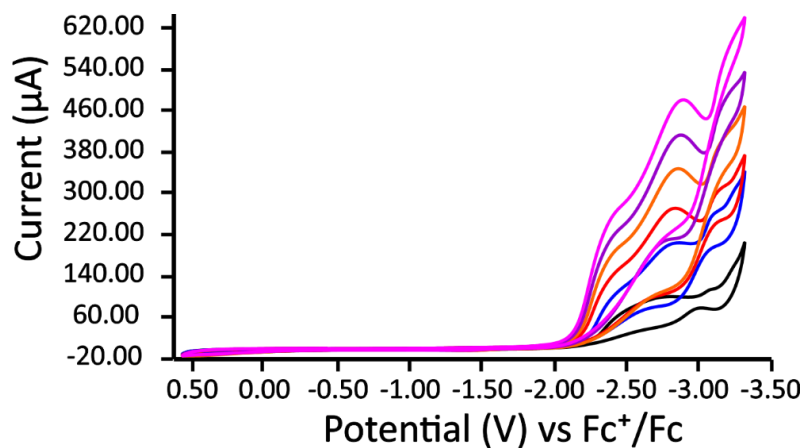


Figure A-23. Cyclic voltammetry of Zn(HDMTH)(OAc) in acetonitrile with acetic acid, full data, scan rate (0.2 V/s).

Each addition is 6mM with background subtraction of the corresponding concentration of acid.

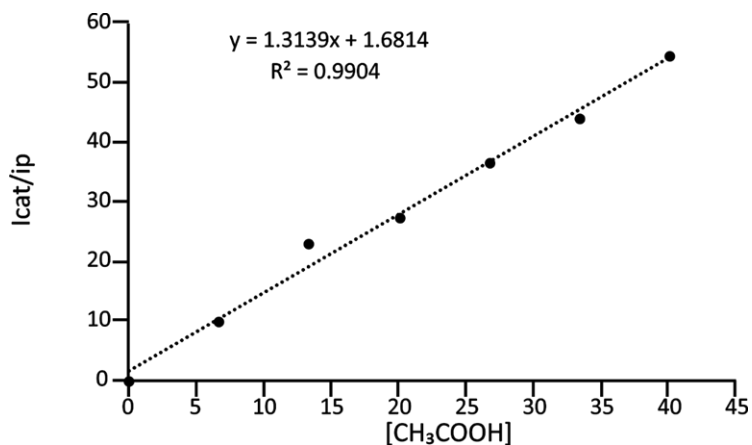


Figure A-24. I_{cat}/I_p vs [CH₃COOH] plot in acetonitrile scan rate (0.2V/s) for Zn(HDMTH)(OAc)

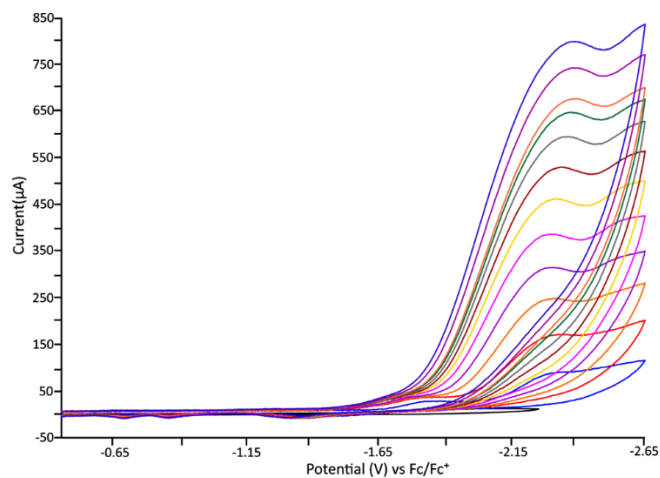


Figure A-25. Cyclic voltammetry of Zn(DMTMH) in acetonitrile with acetic acid, full data, scan rate (0.2 V/s).

Each addition is 6 mM acetic acid with background subtraction of the corresponding concentration of acid.

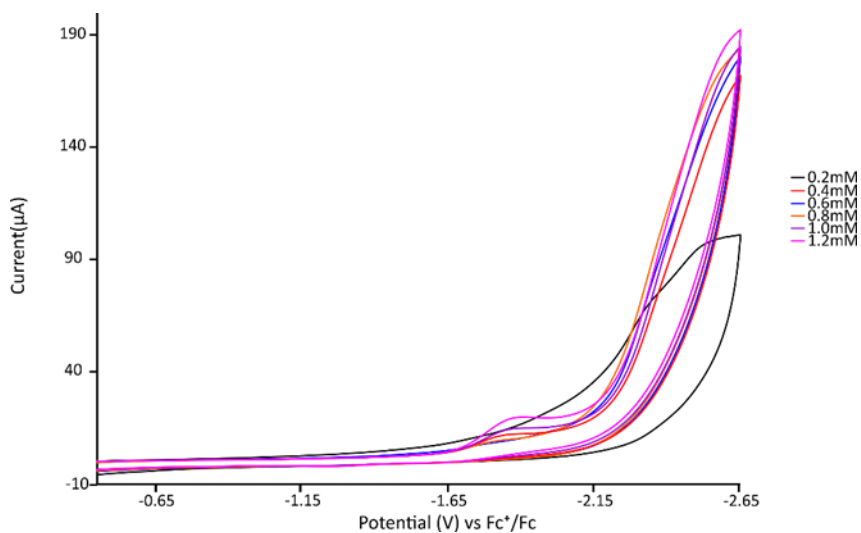


Figure A-26. Catalyst Dependence study for Zn(DMTMH) in acetonitrile, scan rate (0.2 V/s).

Each addition is 0.2 mM with background subtraction of the corresponding concentration of acid.

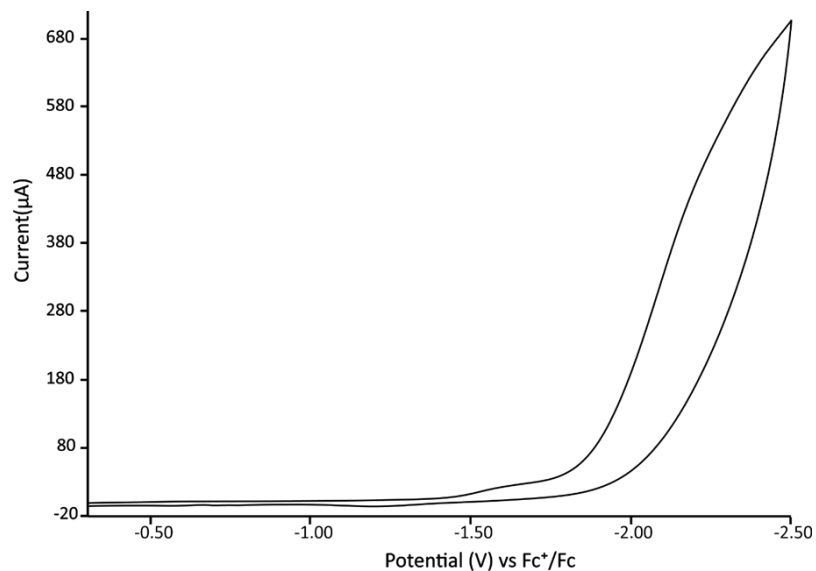


Figure A-27. Cyclic voltammetry of Zn(DMTMH) in acetonitrile with acetic acid (D₄), (scan 1) scan rate (1.0 V/s).

With background subtraction of the corresponding concentration of acid.

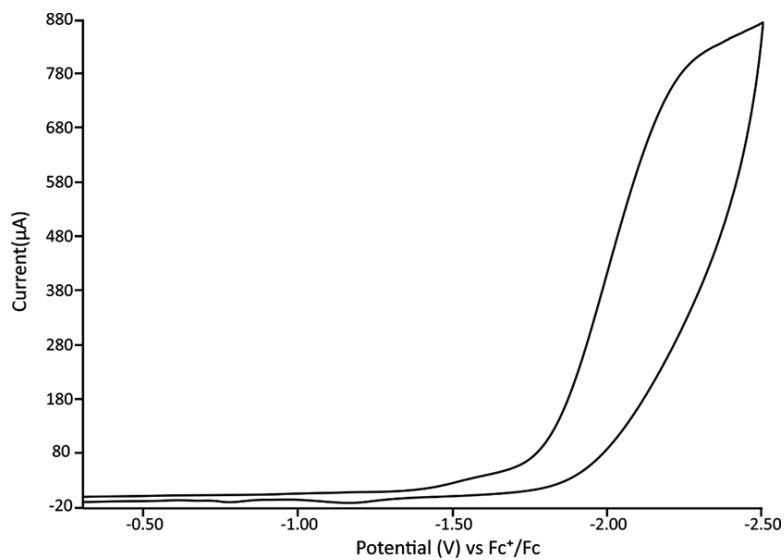


Figure A-28. Cyclic voltammetry of Zn(DMTMH) in acetonitrile with acetic acid (D₄), (scan 2) scan rate (1.0 V/s).

With background subtraction of the corresponding concentration of acid.

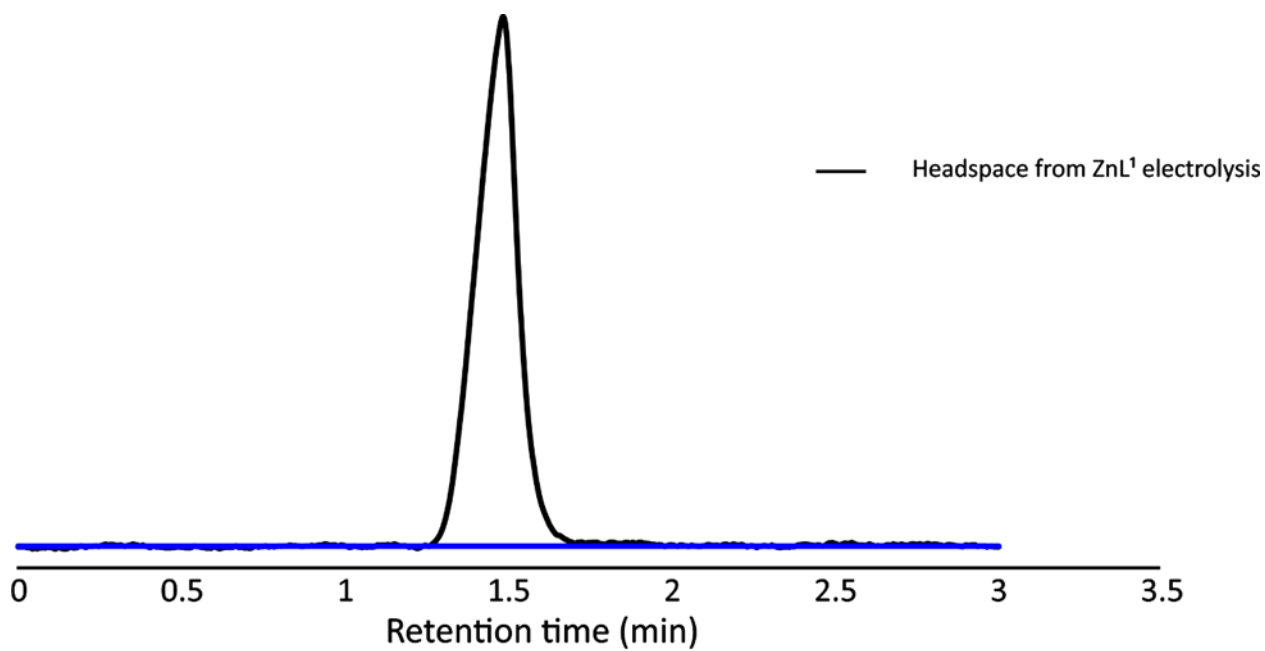


Figure A-29. GC/Headspace readout for Zn(DMTH).

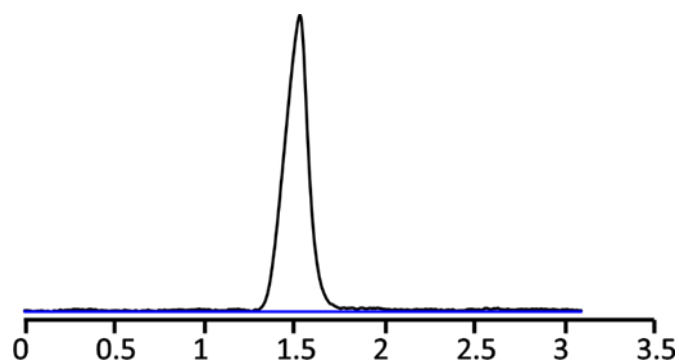


Figure A-30. GC/Headspace readout for Zn(DMTMH).

Table A-9. Compilation of CPC experiments for HER.

Catalyst	Displacement (cm)	Volume (mL)	Number of moles (mol)	Charge (C)	Charge with blank subtracted	Moles with blank subtracted	TON	Theoretical moles	Faradaic efficiency
ZnL ¹	7.00	6.89	28.2 x 10 ⁻⁵	104.5	51.4	189 x 10 ⁻⁶	189	266 x 10 ⁻⁶	71.0
ZnL ²	0.40	0.39	1.61 x 10 ⁻⁵	3.54	1.84	8.45 x 10 ⁻⁶	845	9.53 x 10 ⁻⁶	88.6
Blank ZnL ¹	2.30	2.26	9.26 x 10 ⁻⁵	51.3					
Blank ZnL ²	0.19	0.19	2.01 x 10 ⁻⁵	1.7					

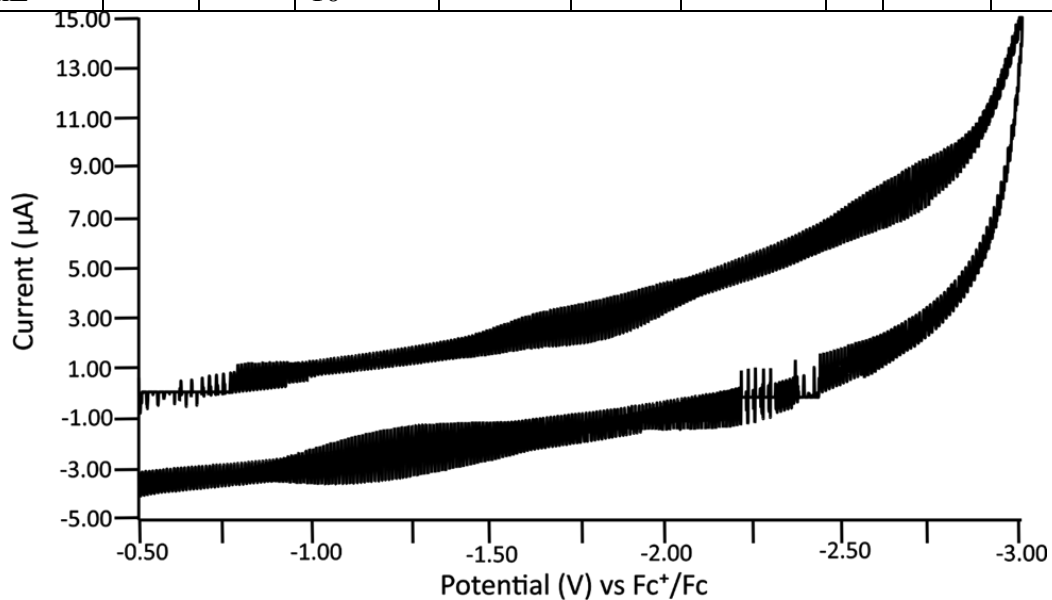


Figure A-31. Cyclic voltammogram of electrode following soak test of Zn(DMTH).

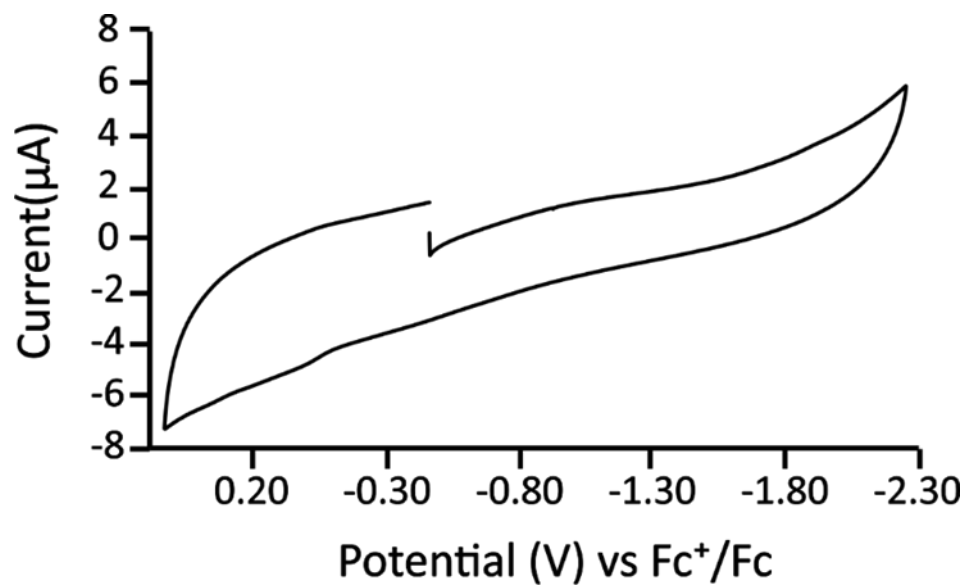


Figure A-32. Cyclic voltammogram of electrode following soak test of Zn(DMTMH).

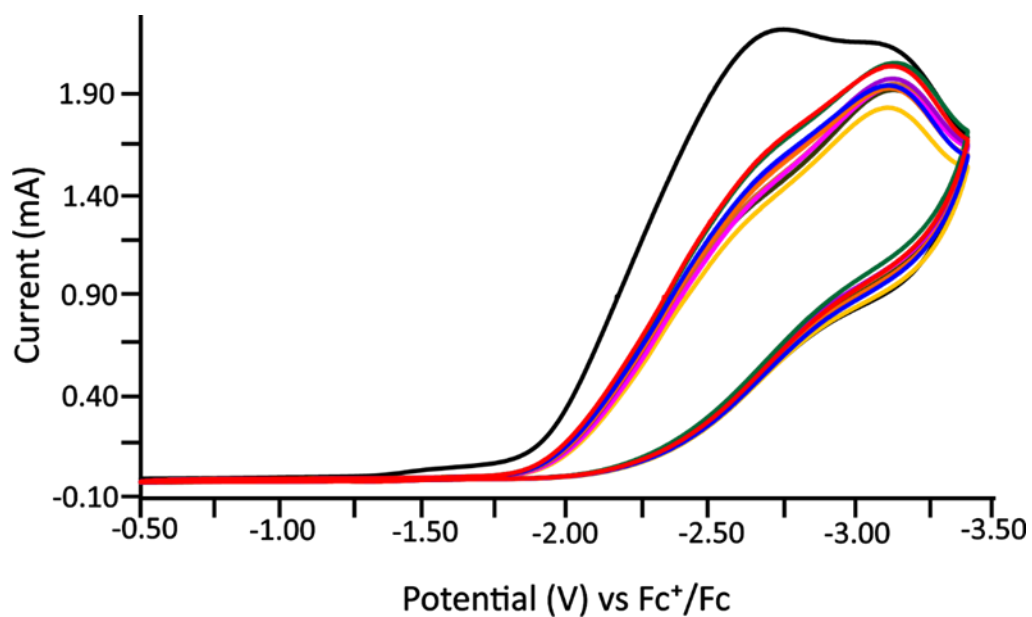


Figure A-33. Cyclic voltammetry multiple cycles (10-cycles) for Zn(DMTH) CV.

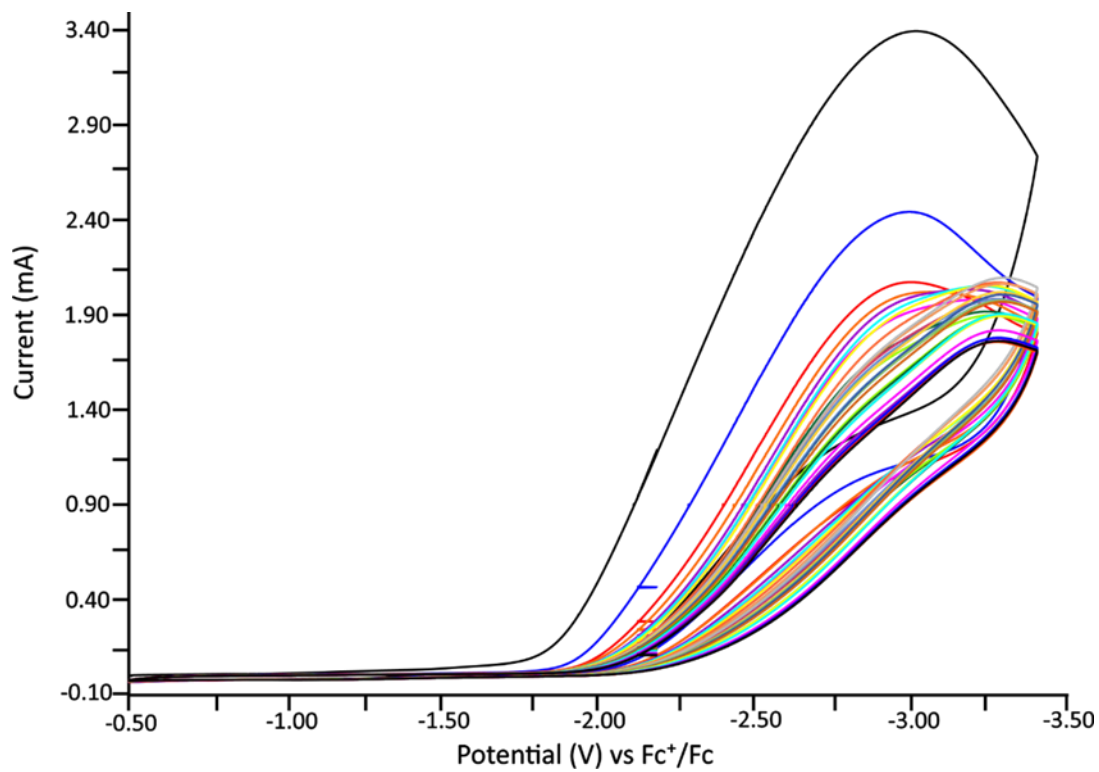


Figure A-34. Cyclic voltammetry multiple cycles (30-cycles) for Zn(DMTH) CV.

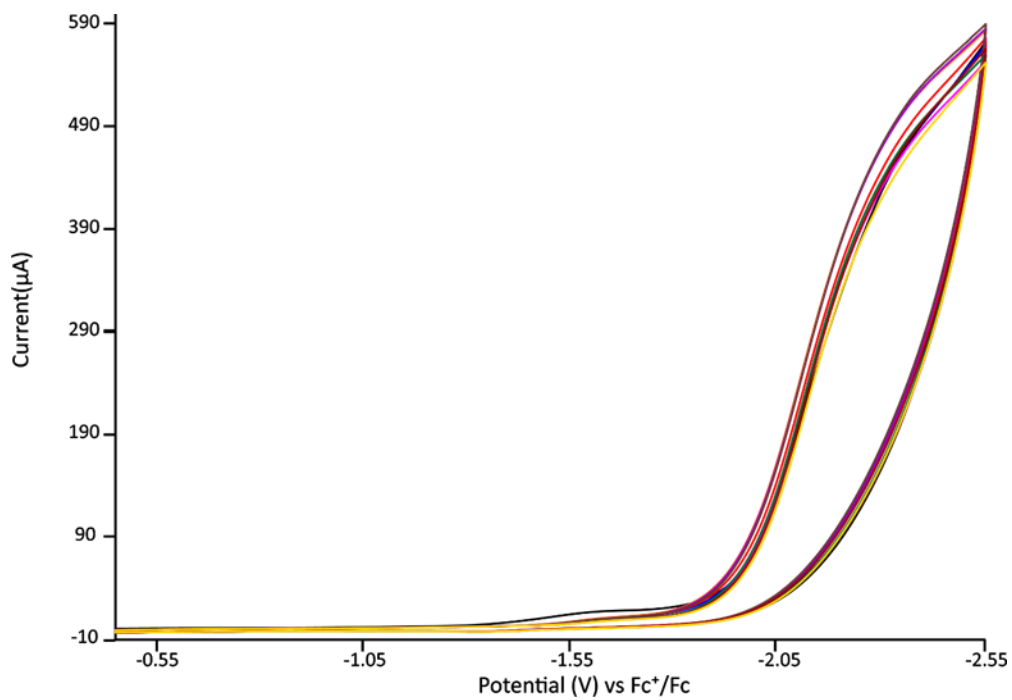


Figure A-35. Cyclic voltammetry multiple cycles (10-cycles) for Zn(DMTMH) CV.

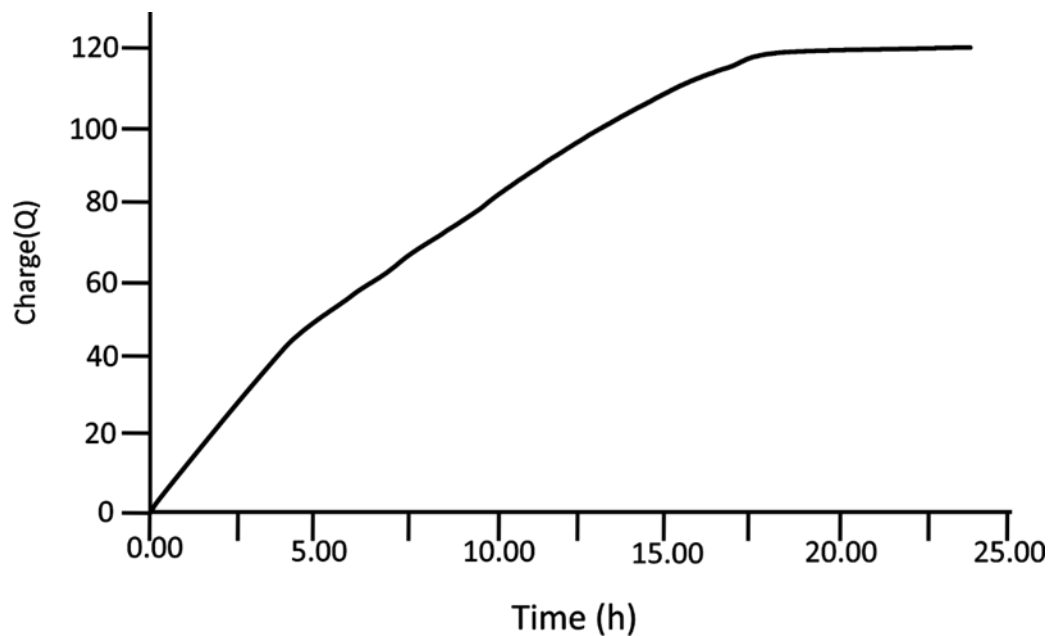


Figure A-36. Bulk electrolysis for depositing of Zn(DMTH).

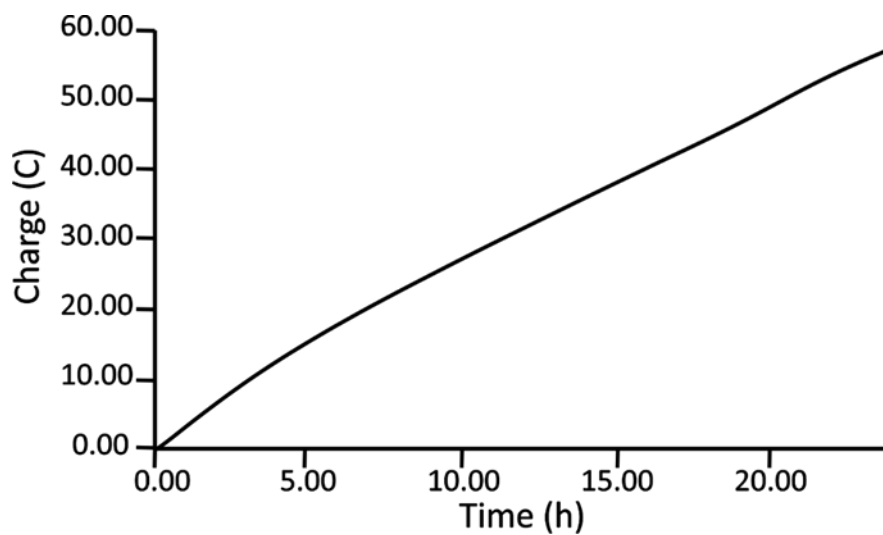


Figure A-37. Bulk electrolysis for depositing of Zn(DMTMH).

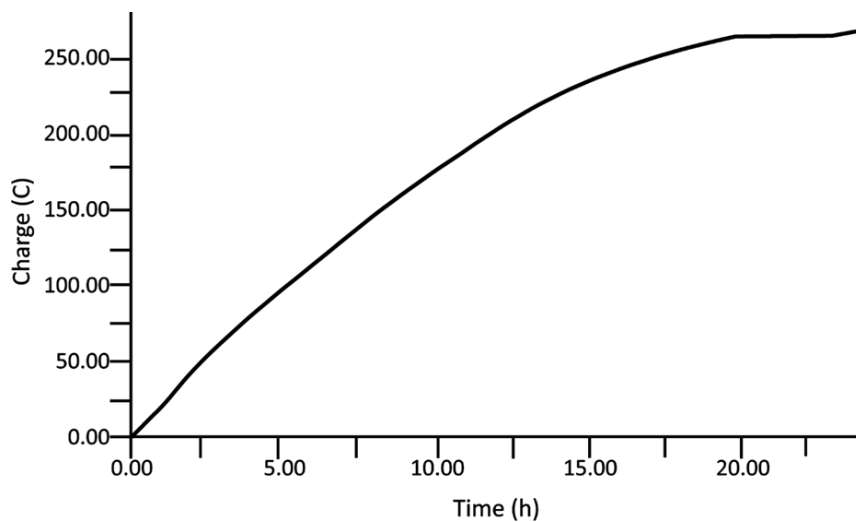


Figure A-38. Bulk electrolysis for depositing of Zn(DMTH) for XPS.

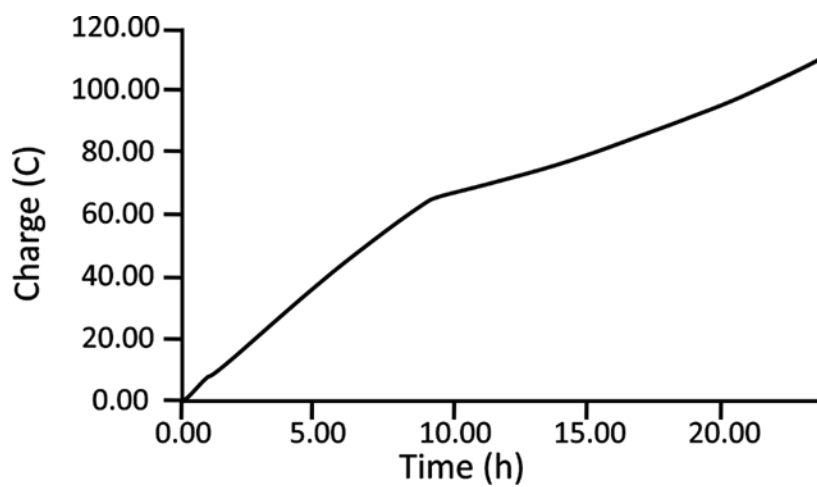


Figure A-39. Bulk electrolysis for depositing of Zn(DMTMH) for XPS.

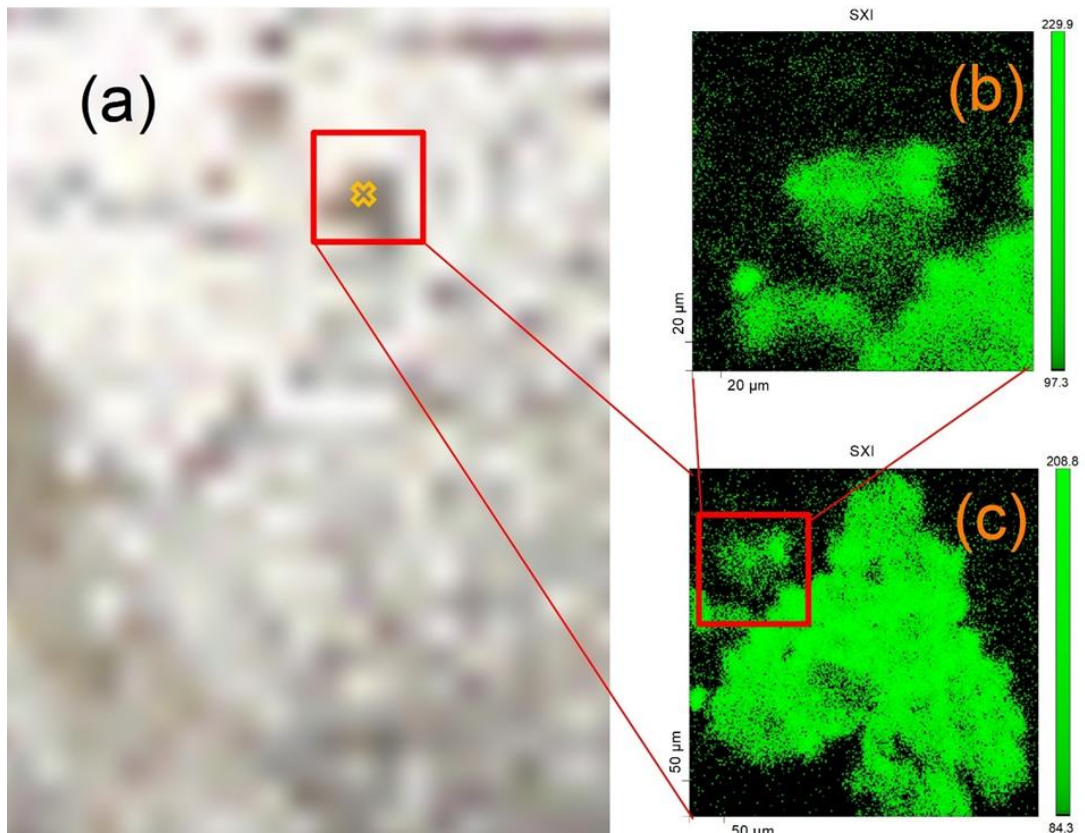


Figure A-40. SXI Image for Zn(DMTMH).

Optical image (a) and x-ray beam induced secondary electron images (SXI) (b) and (c) with scale bar indicated.

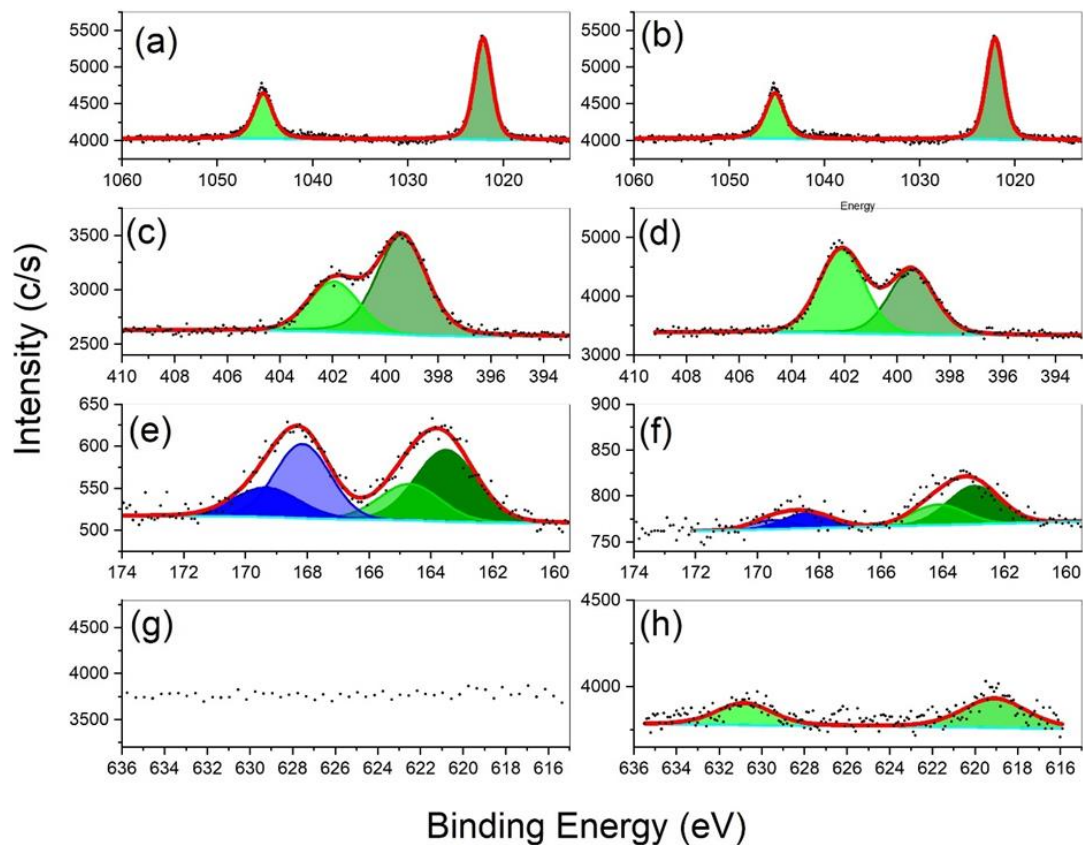


Figure A-41. HR XPS for Zn(DMTH) and Zn(DMTMH).

Zn 2p (a), N 1s (c), S 2p (e) and I 3d (g) spectra of 1sample. HR XPS Zn 2p (b), N 1s (d), S 2p (f) and I 3d (h) spectra of 3 sample. Black dots represents experimental data, red color represent generated fit. Dark green and light green for (a, b) represents Zn 2p_{3/2} and Zn 2p_{1/2} transition respectively. Dark green and light green for (c, d) represents two different N species. Dark green and light green for (e, f) represents S 2p_{3/2} and S2p_{1/2}¹⁶⁹ while dark and light blue represents S 2p_{3/2} and S2p_{1/2}.¹⁷⁰ Light green for (h) represents I3d_{5/2} and I3d_{3/2} spin-orbit split components. See Tables S10 and S11 for corresponding fitting parameters.

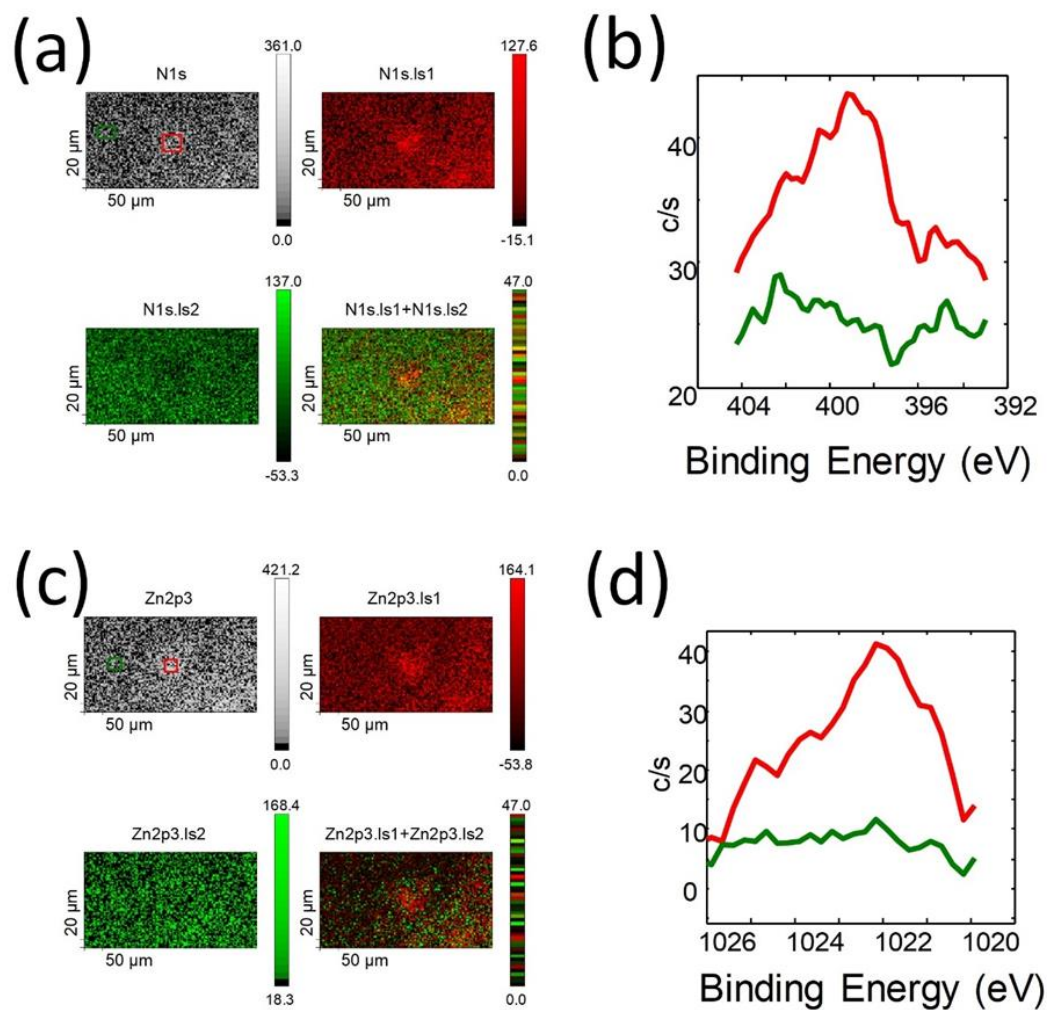


Figure A-42. Elemental mapping for Zn(DMTMH).

Elemental N 1s (a, b) and Zn 2p_{3/2} (c, d) mapping for feature in red square of sample 3 (see Fig. S54). Pixels were integrated across the red and green squares resulting in corresponding XPS spectra (b) and (c) with enhanced Zn and N lateral distribution within SXI feature.

Table A-10. Compilation of expected, normalized, and actual atomic percentages for XPS of Zn(DMTH) and Zn(DMTMH).

	1	3
N _{expected}	0.75	0.667
S _{expected}	0.125	0.111
Zn _{expected}	0.125	0.111
I _{expected}	0	0.111
N _{actual}	0.772	0.898
S _{actual}	0.09	0.03
Zn _{actual}	0.138	0.133
I _{actual}	0	0.006
N _{normalized}	6	6
Zn _{normalized}	1.07	0.88
S _{normalized}	0.699	0.200
I _{normalized}	0	0.04

Table A-11. Compilation of fitting parameters for all elements for XPS for Zn(DMTH).

Element	Band	Position, eV	PosSep, eV	FWHM, eV	% Gauss	% Area	Chi Squared
S2p	1	163.51	0.00	2.33	90	35.13	1.27
	2	164.69	1.18	2.33	90	17.88	
	3	168.16	4.65	2.11	100	31.32	
	4	169.34	5.83	2.51	89	15.66	
Zn2p	1	1022.11	0.00	2.16	69	65.27	1.55
	2	1045.20	23.09	2.37	50	34.73	
N1s	1	399.38	0.00	2.21	74	68.31	1.09
	2	401.95	2.57	2.21	94	31.69	

Table A-12. Compilation of fitting parameters for all elements for XPS for Zn(DMTMH).

Element	Band	Position, eV	PosSep, eV	FWHM, eV	% Gauss	%Area	Chi Squared
S2p	1	162.97	0.00	2.04	90	48.72	1.13
	2	164.15	1.18	2.04	100	24.80	
	3	168.38	5.38	1.94	100	17.65	
	4	169.53	6.56	1.63	100	8.83	
Zn2p	1	1022.19	0.00	2.28	90	69.27	0.97
	2	1045.30	23.11	2.37	50	31.73	
N	1	399.46	0.00	2.04	78	44.94	1.41
	2	402.11	2.65	2.04	88	55.06	
I3d	1	619.08	0.00	3.55	70	60.26	1.23
	2	630.83	11.76	3.11	70	39.74	

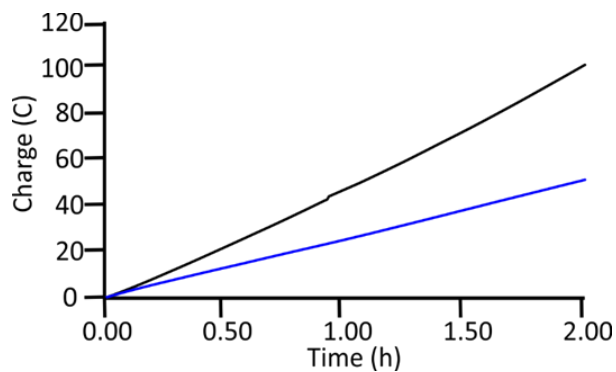


Figure A-43. H-cell electrolysis test for Zn(DMTMH).

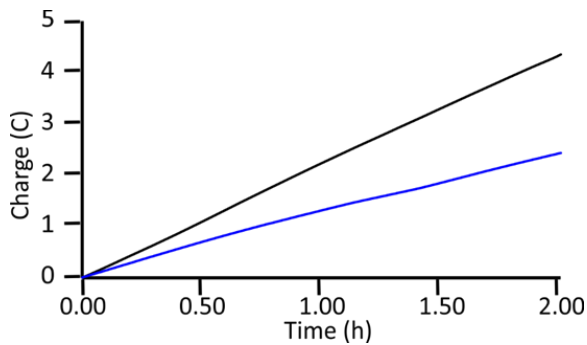


Figure A-44. H-cell electrolysis test for Zn(DMTMH).

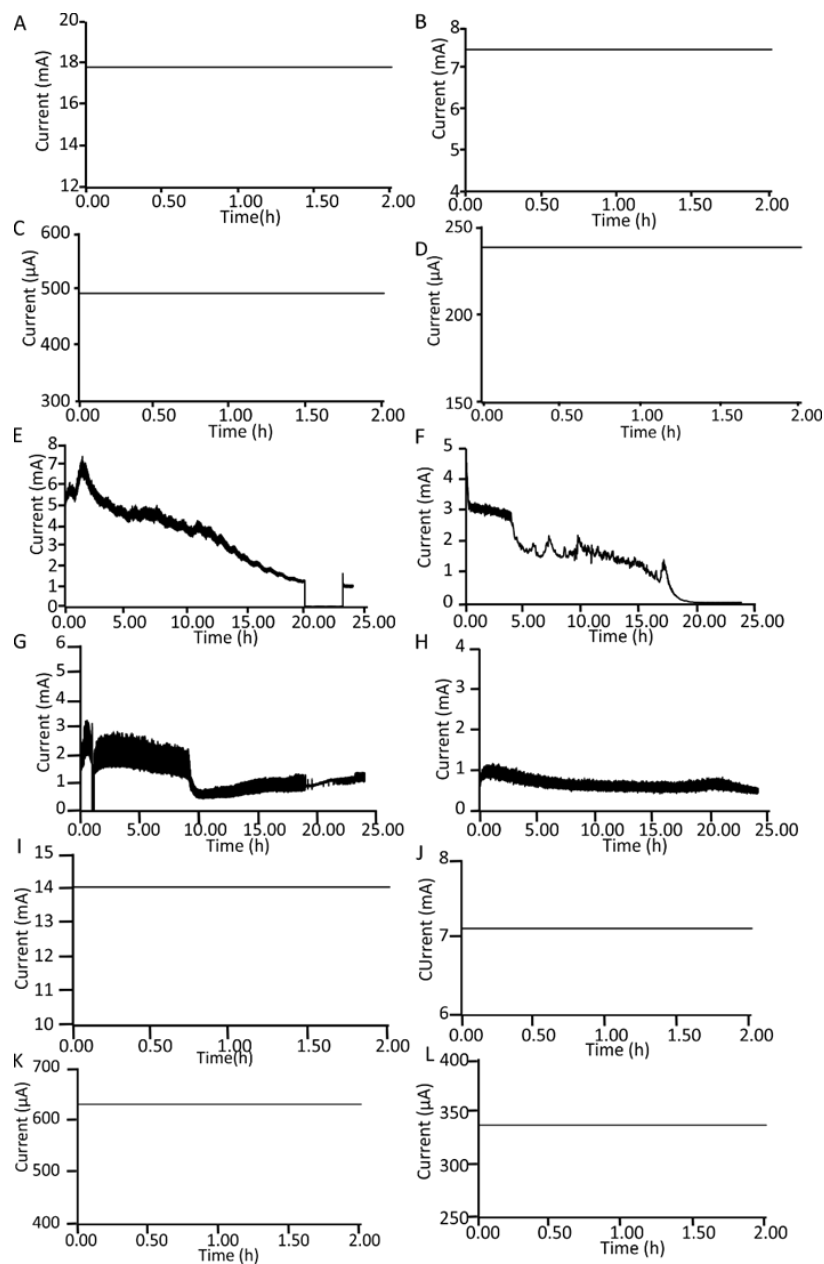


Figure A-45. All current vs time plots for all CPC experiments.

A. Bulk electrolysis for Faradaic efficiency of **1** (Figure III-9A Black) B. Bulk electrolysis for Faradaic efficiency of the blank of **1** (Figure III-9A red) C. Bulk electrolysis for Faradaic efficiency of **3** (Figure III-9B Black) D. Bulk electrolysis for Faradaic efficiency of the blank of **3** (Figure III-9B red) E. Bulk Electrolysis for XPS of **1** (Figure A-37) F.

Bulk Electrolysis for depositing **1** (Figure A-35) G. Bulk Electrolysis for depositing **3** for XPS (Figure A-38) H. Bulk Electrolysis for depositing **3** (Figure A-36) I. H-Cell test for **1** with catalyst (Figure A-42 black) J. H-Cell test for **1** post run after rinse with DI H₂O (Figure A-42 Blue) K. H-Cell test for **3** with catalysts (Figure A-43 black) L. H-Cell test for **3** post run after rinse with DI H₂O (Figure A-43 Blue).

Table A-13. Comparison of computational distances and actual distance for Zn(DMTH).

Bond	Actual(Å)	Computed(Å)
Zn-S	2.3279	2.37
Zn-N ₁	2.106	2.12
Zn-N ₃	2.098	2.10
Zn-N ₅	2.057	2.06

Table A-14. Compilation of calculated reduction potentials from Born-Haber, Fc⁺/Fc direct, and experimental.

Reduction event	Fc ⁺ /Fc direct (V)	Born-Haber (V)	Experimental (V)
2-H ⁺ /2-H	-1.83	-1.78	-1.97
2-H ₂ ⁺ /2-H ₂	-1.36	-1.31	-2.67
2-H/2-H ⁻	-2.47	-2.42	-2.67

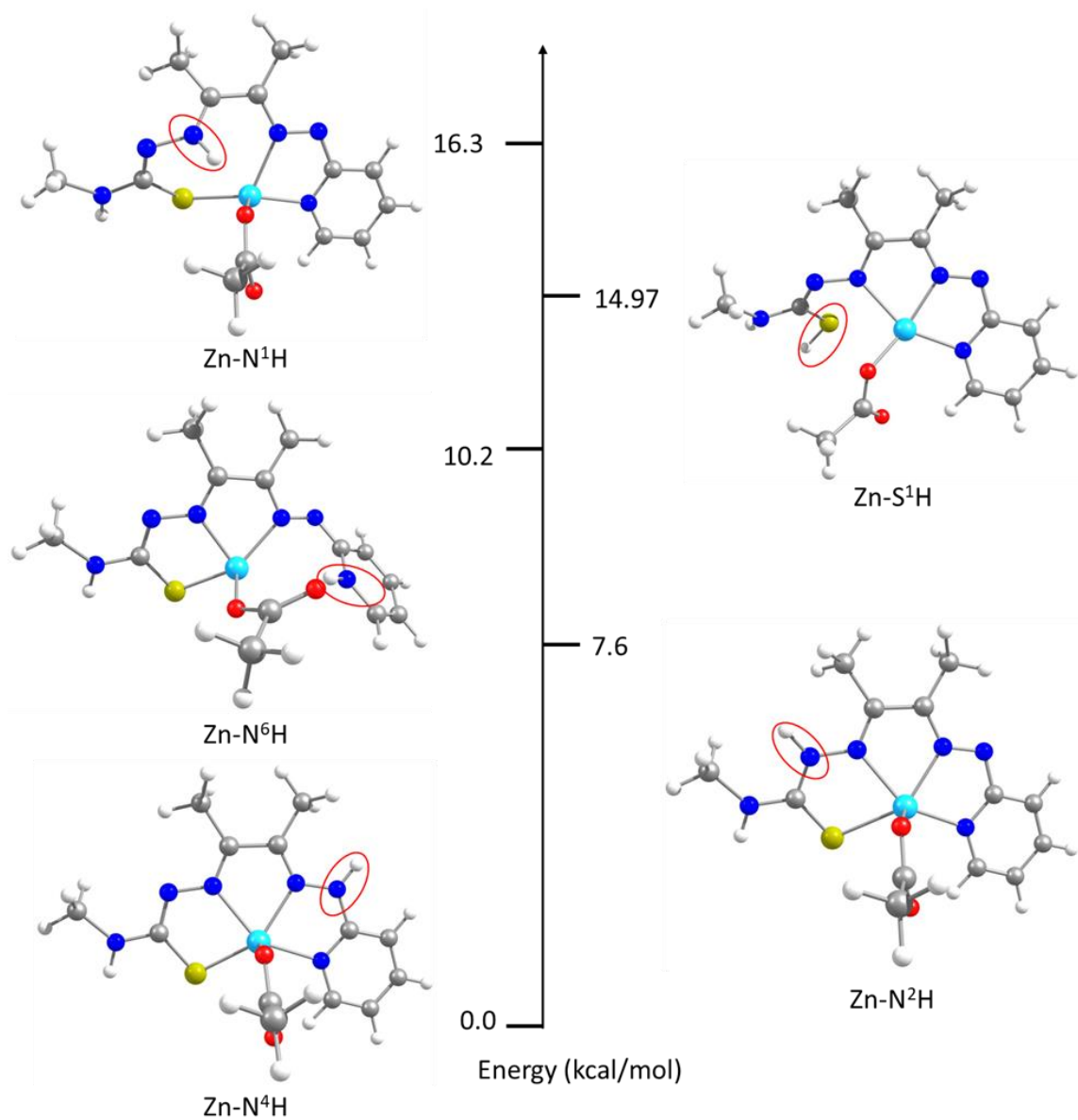


Figure A-46. Relative energy diagram for different computed tautomers of Zn(HDMTH)(OAc).

Energy diagram of the protonated species of ZnL¹ (2) computed by DFT with B3LYP/6-311g (d,p) (S=0, q=0) in PCM solvent model using acetonitrile as a solvent

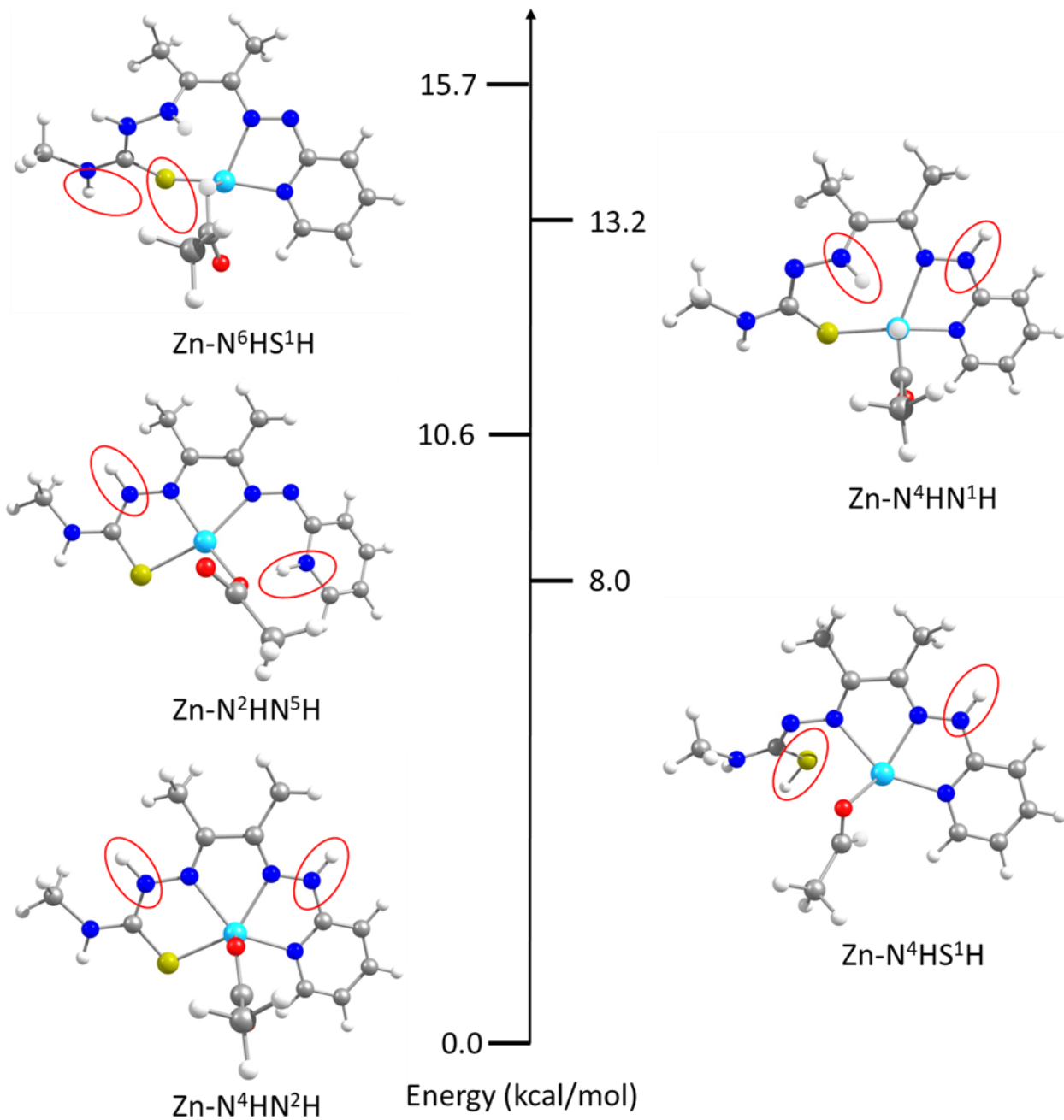


Figure A-47. Relative energy diagram for $\text{Zn}(\text{H}_2\text{DMTH})(\text{OAc})^+$.

Energy diagram of the protonated/protonated species of $\text{ZnL}^1 (2\text{-H}^+)$ computed by DFT with B3LYP/6-311g(d,p) ($S=0, q=1$) in PCM solvent model using acetonitrile as a solvent.

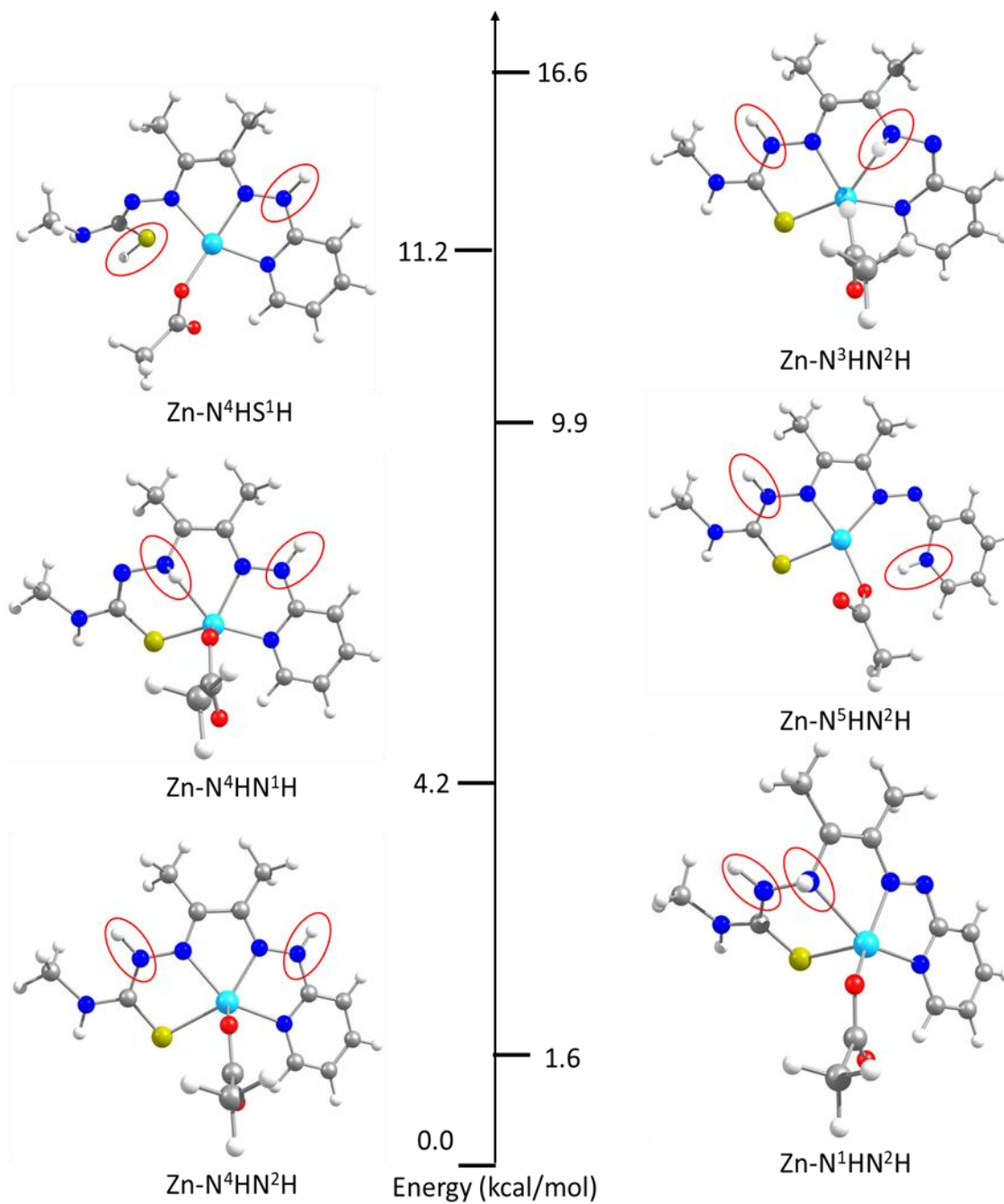


Figure A-48. Relative energy diagram for Zn(H₂DMTH)(OAc).

Energy diagram of the protonated/protonated/reduced species of ZnL¹ (2-H) computed by DFT with B3LYP/6-311g(d,p) ($S=1/2$, $q=0$) in PCM solvent model using acetonitrile as a solvent.

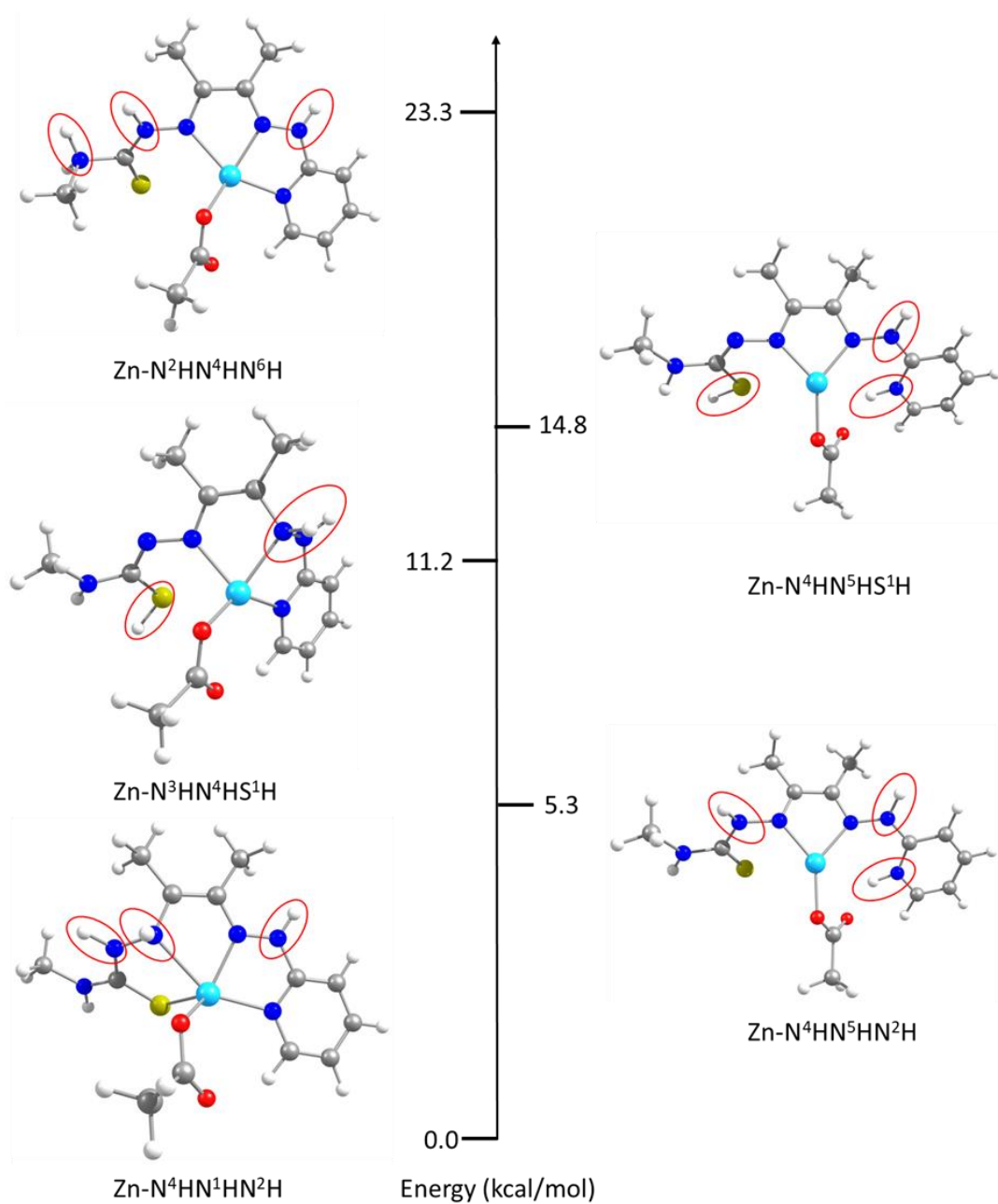


Figure A-49. Relative energy diagram for $\text{Zn}(\text{H}_3\text{DMTH})(\text{OAc})^+$.

Energy diagram of the protonated/protonated/reduced/protonated species of ZnL^1 (2-H_2^+) computed by DFT with B3LYP/6-311g(d,p) ($S = 1/2$, $q=1$) in PCM solvent model using acetonitrile as a solvent.

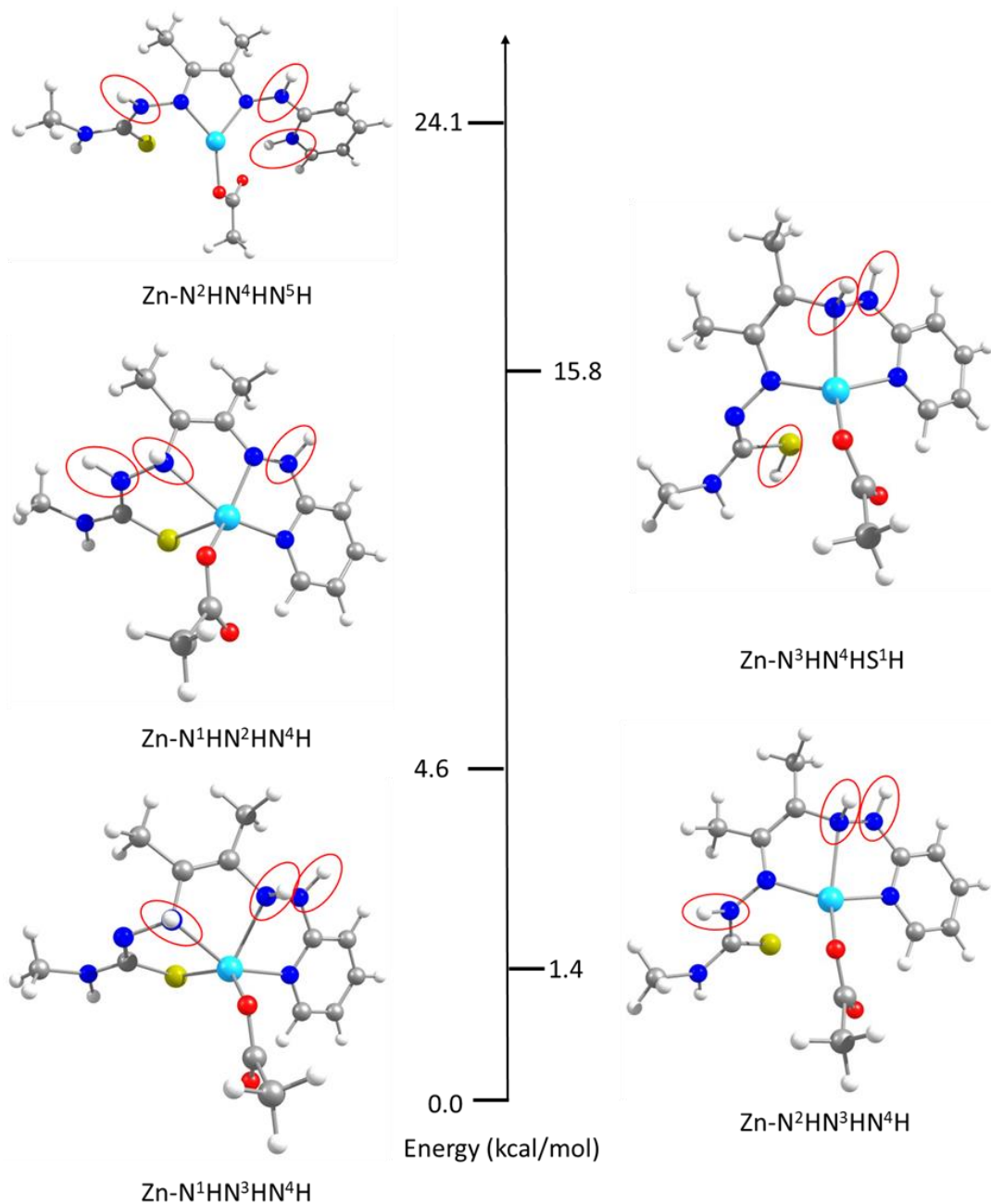


Figure A-50. Relative energy diagram for Zn(H₃DMTH)(OAc).

*Energy diagram of the protonated/protonated/reduced/protonated/reduced species of ZnL¹ (2-H₂) computed by DFT with B3LYP/6-311g(d,p) (*S* = 0, *q* = 0) in PCM solvent model using acetonitrile as a solvent.*

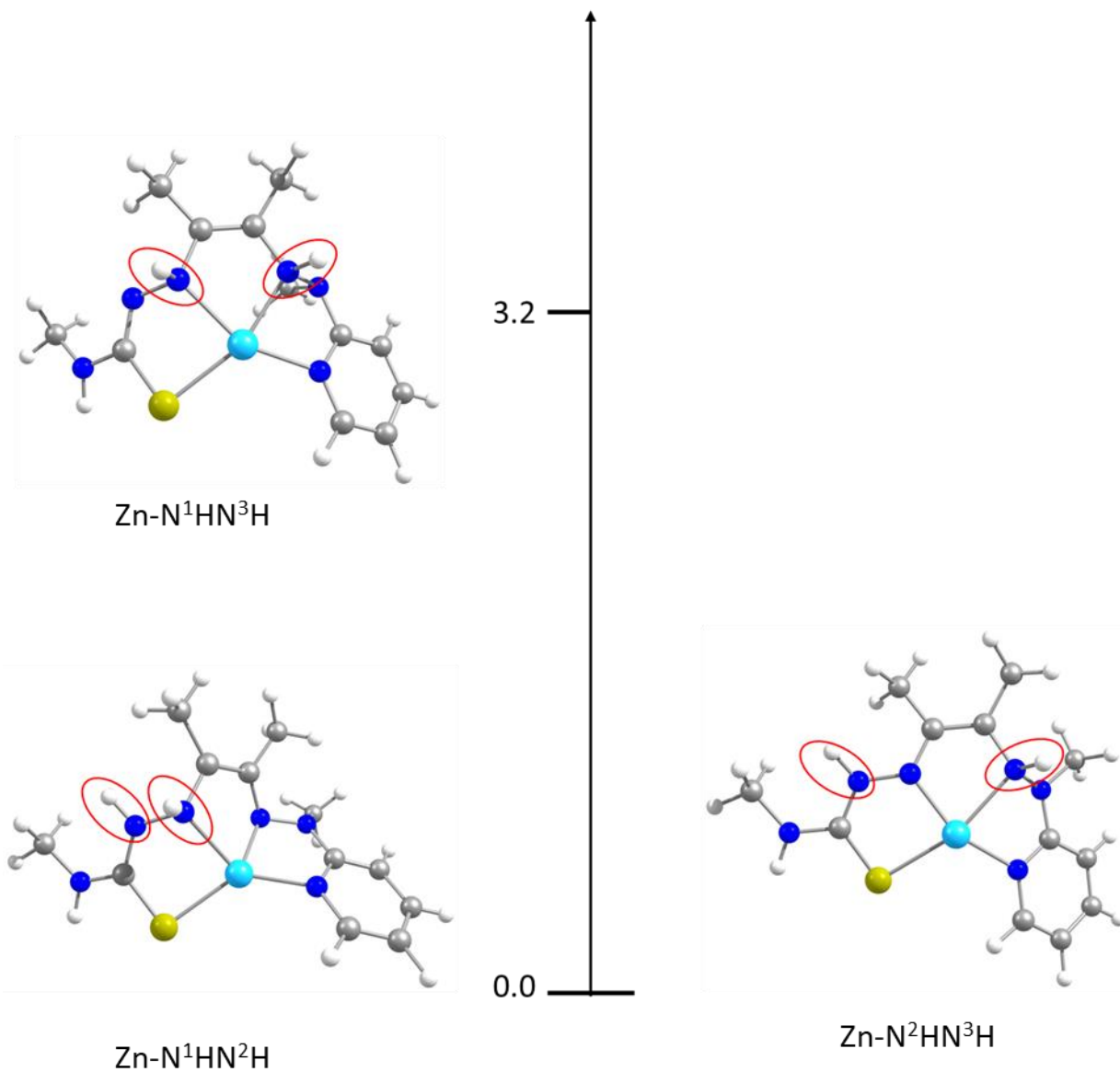


Figure A-51. Relative energy diagram for $\text{Zn}(\text{H}_2\text{DMTMH})^{2+}$.

Energy diagram of the protonated/protonated/reduced/protonated/reduced species of 3 (H_2^{2+}) computed by DFT with B3LYP/6-311g(d,p) ($S=0$, $q=+2$) in PCM solvent model using acetonitrile as a solvent.

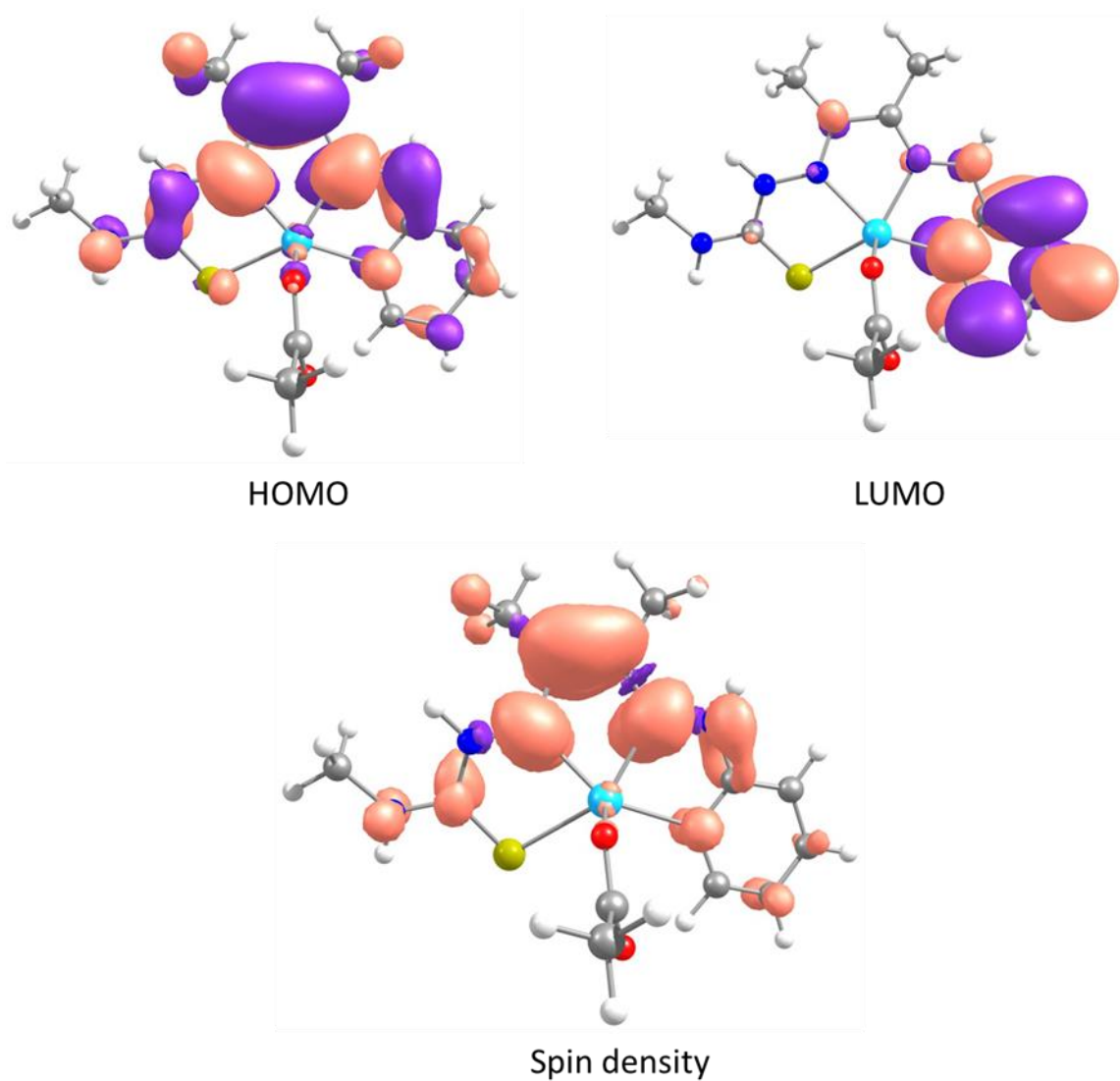


Figure A-52. HOMO/LUMO and plot of spin density for Zn(H₂DMTH)(OAc).

Frontier molecular orbital (HOMO, LUMO) and the spin density depiction for Zn-N⁴HN²H (S=1/2, q=0) structure.

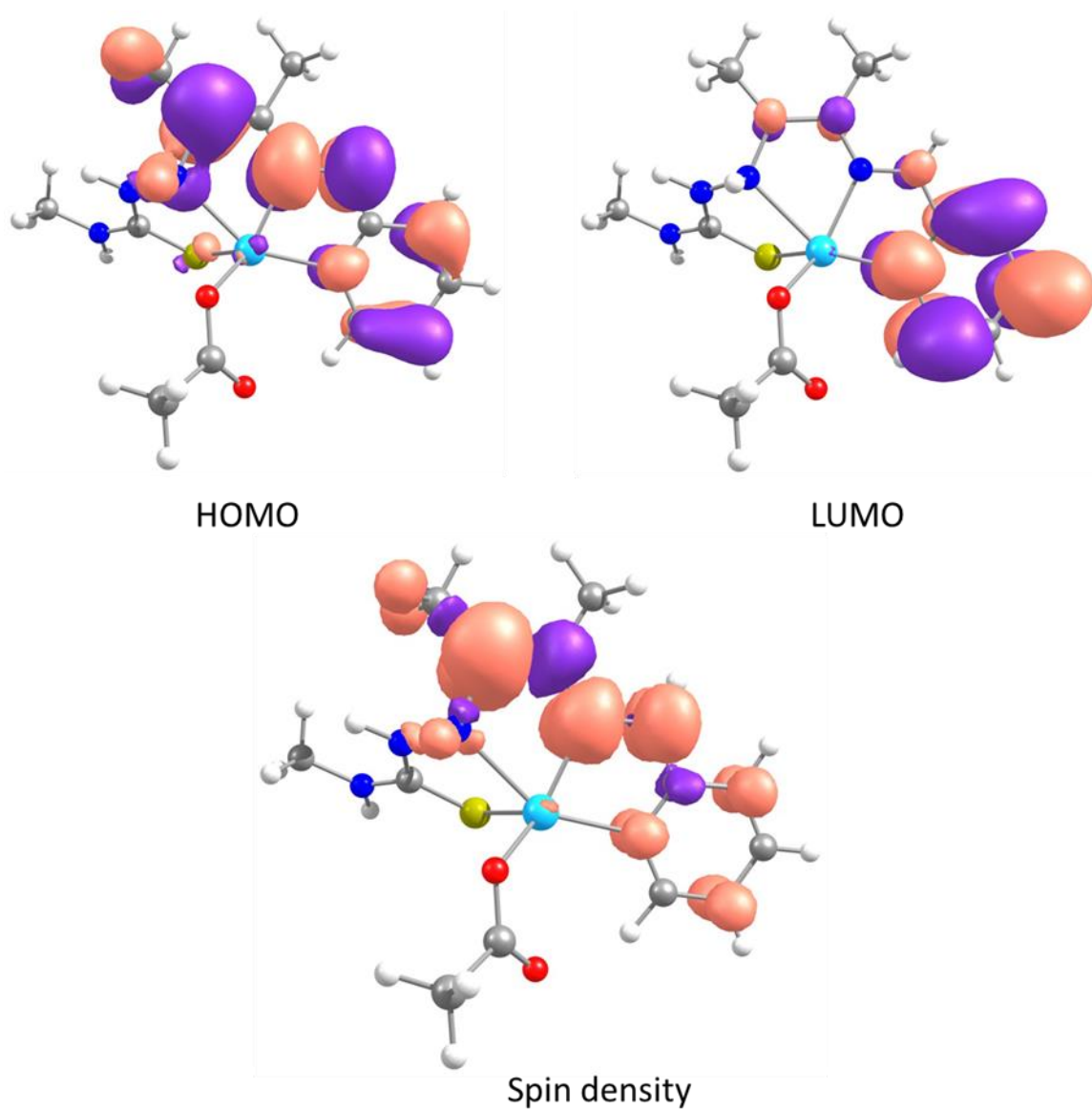


Figure A-53. HOMO/LUMO and plot of spin density for $\text{Zn}(\text{H}_3\text{DMTH})(\text{OAc})^+$.

Frontier molecular orbital (HOMO, LUMO) and the spin density depiction for Zn- $N^4HN^1HN^2H$ ($S=1/2$, $q=1$) structure.

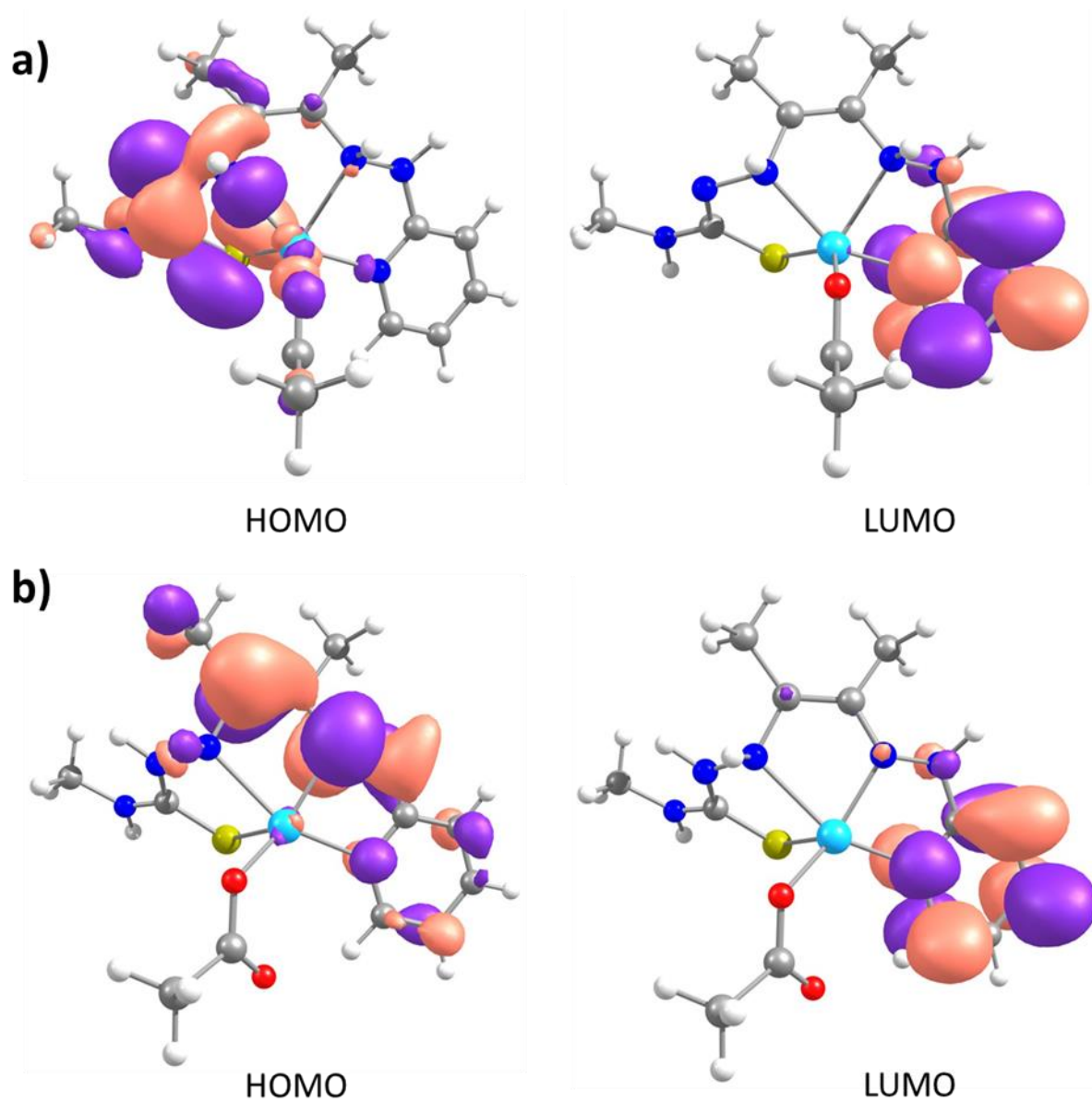


Figure A-54. HOMO/LUMO and plot of spin density for Zn(H₃DMTH)(OAc).

Frontier molecular orbital (HOMO, LUMO) for a) Zn-N¹HN³HN⁴H (S=0, q=0) b) Zn-N¹HN²HN⁴H (S=0, q=0).

A.3 Chapter 4 Figures and Tables

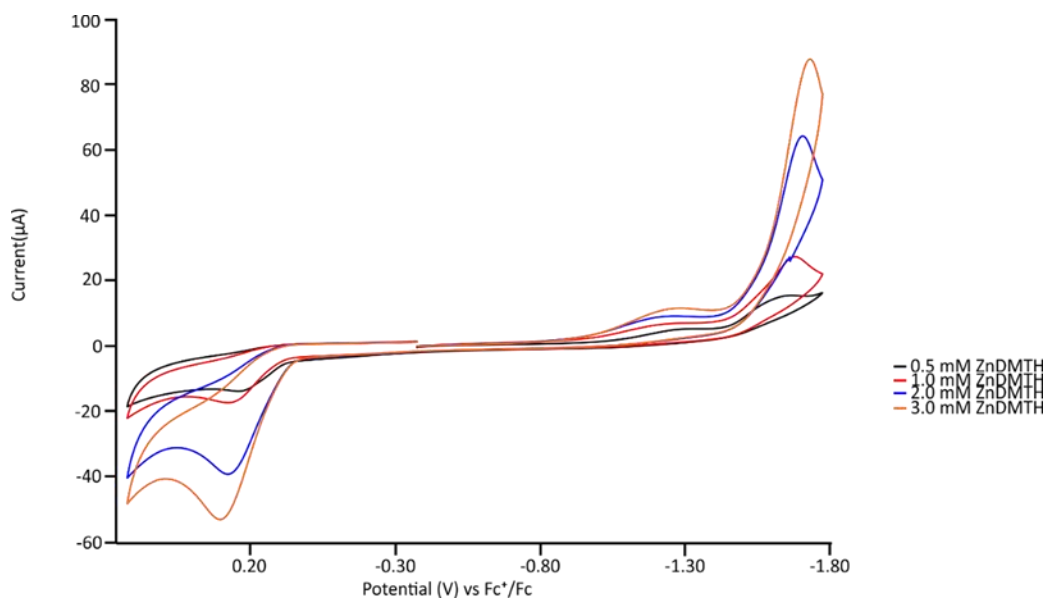


Figure A-55. Catalysts concentration dependence CVs for CO₂ binding.

Solvent = methanol, no acid, scan rate = 200 mV/s scan from -0.50 V to -1.80 V to 0.60 V to -0.50 V.

Table A-15. K values for each pressure of CO ₂ .							
Absorbance	[CO ₂] in ppm	[CO ₂] (M)	ε[Zn (HD MTH) (CO ₃ CH ₃)]	[Zn (HDMTH) (CO ₃ CH ₃) (M)	ε[Zn (DMTH)]	[Zn (DMTH)] (M)	K
0.116945	1000	14.8 x 10 ⁻⁵	391.4395	6.11 x 10 ⁻⁵	2393.616	3.89 x 10 ⁻⁵	10.6 x 10 ³
0.145383	900	13.3 x10 ⁻⁵	391.4395	4.69 x 10 ⁻⁵	2393.616	5.31 x10 ⁻⁵	6.64 x 10 ³
0.148217	800	11.8 x 10 ⁻⁵	391.4395	4.55 x 10 ⁻⁵	2393.616	5.45 x10 ⁻⁵	7.06 x 10 ³
0.160975	700	10.4 x 10 ⁻⁵	391.4395	3.92 x 10 ⁻⁵	2393.616	6.08 x10 ⁻⁵	6.21 x 10 ³
0.163898	600	8.88 x 10 ⁻⁵	391.4395	3.77 x 10 ⁻⁵	2393.616	6.23 x10 ⁻⁵	6.81 x 10 ³

0.185974	500	7.4 x 10 ⁻⁵	391.4395	2.67 x 10 ⁻⁵	2393.616	7.33 x10 ⁻⁵	4.92 x 10 ³
0.187831	400	5.92 x 10 ⁻⁵	391.4395	2.57 x 10 ⁻⁵	2393.616	7.43 x10 ⁻⁵	5.86 x 10 ³

Utilizing the average and std dev functions within excel, we can get an average of 6.88 x 10³ and a standard deviation of 1804 or 6.88 x 10³ ± 1.8.

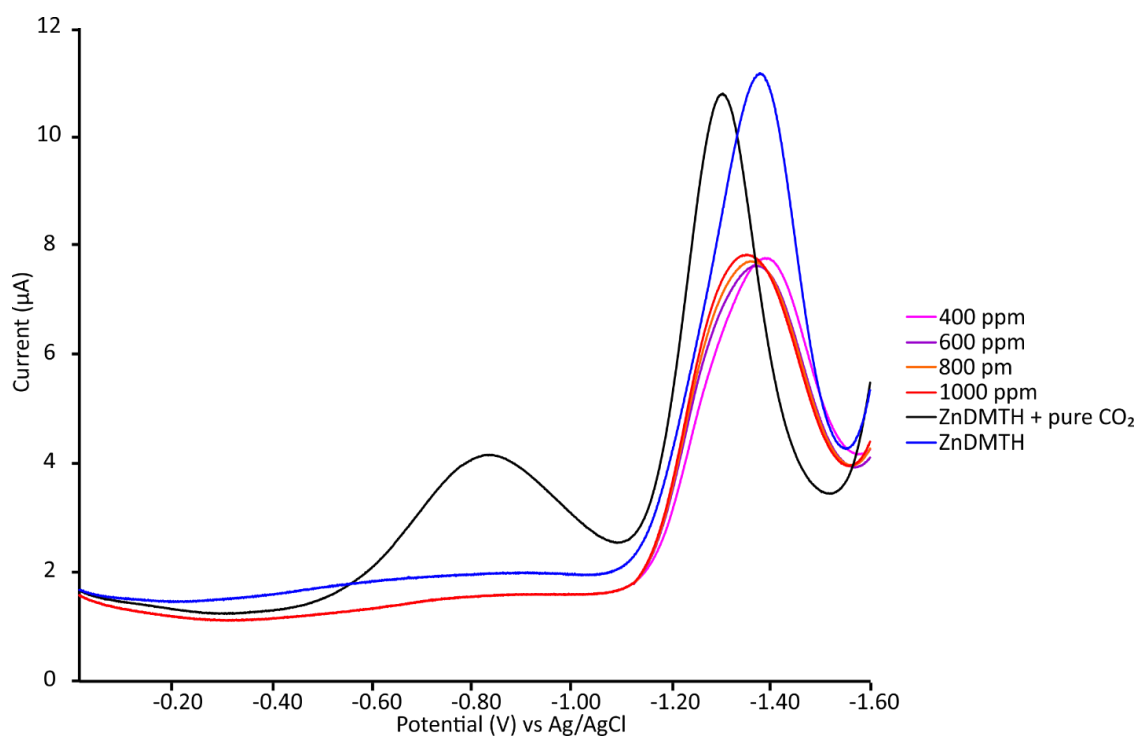


Figure A-56. Square wave voltammetry of varying CO₂ concentration.

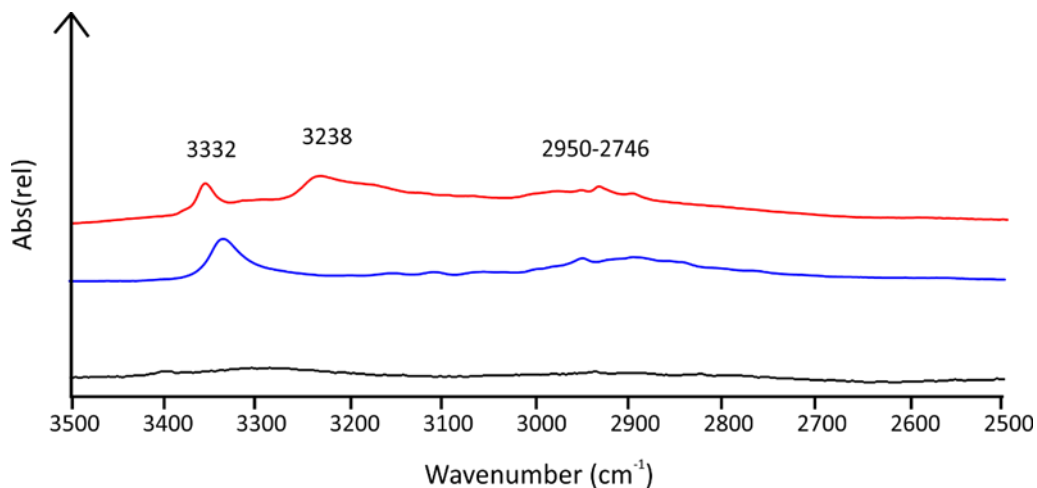


Figure A-57. FT-IR of crystals of Zn(DMTH)(MeOH) (black), Zn(HDMTH)(CO₃CH₃) (blue), and Zn(HDMTH)(OAc).

From 3500-2500 cm⁻¹.

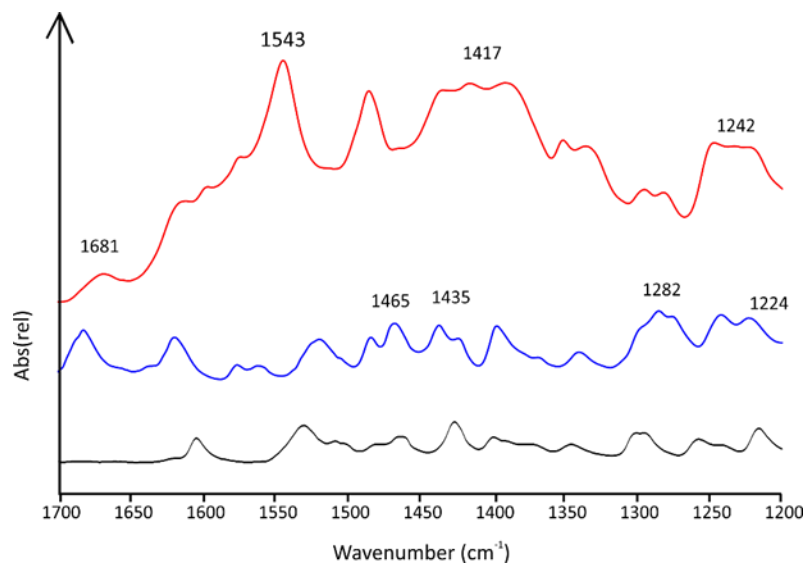


Figure A-58. FT-IR of crystals of Zn(DMTH)(MeOH) (black), Zn(HDMTH)(CO₃CH₃) (blue), and Zn(HDMTH)(OAc).

From 1700-1200 cm⁻¹.

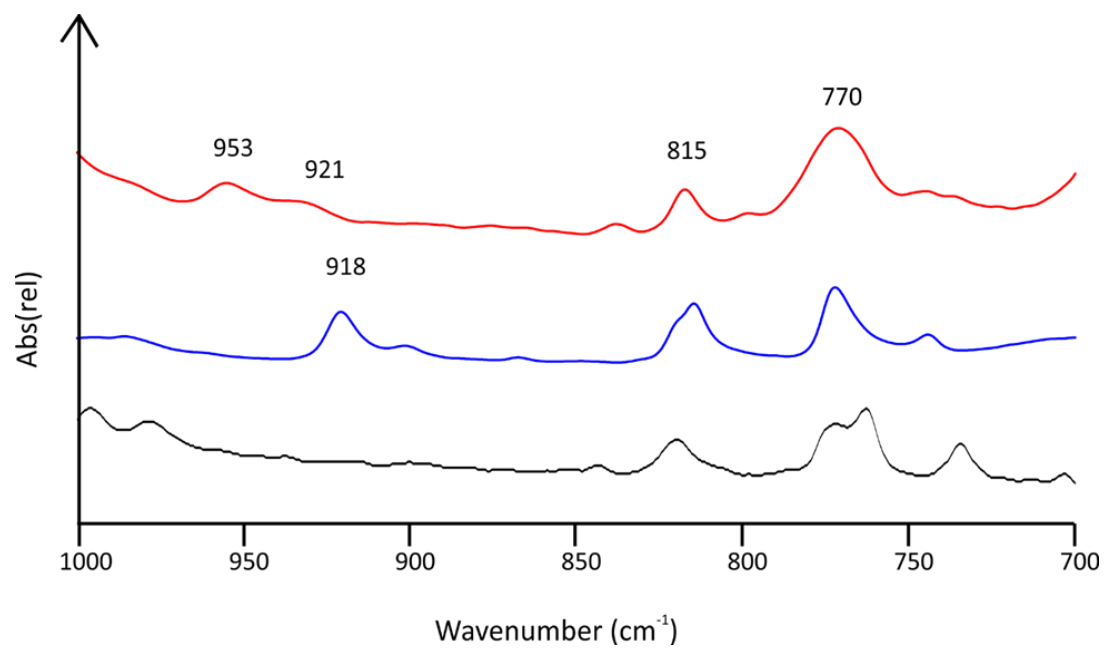


Figure A-59. FT-IR of crystals of Zn(DMTH)(MeOH) (black), Zn(HDMTH)(CO₃CH₃) (blue), and Zn(HDMTH)(OAc).

From 1000-700 cm⁻¹.

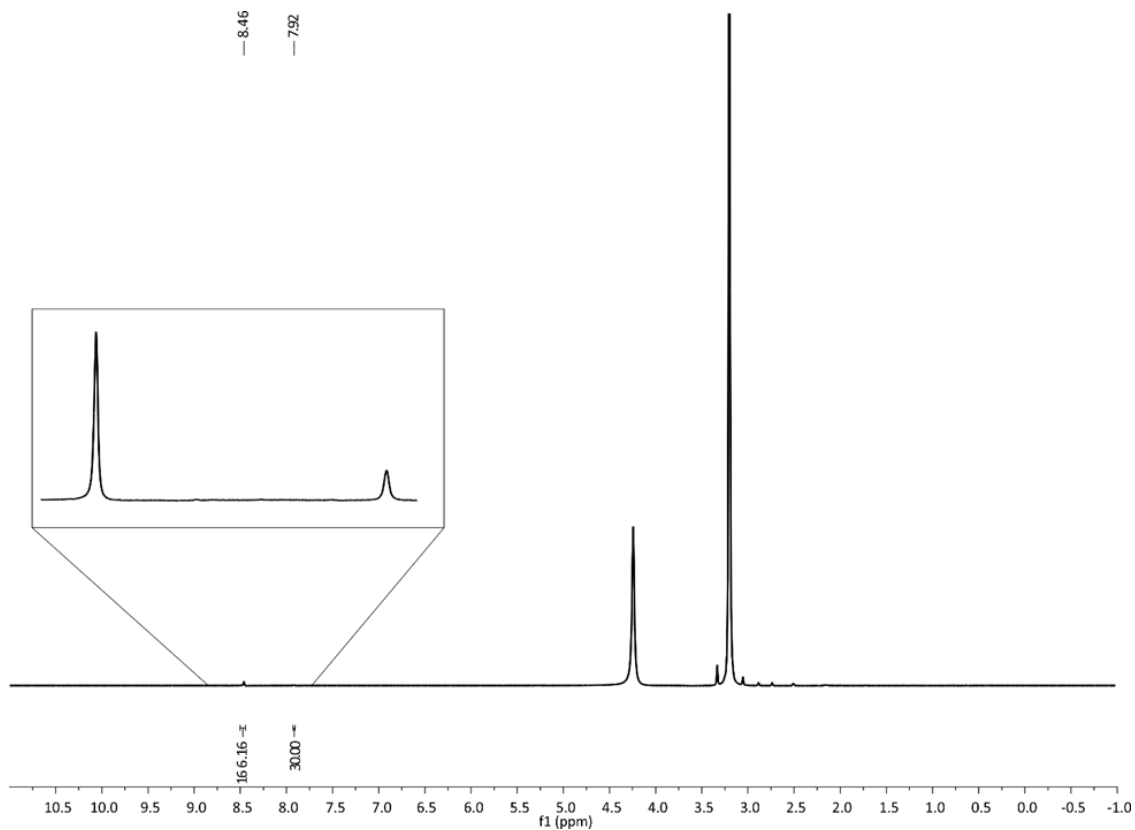


Figure A-60. ¹H NMR for the reaction of Zn(DMTH) and NaBH₄ in the presence of pure CO₂.

Solvent= methanol.

NMR solvent DMSO-d₆. Integrations are referenced to the 30 mM DMF standard.

Total concentration of formate is 170 mM.

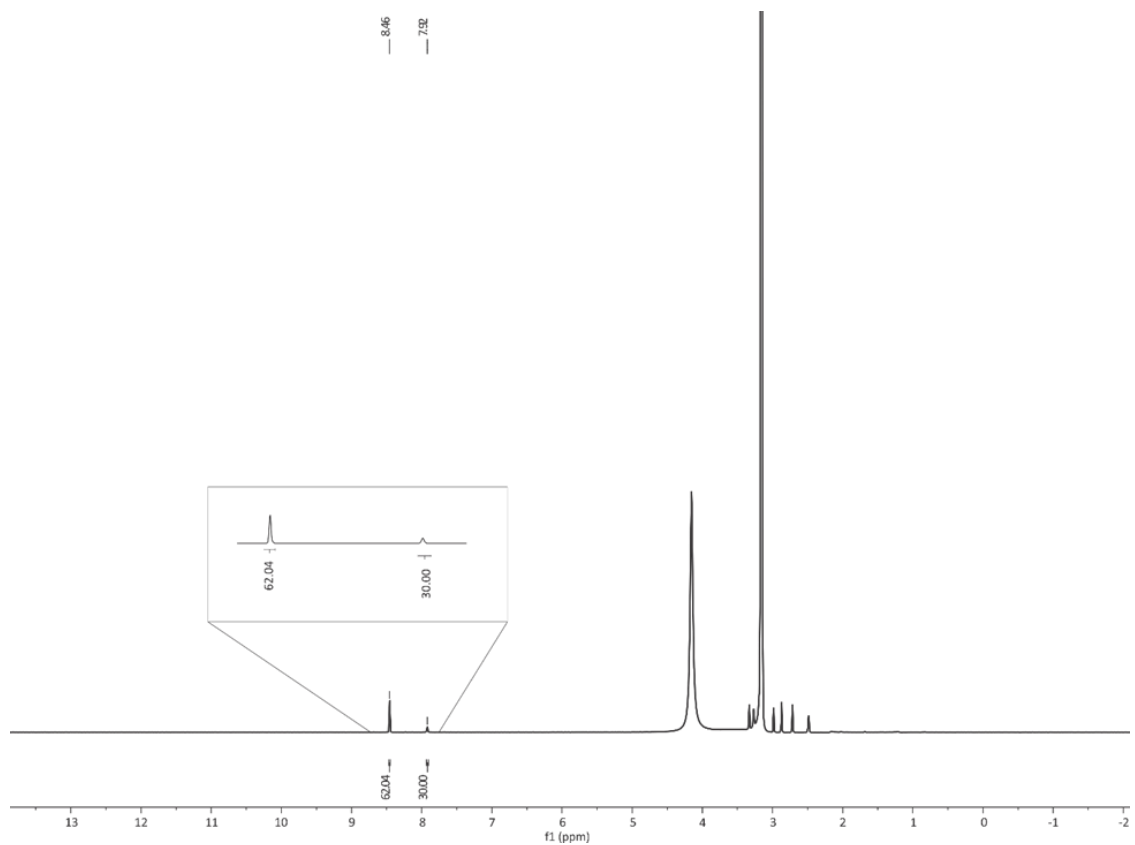


Figure A-61. ¹H NMR for the blank of the reaction of Zn(DMTH) and NaBH₄ in the presence of pure CO₂.

Solvent= methanol.

NMR solvent DMSO-d₆. Integrations are referenced to the 30 mM DMF standard.

Total concentration of formate is 62 mM.

R u n	Electrode	CO ₂ Source	Solvent	Charge	Numb er of Moles of Forma te (x10 ⁻⁴)	Charg e From Blank Subtr acted	Theoreti cal Moles of Formate (x10 ⁻⁴)	Faradaic Efficiency of Formate
1	GC	Pure	MeOH	98.3	12.26	24.9	12.90	95.0%
2	GC	Pure	MeOH	97.95	9.54	24.55	12.72	75.0%
3	Platinum	Pure	MeOH	55.78	8.70	17.17	8.90	97.8%
4	Platinum	Pure	MeOH	49.67	4.03	11.06	5.73	70.3%
5	GC	Air	MeOH	51.90	3.87	15.66	8.115	47.8%
6	GC	Air	MeOH	63.30	5.18	27.10	14.04	36.9%
7	GC	Pure	MeCN/ MeOH	102.7	15.55	31.4	16.27	95.5%
8	GC	Pure	MeCN/ MeOH	101.1	14.50	29.8	15.44	93.8%
9	GC	Pure	MeCN/ MeOH	6.32	27.77	5.98	30.00	92.5%
Bl an k	GC	Pure	MeOH	73.10	0			

Bl an k	Platinum	Pure	MeOH	38.61	0			
Bl an k	GC	Air	MeOH	36.24	0			
Bl an k	GC	Pure	MeCN/ MeOH	71.3	0			
Concentration of CO ₂ in pure phase is 6.511 mM. Concentration with air is 5.917 x 10 ⁻² mM. GC = glassy carbon								

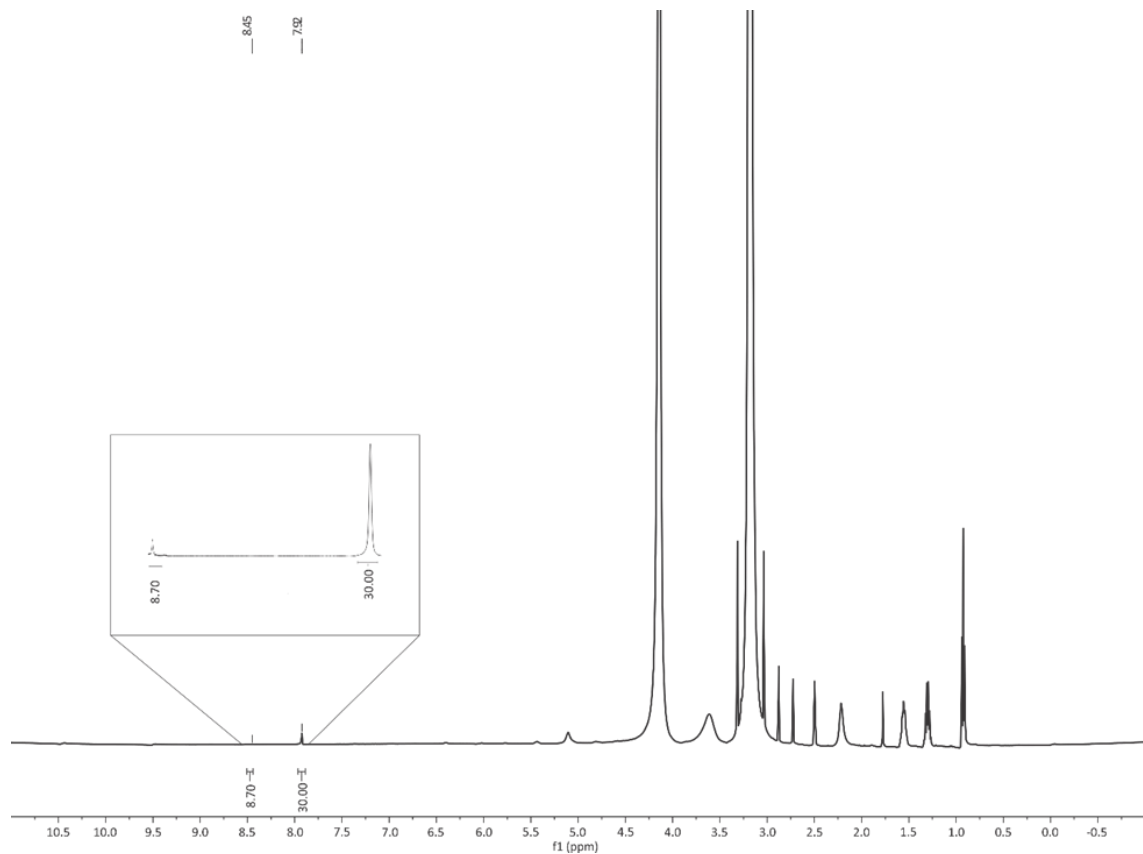


Figure A-62. ¹H NMR for run 1 of the reaction of Zn(DMTH) and 10 mM acetic acid in the presence of pure CO₂ on a platinum working electrode.

Solvent= methanol.

NMR solvent DMSO-d₆. Integrations are referenced to the 30 mM DMF standard.

Total concentration of formate is 8.70 mM.

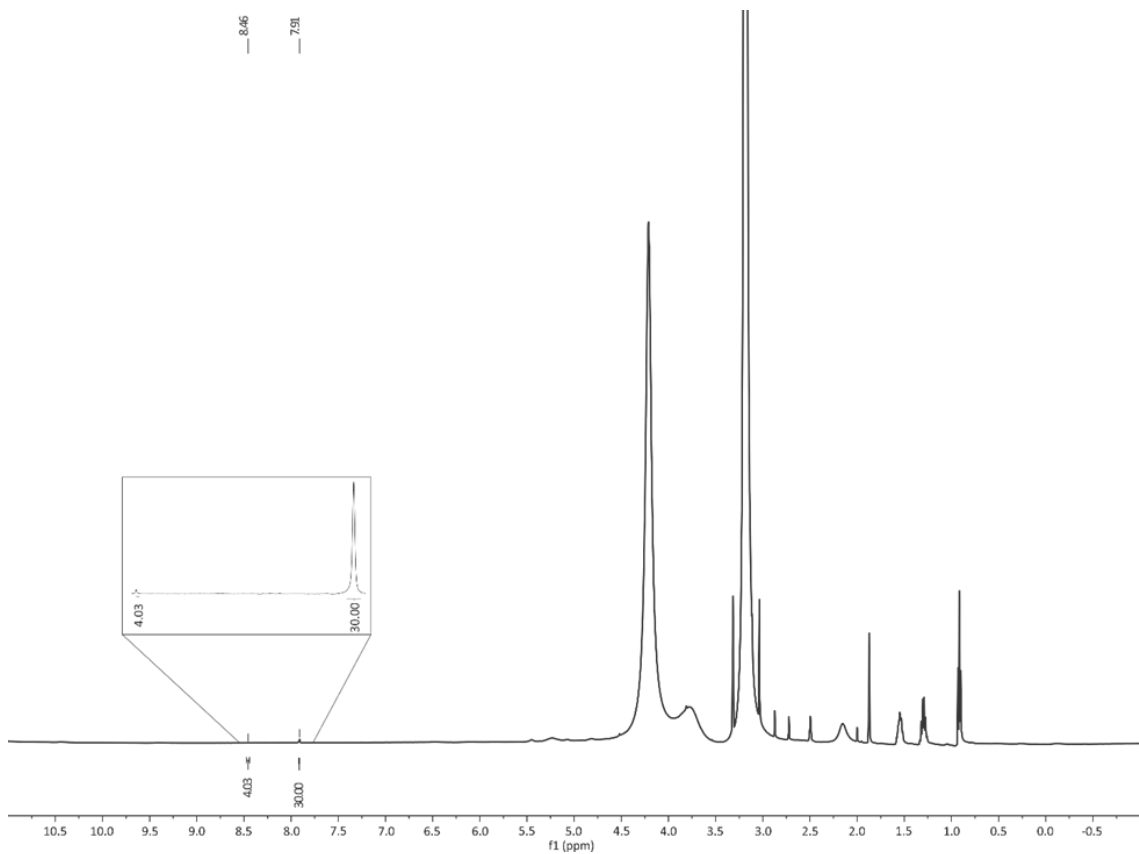


Figure A-63. ¹H NMR for run 2 of the reaction of Zn(DMTH) and 10 mM acetic acid in the presence of pure CO₂ on a platinum working electrode.

Solvent= methanol.

NMR solvent DMSO-d₆. Integrations are referenced to the 30 mM DMF standard.

Total concentration of formate is 4.08 mM.

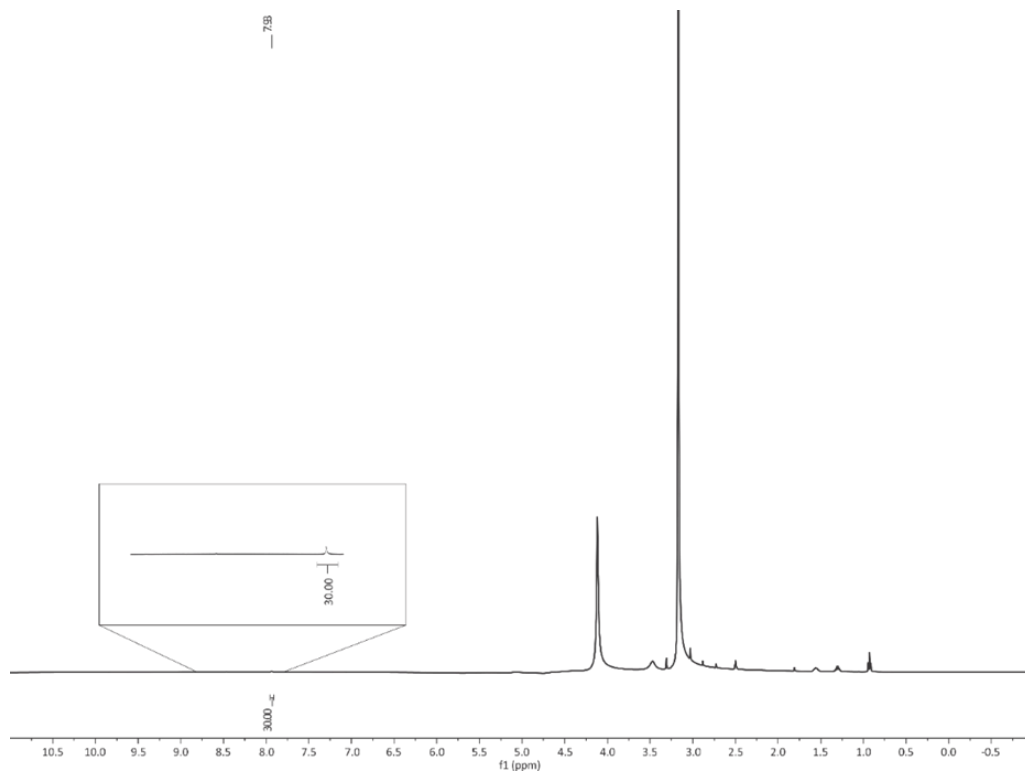


Figure A-64. ^1H NMR for the blank of the reaction of Zn(DMTH) and 10 mM acetic acid in the presence of pure CO_2 on a platinum working electrode.

Solvent= methanol.

NMR solvent DMSO-d₆. Integrations are referenced to the 30 mM DMF standard.

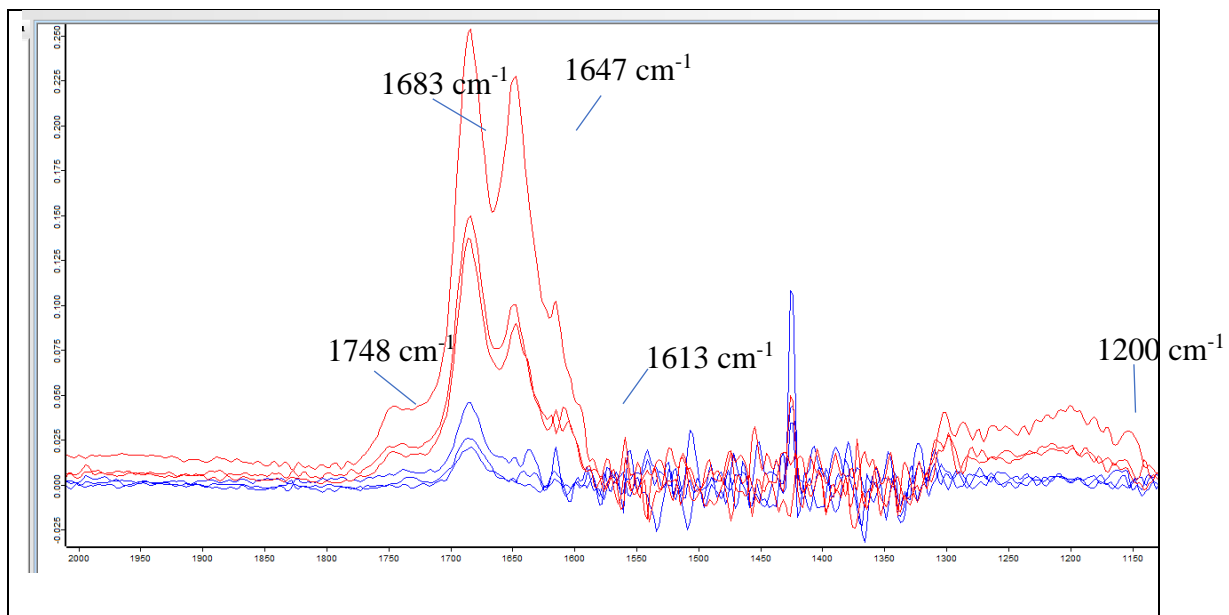


Figure A-65. FT-IR of Zn(DMTH)(MeCN) CO₂ purged held at -1.75 V vs Fc⁺/Fc.

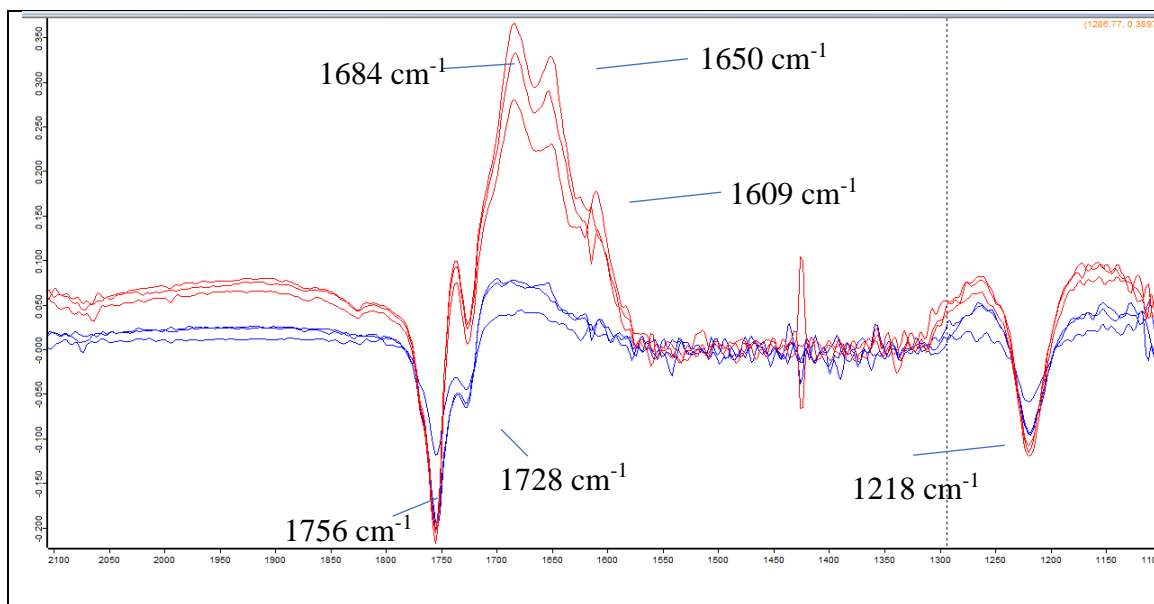


Figure A-66. FT-IR of Zn(DMTH)(MeCN) CO₂ purged held at -2.55 V vs Fc⁺/Fc.

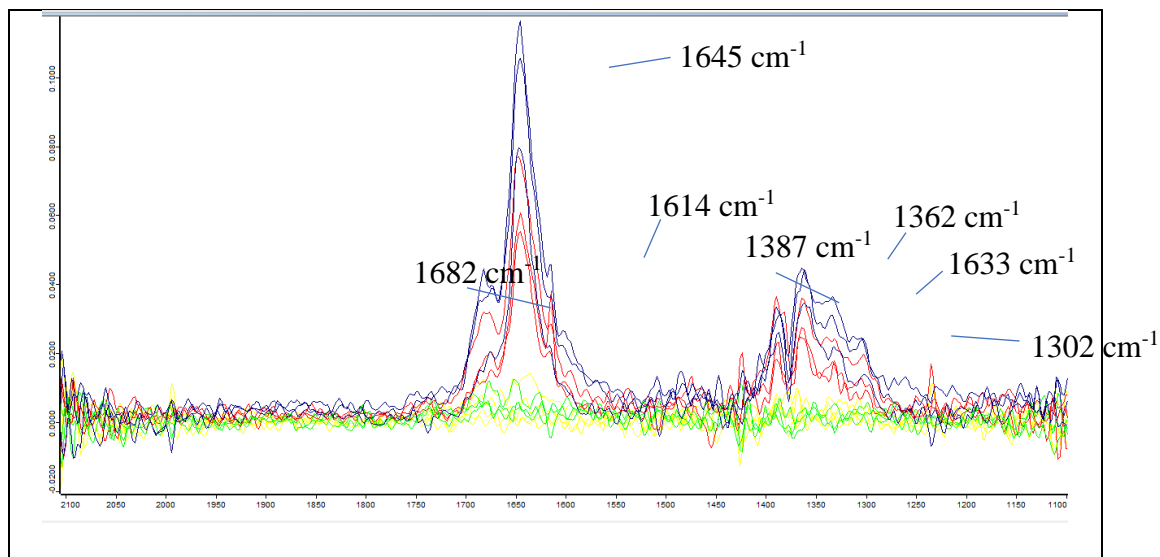


Figure A-67. FT-IR of Zn(DMTH)(MeCN) CO₂ purged with acetic acid.

Yellow: -1.75 V vs Fc⁺/Fc, Red: -2.55 V vs Fc⁺/Fc

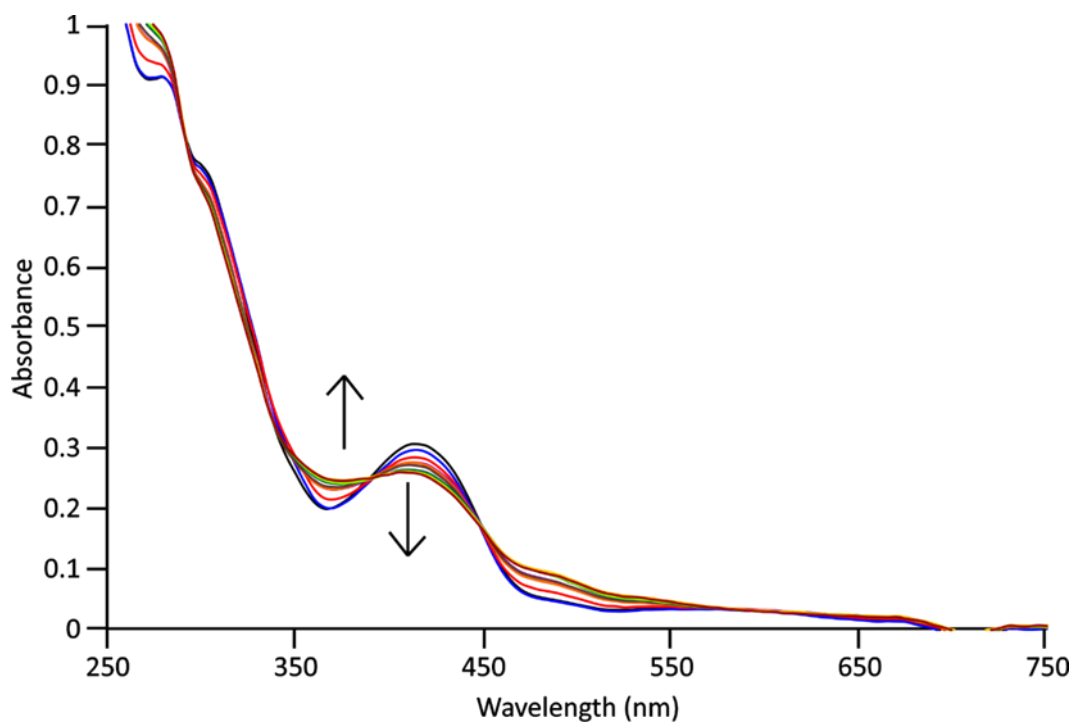


Figure A-68. UV/vis titration of Zn(HDMTH)(CO₃CH₃)

Each addition is 0.4mM. Black is no acid to red is 3.6 mM acetic acid.

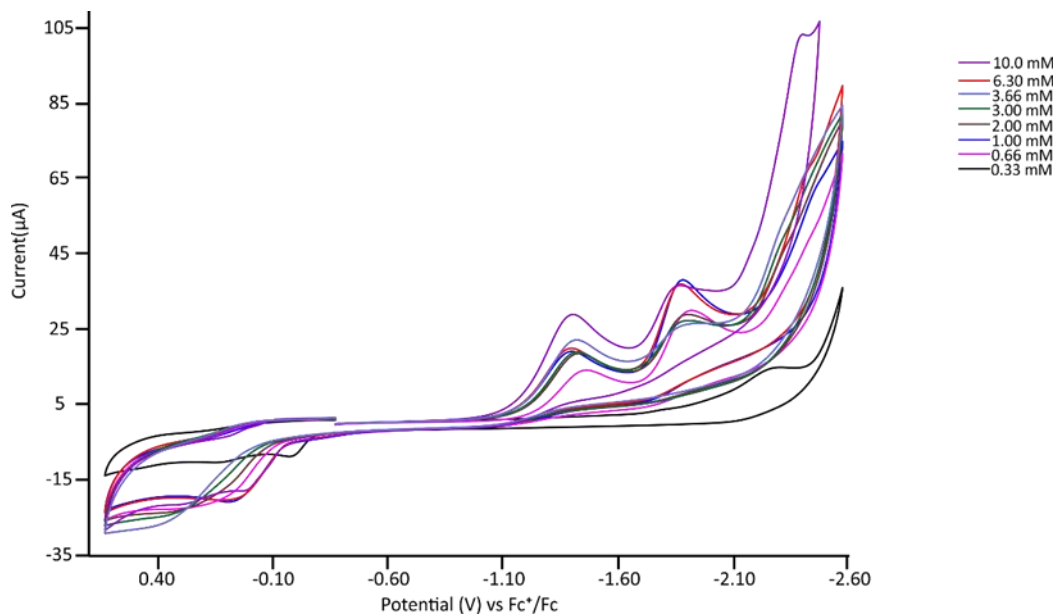


Figure A-69. CV of Zn(DMTH) with CO₂ in 9:1 acetonitrile/methanol at a $\nu=200$ mV/s. Additions of acetic acid from 0.33 mM to 10 mM.

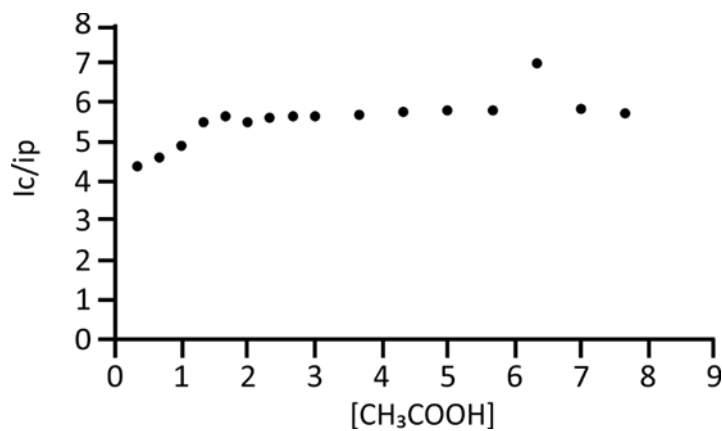


Figure A-70. i_{cat}/i_p vs $[\text{CH}_3\text{COOH}]$ in mM.

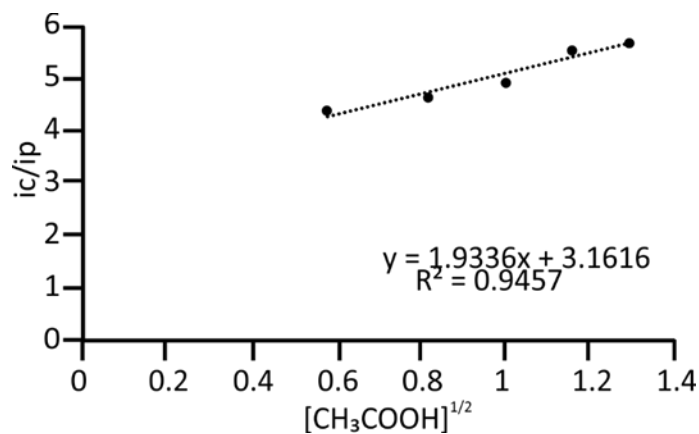


Figure A-71. $i_{\text{cat}}/i_{\text{p}}$ vs $[\text{CH}_3\text{COOH}]^{0.5}$ in mM linear region

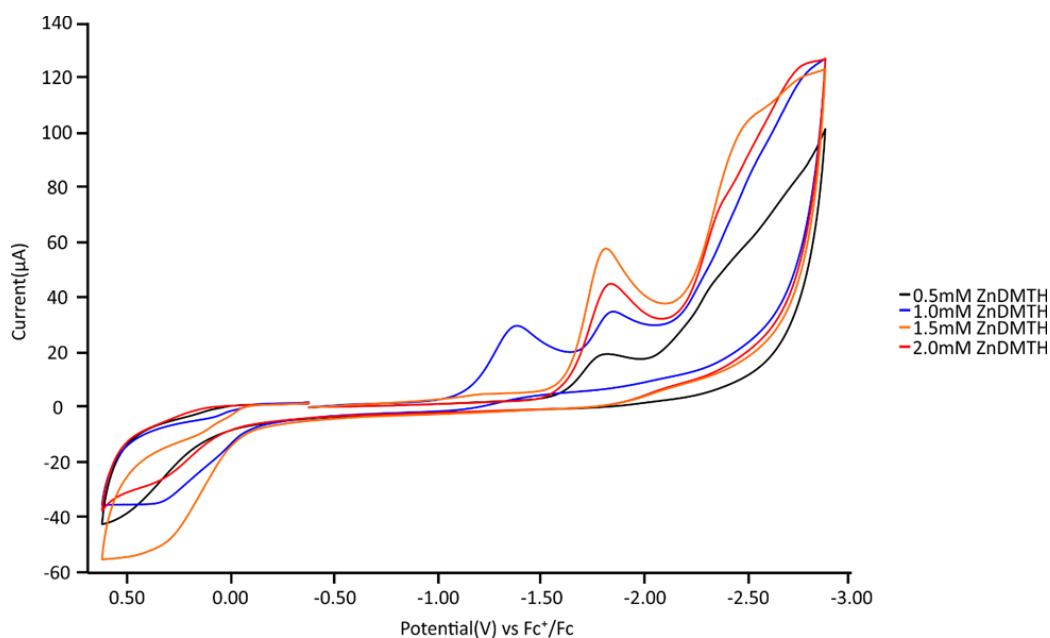


Figure A-72. Catalyst concentration dependence CV under a CO_2 atmosphere in 9:1 acetonitrile:methanol at a $\nu=200$ mV/s and 10 mM acetic acid added.

It should be noted that in the trace at 0.5mM the peak at -1.40 V is present, and at higher concentrations (1.5 mM/2.0 mM) it is absent as a result of the K for this reaction of 9.3×10^{-3} . All are at the same concentration of acid, thereby limiting protonation to generate the doubly protonated species.

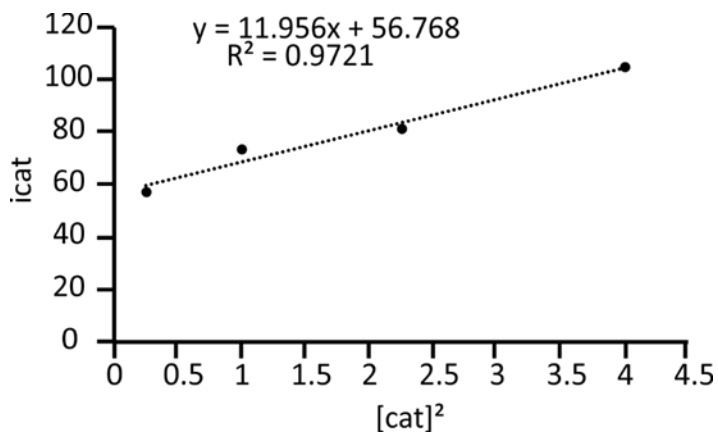


Figure A-73. i_{cat} vs $[cat]^2$ at a $v=200$ mV/s and 10 mM acetic acid

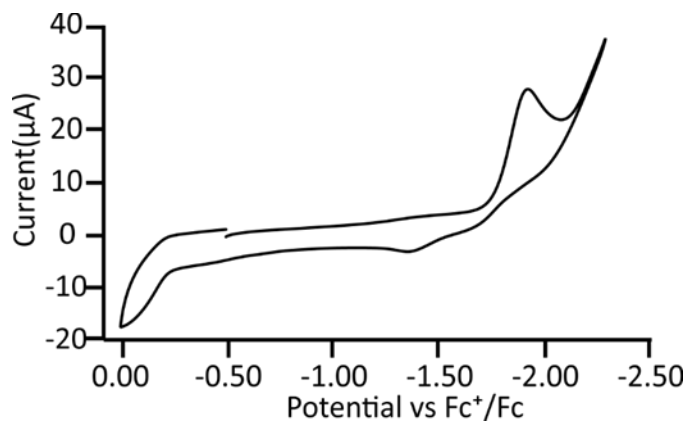


Figure A-74. CV of Zn(DMTH) in 9:1 acetontirle:methanol at $v=200$ mV/s and 98.6 mM phenol.

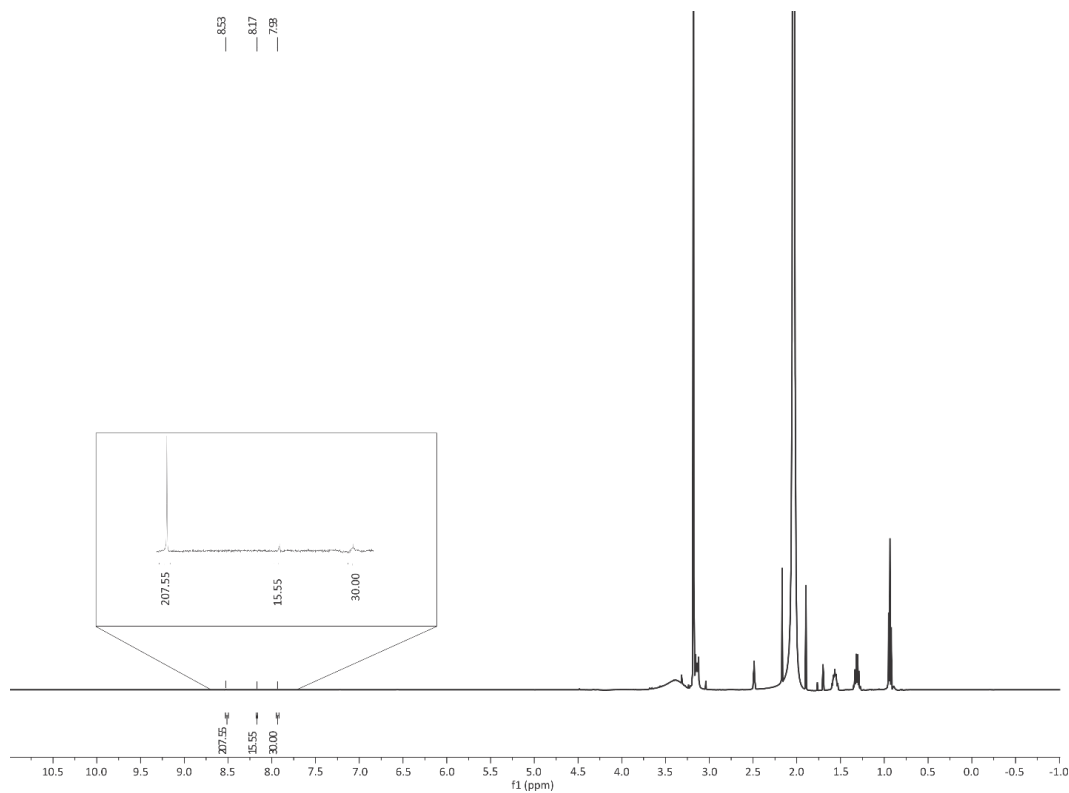


Figure A-75. ¹H NMR for run 1 of the reaction of Zn(DMTH) and 10 mM acetic acid in the presence of pure CO₂ on a glassy carbon working electrode in 9:1 acetonitrile:methanol.

Integrations are referenced to the 30 mM DMF standard.

Concentration of formic acid is 15.55 mM

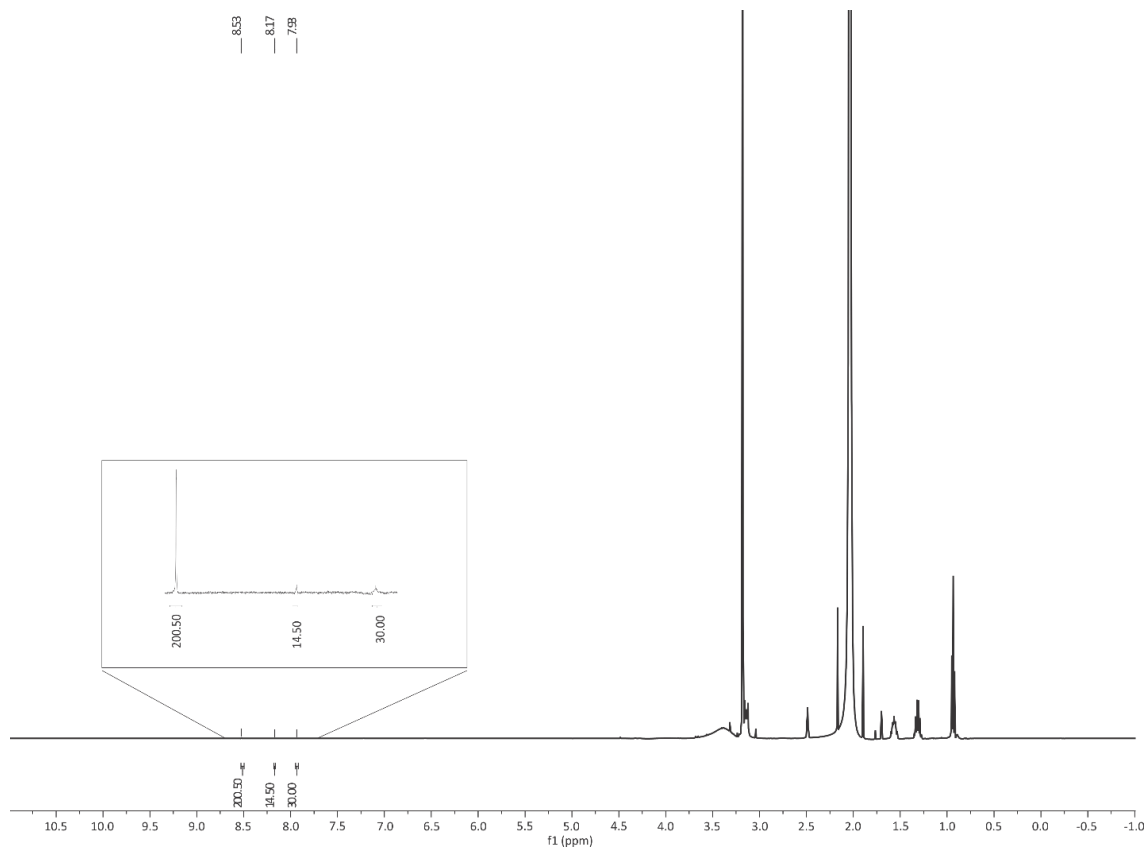


Figure A-76. ¹H NMR for run 2 of the reaction of Zn(DMTH) and 10 mM acetic acid in the presence of pure CO₂ on a glassy carbon working electrode in 9:1 acetonitrile:methanol.

Integrations are referenced to the 30 mM DMF standard.

Concentration of formic acid is 14.50 mM

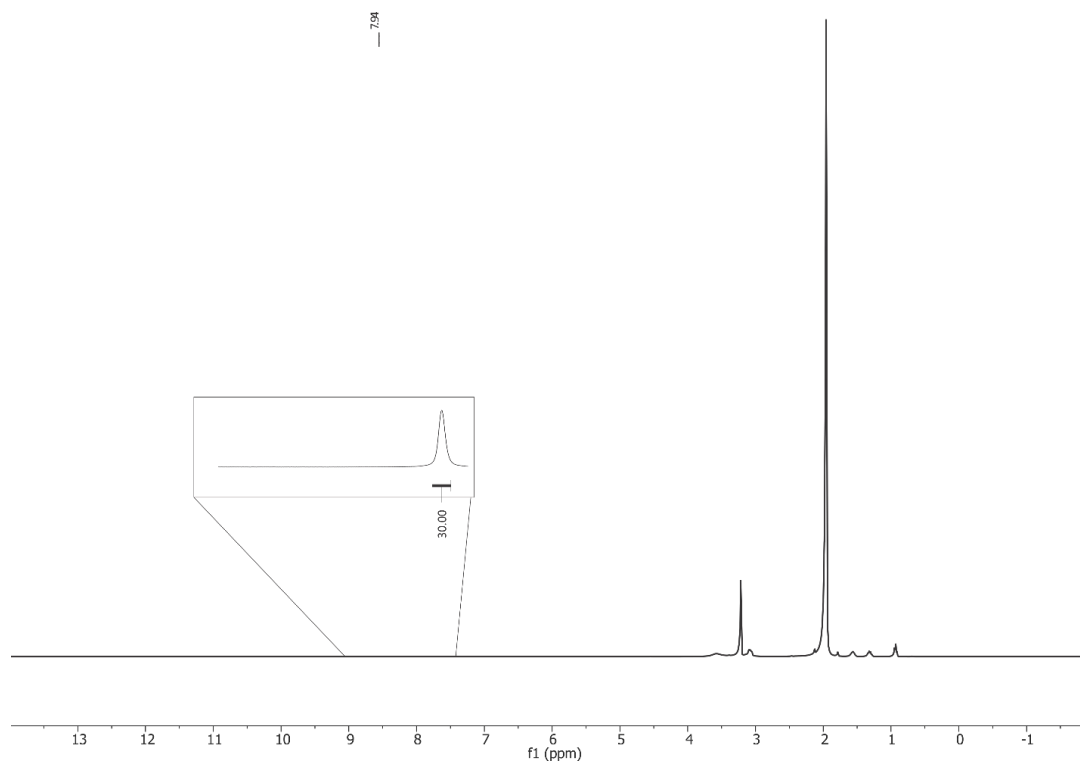


Figure A-77. ¹H NMR for the blank of of the reaction of Zn(DMTH) and 10 mM acetic acid in the presence of pure CO₂ on a glassy carbon working electrode in 9:1 acetonitrile:methanol.

Integrations are referenced to the 30 mM DMF standard.

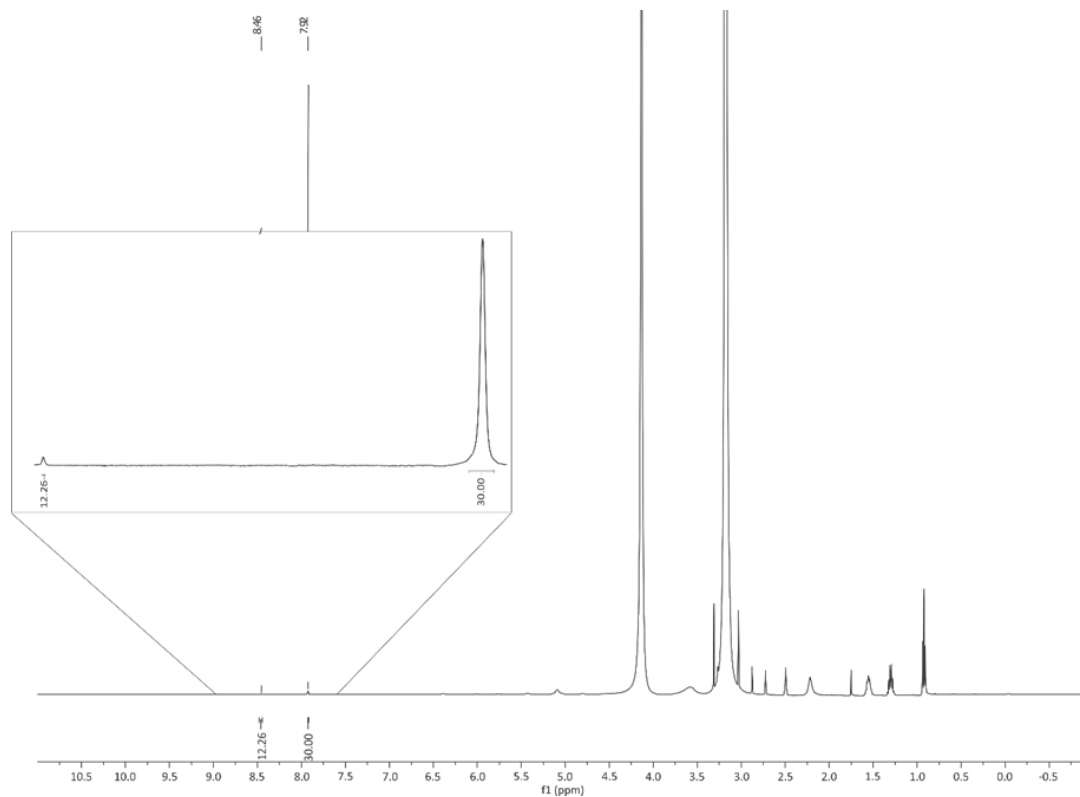


Figure A-78. ¹H NMR for run 1 of the reaction of Zn(DMTH) and 10 mM acetic acid in the presence of pure CO₂ on a glassy carbon working electrode in methanol.

Integrations are referenced to the 30 mM DMF standard.

Total concentration of formate is 12.26 mM.

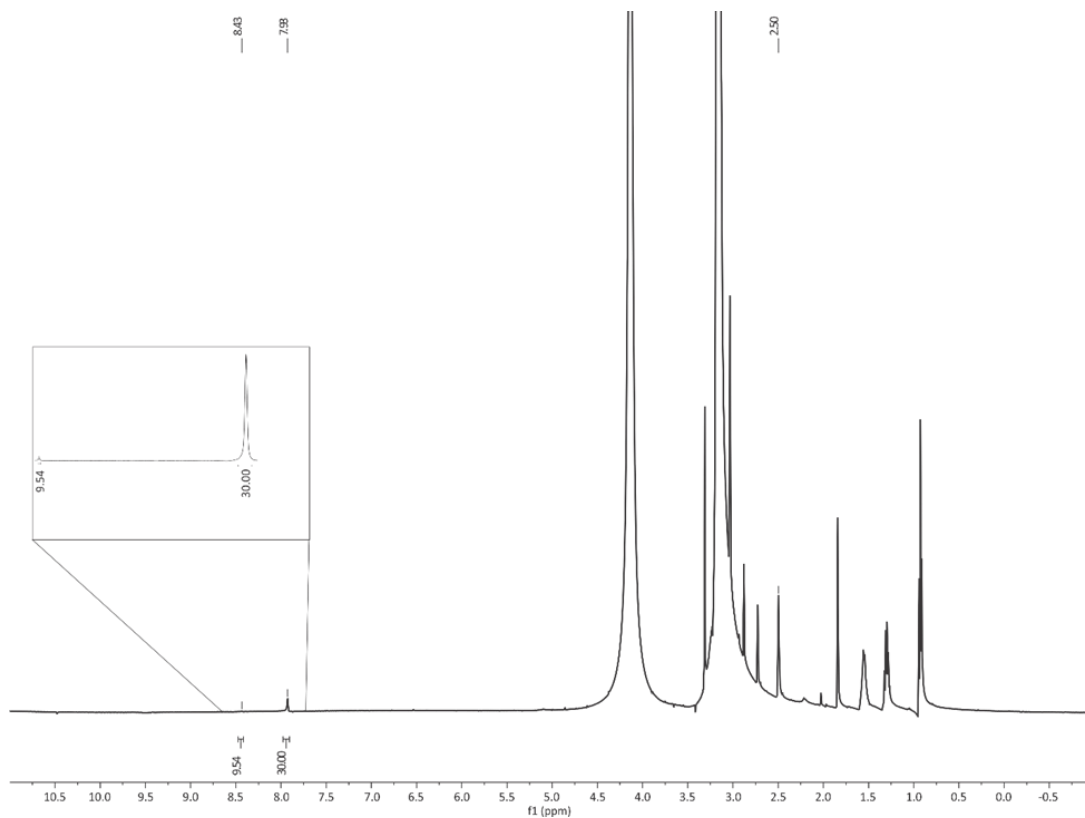


Figure A-79. ¹H NMR for run 2 of the reaction of Zn(DMTH) and 10 mM acetic acid in the presence of pure CO₂ on a glassy carbon working electrode in methanol.

Integrations are referenced to the 30 mM DMF standard.

Total concentration of formate is 9.54 mM

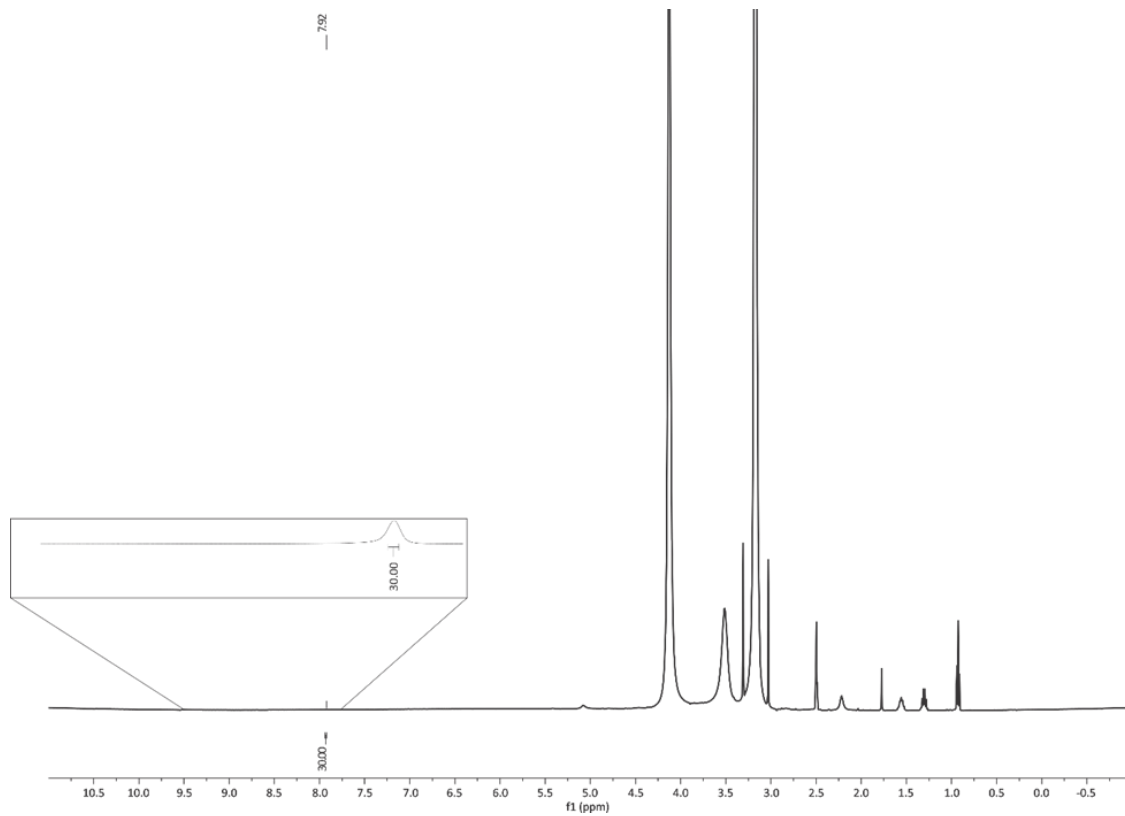


Figure A-80. ¹H NMR for the blank of the reaction of Zn(DMTH) and 10 mM acetic acid in the presence of pure CO₂ on a glassy carbon working electrode in methanol.

Integrations are referenced to the 30 mM DMF standard.

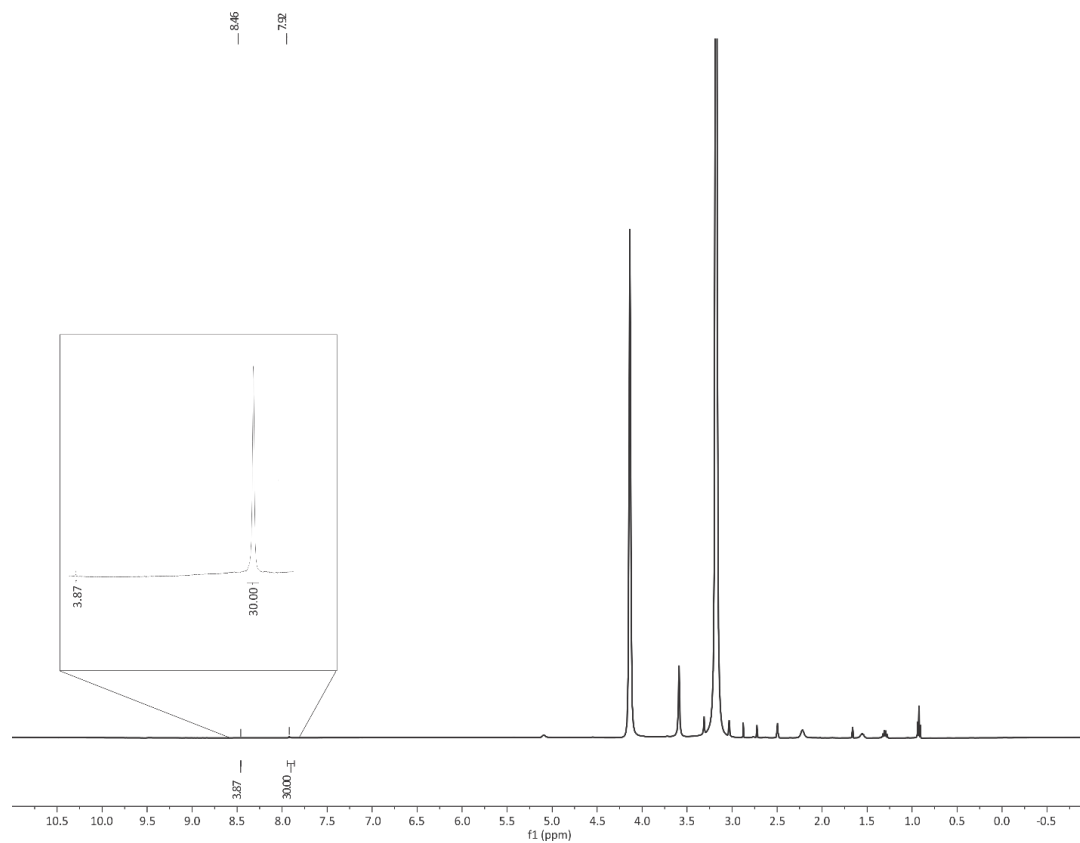


Figure A-81. ^1H NMR for run 1 of the reaction of Zn(DMTH) and 10 mM acetic acid in the presence of air on a glassy carbon working electrode in methanol.

Integrations are referenced to the 30 mM DMF standard.

Total concentration of formate is 3.87 mM

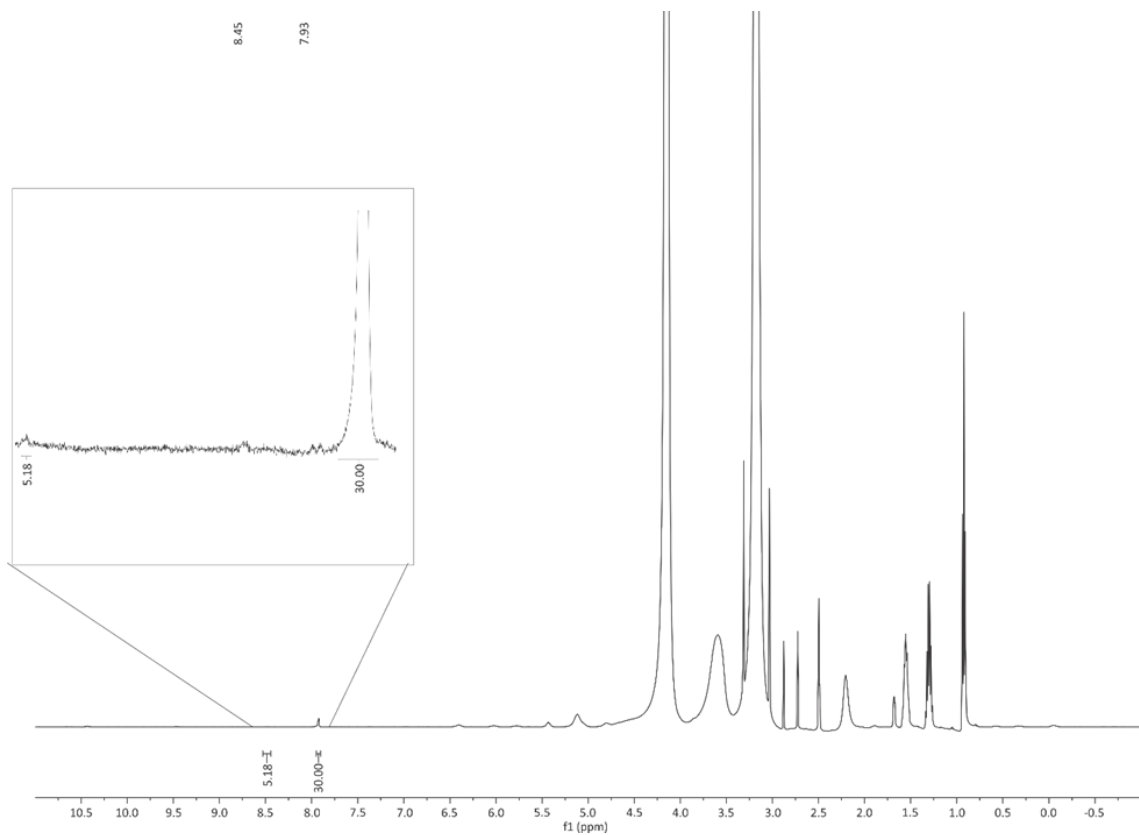


Figure A-82. ¹H NMR for run 2 of the reaction of Zn(DMTH) and 10 mM acetic acid in the presence of air on a glassy carbon working electrode in methanol.

Integrations are referenced to the 30 mM DMF standard.

Total concentration of formate is 5.18 mM

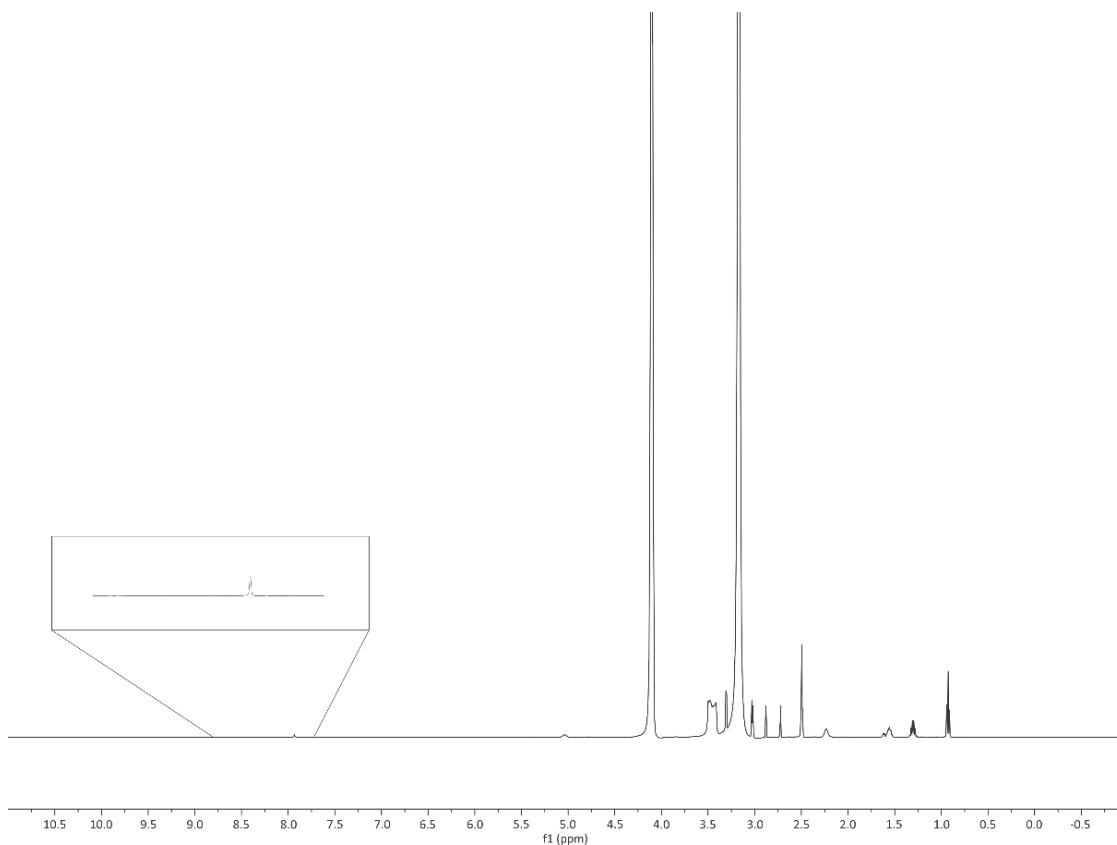


Figure A-83. ¹H NMR for the blank of the reaction of Zn(DMTH) and 10 mM acetic acid in the presence of air on a glassy carbon working electrode in methanol.

Integrations are referenced to the 30 mM DMF standard.

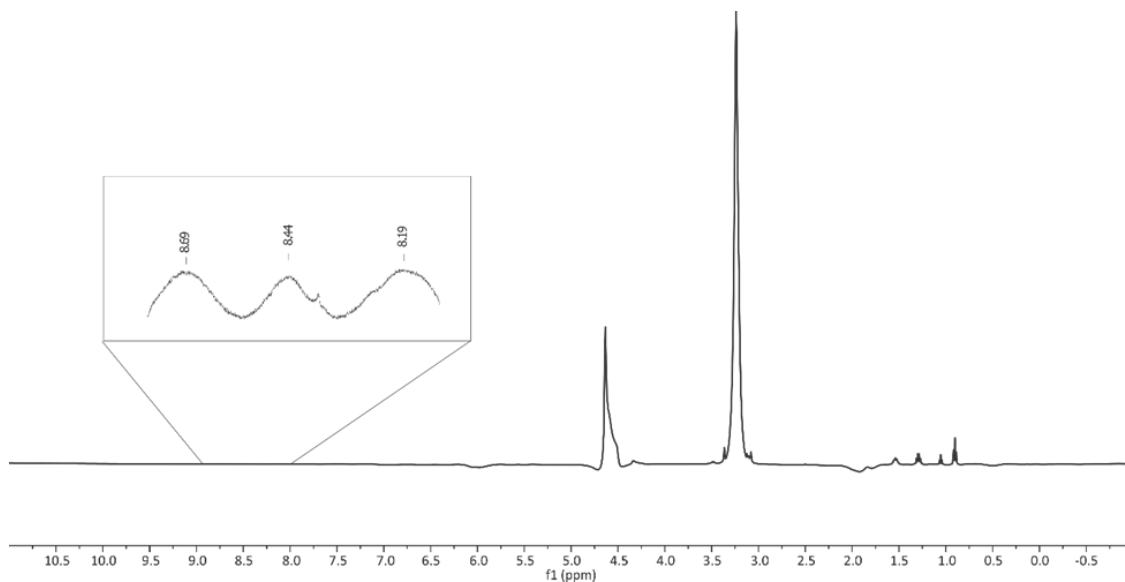


Figure A-84. ^1H NMR of $^{13}\text{CO}_2$ reduction shows characteristic splitting of $\text{H}^{13}\text{CO}_2^-$ (8.44 ppm).

$J_{\text{C-H}} = 138.75 \text{ Hz (500 mHZ)}$

Sample Calculations

Determination of K for each pressure of CO_2 .

The overall reaction is found in the equation below:



Because methanol is the solvent it was left out of the equilibrium calculations. The molar absorptivities of $\text{Zn}(\text{DMTH})$ and $\text{Zn}(\text{HDMTH})(\text{CO}_3\text{CH}_3)$ at 500 nm are 2390 and 391. The absorbance at 500 nm is then simplified to, assuming a 1cm cuvette:

$$A = \varepsilon_1[\text{Zn}(\text{DMTH})] + \varepsilon_2[\text{Zn}(\text{HDMTH})(\text{CO}_3\text{CH}_3)] \quad \text{A-(1)}$$

Given that the starting concentration is = 0.1mM a second equation can be written.

$$[\text{Zn}(\text{DMTH})] + [\text{Zn}(\text{HDMTH})(\text{CO}_3\text{CH}_3)] = 0.0001 \quad \text{A-(2)}$$

Which can be subsequently rearranged as

$$[\text{Zn}(\text{HDMTH})(\text{CO}_3\text{CH}_3)] = 0.0001 - [\text{Zn}(\text{DMTH})] \quad \text{A-(3)}$$

Substitution of A-3 into equation A-1 yields:

$$A = \varepsilon_1[\text{Zn(DMTH)}] + \varepsilon_2(0.0001 - [\text{Zn(DMTH)}]) \quad \text{A-(4)}$$

Which can then be rearranged as

$$[\text{Zn(DMTH)}] = \frac{A - 0.0001\varepsilon_2}{\varepsilon_1 - \varepsilon_2} \quad \text{A-(5)}$$

This could then be substituted into equation A-3 to determine $[\text{Zn(HDMTH)}(\text{CO}_3\text{CH}_3)]$

CO₂ concentrations were varied by diluting the initial tank concentration of 1000 ppm with N₂. (i.e. a 50/50 mix of the two gas streams at the same pressures would result in a 500 ppm CO₂ stream) Since the solution was bubbled for 30 minutes, the [CO₂] remained constant for resulting stream. Conversion from ppm to M as shown below:

$$1,000 \text{ ppm} \times \frac{1 \text{ mg}}{\text{L}} \times \frac{1 \text{ g}}{1000 \text{ mg}} \times \frac{1 \text{ mol}}{44.01 \text{ g}} = 0.0227 \text{ M} \quad \text{A-(6)}$$

However, this concentration assumes that 100% of the CO₂ is dissolved in the methanol. At 1 atm the solubility and mole fraction dissolved can be related to the following equation:

$$\ln x_{\text{CO}_2} = -49.919 + 3484.7 (T/K) + 5.8265 \ln (T/K)^{171} \quad \text{A-(7)}$$

Therefore the [CO₂] found can be displayed as below:

$$[\text{CO}_2]_{\text{dissolved}} = x_{\text{CO}_2} [\text{CO}_2] \quad \text{A-(8)}$$

$$[\text{CO}_2]_{\text{dissolved}} = (0.006511)(0.0227) = 1.48 \times 10^{-4} \text{ M} \quad \text{A-(9)}$$

The equilibrium K for binding of CO₂ can be determined using $[\text{Zn(HDMTH)}(\text{CO}_3\text{CH}_3)]$, [CO₂], and [Zn(DMTH)] and the equation presented at the beginning of this section. A summary of all calculations are presented in Appendix A Table A-14.

$$K = \frac{[\text{Zn(HDMTH)}(\text{CO}_3\text{CH}_3)]}{[\text{Zn(DMTH)}][\text{CO}_2]} \quad \text{A-(10)}$$

TOF_{max} sample calculation for Zn(DMTH) in methanol

$$\text{TOF}/k_{\text{obs}} \text{ is } k_{\text{obs}} = 1.94v\left[\frac{i_{\text{cat}}}{i_{\text{p}}}\right]^2. \quad \text{A-(11)}$$

Derevation of this equation can be found in Haddad *et al.*⁵⁸

Scan rate independence is $v = 9.0 \text{ V/s}$

$$i_{\text{cat}} = 284.5 \mu\text{A}$$

$$i_{\text{p}} = 138.8 \mu\text{A}$$

$$i_{\text{cat}}/i_{\text{p}} = 2.05$$

$$\text{TOF}_{\text{max}} = 73.4 \text{ s}^{-1}$$

Overpotential calculation at the potential of half catalytic current ($E_{\text{cat}/2}$); Zn(DMTH) in acetonitrile:methanol:

$$\eta = |E_{1/2}^{\text{T}} - E_{\text{cat}/2}| \quad \text{A-(12)}$$

$$\eta = -1.36 - (-2.22) = 0.86 \text{ V} \quad \text{A-(13)}$$

A.4 Chapter 5 Figures and Tables

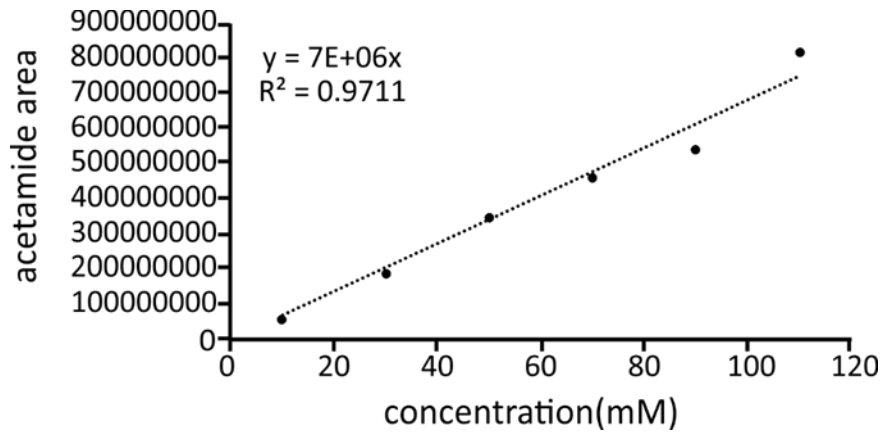


Figure A-85. Calibration curve for acetamide.

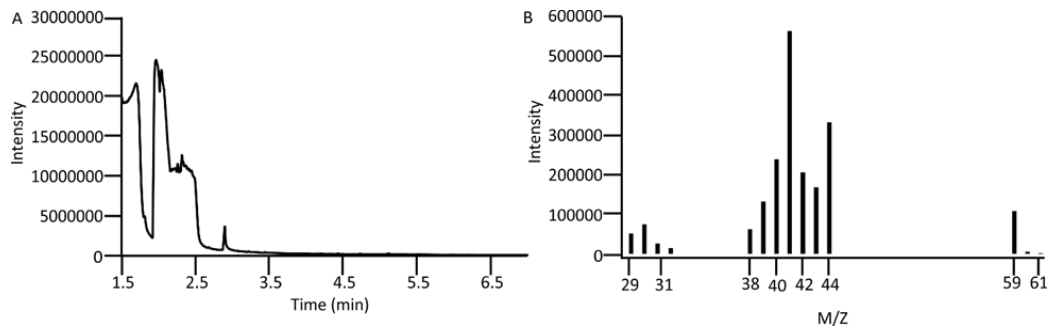


Figure A-86. GC/MS for long term study of Zn(DMTH) with water and acetonitrile.

- A. GC for long term study of Zn(DMTH), water, and acetonitrile B. MS for long term study of Zn(DMTH), water, and acetonitrile at = 2.40 min.

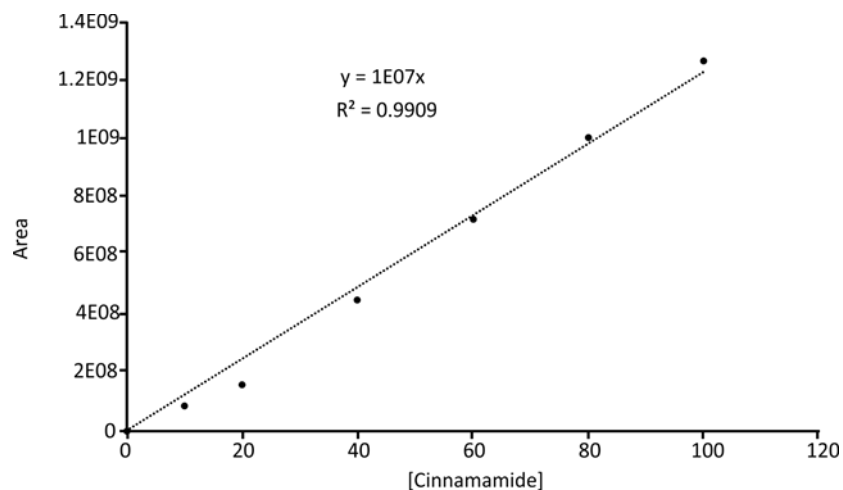


Figure A-87. Calibration curve for cinnamamide.

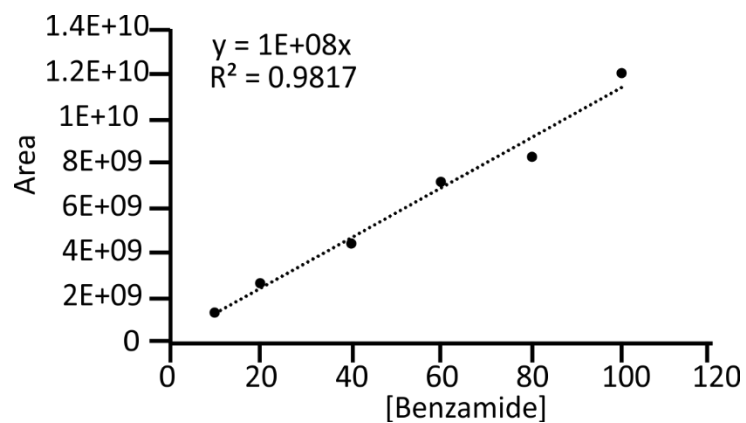


Figure A-88. Calibration curve for benzamide.

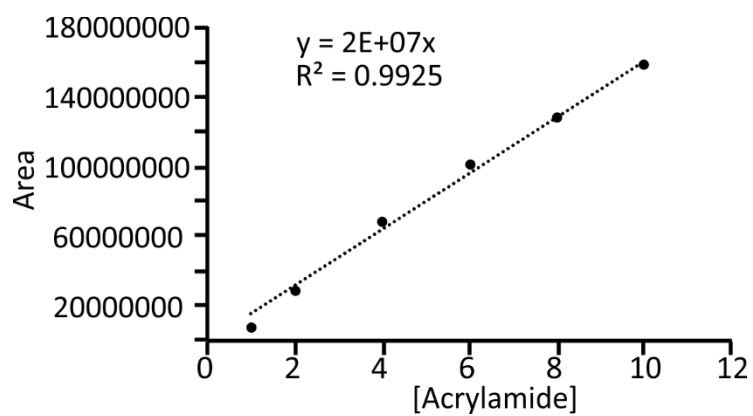


Figure A-89. Calibration curve for acrylamide.

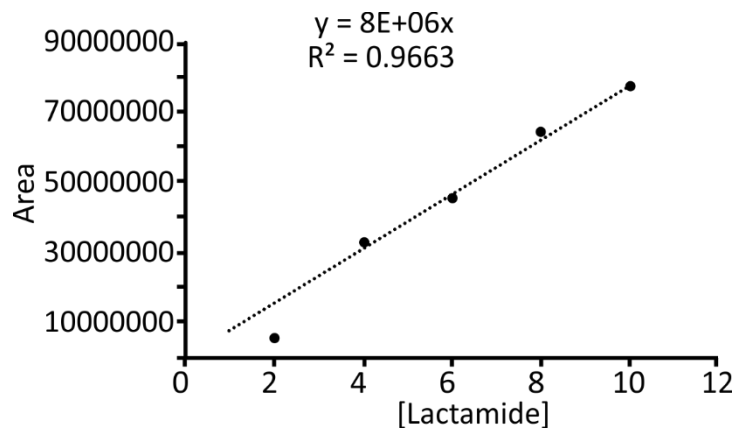


Figure A-90. Calibration curve for lactamide.

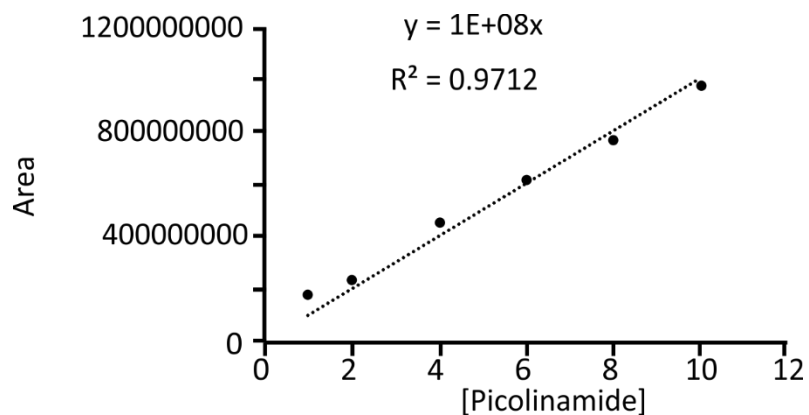


Figure A-91. Calibration curve for picolinamide.

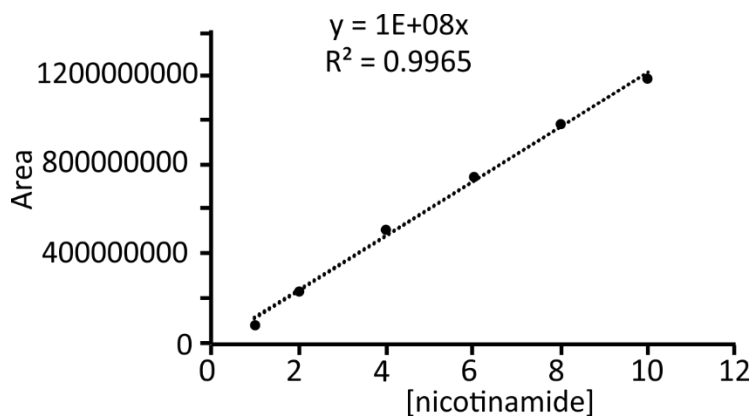


Figure A-92. Calibration curve for nicotinamide.

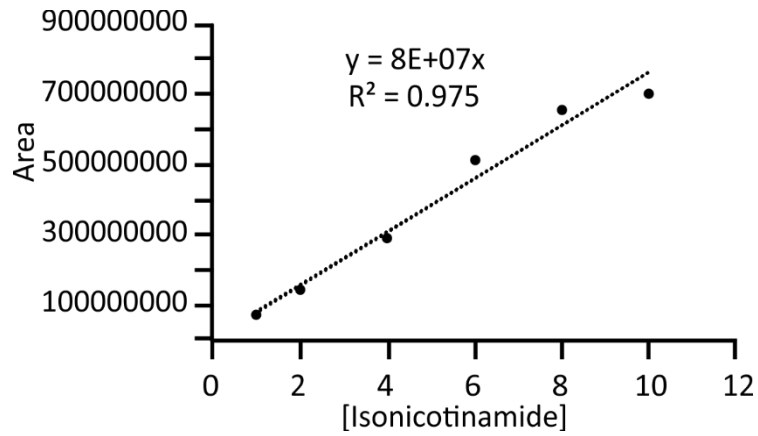


Figure A-93. Calibration curve for isonicotinamide.

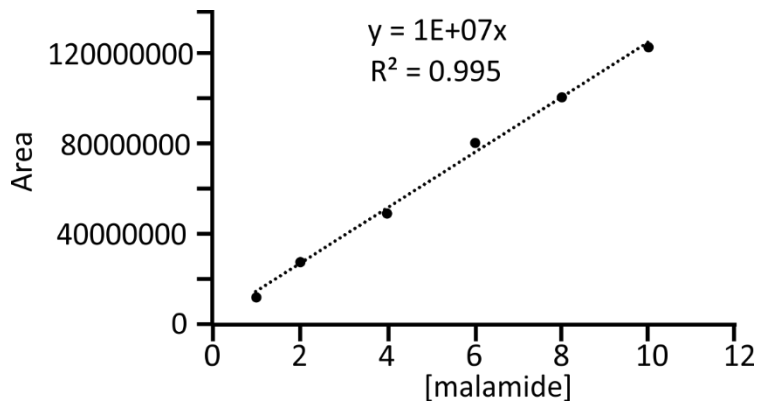


Figure A-94. Calibration curve for malamide.

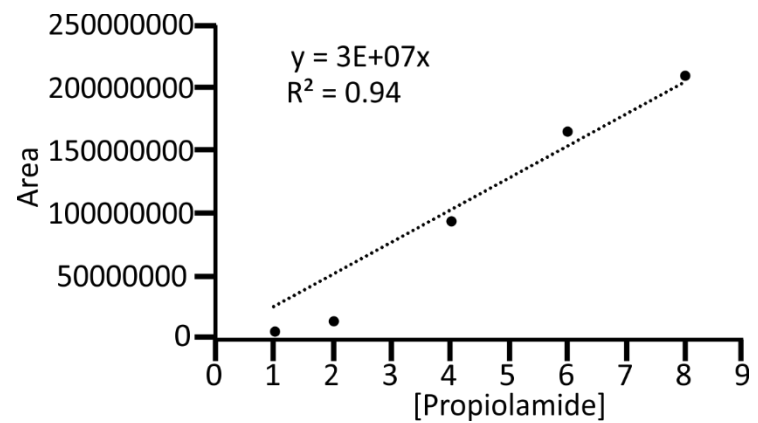


Figure A-95. Calibration curve for propiolamide.

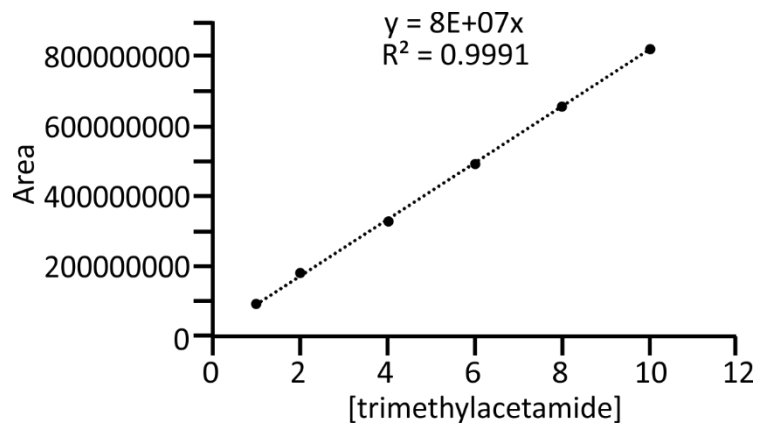


Figure A-96. Calibration curve for trimethylacetamide.

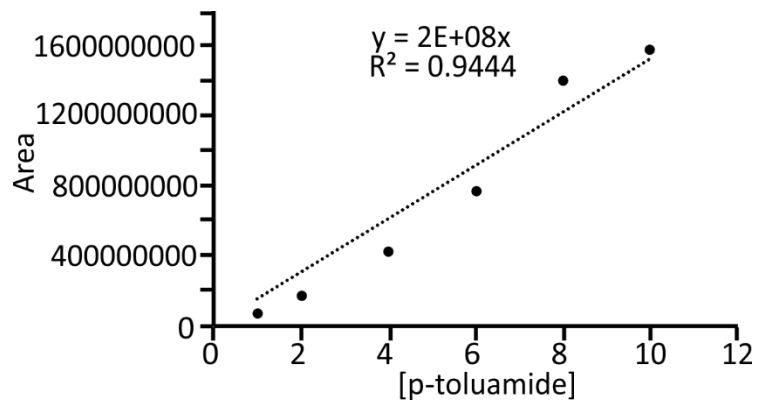


Figure A-97. Calibration curve for p-toluamide.

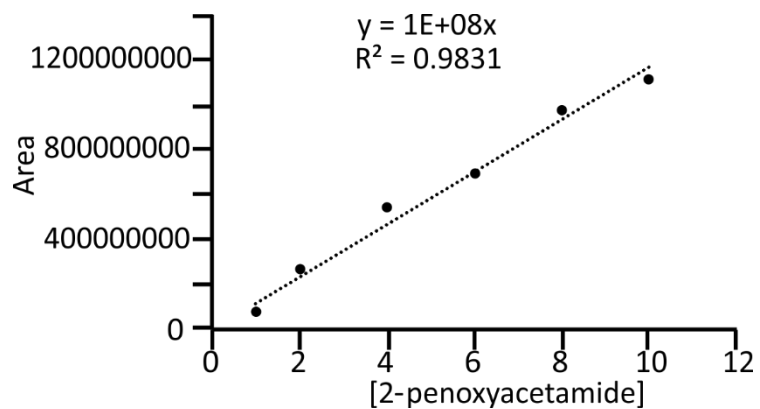


Figure A-98. Calibration curve for phenoxyacetamide.

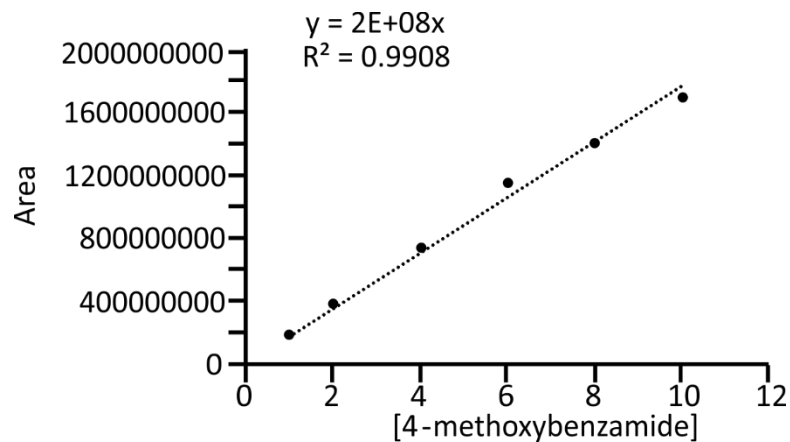


Figure A-99. Calibration curve for 4-methoxybenzamide.

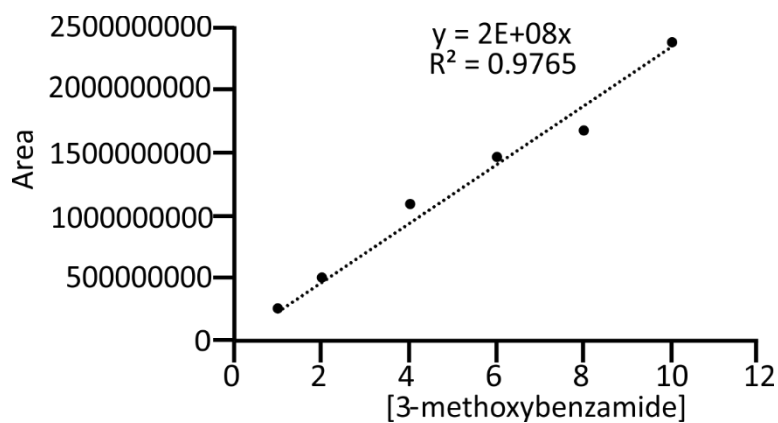


Figure A-100. Calibration curve for 3-methoxybenzamide.

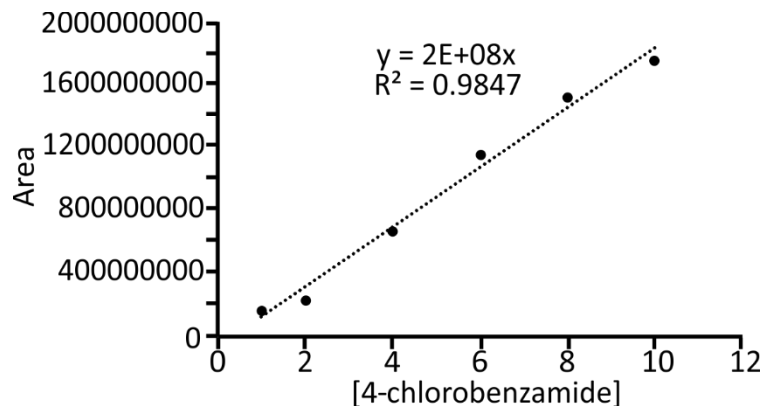


Figure A-101. Calibration curve for 4-chlorobenzamide.

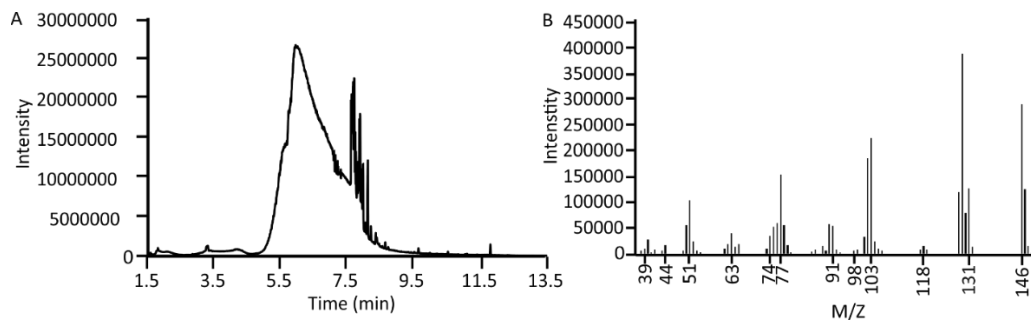


Figure A-102. GC/MS for the hydration of cinnamanonitrile.

A. GC for the hydration of cinnamanonitrile B. MS for the hydration of cinnamanonitrile at $t = 8.38$ min

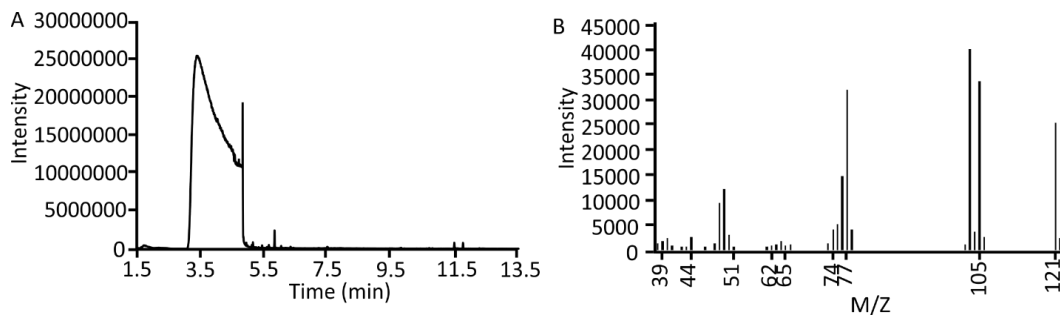


Figure A-103. GC/MS for the hydration of benzonitrile.

A. GC for the hydration of benzonitrile B. MS for the hydration of benzonitrile at $t = 6.07$ min

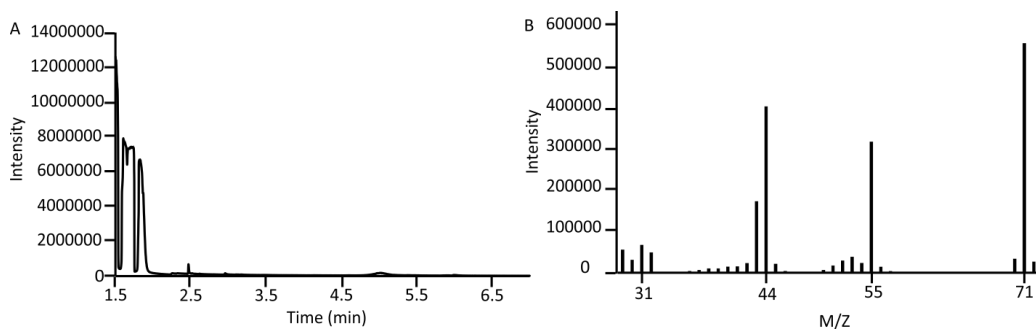


Figure A-104. GC/MS for the hydration of acrylonitrile.

A. GC for the hydration of acrylonitrile B. MS for the hydration of acrylonitrile at $t = 2.80$ min

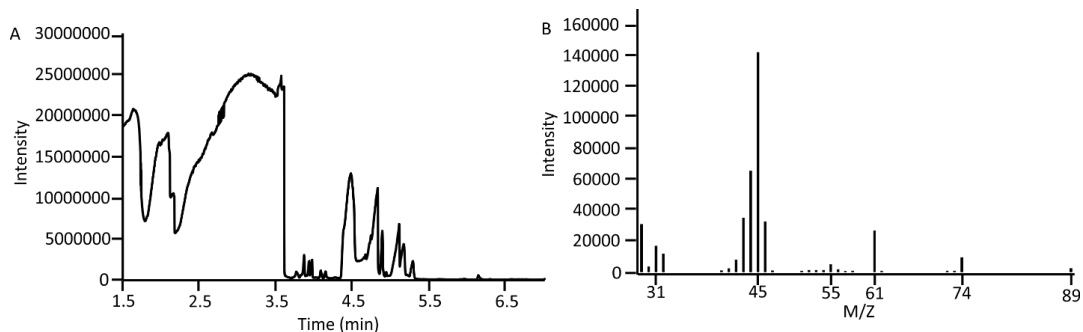


Figure A-105. GC/MS for the hydration of lactonitrile.

A. GC for the hydration of lactonitrile B. MS for the hydration of lactonitrile at $t = 4.77$ min

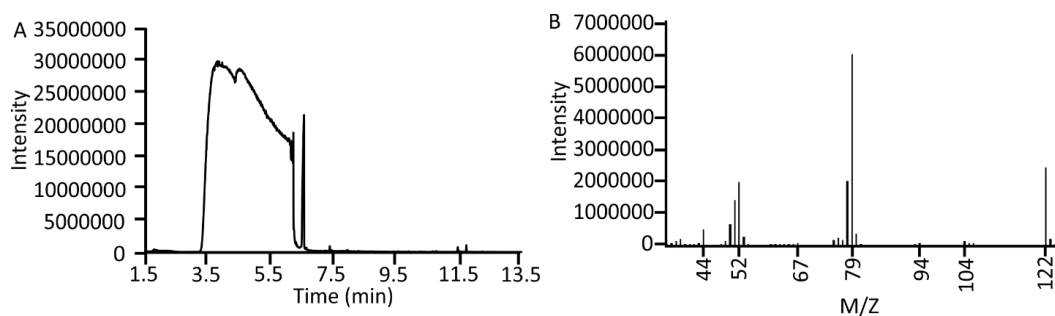


Figure A-106. GC/MS for the hydration of 2-pyridinecarbonitrile.

A. GC for the hydration of 2-pyridinecarbonitrile B. MS for the hydration of 2-pyridinecarbonitrile at $t = 6.54$ min

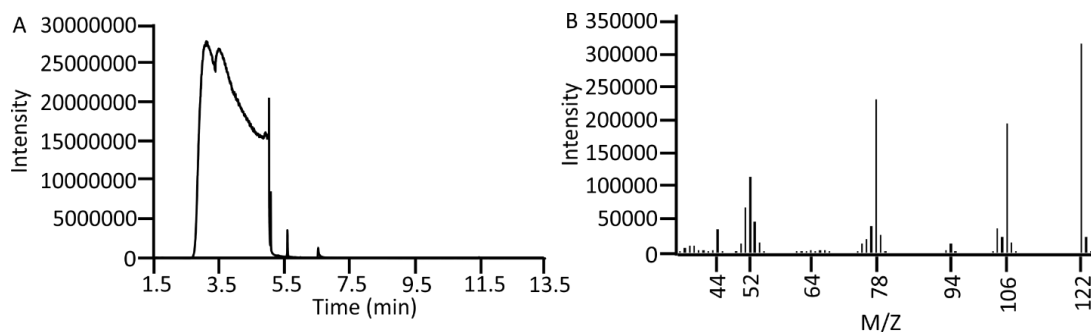


Figure A-107. GC/MS for the hydration of 3-pyridinecarbonitrile.

A. GC for the hydration of 3-pyridinecarbonitrile B. MS for the hydration of 3-pyridinecarbonitrile at $t = 6.56$ min

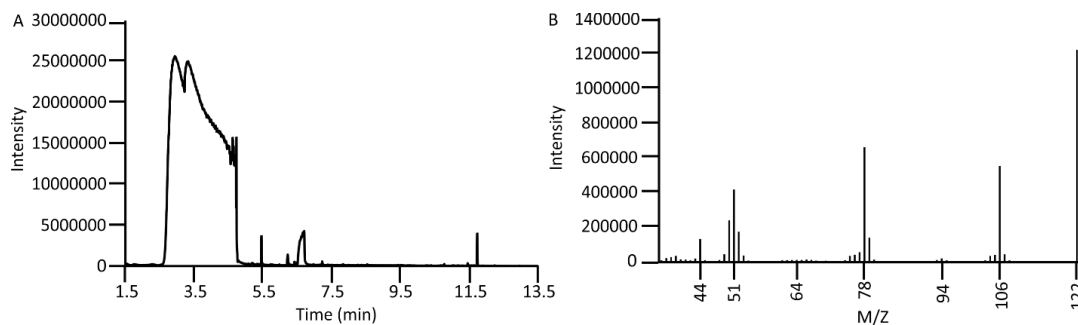


Figure A-108. GC/MS for the hydration of 4-pyridinecarbonitrile.

A. GC for the hydration of 4-pyridinecarbonitrile B. MS for the hydration of 4-pyridinecarbonitrile at $t = 6.68$ min

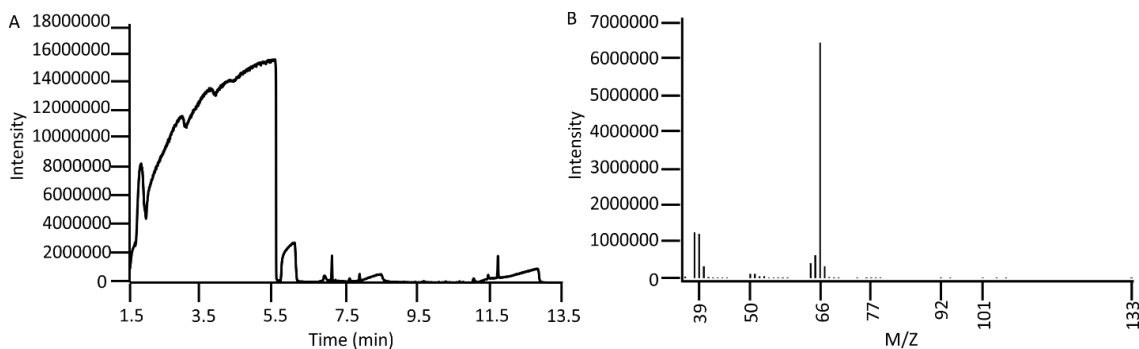


Figure A-109. GC/MS for the hydration of malonitrile.

A. GC for the hydration of malonitrile B. MS for the hydration of malonitrile at $t = 6.97$ min

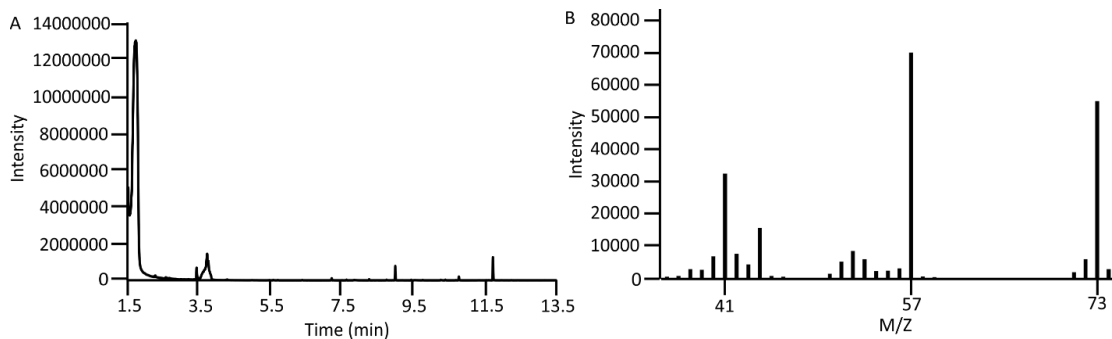


Figure A-110. GC/MS for the hydration of propionitrile.

A. GC for the hydration of propionitrile B. MS for the hydration of propionitrile at $t = 2.52$ min

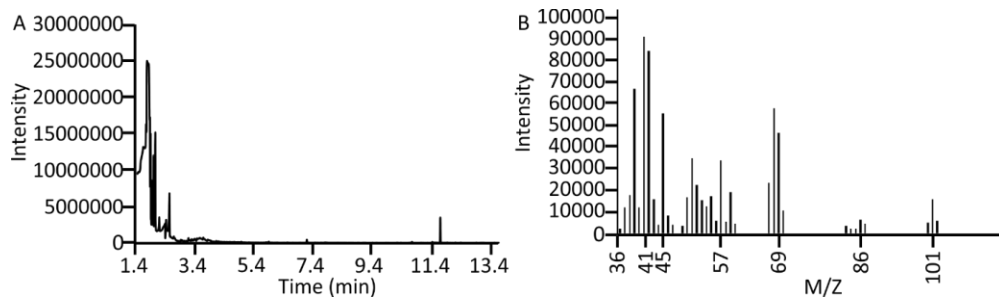


Figure A-111. GC/MS for the hydration of trimethylacetonitrile.

A. GC for the hydration of trimethylacetonitrile B. MS for the hydration of trimethylacetonitrile at $t = 2.45$ min

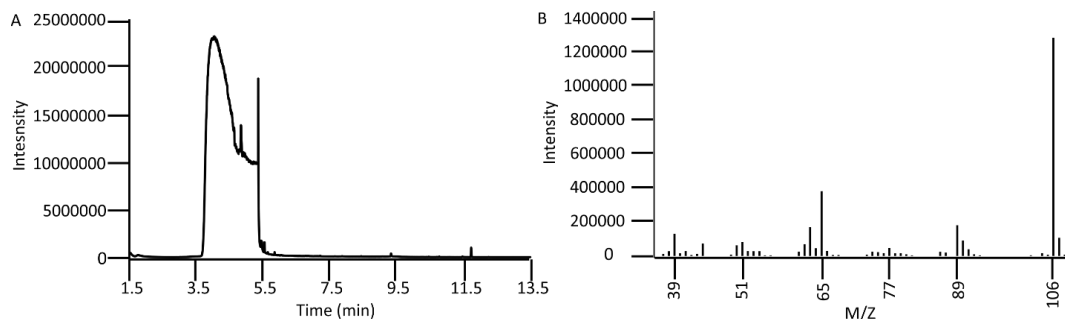


Figure A-112. GC/MS for the hydration of p-tolunitrile.

A. GC for the hydration of p-tolunitrile B. MS for the hydration of p-tolunitrile at $t = 7.02$ min

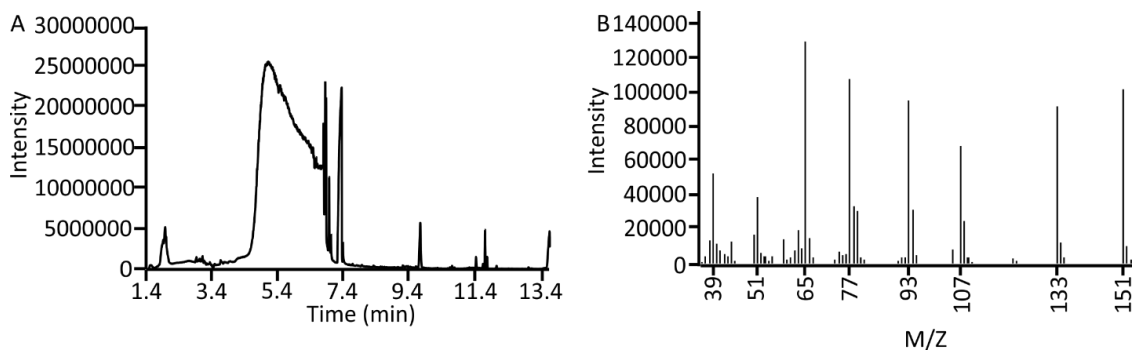


Figure A-113. GC/MS for the hydration of phenoxyacetonitrile.

A. GC for the hydration of phenoxyacetonitrile B. MS for the hydration of phenoxyacetonitrile at $t = 7.39$ min

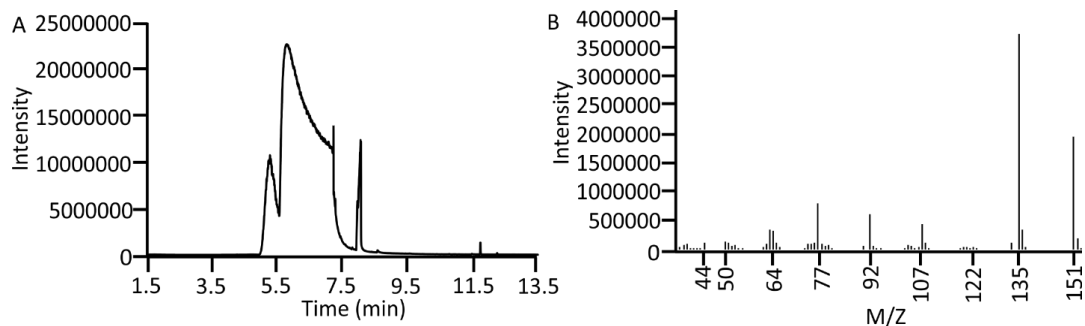


Figure A-114. GC/MS for the hydration of 4-methoxybenzonitrile.

A. GC for the hydration of 4-methoxybenzonitrile B. MS for the hydration of 4-methoxybenzonitrile at t= 8.05 min.

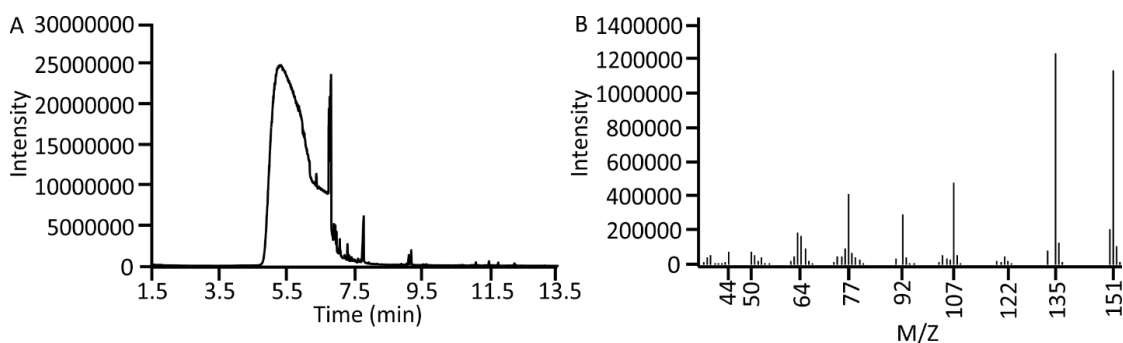


Figure A-115. GC/MS for the hydration of 3-methoxybenzonitrile.

A. GC for the hydration of 3-methoxybenzonitrile B. MS for the hydration of 3-methoxybenzonitrile at t= 8.05 min.

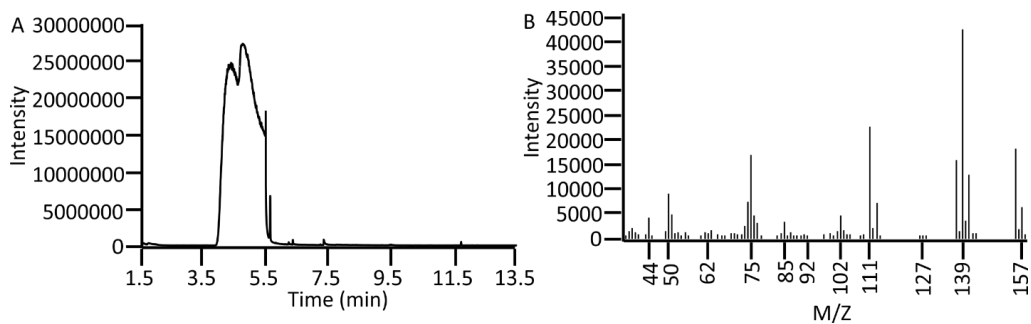


Figure A-116. GC/MS for the hydration of 4-chlorobenzonitrile.

A. GC for the hydration of 4-chlorobenzonitrile B. MS for the hydration of 4-chlorobenzonitrile at t= 7.34 min.

APPENDIX B
COMPUTATIONAL COORDINATES

Initial structure (Zn-L)

0 1

S -1.51917200 -2.28021900 -0.00688000
N -2.82075100 0.21238000 0.00391500
N -1.55842300 0.70446700 -0.00270500
N 2.25624800 -0.82602700 0.00106800
N -4.11997000 -1.67613600 0.00066900
C -2.88289200 -1.11568400 -0.00089600
C -1.32304800 1.99661100 -0.00570000
C 0.09508300 2.40297400 0.00050200
C 2.93624700 0.37542800 0.00037100
C 4.36140100 0.36997300 0.00350800
H 4.87744100 1.32907800 0.00333200
C 5.04944300 -0.83117900 0.00635700
H 2.33679900 -2.89241000 0.00273500
C 4.33401600 -2.05266800 0.00602400
H 4.84184500 -3.01474100 0.00797600
C 2.94604100 -1.98733400 0.00322000
H 6.13988900 -0.83350700 0.00880700
C -5.36215100 -0.90984200 0.01318600
H -5.41974700 -0.26861900 0.90400800
H -6.19591500 -1.61927300 0.02059700
H -5.43724900 -0.26755100 -0.87560900

C -2.40338200 3.04628400 -0.00466400
H -2.48834900 3.51279400 0.98967500
H -3.36970900 2.60084300 -0.25803500
H -2.17022900 3.85007800 -0.71560000
C 0.48224000 3.85838700 0.00697300
H 0.27785500 4.33022800 -0.96764400
H 1.55203700 3.95719200 0.21720900
H -0.08924000 4.41953800 0.75957600
H -4.17275400 -2.68377200 0.00485500
Zn 0.17265900 -0.55779500 -0.00404800
N 0.96179100 1.41310000 -0.00356500
N 2.28772300 1.58361000 -0.00561900

First protonated structure Zn-N4H

0 1

Zn 0.22480200 -0.23812200 -0.14062200
O -0.05899600 -1.14785100 1.59047900
O 0.78825800 -3.03416700 0.72678700
N 2.26602800 -0.29109300 -0.53180300
C -2.91835400 -0.66436600 -0.89166300
C -1.38074800 2.25536700 0.36464100
C 0.01163500 2.69373400 0.48049400
C 2.88828500 0.89404000 -0.27806000
C 4.29115200 1.00002200 -0.42382600
H 4.75745900 1.95377800 -0.21256700
C 5.01963500 -0.09713000 -0.82932800
H 2.43102100 -2.27291900 -1.04910200
C 4.36355800 -1.31313000 -1.08349800
H 4.90504100 -2.19644900 -1.39479700
C 2.99292300 -1.35726400 -0.91206100
H 6.09487500 -0.02120900 -0.94689500

C -5.37562100 -0.59724100 -0.47604400
H -5.34109900 -0.51976000 0.61458400
H -6.20104100 -1.25187200 -0.74454200
H -5.56597300 0.39080700 -0.90544300
C -2.52446800 3.18852000 0.63861500
H -3.04373300 2.90448800 1.56041600
H -3.25141200 3.15666000 -0.17823700
H -2.18937400 4.21610700 0.75260600
C 0.38889100 4.09621000 0.86227800
H 0.09661600 4.82188100 0.09530900
H 1.46958400 4.14888900 0.98186300
H -0.08406600 4.40186300 1.79956400
C 0.28350100 -2.38954100 1.65425800
C 0.02105900 -3.05099700 3.00200900
H -1.04232900 -2.98376900 3.24578600
H 0.56543200 -2.51819800 3.78603300
H 0.32788900 -4.09623200 2.99114800
N 0.89013500 1.76894000 0.16949600
N -1.55149000 1.02283300 -0.01761500
N -2.79619300 0.50234500 -0.21492500
N -4.13831017 -1.18384062 -1.01070539
H -4.21830586 -1.31748392 -1.99850100
S -1.51586122 -1.47710267 -1.62710376
N 2.18761100 2.00916100 0.11198600
H 2.76816170 2.20624702 0.90199738

First protonated structure Zn-N2H

O 1

Zn 0.22480200 -0.23812200 -0.14062200
S -1.56312600 -1.44971300 -1.60231900
O -0.05899600 -1.14785100 1.59047900

O 0.78825800 -3.03416700 0.72678700
N 2.18761100 2.00916100 0.11198600
N 2.26602800 -0.29109300 -0.53180300
N -4.14698700 -1.17972700 -1.00695600
H -4.20909600 -2.03924000 -1.52992000
C -2.91835400 -0.66436600 -0.89166300
C -1.38074800 2.25536700 0.36464100
C 0.01163500 2.69373400 0.48049400
C 2.88828500 0.89404000 -0.27806000
C 4.29115200 1.00002200 -0.42382600
H 4.75745900 1.95377800 -0.21256700
C 5.01963500 -0.09713000 -0.82932800
H 2.43102100 -2.27291900 -1.04910200
C 4.36355800 -1.31313000 -1.08349800
H 4.90504100 -2.19644900 -1.39479700
C 2.99292300 -1.35726400 -0.91206100
H 6.09487500 -0.02120900 -0.94689500
C -5.37562100 -0.59724100 -0.47604400
H -5.34109900 -0.51976000 0.61458400
H -6.20104100 -1.25187200 -0.74454200
H -5.56597300 0.39080700 -0.90544300
C -2.52446800 3.18852000 0.63861500
H -3.04373300 2.90448800 1.56041600
H -3.25141200 3.15666000 -0.17823700
H -2.18937400 4.21610700 0.75260600
C 0.38889100 4.09621000 0.86227800
H 0.09661600 4.82188100 0.09530900
H 1.46958400 4.14888900 0.98186300
H -0.08406600 4.40186300 1.79956400
C 0.28350100 -2.38954100 1.65425800

C 0.02105900 -3.05099700 3.00200900
H -1.04232900 -2.98376900 3.24578600
H 0.56543200 -2.51819800 3.78603300
H 0.32788900 -4.09623200 2.99114800
N 0.89013500 1.76894000 0.16949600
N -1.55149000 1.02283300 -0.01761500
N -2.79619300 0.50234500 -0.21492500
H -3.60034100 0.92381800 0.23363800

First protonated structure Zn-N5H

0 1

Zn 0.22480200 -0.23812200 -0.14062200
O -0.05899600 -1.14785100 1.59047900
O 0.78825800 -3.03416700 0.72678700
C -2.91835400 -0.66436600 -0.89166300
C -1.38074800 2.25536700 0.36464100
C 0.01163500 2.69373400 0.48049400
C 2.88828500 0.89404000 -0.27806000
C 4.29115200 1.00002200 -0.42382600
H 4.75745900 1.95377800 -0.21256700
C 5.01963500 -0.09713000 -0.82932800
H 2.43102100 -2.27291900 -1.04910200
C 4.36355800 -1.31313000 -1.08349800
H 4.90504100 -2.19644900 -1.39479700
C 2.99292300 -1.35726400 -0.91206100
H 6.09487500 -0.02120900 -0.94689500
C -5.37562100 -0.59724100 -0.47604400
H -5.34109900 -0.51976000 0.61458400
H -6.20104100 -1.25187200 -0.74454200
H -5.56597300 0.39080700 -0.90544300
C -2.52446800 3.18852000 0.63861500

H -3.04373300 2.90448800 1.56041600
H -3.25141200 3.15666000 -0.17823700
H -2.18937400 4.21610700 0.75260600
C 0.38889100 4.09621000 0.86227800
H 0.09661600 4.82188100 0.09530900
H 1.46958400 4.14888900 0.98186300
H -0.08406600 4.40186300 1.79956400
C 0.28350100 -2.38954100 1.65425800
C 0.02105900 -3.05099700 3.00200900
H -1.04232900 -2.98376900 3.24578600
H 0.56543200 -2.51819800 3.78603300
H 0.32788900 -4.09623200 2.99114800
N 0.89013500 1.76894000 0.16949600
N -1.55149000 1.02283300 -0.01761500
N -2.79619300 0.50234500 -0.21492500
N -4.13831017 -1.18384062 -1.01070539
H -4.21830586 -1.31748392 -1.99850100
S -1.51586122 -1.47710267 -1.62710376
N 2.18761100 2.00916100 0.11198600
N 2.26602800 -0.29109300 -0.53180300
H 1.78053789 -1.13177729 -0.29190870

First protonated structure Zn-S1H

0 1

Zn 0.22480200 -0.23812200 -0.14062200
O -0.05899600 -1.14785100 1.59047900
O 0.78825800 -3.03416700 0.72678700
N 2.18761100 2.00916100 0.11198600
N 2.26602800 -0.29109300 -0.53180300
C -2.91835400 -0.66436600 -0.89166300
C -1.38074800 2.25536700 0.36464100

C 0.01163500 2.69373400 0.48049400
C 2.88828500 0.89404000 -0.27806000
C 4.29115200 1.00002200 -0.42382600
H 4.75745900 1.95377800 -0.21256700
C 5.01963500 -0.09713000 -0.82932800
H 2.43102100 -2.27291900 -1.04910200
C 4.36355800 -1.31313000 -1.08349800
H 4.90504100 -2.19644900 -1.39479700
C 2.99292300 -1.35726400 -0.91206100
H 6.09487500 -0.02120900 -0.94689500
C -5.37562100 -0.59724100 -0.47604400
H -5.34109900 -0.51976000 0.61458400
H -6.20104100 -1.25187200 -0.74454200
H -5.56597300 0.39080700 -0.90544300
C -2.52446800 3.18852000 0.63861500
H -3.04373300 2.90448800 1.56041600
H -3.25141200 3.15666000 -0.17823700
H -2.18937400 4.21610700 0.75260600
C 0.38889100 4.09621000 0.86227800
H 0.09661600 4.82188100 0.09530900
H 1.46958400 4.14888900 0.98186300
H -0.08406600 4.40186300 1.79956400
C 0.28350100 -2.38954100 1.65425800
C 0.02105900 -3.05099700 3.00200900
H -1.04232900 -2.98376900 3.24578600
H 0.56543200 -2.51819800 3.78603300
H 0.32788900 -4.09623200 2.99114800
N 0.89013500 1.76894000 0.16949600
N -1.55149000 1.02283300 -0.01761500
N -2.79619300 0.50234500 -0.21492500

N -4.13831017 -1.18384062 -1.01070539
H -4.21830586 -1.31748392 -1.99850100
S -1.51586122 -1.47710267 -1.62710376
H -1.92219624 -2.51988884 -2.30797736

First protonated structure Zn-N1H

0 1

Zn 0.38011600 -0.42391300 -0.50929300
S -1.59008100 -0.69340600 -1.80856300
O -0.10623000 -1.16496900 1.28915100
O 0.53795700 -3.24446500 0.78114300
N -3.01254400 0.40779600 0.33408800
N 2.10929000 1.81185200 0.38238200
N 2.39281800 -0.35554000 -0.59114200
N -4.10889700 -1.01643800 -1.06400200
H -4.07989200 -1.58393200 -1.89417800
C -2.96912900 -0.38599200 -0.71210800
C -1.41588000 2.20084200 0.50238500
C -0.02537900 2.52929100 0.61325000
C 2.91178400 0.79155900 -0.08308700
C 4.30896200 0.96580000 -0.01252300
H 4.69037600 1.89342600 0.39313100
C 5.14322800 -0.04139000 -0.45225700
H 2.73344000 -2.22982700 -1.38388400
C 4.59197200 -1.22631700 -0.96174800
H 5.21519200 -2.03885000 -1.30962900
C 3.21567900 -1.33515300 -1.00931800
H 6.21859900 0.08272000 -0.40048100
C -5.37977300 -0.81631100 -0.38490400
H -5.28458300 -1.03098600 0.68178400
H -6.11099200 -1.49493500 -0.82166000

H -5.73720700 0.21230000 -0.49477100
C -2.44573800 3.22831500 0.15276100
H -2.67693500 3.82626900 1.04097500
H -3.36233800 2.74918400 -0.18138800
H -2.07755300 3.90671700 -0.61729400
C 0.45797200 3.90751900 0.94959000
H 1.09565200 4.29807900 0.15068500
H 1.07660300 3.87745600 1.85171400
H -0.36629100 4.59775900 1.12016100
C 0.02092700 -2.43162100 1.54810600
C -0.51941100 -2.85527000 2.90525300
H -1.58467900 -2.61824100 2.96666100
H -0.01751200 -2.28977500 3.69437900
H -0.37188000 -3.92201200 3.06842400
N 0.82436600 1.55045400 0.30338200
N -1.77478400 0.94100000 0.67454800
H -1.15900200 0.29049800 1.18162700

Protonation/protonation step (Zn-N4HN2H)

1 1

Zn 0.17423800 -0.33379300 -0.17894400
S -1.58507100 -1.68184000 -1.36370400
O 0.08091300 -0.96096600 1.68694300
O 1.00889900 -2.83262400 0.89461200
N -1.65950500 0.97188300 -0.03842800
N 0.75323500 1.75472000 0.09143500
N 2.07104100 1.95175400 0.03514400
H 2.48045300 2.86809100 0.16735800
N 2.24443500 -0.27154200 -0.62278300
N -4.18475300 -1.32029700 -0.97449500
H -4.22659800 -2.22666100 -1.41577300

C -2.96274800 -0.81713300 -0.81666500
C -1.52289000 2.20312200 0.31880900
C -0.10426600 2.65309500 0.43886200
C 2.86458600 0.89537600 -0.39472100
C 4.24306400 1.06528100 -0.56694400
H 4.70533400 2.02375400 -0.36813800
C 4.98213400 -0.02284400 -0.99536100
H 2.43346100 -2.24905200 -1.15311500
C 4.34479400 -1.24520800 -1.23296100
H 4.89712400 -2.11498400 -1.56120300
C 2.98040400 -1.32495700 -1.02698400
H 6.05083300 0.07683900 -1.14075000
C -5.44273300 -0.67802900 -0.59698900
H -5.49346100 -0.50880200 0.48162200
H -6.25388700 -1.34485100 -0.87689100
H -5.57639800 0.26879700 -1.12711200
C -2.65251600 3.15360500 0.57513500
H -2.36140200 4.17966500 0.35829600
H -2.96208700 3.10808200 1.62469100
H -3.51978300 2.92327600 -0.04591800
C 0.26062900 4.03626000 0.88402000
H 0.42669500 4.69601800 0.02527200
H 1.17678200 4.01956100 1.47945200
H -0.51894700 4.47870400 1.50068300
C 0.54116600 -2.16025700 1.82290600
C 0.47716500 -2.71691800 3.23589000
H -0.55744800 -2.71140700 3.58784300
H 1.05052000 -2.07542400 3.90986800
H 0.87175900 -3.73126700 3.27328300
N -2.87451400 0.40786000 -0.22631900

H -3.70974100 0.88259900 0.09381600
Protonation/protonation step (Zn-N4HS1H)
1 1
Zn 0.17423800 -0.33379300 -0.17894400
O 0.08091300 -0.96096600 1.68694300
O 1.00889900 -2.83262400 0.89461200
N -4.18475300 -1.32029700 -0.97449500
H -4.22659800 -2.22666100 -1.41577300
C -2.96274800 -0.81713300 -0.81666500
C -1.52289000 2.20312200 0.31880900
C -0.10426600 2.65309500 0.43886200
C 2.86458600 0.89537600 -0.39472100
C 4.24306400 1.06528100 -0.56694400
H 4.70533400 2.02375400 -0.36813800
C 4.98213400 -0.02284400 -0.99536100
H 2.43346100 -2.24905200 -1.15311500
C 4.34479400 -1.24520800 -1.23296100
H 4.89712400 -2.11498400 -1.56120300
C 2.98040400 -1.32495700 -1.02698400
H 6.05083300 0.07683900 -1.14075000
C -5.44273300 -0.67802900 -0.59698900
H -5.49346100 -0.50880200 0.48162200
H -6.25388700 -1.34485100 -0.87689100
H -5.57639800 0.26879700 -1.12711200
C -2.65251600 3.15360500 0.57513500
H -2.36140200 4.17966500 0.35829600
H -2.96208700 3.10808200 1.62469100
H -3.51978300 2.92327600 -0.04591800
C 0.26062900 4.03626000 0.88402000
H 0.42669500 4.69601800 0.02527200

H 1.17678200 4.01956100 1.47945200
H -0.51894700 4.47870400 1.50068300
C 0.54116600 -2.16025700 1.82290600
C 0.47716500 -2.71691800 3.23589000
H -0.55744800 -2.71140700 3.58784300
H 1.05052000 -2.07542400 3.90986800
H 0.87175900 -3.73126700 3.27328300
N -2.87451400 0.40786000 -0.22631900
N 2.24443500 -0.27154200 -0.62278300
N -1.65950500 0.97188300 -0.03842800
N 0.75323500 1.75472000 0.09143500
N 2.07104100 1.95175400 0.03514400
H 2.66027072 2.11873176 0.82566709
S -1.53376379 -1.71404327 -1.38407673
H -1.91441528 -2.84045444 -1.93398792

Protonation/protonation step (Zn-N2HN5H)

1 1

Zn 0.17423800 -0.33379300 -0.17894400
S -1.58507100 -1.68184000 -1.36370400
O 0.08091300 -0.96096600 1.68694300
O 1.00889900 -2.83262400 0.89461200
N 2.07104100 1.95175400 0.03514400
N -4.18475300 -1.32029700 -0.97449500
H -4.22659800 -2.22666100 -1.41577300
C -2.96274800 -0.81713300 -0.81666500
C -1.52289000 2.20312200 0.31880900
C -0.10426600 2.65309500 0.43886200
C 2.86458600 0.89537600 -0.39472100
C 4.24306400 1.06528100 -0.56694400
H 4.70533400 2.02375400 -0.36813800

C 4.98213400 -0.02284400 -0.99536100
H 2.43346100 -2.24905200 -1.15311500
C 4.34479400 -1.24520800 -1.23296100
H 4.89712400 -2.11498400 -1.56120300
C 2.98040400 -1.32495700 -1.02698400
H 6.05083300 0.07683900 -1.14075000
C -5.44273300 -0.67802900 -0.59698900
H -5.49346100 -0.50880200 0.48162200
H -6.25388700 -1.34485100 -0.87689100
H -5.57639800 0.26879700 -1.12711200
C -2.65251600 3.15360500 0.57513500
H -2.36140200 4.17966500 0.35829600
H -2.96208700 3.10808200 1.62469100
H -3.51978300 2.92327600 -0.04591800
C 0.26062900 4.03626000 0.88402000
H 0.42669500 4.69601800 0.02527200
H 1.17678200 4.01956100 1.47945200
H -0.51894700 4.47870400 1.50068300
C 0.54116600 -2.16025700 1.82290600
C 0.47716500 -2.71691800 3.23589000
H -0.55744800 -2.71140700 3.58784300
H 1.05052000 -2.07542400 3.90986800
H 0.87175900 -3.73126700 3.27328300
N -2.87451400 0.40786000 -0.22631900
H -3.70974100 0.88259900 0.09381600
N -1.65950500 0.97188300 -0.03842800
N 0.75323500 1.75472000 0.09143500
N 2.24443500 -0.27154200 -0.62278300
H 1.76370537 -1.11012767 -0.36651538

Protonation/protonation step (Zn-N4HN1H)

1 1

Zn 0.17423800 -0.33379300 -0.17894400
S -1.58507100 -1.68184000 -1.36370400
O 0.08091300 -0.96096600 1.68694300
O 1.00889900 -2.83262400 0.89461200
N -4.18475300 -1.32029700 -0.97449500
H -4.22659800 -2.22666100 -1.41577300
C -2.96274800 -0.81713300 -0.81666500
C -1.52289000 2.20312200 0.31880900
C -0.10426600 2.65309500 0.43886200
C 2.86458600 0.89537600 -0.39472100
C 4.24306400 1.06528100 -0.56694400
H 4.70533400 2.02375400 -0.36813800
C 4.98213400 -0.02284400 -0.99536100
H 2.43346100 -2.24905200 -1.15311500
C 4.34479400 -1.24520800 -1.23296100
H 4.89712400 -2.11498400 -1.56120300
C 2.98040400 -1.32495700 -1.02698400
H 6.05083300 0.07683900 -1.14075000
C -5.44273300 -0.67802900 -0.59698900
H -5.49346100 -0.50880200 0.48162200
H -6.25388700 -1.34485100 -0.87689100
H -5.57639800 0.26879700 -1.12711200
C -2.65251600 3.15360500 0.57513500
H -2.36140200 4.17966500 0.35829600
H -2.96208700 3.10808200 1.62469100
H -3.51978300 2.92327600 -0.04591800
C 0.26062900 4.03626000 0.88402000
H 0.42669500 4.69601800 0.02527200
H 1.17678200 4.01956100 1.47945200

H -0.51894700 4.47870400 1.50068300
C 0.54116600 -2.16025700 1.82290600
C 0.47716500 -2.71691800 3.23589000
H -0.55744800 -2.71140700 3.58784300
H 1.05052000 -2.07542400 3.90986800
H 0.87175900 -3.73126700 3.27328300
N -2.87451400 0.40786000 -0.22631900
N 2.24443500 -0.27154200 -0.62278300
N -1.65950500 0.97188300 -0.03842800
H -1.25101822 0.35443018 0.63380006
N 0.75323500 1.75472000 0.09143500
N 2.07104100 1.95175400 0.03514400
H 2.66027072 2.11873176 0.82566709

Protonation/protonation step (Zn-N2HN1H)

1 1

Zn 0.17423800 -0.33379300 -0.17894400
S -1.58507100 -1.68184000 -1.36370400
O 0.08091300 -0.96096600 1.68694300
O 1.00889900 -2.83262400 0.89461200
N 0.75323500 1.75472000 0.09143500
N 2.07104100 1.95175400 0.03514400
N 2.24443500 -0.27154200 -0.62278300
N -4.18475300 -1.32029700 -0.97449500
H -4.22659800 -2.22666100 -1.41577300
C -2.96274800 -0.81713300 -0.81666500
C -1.52289000 2.20312200 0.31880900
C -0.10426600 2.65309500 0.43886200
C 2.86458600 0.89537600 -0.39472100
C 4.24306400 1.06528100 -0.56694400
H 4.70533400 2.02375400 -0.36813800

C 4.98213400 -0.02284400 -0.99536100
H 2.43346100 -2.24905200 -1.15311500
C 4.34479400 -1.24520800 -1.23296100
H 4.89712400 -2.11498400 -1.56120300
C 2.98040400 -1.32495700 -1.02698400
H 6.05083300 0.07683900 -1.14075000
C -5.44273300 -0.67802900 -0.59698900
H -5.49346100 -0.50880200 0.48162200
H -6.25388700 -1.34485100 -0.87689100
H -5.57639800 0.26879700 -1.12711200
C -2.65251600 3.15360500 0.57513500
H -2.36140200 4.17966500 0.35829600
H -2.96208700 3.10808200 1.62469100
H -3.51978300 2.92327600 -0.04591800
C 0.26062900 4.03626000 0.88402000
H 0.42669500 4.69601800 0.02527200
H 1.17678200 4.01956100 1.47945200
H -0.51894700 4.47870400 1.50068300
C 0.54116600 -2.16025700 1.82290600
C 0.47716500 -2.71691800 3.23589000
H -0.55744800 -2.71140700 3.58784300
H 1.05052000 -2.07542400 3.90986800
H 0.87175900 -3.73126700 3.27328300
N -2.87451400 0.40786000 -0.22631900
H -3.70974100 0.88259900 0.09381600
N -1.65950500 0.97188300 -0.03842800
H -1.24539057 0.36252745 0.63773400

Protonation/protonation/reduction step (Zn-N4HN2H)

0 2

Zn 0.17423800 -0.33379300 -0.17894400

S -1.58507100 -1.68184000 -1.36370400
O 0.08091300 -0.96096600 1.68694300
O 1.00889900 -2.83262400 0.89461200
N -1.65950500 0.97188300 -0.03842800
N 0.75323500 1.75472000 0.09143500
N 2.07104100 1.95175400 0.03514400
H 2.48045300 2.86809100 0.16735800
N 2.24443500 -0.27154200 -0.62278300
N -4.18475300 -1.32029700 -0.97449500
H -4.22659800 -2.22666100 -1.41577300
C -2.96274800 -0.81713300 -0.81666500
C -1.52289000 2.20312200 0.31880900
C -0.10426600 2.65309500 0.43886200
C 2.86458600 0.89537600 -0.39472100
C 4.24306400 1.06528100 -0.56694400
H 4.70533400 2.02375400 -0.36813800
C 4.98213400 -0.02284400 -0.99536100
H 2.43346100 -2.24905200 -1.15311500
C 4.34479400 -1.24520800 -1.23296100
H 4.89712400 -2.11498400 -1.56120300
C 2.98040400 -1.32495700 -1.02698400
H 6.05083300 0.07683900 -1.14075000
C -5.44273300 -0.67802900 -0.59698900
H -5.49346100 -0.50880200 0.48162200
H -6.25388700 -1.34485100 -0.87689100
H -5.57639800 0.26879700 -1.12711200
C -2.65251600 3.15360500 0.57513500
H -2.36140200 4.17966500 0.35829600
H -2.96208700 3.10808200 1.62469100
H -3.51978300 2.92327600 -0.04591800

C 0.26062900 4.03626000 0.88402000
H 0.42669500 4.69601800 0.02527200
H 1.17678200 4.01956100 1.47945200
H -0.51894700 4.47870400 1.50068300
C 0.54116600 -2.16025700 1.82290600
C 0.47716500 -2.71691800 3.23589000
H -0.55744800 -2.71140700 3.58784300
H 1.05052000 -2.07542400 3.90986800
H 0.87175900 -3.73126700 3.27328300
N -2.87451400 0.40786000 -0.22631900
H -3.70974100 0.88259900 0.09381600

Protonation/protonation/reduction step (Zn-N1HN2H)

0 2

Zn 0.17423800 -0.33379300 -0.17894400
S -1.58507100 -1.68184000 -1.36370400
O 0.08091300 -0.96096600 1.68694300
O 1.00889900 -2.83262400 0.89461200
N 0.75323500 1.75472000 0.09143500
N 2.07104100 1.95175400 0.03514400
N 2.24443500 -0.27154200 -0.62278300
N -4.18475300 -1.32029700 -0.97449500
H -4.22659800 -2.22666100 -1.41577300
C -2.96274800 -0.81713300 -0.81666500
C -1.52289000 2.20312200 0.31880900
C -0.10426600 2.65309500 0.43886200
C 2.86458600 0.89537600 -0.39472100
C 4.24306400 1.06528100 -0.56694400
H 4.70533400 2.02375400 -0.36813800
C 4.98213400 -0.02284400 -0.99536100
H 2.43346100 -2.24905200 -1.15311500

C 4.34479400 -1.24520800 -1.23296100
H 4.89712400 -2.11498400 -1.56120300
C 2.98040400 -1.32495700 -1.02698400
H 6.05083300 0.07683900 -1.14075000
C -5.44273300 -0.67802900 -0.59698900
H -5.49346100 -0.50880200 0.48162200
H -6.25388700 -1.34485100 -0.87689100
H -5.57639800 0.26879700 -1.12711200
C -2.65251600 3.15360500 0.57513500
H -2.36140200 4.17966500 0.35829600
H -2.96208700 3.10808200 1.62469100
H -3.51978300 2.92327600 -0.04591800
C 0.26062900 4.03626000 0.88402000
H 0.42669500 4.69601800 0.02527200
H 1.17678200 4.01956100 1.47945200
H -0.51894700 4.47870400 1.50068300
C 0.54116600 -2.16025700 1.82290600
C 0.47716500 -2.71691800 3.23589000
H -0.55744800 -2.71140700 3.58784300
H 1.05052000 -2.07542400 3.90986800
H 0.87175900 -3.73126700 3.27328300
N -2.87451400 0.40786000 -0.22631900
H -3.70974100 0.88259900 0.09381600
N -1.65950500 0.97188300 -0.03842800
H -1.24539057 0.36252745 0.63773400

Protonation/protonation/reduction step (Zn-N4HN1H)

O 2

Zn 0.17423800 -0.33379300 -0.17894400
S -1.58507100 -1.68184000 -1.36370400
O 0.08091300 -0.96096600 1.68694300

O 1.00889900 -2.83262400 0.89461200
N -4.18475300 -1.32029700 -0.97449500
H -4.22659800 -2.22666100 -1.41577300
C -2.96274800 -0.81713300 -0.81666500
C -1.52289000 2.20312200 0.31880900
C -0.10426600 2.65309500 0.43886200
C 2.86458600 0.89537600 -0.39472100
C 4.24306400 1.06528100 -0.56694400
H 4.70533400 2.02375400 -0.36813800
C 4.98213400 -0.02284400 -0.99536100
H 2.43346100 -2.24905200 -1.15311500
C 4.34479400 -1.24520800 -1.23296100
H 4.89712400 -2.11498400 -1.56120300
C 2.98040400 -1.32495700 -1.02698400
H 6.05083300 0.07683900 -1.14075000
C -5.44273300 -0.67802900 -0.59698900
H -5.49346100 -0.50880200 0.48162200
H -6.25388700 -1.34485100 -0.87689100
H -5.57639800 0.26879700 -1.12711200
C -2.65251600 3.15360500 0.57513500
H -2.36140200 4.17966500 0.35829600
H -2.96208700 3.10808200 1.62469100
H -3.51978300 2.92327600 -0.04591800
C 0.26062900 4.03626000 0.88402000
H 0.42669500 4.69601800 0.02527200
H 1.17678200 4.01956100 1.47945200
H -0.51894700 4.47870400 1.50068300
C 0.54116600 -2.16025700 1.82290600
C 0.47716500 -2.71691800 3.23589000
H -0.55744800 -2.71140700 3.58784300

H 1.05052000 -2.07542400 3.90986800
H 0.87175900 -3.73126700 3.27328300
N -2.87451400 0.40786000 -0.22631900
N 2.24443500 -0.27154200 -0.62278300
N -1.65950500 0.97188300 -0.03842800
H -1.25101822 0.35443018 0.63380006
N 0.75323500 1.75472000 0.09143500
N 2.07104100 1.95175400 0.03514400
H 2.66027072 2.11873176 0.82566709

Protonation/protonation/reduction step (Zn-N5HN2H)

0 2

Zn 0.17423800 -0.33379300 -0.17894400
S -1.58507100 -1.68184000 -1.36370400
O 0.08091300 -0.96096600 1.68694300
O 1.00889900 -2.83262400 0.89461200
N 2.07104100 1.95175400 0.03514400
N -4.18475300 -1.32029700 -0.97449500
H -4.22659800 -2.22666100 -1.41577300
C -2.96274800 -0.81713300 -0.81666500
C -1.52289000 2.20312200 0.31880900
C -0.10426600 2.65309500 0.43886200
C 2.86458600 0.89537600 -0.39472100
C 4.24306400 1.06528100 -0.56694400
H 4.70533400 2.02375400 -0.36813800
C 4.98213400 -0.02284400 -0.99536100
H 2.43346100 -2.24905200 -1.15311500
C 4.34479400 -1.24520800 -1.23296100
H 4.89712400 -2.11498400 -1.56120300
C 2.98040400 -1.32495700 -1.02698400
H 6.05083300 0.07683900 -1.14075000

C -5.44273300 -0.67802900 -0.59698900
H -5.49346100 -0.50880200 0.48162200
H -6.25388700 -1.34485100 -0.87689100
H -5.57639800 0.26879700 -1.12711200
C -2.65251600 3.15360500 0.57513500
H -2.36140200 4.17966500 0.35829600
H -2.96208700 3.10808200 1.62469100
H -3.51978300 2.92327600 -0.04591800
C 0.26062900 4.03626000 0.88402000
H 0.42669500 4.69601800 0.02527200
H 1.17678200 4.01956100 1.47945200
H -0.51894700 4.47870400 1.50068300
C 0.54116600 -2.16025700 1.82290600
C 0.47716500 -2.71691800 3.23589000
H -0.55744800 -2.71140700 3.58784300
H 1.05052000 -2.07542400 3.90986800
H 0.87175900 -3.73126700 3.27328300
N -2.87451400 0.40786000 -0.22631900
H -3.70974100 0.88259900 0.09381600
N -1.65950500 0.97188300 -0.03842800
N 0.75323500 1.75472000 0.09143500
N 2.24443500 -0.27154200 -0.62278300
H 1.76370537 -1.11012767 -0.36651538

Protonation/protonation/reduction step (Zn-N4HS1H)

O 2

Zn 0.17423800 -0.33379300 -0.17894400
O 0.08091300 -0.96096600 1.68694300
O 1.00889900 -2.83262400 0.89461200
N -4.18475300 -1.32029700 -0.97449500
H -4.22659800 -2.22666100 -1.41577300

C -2.96274800 -0.81713300 -0.81666500
C -1.52289000 2.20312200 0.31880900
C -0.10426600 2.65309500 0.43886200
C 2.86458600 0.89537600 -0.39472100
C 4.24306400 1.06528100 -0.56694400
H 4.70533400 2.02375400 -0.36813800
C 4.98213400 -0.02284400 -0.99536100
H 2.43346100 -2.24905200 -1.15311500
C 4.34479400 -1.24520800 -1.23296100
H 4.89712400 -2.11498400 -1.56120300
C 2.98040400 -1.32495700 -1.02698400
H 6.05083300 0.07683900 -1.14075000
C -5.44273300 -0.67802900 -0.59698900
H -5.49346100 -0.50880200 0.48162200
H -6.25388700 -1.34485100 -0.87689100
H -5.57639800 0.26879700 -1.12711200
C -2.65251600 3.15360500 0.57513500
H -2.36140200 4.17966500 0.35829600
H -2.96208700 3.10808200 1.62469100
H -3.51978300 2.92327600 -0.04591800
C 0.26062900 4.03626000 0.88402000
H 0.42669500 4.69601800 0.02527200
H 1.17678200 4.01956100 1.47945200
H -0.51894700 4.47870400 1.50068300
C 0.54116600 -2.16025700 1.82290600
C 0.47716500 -2.71691800 3.23589000
H -0.55744800 -2.71140700 3.58784300
H 1.05052000 -2.07542400 3.90986800
H 0.87175900 -3.73126700 3.27328300
N -2.87451400 0.40786000 -0.22631900

N 2.24443500 -0.27154200 -0.62278300
N -1.65950500 0.97188300 -0.03842800
N 0.75323500 1.75472000 0.09143500
N 2.07104100 1.95175400 0.03514400
H 2.66027072 2.11873176 0.82566709
S -1.53376379 -1.71404327 -1.38407673
H -1.91441528 -2.84045444 -1.93398792

Protonation/protonation/reduction step (Zn-N3HN2H)

0 2

Zn 0.17423800 -0.33379300 -0.17894400
S -1.58507100 -1.68184000 -1.36370400
O 0.08091300 -0.96096600 1.68694300
O 1.00889900 -2.83262400 0.89461200
N 2.07104100 1.95175400 0.03514400
N 2.24443500 -0.27154200 -0.62278300
N -4.18475300 -1.32029700 -0.97449500
H -4.22659800 -2.22666100 -1.41577300
C -2.96274800 -0.81713300 -0.81666500
C -1.52289000 2.20312200 0.31880900
C -0.10426600 2.65309500 0.43886200
C 2.86458600 0.89537600 -0.39472100
C 4.24306400 1.06528100 -0.56694400
H 4.70533400 2.02375400 -0.36813800
C 4.98213400 -0.02284400 -0.99536100
H 2.43346100 -2.24905200 -1.15311500
C 4.34479400 -1.24520800 -1.23296100
H 4.89712400 -2.11498400 -1.56120300
C 2.98040400 -1.32495700 -1.02698400
H 6.05083300 0.07683900 -1.14075000
C -5.44273300 -0.67802900 -0.59698900

H -5.49346100 -0.50880200 0.48162200
H -6.25388700 -1.34485100 -0.87689100
H -5.57639800 0.26879700 -1.12711200
C -2.65251600 3.15360500 0.57513500
H -2.36140200 4.17966500 0.35829600
H -2.96208700 3.10808200 1.62469100
H -3.51978300 2.92327600 -0.04591800
C 0.26062900 4.03626000 0.88402000
H 0.42669500 4.69601800 0.02527200
H 1.17678200 4.01956100 1.47945200
H -0.51894700 4.47870400 1.50068300
C 0.54116600 -2.16025700 1.82290600
C 0.47716500 -2.71691800 3.23589000
H -0.55744800 -2.71140700 3.58784300
H 1.05052000 -2.07542400 3.90986800
H 0.87175900 -3.73126700 3.27328300
N -2.87451400 0.40786000 -0.22631900
H -3.70974100 0.88259900 0.09381600
N -1.65950500 0.97188300 -0.03842800
N 0.75323500 1.75472000 0.09143500
H 0.69602815 0.96995593 0.70858388

Protonation/protonation/reduction/protonation step (Zn-N4HN1HN2H)

1 2

Zn 0.31941700 0.27771100 -0.46863400
S -0.94950500 0.62182400 1.79145300
O -0.15956700 1.87655000 -1.48385500
O 1.07670900 3.32054600 -0.28413300
N 0.64193300 -1.67058100 -0.74609500
N 1.84930700 -2.11877300 -0.17754800
H 2.26935500 -2.94539900 -0.58597400

N 2.29011000 0.10969700 0.30566200
N -3.59138000 0.77087600 1.94231300
H -3.36101600 1.15732700 2.84390400
C -2.54374400 0.42502400 1.18303900
C -1.69250200 -2.03829100 -0.86375700
C -0.42253000 -2.53235000 -0.71379200
C 2.73073800 -1.16698600 0.24415000
C 4.05450100 -1.50592000 0.61516500
H 4.38716200 -2.53425800 0.53963700
C 4.88416200 -0.51301300 1.08050700
H 2.69948400 2.06816600 0.75887400
C 4.41585800 0.81352600 1.16550300
H 5.04988400 1.61410500 1.52249500
C 3.12396100 1.07088200 0.76215900
H 5.89818300 -0.75486600 1.37818700
C -4.99705400 0.67603400 1.56362600
H -5.21274700 1.28001400 0.67746500
H -5.59415900 1.05501700 2.38959300
H -5.29138200 -0.36099400 1.37628200
C -2.94692000 -2.80403800 -1.18255700
H -2.76770500 -3.87496000 -1.26768100
H -3.37880700 -2.47617000 -2.13999100
H -3.72987500 -2.67458100 -0.42407700
C -0.14322900 -4.00803300 -0.57135900
H 0.40351200 -4.19058600 0.35872000
H 0.48306300 -4.37496200 -1.39244900
H -1.05077500 -4.60563400 -0.54461200
C 0.27242500 3.05696600 -1.18287500
C -0.30309000 4.16680100 -2.05430600
H -1.39397800 4.16039800 -1.98963500

H -0.04090300 3.98641200 -3.10005100
H 0.07709000 5.14000200 -1.74613800
N -2.81200500 -0.06638400 -0.04190200
H -3.77222500 -0.24343900 -0.30697800
N -1.80395800 -0.58290000 -0.89117500
H -2.01523500 -0.22004200 -1.81967000

Protonation/protonation/reduction/protonation step (Zn-N4HN5HN2H)

1 2

Zn 0.31941700 0.27771100 -0.46863400
S -0.94950500 0.62182400 1.79145300
O -0.15956700 1.87655000 -1.48385500
O 1.07670900 3.32054600 -0.28413300
N 1.84930700 -2.11877300 -0.17754800
H 2.26935500 -2.94539900 -0.58597400
C -2.54374400 0.42502400 1.18303900
C -1.69250200 -2.03829100 -0.86375700
C -0.42253000 -2.53235000 -0.71379200
C 2.73073800 -1.16698600 0.24415000
C 4.05450100 -1.50592000 0.61516500
H 4.38716200 -2.53425800 0.53963700
C 4.88416200 -0.51301300 1.08050700
H 2.69948400 2.06816600 0.75887400
C 4.41585800 0.81352600 1.16550300
H 5.04988400 1.61410500 1.52249500
C 3.12396100 1.07088200 0.76215900
H 5.89818300 -0.75486600 1.37818700
C -4.99705400 0.67603400 1.56362600
H -5.21274700 1.28001400 0.67746500
H -5.59415900 1.05501700 2.38959300
H -5.29138200 -0.36099400 1.37628200

C -2.94692000 -2.80403800 -1.18255700
H -2.76770500 -3.87496000 -1.26768100
H -3.37880700 -2.47617000 -2.13999100
H -3.72987500 -2.67458100 -0.42407700
C -0.14322900 -4.00803300 -0.57135900
H 0.40351200 -4.19058600 0.35872000
H 0.48306300 -4.37496200 -1.39244900
H -1.05077500 -4.60563400 -0.54461200
C 0.27242500 3.05696600 -1.18287500
C -0.30309000 4.16680100 -2.05430600
H -1.39397800 4.16039800 -1.98963500
H -0.04090300 3.98641200 -3.10005100
H 0.07709000 5.14000200 -1.74613800
N -2.81200500 -0.06638400 -0.04190200
N -3.58066135 0.77159920 1.94520059
H -3.88097186 0.03561146 1.33845876
H -3.65870950 1.69618659 2.31809018
N -1.80395800 -0.58290000 -0.89117500
N 0.64193300 -1.67058100 -0.74609500
N 2.29011000 0.10969700 0.30566200
H 1.91324116 1.03465272 0.25639952

Protonation/protonation/reduction/protonation step (Zn-N3HN4HS1H)

1 2

Zn 0.31941700 0.27771100 -0.46863400
O -0.15956700 1.87655000 -1.48385500
O 1.07670900 3.32054600 -0.28413300
N 1.84930700 -2.11877300 -0.17754800
H 2.26935500 -2.94539900 -0.58597400
C -2.54374400 0.42502400 1.18303900
C -1.69250200 -2.03829100 -0.86375700

C -0.42253000 -2.53235000 -0.71379200
C 2.73073800 -1.16698600 0.24415000
C 4.05450100 -1.50592000 0.61516500
H 4.38716200 -2.53425800 0.53963700
C 4.88416200 -0.51301300 1.08050700
H 2.69948400 2.06816600 0.75887400
C 4.41585800 0.81352600 1.16550300
H 5.04988400 1.61410500 1.52249500
C 3.12396100 1.07088200 0.76215900
H 5.89818300 -0.75486600 1.37818700
C -4.99705400 0.67603400 1.56362600
H -5.21274700 1.28001400 0.67746500
H -5.59415900 1.05501700 2.38959300
H -5.29138200 -0.36099400 1.37628200
C -2.94692000 -2.80403800 -1.18255700
H -2.76770500 -3.87496000 -1.26768100
H -3.37880700 -2.47617000 -2.13999100
H -3.72987500 -2.67458100 -0.42407700
C -0.14322900 -4.00803300 -0.57135900
H 0.40351200 -4.19058600 0.35872000
H 0.48306300 -4.37496200 -1.39244900
H -1.05077500 -4.60563400 -0.54461200
C 0.27242500 3.05696600 -1.18287500
C -0.30309000 4.16680100 -2.05430600
H -1.39397800 4.16039800 -1.98963500
H -0.04090300 3.98641200 -3.10005100
H 0.07709000 5.14000200 -1.74613800
N -3.58066135 0.77159920 1.94520059
H -3.65870950 1.69618659 2.31809018
N 2.29011000 0.10969700 0.30566200

N 0.64193300 -1.67058100 -0.74609500
H 0.75239605 -2.64323036 -0.54176406
N -2.81200500 -0.06638400 -0.04190200
N -1.80395800 -0.58290000 -0.89117500
S -0.89168357 0.62896174 1.81351956
H -0.94359927 0.92272537 3.08910087

Protonation/protonation/reduction/protonation step (Zn-N4HN5HS1H)

1 2

Zn 0.31941700 0.27771100 -0.46863400
O -0.15956700 1.87655000 -1.48385500
O 1.07670900 3.32054600 -0.28413300
N 1.84930700 -2.11877300 -0.17754800
H 2.26935500 -2.94539900 -0.58597400
C -2.54374400 0.42502400 1.18303900
C -1.69250200 -2.03829100 -0.86375700
C -0.42253000 -2.53235000 -0.71379200
C 2.73073800 -1.16698600 0.24415000
C 4.05450100 -1.50592000 0.61516500
H 4.38716200 -2.53425800 0.53963700
C 4.88416200 -0.51301300 1.08050700
H 2.69948400 2.06816600 0.75887400
C 4.41585800 0.81352600 1.16550300
H 5.04988400 1.61410500 1.52249500
C 3.12396100 1.07088200 0.76215900
H 5.89818300 -0.75486600 1.37818700
C -4.99705400 0.67603400 1.56362600
H -5.21274700 1.28001400 0.67746500
H -5.59415900 1.05501700 2.38959300
H -5.29138200 -0.36099400 1.37628200
C -2.94692000 -2.80403800 -1.18255700

H -2.76770500 -3.87496000 -1.26768100
H -3.37880700 -2.47617000 -2.13999100
H -3.72987500 -2.67458100 -0.42407700
C -0.14322900 -4.00803300 -0.57135900
H 0.40351200 -4.19058600 0.35872000
H 0.48306300 -4.37496200 -1.39244900
H -1.05077500 -4.60563400 -0.54461200
C 0.27242500 3.05696600 -1.18287500
C -0.30309000 4.16680100 -2.05430600
H -1.39397800 4.16039800 -1.98963500
H -0.04090300 3.98641200 -3.10005100
H 0.07709000 5.14000200 -1.74613800
N -3.58066135 0.77159920 1.94520059
H -3.65870950 1.69618659 2.31809018
N 0.64193300 -1.67058100 -0.74609500
N -2.81200500 -0.06638400 -0.04190200
N -1.80395800 -0.58290000 -0.89117500
S -0.89168357 0.62896174 1.81351956
H -0.94359927 0.92272537 3.08910087
N 2.29011000 0.10969700 0.30566200
H 1.93088189 1.03710908 0.20144105

Protonation/protonation/reduction/protonation step (Zn-N₂HN₄HN₆H)

1 2

Zn 0.31941700 0.27771100 -0.46863400
S -0.94950500 0.62182400 1.79145300
O -0.15956700 1.87655000 -1.48385500
O 1.07670900 3.32054600 -0.28413300
N 1.84930700 -2.11877300 -0.17754800
H 2.26935500 -2.94539900 -0.58597400
N 2.29011000 0.10969700 0.30566200

C -2.54374400 0.42502400 1.18303900
C -1.69250200 -2.03829100 -0.86375700
C -0.42253000 -2.53235000 -0.71379200
C 2.73073800 -1.16698600 0.24415000
C 4.05450100 -1.50592000 0.61516500
H 4.38716200 -2.53425800 0.53963700
C 4.88416200 -0.51301300 1.08050700
H 2.69948400 2.06816600 0.75887400
C 4.41585800 0.81352600 1.16550300
H 5.04988400 1.61410500 1.52249500
C 3.12396100 1.07088200 0.76215900
H 5.89818300 -0.75486600 1.37818700
C -4.99705400 0.67603400 1.56362600
H -5.21274700 1.28001400 0.67746500
H -5.59415900 1.05501700 2.38959300
H -5.29138200 -0.36099400 1.37628200
C -2.94692000 -2.80403800 -1.18255700
H -2.76770500 -3.87496000 -1.26768100
H -3.37880700 -2.47617000 -2.13999100
H -3.72987500 -2.67458100 -0.42407700
C -0.14322900 -4.00803300 -0.57135900
H 0.40351200 -4.19058600 0.35872000
H 0.48306300 -4.37496200 -1.39244900
H -1.05077500 -4.60563400 -0.54461200
C 0.27242500 3.05696600 -1.18287500
C -0.30309000 4.16680100 -2.05430600
H -1.39397800 4.16039800 -1.98963500
H -0.04090300 3.98641200 -3.10005100
H 0.07709000 5.14000200 -1.74613800
N -2.81200500 -0.06638400 -0.04190200

H -3.77222500 -0.24343900 -0.30697800
N -1.80395800 -0.58290000 -0.89117500
N 0.64193300 -1.67058100 -0.74609500
N -3.58066135 0.77159920 1.94520059
H -3.88097186 0.03561146 1.33845876
H -3.65870950 1.69618659 2.31809018

Protonation/protonation/reduction/protonation/reduction step (Zn-N1HN3HN4H)

O 1

Zn 0.31941700 0.27771100 -0.46863400
O -0.15956700 1.87655000 -1.48385500
O 1.07670900 3.32054600 -0.28413300
N 1.84930700 -2.11877300 -0.17754800
H 2.26935500 -2.94539900 -0.58597400
C -2.54374400 0.42502400 1.18303900
C -1.69250200 -2.03829100 -0.86375700
C -0.42253000 -2.53235000 -0.71379200
C 2.73073800 -1.16698600 0.24415000
C 4.05450100 -1.50592000 0.61516500
H 4.38716200 -2.53425800 0.53963700
C 4.88416200 -0.51301300 1.08050700
H 2.69948400 2.06816600 0.75887400
C 4.41585800 0.81352600 1.16550300
H 5.04988400 1.61410500 1.52249500
C 3.12396100 1.07088200 0.76215900
H 5.89818300 -0.75486600 1.37818700
C -4.99705400 0.67603400 1.56362600
H -5.21274700 1.28001400 0.67746500
H -5.59415900 1.05501700 2.38959300
H -5.29138200 -0.36099400 1.37628200
C -2.94692000 -2.80403800 -1.18255700

H -2.76770500 -3.87496000 -1.26768100
H -3.37880700 -2.47617000 -2.13999100
H -3.72987500 -2.67458100 -0.42407700
C -0.14322900 -4.00803300 -0.57135900
H 0.40351200 -4.19058600 0.35872000
H 0.48306300 -4.37496200 -1.39244900
H -1.05077500 -4.60563400 -0.54461200
C 0.27242500 3.05696600 -1.18287500
C -0.30309000 4.16680100 -2.05430600
H -1.39397800 4.16039800 -1.98963500
H -0.04090300 3.98641200 -3.10005100
H 0.07709000 5.14000200 -1.74613800
N -3.58066135 0.77159920 1.94520059
H -3.65870950 1.69618659 2.31809018
N 2.29011000 0.10969700 0.30566200
S -0.89168357 0.62896174 1.81351956
N 0.64193300 -1.67058100 -0.74609500
H 0.75239605 -2.64323036 -0.54176406
N -2.81200500 -0.06638400 -0.04190200
N -1.80395800 -0.58290000 -0.89117500
H -2.03680117 -0.25072510 -1.80520120

Protonation/protonation/reduction/protonation/reduction step (Zn-N₂HN₃HN₄H)

0 1

Zn 0.31941700 0.27771100 -0.46863400
O -0.15956700 1.87655000 -1.48385500
O 1.07670900 3.32054600 -0.28413300
N 1.84930700 -2.11877300 -0.17754800
H 2.26935500 -2.94539900 -0.58597400
C -2.54374400 0.42502400 1.18303900
C -1.69250200 -2.03829100 -0.86375700

C -0.42253000 -2.53235000 -0.71379200
C 2.73073800 -1.16698600 0.24415000
C 4.05450100 -1.50592000 0.61516500
H 4.38716200 -2.53425800 0.53963700
C 4.88416200 -0.51301300 1.08050700
H 2.69948400 2.06816600 0.75887400
C 4.41585800 0.81352600 1.16550300
H 5.04988400 1.61410500 1.52249500
C 3.12396100 1.07088200 0.76215900
H 5.89818300 -0.75486600 1.37818700
C -4.99705400 0.67603400 1.56362600
H -5.21274700 1.28001400 0.67746500
H -5.59415900 1.05501700 2.38959300
H -5.29138200 -0.36099400 1.37628200
C -2.94692000 -2.80403800 -1.18255700
H -2.76770500 -3.87496000 -1.26768100
H -3.37880700 -2.47617000 -2.13999100
H -3.72987500 -2.67458100 -0.42407700
C -0.14322900 -4.00803300 -0.57135900
H 0.40351200 -4.19058600 0.35872000
H 0.48306300 -4.37496200 -1.39244900
H -1.05077500 -4.60563400 -0.54461200
C 0.27242500 3.05696600 -1.18287500
C -0.30309000 4.16680100 -2.05430600
H -1.39397800 4.16039800 -1.98963500
H -0.04090300 3.98641200 -3.10005100
H 0.07709000 5.14000200 -1.74613800
N -3.58066135 0.77159920 1.94520059
H -3.65870950 1.69618659 2.31809018
N -1.80395800 -0.58290000 -0.89117500

N 2.29011000 0.10969700 0.30566200
S -0.89168357 0.62896174 1.81351956
N 0.64193300 -1.67058100 -0.74609500
H 0.75239605 -2.64323036 -0.54176406
N -2.81200500 -0.06638400 -0.04190200
H -3.20935442 0.57943334 -0.69384785

Protonation/protonation/reduction/protonation/reduction step (Zn-N1HN2HN4H)

O 1

Zn 0.31941700 0.27771100 -0.46863400
S -0.94950500 0.62182400 1.79145300
O -0.15956700 1.87655000 -1.48385500
O 1.07670900 3.32054600 -0.28413300
N 1.84930700 -2.11877300 -0.17754800
H 2.26935500 -2.94539900 -0.58597400
N 2.29011000 0.10969700 0.30566200
C -2.54374400 0.42502400 1.18303900
C -1.69250200 -2.03829100 -0.86375700
C -0.42253000 -2.53235000 -0.71379200
C 2.73073800 -1.16698600 0.24415000
C 4.05450100 -1.50592000 0.61516500
H 4.38716200 -2.53425800 0.53963700
C 4.88416200 -0.51301300 1.08050700
H 2.69948400 2.06816600 0.75887400
C 4.41585800 0.81352600 1.16550300
H 5.04988400 1.61410500 1.52249500
C 3.12396100 1.07088200 0.76215900
H 5.89818300 -0.75486600 1.37818700
C -4.99705400 0.67603400 1.56362600
H -5.21274700 1.28001400 0.67746500
H -5.59415900 1.05501700 2.38959300

H -5.29138200 -0.36099400 1.37628200
C -2.94692000 -2.80403800 -1.18255700
H -2.76770500 -3.87496000 -1.26768100
H -3.37880700 -2.47617000 -2.13999100
H -3.72987500 -2.67458100 -0.42407700
C -0.14322900 -4.00803300 -0.57135900
H 0.40351200 -4.19058600 0.35872000
H 0.48306300 -4.37496200 -1.39244900
H -1.05077500 -4.60563400 -0.54461200
C 0.27242500 3.05696600 -1.18287500
C -0.30309000 4.16680100 -2.05430600
H -1.39397800 4.16039800 -1.98963500
H -0.04090300 3.98641200 -3.10005100
H 0.07709000 5.14000200 -1.74613800
N -2.81200500 -0.06638400 -0.04190200
N 0.64193300 -1.67058100 -0.74609500
N -3.58066135 0.77159920 1.94520059
H -3.88097186 0.03561146 1.33845876
H -3.65870950 1.69618659 2.31809018
N -1.80395800 -0.58290000 -0.89117500
H -2.03124877 -0.26063171 -1.81013205

Protonation/protonation/reduction/protonation/reduction step (Zn-N3HN4HS1H)

0 1

Zn 0.31941700 0.27771100 -0.46863400
O -0.15956700 1.87655000 -1.48385500
O 1.07670900 3.32054600 -0.28413300
N 1.84930700 -2.11877300 -0.17754800
H 2.26935500 -2.94539900 -0.58597400
C -2.54374400 0.42502400 1.18303900
C -1.69250200 -2.03829100 -0.86375700

C -0.42253000 -2.53235000 -0.71379200
C 2.73073800 -1.16698600 0.24415000
C 4.05450100 -1.50592000 0.61516500
H 4.38716200 -2.53425800 0.53963700
C 4.88416200 -0.51301300 1.08050700
H 2.69948400 2.06816600 0.75887400
C 4.41585800 0.81352600 1.16550300
H 5.04988400 1.61410500 1.52249500
C 3.12396100 1.07088200 0.76215900
H 5.89818300 -0.75486600 1.37818700
C -4.99705400 0.67603400 1.56362600
H -5.21274700 1.28001400 0.67746500
H -5.59415900 1.05501700 2.38959300
H -5.29138200 -0.36099400 1.37628200
C -2.94692000 -2.80403800 -1.18255700
H -2.76770500 -3.87496000 -1.26768100
H -3.37880700 -2.47617000 -2.13999100
H -3.72987500 -2.67458100 -0.42407700
C -0.14322900 -4.00803300 -0.57135900
H 0.40351200 -4.19058600 0.35872000
H 0.48306300 -4.37496200 -1.39244900
H -1.05077500 -4.60563400 -0.54461200
C 0.27242500 3.05696600 -1.18287500
C -0.30309000 4.16680100 -2.05430600
H -1.39397800 4.16039800 -1.98963500
H -0.04090300 3.98641200 -3.10005100
H 0.07709000 5.14000200 -1.74613800
N -3.58066135 0.77159920 1.94520059
H -3.65870950 1.69618659 2.31809018
N 2.29011000 0.10969700 0.30566200

N 0.64193300 -1.67058100 -0.74609500
H 0.75239605 -2.64323036 -0.54176406
N -2.81200500 -0.06638400 -0.04190200
N -1.80395800 -0.58290000 -0.89117500
S -0.89168357 0.62896174 1.81351956
H -0.94359927 0.92272537 3.08910087

Protonation/protonation/reduction/reduction step (Zn-N1HN2HS1)

-1 1

Zn -6.20249500 8.43221000 8.66594400
S -8.31572400 9.90790400 9.18760400
N -8.54854300 8.80658300 6.74642500
N -7.16333100 9.02858400 6.60697800
N -4.78295000 8.24314600 7.29528600
N -3.49437500 7.99293700 7.75750300
N -4.50823500 8.59671600 9.83362000
N -10.50415900 9.03520500 7.93100100
C -9.17370000 9.18804500 7.86814900
C -6.45211200 8.21193900 5.63295200
C -5.13760800 7.94745100 6.03651100
C -3.40057800 8.21663800 9.05797000
C -2.12692600 8.08514700 9.72305700
H -1.27546700 7.79890600 9.11511100
C -2.00835200 8.31129200 11.06321300
H -5.25389700 9.07342600 11.69543500
C -3.15430400 8.68296300 11.82975400
H -3.09552700 8.86440100 12.89519800
C -4.34837500 8.80000900 11.15736900
H -1.04202200 8.20701800 11.54767000
C -11.33897600 8.44776100 6.89013500
H -11.28758600 9.02809200 5.96354600

H -12.36932800 8.45362300 7.23804400
H -11.04970300 7.41319300 6.68274500
C -6.92196500 8.33552100 4.20713800
H -6.32362800 7.72791500 3.52692500
H -6.88248900 9.37540300 3.83144800
H -7.96028800 8.00208700 4.06706800
C -4.11261100 7.35998500 5.09733100
H -3.54938100 6.57859800 5.61095300
H -3.38275500 8.12173600 4.80108000
H -4.55748700 6.94375600 4.19494500
C -6.93561100 5.65256900 9.28120800
O -5.76401600 5.32719400 9.49816100
O -7.35692500 6.83423300 8.98873300
C -8.04554400 4.60113400 9.34873400
H -8.81254200 4.91323300 10.06225100
H -7.64826900 3.62857800 9.63967700
H -8.53015200 4.51755100 8.37193800
H -10.93537700 9.31964500 8.79570300
H -7.04092200 10.02863900 6.41613100
H -9.06569700 8.49665400 5.93402900

ZnL2

(Zn-N1HN2H) with two equivalents of acids and reduced twice

1 1

Zn 0.07785700 -0.42360100 0.04301700
S 1.94252500 -1.98400800 -0.45200200
N -1.76526300 1.47181500 0.96311900
N -1.73785500 0.20704000 -0.98764700
N 4.46202200 -1.26692700 0.02362600
H 4.57367900 -2.26310500 0.12938500
C 3.21888800 -0.84884100 -0.23170500

C 1.44548900 2.31591500 -0.26662500
C 0.31098500 2.44395100 0.48034400
C -2.45650900 0.90075400 -0.06827900
C -3.86502200 1.01569300 -0.18810600
H -4.43485100 1.55736900 0.55383400
C -4.48856600 0.45296400 -1.28201400
H -5.56313700 0.54804800 -1.39263800
C -3.73578800 -0.23072900 -2.24891800
H -4.19743800 -0.67704600 -3.11943900
C -2.37347200 -0.33258600 -2.04131200
H -1.74456200 -0.88155800 -2.73370700
C 5.62507400 -0.41014200 0.23248900
H 5.82343900 0.20821400 -0.64775200
H 6.48868900 -1.04937000 0.39920600
H 5.49453100 0.23428000 1.10633500
C 2.39013700 3.39711900 -0.71859500
H 2.05688700 4.39219300 -0.43001500
H 2.50140200 3.39080600 -1.81117800
H 3.40015900 3.28315200 -0.29943600
C -0.24073300 3.79994200 0.85634100
H -1.29367100 3.86047200 0.57135700
H -0.19223400 3.94589900 1.94020700
H 0.28287400 4.62324200 0.37641400
C -2.42692600 1.77379600 2.22954700
H -1.64902500 1.84456000 2.98615200
H -3.12629300 0.98124400 2.51612600
H -2.96894600 2.72523300 2.19612200
N 3.00705100 0.47571500 -0.31952000
H 3.79186300 1.11426600 -0.35004400
N -0.35149300 1.32200300 0.95746200

N 1.75183200 0.98091100 -0.75568100

H 1.78197100 0.98991000 -1.77635000

ZnL2

(Zn-N2HN3H) with two equivalents of acids and reduced twice

1 1

Zn 0.03331200 -0.29854800 -0.44710800

S 1.84646300 -1.97012100 -1.19682400

N -2.10242200 1.72367500 -0.02998600

N -2.03206900 -0.45735800 -0.96885600

N 4.37815700 -1.48343500 -0.46390400

H 4.45228800 -2.47521800 -0.61983000

C 3.12484700 -0.97850300 -0.56136500

C 1.48467100 2.16646400 0.03949800

C 0.21597600 2.69307500 -0.03936000

C -2.75470700 0.53908700 -0.42560900

C -4.15235100 0.44085800 -0.30720100

H -4.71582600 1.26439600 0.11062300

C -4.78466200 -0.69830000 -0.76624700

H -5.86230800 -0.78487400 -0.69207600

C -4.02966900 -1.72260500 -1.35126100

H -4.49464200 -2.61945000 -1.73800000

C -2.66120200 -1.55780400 -1.42352900

H -2.02363700 -2.32348900 -1.84777200

C 5.50519400 -0.79491900 0.14687700

H 5.74456900 0.12668400 -0.39316600

H 6.37361200 -1.44792200 0.09265200

H 5.31985600 -0.55143200 1.20004000

C 2.65601600 3.00535000 0.48337400

H 2.35116400 4.01965500 0.73034000

H 3.42235700 3.06654200 -0.29755100

H 3.12564100 2.58347400 1.37915800
C -0.12691200 4.16479500 0.05361500
H -1.12723100 4.33217300 -0.35335700
H -0.13653000 4.55251500 1.07987500
H 0.55683100 4.79841800 -0.52272700
C -2.16772200 2.03879400 1.40711200
H -1.45703600 1.42955500 1.97440700
H -3.17653500 1.82041000 1.75260900
H -1.97178600 3.09566600 1.57106000
N 1.67597600 0.87199400 -0.34914100
N -0.75244100 1.77231100 -0.59927400
H -0.92015900 2.01335000 -1.57625200
N 2.91348200 0.28178900 -0.18599500
H 3.68050200 0.83325200 0.17701000

ZnL2

(Zn-N1HN3H) with two equivalents of acids and reduced twice

1 1

Zn 0.02219700 -0.35190300 -0.53277100
S 1.75966000 -1.75581300 -1.52623100
N -2.13306500 1.64027000 0.09650100
N -2.08164800 -0.55623100 -0.83347000
N 4.17522000 -1.50952100 -0.39683100
H 4.09134000 -2.51348100 -0.41749700
C 3.01156200 -0.83291400 -0.64659800
C 1.42262400 2.30842000 -0.12050800
C 0.12765600 2.67465300 -0.07051800
C -2.79683100 0.44953100 -0.30769800
C -4.18846300 0.36662300 -0.17114900
H -4.73826600 1.20605500 0.23323400
C -4.83075000 -0.78678000 -0.58587100

H -5.90725800 -0.86914900 -0.49582400
C -4.08418000 -1.82920200 -1.14395300
H -4.55515500 -2.73846200 -1.49255100
C -2.71541600 -1.66962600 -1.24587400
H -2.08476600 -2.44785400 -1.65709000
C 5.22173200 -0.94786700 0.44434100
H 5.56820000 -0.00052900 0.02787000
H 6.05624600 -1.64878100 0.46817100
H 4.88339200 -0.76015100 1.47071800
C 2.56714000 3.18001100 0.29686300
H 2.22313400 4.09416900 0.77771100
H 3.18425000 3.44904200 -0.56783200
H 3.21222900 2.63788400 0.98983200
C -0.35176000 4.06908300 0.26762100
H -1.40450000 4.17920100 0.00613400
H -0.24298900 4.30681900 1.32920000
H 0.20849500 4.81888700 -0.29568500
C -2.06216800 1.79267700 1.56900700
H -1.26597700 1.17115400 1.98929800
H -3.01765800 1.47031500 1.97821600
H -1.91699000 2.83593600 1.83648900
N 2.93173600 0.41261100 -0.27837500
N 1.71802700 1.03114300 -0.72006000
H 1.77940600 1.16295300 -1.73204000
N -0.82143200 1.69200100 -0.56073600
H -1.05061300 1.92714900 -1.52633000

Acetic acid

0 1

C -4.52784843 1.57031930 -0.04573389
H -4.36879538 0.54975879 -0.32512318

H -4.10280710 2.21360963 -0.78763511
H -5.57818060 1.75956169 0.03101022
C -3.85681462 1.84093873 1.31370671
O -4.59094730 1.64477294 2.52509772
H -4.26958498 2.25171084 3.19588282
O -2.66244737 2.23469935 1.35853980

Acetate ion

-1 1

C -4.52784843 1.57031930 -0.04573389
H -4.36879538 0.54975879 -0.32512318
H -4.10280710 2.21360963 -0.78763511
H -5.57818060 1.75956169 0.03101022
C -3.85681462 1.84093873 1.31370671
O -4.59094730 1.64477294 2.52509772
O -2.66244737 2.23469935 1.35853980

Input coordinates for ferrocene

0 1

C -0.71935400 -0.43194800 -0.98126300
H -0.04897000 0.29073400 -1.43758900
C -0.87831800 -0.66282800 0.42601800
H -0.34944300 -0.14532800 1.22130200
C -1.81064000 -1.74013200 0.59595900
H -2.11246900 -2.17880500 1.54272300
C -1.55332900 -1.36694200 -1.68093400
H -1.62573900 -1.47436500 -2.75941400
C -2.22789100 -2.17532500 -0.70616600
H -2.89977300 -3.00225100 -0.91742300
C 1.82112500 -2.50346500 -0.40593100
H 2.49991300 -1.66473000 -0.28116800
C 1.33489600 -3.01518700 -1.65534300

H 1.58270100 -2.63271200 -2.64137300
C 0.41673300 -4.08058100 -1.37118300
H -0.15230500 -4.64500200 -2.10436300
C 1.20319200 -3.25271100 0.65047200
H 1.33267500 -3.08074700 1.71516100
C 0.33554200 -4.22739100 0.05387700
H -0.30591900 -4.92257600 0.58789500
Fe -0.20779900 -2.34594300 -0.50674100

Input coordinates for ferrocenium

1 2

C -0.71935400 -0.43194800 -0.98126300
H -0.04897000 0.29073400 -1.43758900
C -0.87831800 -0.66282800 0.42601800
H -0.34944300 -0.14532800 1.22130200
C -1.81064000 -1.74013200 0.59595900
H -2.11246900 -2.17880500 1.54272300
C -1.55332900 -1.36694200 -1.68093400
H -1.62573900 -1.47436500 -2.75941400
C -2.22789100 -2.17532500 -0.70616600
H -2.89977300 -3.00225100 -0.91742300
C 1.82112500 -2.50346500 -0.40593100
H 2.49991300 -1.66473000 -0.28116800
C 1.33489600 -3.01518700 -1.65534300
H 1.58270100 -2.63271200 -2.64137300
C 0.41673300 -4.08058100 -1.37118300
H -0.15230500 -4.64500200 -2.10436300
C 1.20319200 -3.25271100 0.65047200
H 1.33267500 -3.08074700 1.71516100
C 0.33554200 -4.22739100 0.05387700
H -0.30591900 -4.92257600 0.58789500

Fe -0.20779900 -2.34594300 -0.50674100

CURRICULUM VITA

Steve P. Cronin
211 Cannons Lane,
Louisville, KY 40206

859-866-8975 (Cell)

Spcron01@louisville.edu

Professional Appointments

2017 – present	Graduate Research Assistant	University of Louisville
2015-2017	Graduate Teaching Assistant	University of Louisville
2013-2015	Chemistry Teacher	Cooper High School
2012-2013	Chemistry Teacher	Holmes High School

Education

2015 – current	Ph.D. in inorganic chemistry
	University of Louisville
	Louisville, KY

Advisor: Prof Craig A. Grapperhaus

2009-2012

BA in chemistry and secondary education

Northern Kentucky University

Highland Heights, KY

Advisor : Dr. Pamela Ball

2007-2009

Undergraduate Studies

University of Louisville

Louisville, KY

Advisor: Jim Watters

Honors and Awards

2019

ACS Green Chemistry most outstanding poster

2016

University of Louisville, faculty favorites

Professional Societies and Activities

2019 -

Member of the American Chemical Society

Publications (citations = 44)

1. Haddad, A. Z.; Cronin, S. P.; Mashuta, M. S.; Buchanan, R. M.; Grapperhaus, C. A., Metal-Assisted Ligand-Centered Electrocatalytic Hydrogen Evolution upon Reduction of a Bis(thiosemicarbazonato)Cu(II) Complex. *Inorganic Chemistry* **2017**, *56* (18), 11254-11265.
2. Cronin, S. P.; Mamun, A. A.; Toda, M. J.; Mashuta, M. S.; Losovyj, Y.; Kozlowski, P. M.; Buchanan, R. M.; Grapperhaus, C. A., Utilizing Charge Effects and Minimizing Intramolecular Proton Rearrangement to Improve the

Overpotential of a Thiosemicarbazonato Zinc HER Catalyst. *Inorganic Chemistry* **2019**, *58* (19), 12986-12997.

- Cronin, S. P.; Strain, J. M.; Mashuta, M. S.; Spurgeon, J. M.; Buchanan, R. M.; Grapperhaus, C. A., Exploiting Metal–Ligand Cooperativity to Sequester, Activate, and Reduce Atmospheric Carbon Dioxide with a Neutral Zinc Complex. *Inorganic Chemistry* **2020**, *59* (7), 4835-4841.

Presentations

- Haddad, A. Z.; Cronin, S. P.; Mashuta, M. S.; Buchanan, R. M.; Grapperhaus, C. A., Metal-Assisted Ligand-Centered Electrocatalytic Hydrogen Evolution upon Reduction of a Bis(thiosemicarbazonato)Cu(II) Complex. 2017 Southeast Regional Meeting (SERMACS) Charlotte, NC poster presentation
- Haddad, A. Z.; Cronin, S. P.; Mashuta, M. S.; Buchanan, R. M.; Grapperhaus, C. A., Metal-Assisted Ligand-Centered Electrocatalytic Hydrogen Evolution upon Reduction of a Bis(thiosemicarbazonato)Cu(II) Complex. 2018 UofL Graduate Student Regional Research Conference Louisville, KY poster presentation
- Cronin, S. P.; Ramigula, A. R.; Shaw, M. J.; Mashuta, S. M; Buchanan, R. M.; Grapperhaus, C. A., Homogeneous Reduction of Atmospheric Carbon Dioxide by a Neutral Zinc Complex. 2019 UofL Graduate Student Regional Research Conference Louisville, KY poster presentation
- Cronin, S. P.; Ramigula, A. R.; Shaw, M. J.; Mashuta, S. M; Buchanan, R. M.; Grapperhaus, C. A., Homogeneous Reduction of Atmospheric Carbon Dioxide by a Neutral Zinc Complex. 2019 Gordon Graduate Student Research Conference Galveston, TX poster presentation
- Cronin, S. P.; Ramigula, A. R.; Shaw, M. J.; Mashuta, S. M; Buchanan, R. M.; Grapperhaus, C. A., Homogeneous Reduction of Atmospheric Carbon Dioxide by a Neutral Zinc Complex. 2019 Gordon Research Conference Galveston, TX poster presentation
- Cronin, S. P.; Ramigula, A. R.; Shaw, M. J.; Mashuta, S. M; Buchanan, R. M.; Grapperhaus, C. A., Homogeneous Reduction of Atmospheric Carbon Dioxide by a Neutral Zinc Complex. 2019 Great Lakes Regional Meeting Lisle, IL oral presentation
- Cronin, S. P.; Ramigula, A. R.; Shaw, M. J.; Mashuta, S. M; Buchanan, R. M.; Grapperhaus, C. A., Homogeneous Reduction of Atmospheric Carbon Dioxide by a Neutral Zinc Complex. 2019 23rd ACS Green Chemistry Conference Reston, VA poster presentation
- Cronin, S. P.; Ramigula, A. R.; Shaw, M. J.; Mashuta, S. M; Buchanan, R. M.; Grapperhaus, C. A., Homogeneous Reduction of Atmospheric Carbon Dioxide by a Neutral Zinc Complex. 2019 23rd ACS Green Chemistry Conference Reston, VA impromptu oral presentation
- Cronin, S. P.; Ramigula, A. R.; Shaw, M. J.; Mashuta, S. M; Buchanan, R. M.; Grapperhaus, C. A., Homogeneous Reduction of Atmospheric Carbon Dioxide by a

Neutral Zinc Complex. 2019 ACS Fall National Conference San Diego, CA poster presentation

Persons Mentored

Matthew Turner – 2019-20

Julia Tross -2018-19

Bruce Spigelmyer -2018-19

Brandon Swift -2018

Stephanie Vega -2018

Professional References

Craig A. Grapperhaus Assistant Professor Department of Chemistry University of Louisville 502-852-5932 grapperhaus@louisville.edu	Robert M. Buchanan Associate Dean of Research College of Arts & Sciences University of Louisville 502-852-5635 robert.buchanan@louisville.edu
Pawel Kozlowski Department Chair Department of Chemistry University of Louisville 502-852-6609 pawel@louisville.edu	